UNIVERSIDADE DE SÃO PAULO

CENTRO DE ENERGIA NUCLEAR NA AGRICULTURA

FRANCINE CÔA

Toxicity of carbon nanomaterials in *Caenorhabditis elegans*: effects of biocorona formation on single and co-exposure testing

Piracicaba
2023

FRANCINE CÔA

Toxicity of carbon nanomaterials in *Caenorhabditis elegans*: effects of biocorona formation on single and co-exposure testing

Revised version according the Resoluiton CoPGr 6018 from 2011

Thesis presented to the Center for Nuclear Energy in Agriculture of the University of Sao Paulo as a requisite to the Doctoral Degree in Sciences

Concentration Area: Chemistry in Agriculture and the Environment

Advisor: Prof. Dr. Diego Stéfani Teodoro Martinez

Co-Advisor: Prof. Dr. Cassio Hamilton Abreu-Junior

Piracicaba
2023

Dados Internacionais de Catalogação na Publicação (CIP)

Sessão Técnica de Biblioteca - CENA/USP

Côa, Francine

Toxicidade de nanomateriais de carbono no *Caenorhabditis elegans*: o efeito da formação da biocorona em ensaios de exposição simples e combinada / Toxicity of carbon nanomaterials in *Caenorhabditis elegans*: Effects of biocorona formation on single and co-exposure testing / Francine Côa; orientador Diego Stéfani Teodoro Martinez; co-orientador Cassio Hamilton Abreu-Junior. – Versão revisada de acordo com a Resolução CoPGr 6018 de 2011. - - Piracicaba, 2023.

164 p.

Tese (Doutorado – Programa de Pós-Graduação em Ciências. Área de Concentração: Química na Agricultura e no Ambiente) – Centro de Energia Nuclear na Agricultura, Universidade de São Paulo, 2023.

1. Bioindicadores 2. Ecotoxicologia 3. Nanopartículas 4. Nanotecnologia 5. Nematóides 6. Proteínas 7. Toxicologia ambiental I. Título

CDU 504.5 + 661.97

Elaborada por:
Marilia Ribeiro Garcia Henyei
CRB-8/3631
Resolução CFB Nº 184 de 29 de setembro de 2017

ACKNOWLEDGEMENTS

I am beyond appreciative of all the advice, encouragement, and support I have received during the development of my thesis. I´m extremely grateful to my advisor, Diego Martinez, for his support, ambition, focus on quality, and orientation to results that helped me to progress in my research and personal life.

I have also been fortunate to have a second mentor, Cassio H. Abreu-Junior. I am grateful for receiving me in his laboratory and for his insights and dedication to our analysis. I also thank the support of his analysts, Inês and Everaldo, besides my lab colleagues, Thays and Paulo.

My special gratitude to Mathias, Fabricio, and Manu, who moulded me into the scientist I am today. Mathias, his insights and advice have been a contributor to my growth as a researcher.

I´m grateful for the best training in *C. elegans* I received from Profa. Daiana Avila and Fabricio Delite.

I acknowledge Prof. Iseult Lynch, who received and supported me at the University of Birmingham. I also thank the staff (Chris and Nick) and my lab (Hassan, Hayat, Lisi, Thanawan, Lucia, and Roberta) and office friends (Yongjian Li and Hector) for our funny moments.

My honest gratitude to the Academic league of *C. elegans* (LAECE) in which I had the pleasure of learning more about *C. elegans* and making friends; Likewise, I appreciate the opportunity to join the Nanolegal group promoted by Prof. Ivandick and Mackenzie University and our endless and valuable discussions about the Regulatory aspects of Nanotechnology.

I also must thank my previous lab mates: Lais, Josias, Lidiane, Leandro, Luelc, Luciana, Marcia, Luelc, and Rubens; and my current ones: Aline, Romana, Nathalia, Gabriela, Milena and Cecilia; you are brilliant!

I´m very grateful to the CNPEM analysts who supported me during my analyses: Carol (LNNano), Carlos Costa (LNNano), Cleiton (LNNano), Joice (LNBR), Otavio (LNNano), Bruna (LNNano), Sami (LNBio) and Letícia (LNBR).

I must thank my dear parents, Irineu and Silvana, for their patience, support, and true love. And to my boyfriend Luiz for all the support, true love, and patience with my absence throughout these years of this study. I would acknowledge the support and great love of my friends.

I also acknowledge CENA – USP and LNNano – CNPEM infrastructure, as well as the support of respective amazing staff: Cleide, Marcos and Magali (CENA) and Janaína (LNNano).

I acknowledge the funding sources during these years: CAPES (Coordenação de Aperfeiçoamento Pessoal de Nível Superior) – Finance Code 001, FAPESP-UoB Research Grant (Project. No. 19/07058-0), Brazil-China Center for Research and Innovation on Nanotechnology (CNPq/MCTI) and the National Institute of Functional Complex Materials (INCT-INOMAT).

ABSTRACT

CÔA, F. **Toxicity of carbon nanomaterials in *Caenorhabditis elegans***: Effects of biocorona formation on single and co-exposure testing. 2023. 164 p. Tese (Doutorado em Ciências) - Centro de Energia Nuclear na Agricultura, Universidade de São Paulo, Piracicaba, 2023.

This thesis aimed to evaluate the effects of biocorona formation on carbon nanomaterials (i.e., graphene oxide - GO and multiwalled carbon nanotubes - MWCNT) toxicity in the nematode *Caenorhabditis elegans* model. In the first chapter, a literature review introduced this organism as a valuable model for nanotoxicity research; focusing on carbon nanomaterials toxicity, nanobiointerfaces, and discussing experimental gaps towards harmonization of protocols and best laboratory practices. In the second chapter, bovine serum albumin was exploited as a protein model to investigate the implications of biocorona formation on the toxicity of GO and MWCNT. This study demonstrated that both materials were toxic to nematode survival, growth, reproduction, and fertility, as well as enhanced oxidative stress and permeability of intestinal barrier. They crossed the nematode intestine reaching its secondary organs, but albumin corona hindered the MWCNT translocation, while coated GO was translocated affecting the functionality of crucial organs. As consequence, the effects of GO were 50% attenuated by protein coating, while damages of MWCNT were 100% mitigated. In the third chapter, the combined toxicity of GO and silver nitrate (Ag^{+}) in co-exposure testing was analysed, and the concept of *E. coli* corona formation was addressed for the first time in the literature. Results suggest that GO increased the lethality of Ag^{+} 2.1 times, but it was aggravated 4.6 times when GO was coated by *E. coli* corona. Bare and coated GO were translocated to secondary organs of *C. elegans*, where they promoted the enhancement of apoptotic corpses in germline and potential injuries to neurons. Therefore, these results suggest that assessing the implications of *E. coli* corona formation to nanomaterials toxicity must be a priority in the assays with *C. elegans*. Finally, this thesis provides a fundamental understanding of biocorona role and reinforces the importance of considering its influence on nanomaterials toxicity towards a safer applications of carbon nanomaterials.

Keywords: Nanotoxicology. Protein corona. Combined toxicity. Nanosafety.

RESUMO

CÔA, F. **Toxicidade de nanomateriais de carbono no *Caenorhabditis elegans***: efeitos da formação da biocorona em ensaios de exposição simples e combinada. 2023. 164 p. Tese (Doutorado em Ciências) - Centro de Energia Nuclear na Agricultura, Universidade de São Paulo, Piracicaba, 2023.

Esta tese teve por objetivo avaliar o efeito da formação da biocorona sobre a toxicidade de nanomateriais de carbono (i.e., óxido de grafeno – GO e nanotubos de carbono de paredes múltiplas - MWCNT) no nematoide modelo *Caenorhabditis elegans*. No primeiro capítulo, uma revisão de literatura introduz este organismo como um modelo valioso para estudos de nanotoxicidade; focando na toxicidade de nanomateriais de carbono, nas interfaces nanobiológicas, além de discutir os desafios experimentais na direção da harmonização de protocolos e boas práticas laboratoriais. No segundo capítulo, a albumina sérica bovina foi explorada como proteína modelo para investigar a influência da biocorona sobre a toxicidade do GO e MWCNT. Neste estudo, foi demonstrado que ambos os materiais foram tóxicos à sobrevivência, crescimento, reprodução e fertilidade dos nematoides, assim como aumentaram a produção de estresse oxidativo e a permeabilidade da barreira intestinal. Ambos atravessaram o intestino do nematoide, alcançando seus órgãos secundários; no entanto, a corona de albumina impediu a translocação do MWCNT. Por outro lado, o GO revestido foi translocado afetando a funcionalidade dos órgãos cruciais do *C. elegans*. Como consequência, os efeitos tóxicos do GO foram atenuados em 50% pela corona de proteínas, enquanto os do MWCNT foram 100% mitigados. No terceiro capítulo, a toxicidade combinada do GO com nitrato de prata (Ag^{+}) foi investigada, e a formação da corona de *Escherichia coli* sobre a superfície do GO foi abordado pela primeira vez na literatura. Os resultados sugerem que o GO aumentou a letalidade da prata em 2,1 vezes, mas esta foi agravada 4,6 vezes pelo GO revestido. O GO coronado e não coronado foram translocados para os órgãos secundários do *C. elegans*, onde promoveram aumento dos danos apoptóticos na linhagem germinativa e potenciais danos neuronais. Portanto, esses resultados sugerem que avaliar as implicações da formação da corona de *E. coli* para a toxicidade dos nanomaterials deve ser prioritária em ensaios com o *C. elegans*. Por fim, esta tese fornece um embasamento fundamental para entender o papel da biocorona sobre a toxicidade dos nanomateriais de carbono e reforça a importância de considerar a influencia da mesma sobre a toxicidade destes materiais na direção de uma aplicação segura e responsável.

Palavras-chave: Nanotoxicologia. Corona de proteínas. Toxicidade combinada. Nanossegurança.

SUMMARY

1. INTRODUCTION 11

1.1. Biocorona effect on nanomaterials toxicity and interface with pre-existing contaminants 13

1.2. *Caenorhabditis elegans* as a model organism 15

1.3. Motivation 18

1.4. Outline of this thesis 19

References 20

2. CHAPTER 2. *Caenorhabditis elegans*: CURRENT STATUS AND PERSPECTIVES ON CARBON NANOTOXICITY RESEARCH 27

2.1. Introduction 28

2.2. *Caenorhabditis elegans*: an alternative model to animal experimentation and nanotoxicity assessment 29

2.3. Scientific and methodological challenges in assays with *Caenorhabditis elegans* and nanomaterials 32

2.4. Toxicity of carbon nanomaterials on *Caenorhabditis elegans:* the state-of-the-art 35

2.5. Tools for evaluating nanomaterials internalization and biodistribution in *Caenorhabditis elegans* 45

2.6. Conclusion and perspectives 51

References 52

3. CHAPTER 3. TOXICITY MITIGATION AND BIODISTRIBUTION OF ALBUMIN CORONA COATED GRAPHENE OXIDE AND CARBON NANOTUBES IN *Caenorhabditis elegans* 65

3.1. Introduction 67

3.2. Material and methods 69

3.2.1. Preparation and characterization of GO and MWCNT stock dispersions 70

3.2.2. Albumin corona formation on GO and MWCNT 71

3.2.3. Physico-chemical characterization of nanomaterials 71

3.2.4. Biological assays with *Caenorhabditis elegans* 72

3.2.4.1. Preparation of sub-stocks of bare and coated materials for toxicity assays 72

3.2.4.2. Characterization of colloidal stability 73

3.2.4.3. *Caenorhabditis elegans* maintenance and strain preparation for toxicity assays 74

3.2.4.4. Acute assays 74

3.2.4.5. Oxidative stress measurement 75

3.2.4.6. Nile red staining 75

3.2.4.7. Long-term assay 76

3.2.5. Raman spectroscopy imaging for biodistribution studies 77

3.2.6. Data analysis 78

3.3. Results and Discussion 78
3.3.1. Physico-chemical properties of nanomaterials 78
3.3.2. Dispersion stability of materials in ultrapure water and EPA medium 81
3.3.3. Influence of albumin corona on toxicity and internalization of materials in *Caenorhabditis elegans* 84
3.4. Conclusions 95
References 96
4. CHAPTER 4. INFLUENCE OF *Escherichia coli* CORONA FORMATION ON COMBINED TOXICITY OF GRAPHENE OXIDE WITH SILVER IONS IN *Caenorhabditis elegans* 105
4.1. Introduction 106
4.2. Material and methods 108
4.2.1. Materials 108
4.2.2. *Escherichia coli* lysis and biocorona formation 108
4.2.3. Characterization of graphene oxide with and without corona 109
4.2.4. Adsorption experiments 109
4.2.5. Biological experiments 110
4.2.5.1. Dispersion characterization and colloidal stability studies 110
4.2.5.2. *Caenorhabditis elegans* culturing and synchronization 111
4.2.5.3. Preparation of sub-stocks for toxicity assays 111
4.2.5.4. Lethality assays 111
4.2.5.5. Biodistribution studies by Raman confocal spectroscopy 112
4.2.5.6. Silver internalization by nematodes 112
4.2.5.7. Neuronal effects assessment 113
4.2.5.8. Germline cell apoptosis evaluation 114
4.2.6. Data analysis and statistics 114
4.3. Results and discussion 114
4.3.1. Characterization of *Escherichia coli* corona formation 114
4.3.2. *Escherichia coli* corona influence on GO colloidal behaviour, internalization, and toxicity 118
4.3.3. Influence of GO and *Escherichia coli* corona on silver toxicity 124
4.3.4. Influence of GO and *Escherichia coli* corona on silver bioaccumulation 128
4.4. Conclusions 131
5. CHAPTER 5. GENERAL CONCLUSIONS AND FUTURE OUTLOOK 143
APPENDIX 147
Appendix A. Supplementary Information of Chapter 3 149
Appendix B. Supplementary Information of Chapter 4 157
Appendix C. Scientific publications 163

1. INTRODUCTION

Nanotechnology, as a fundamental enabling technology, touches on every modern life since nanomaterials (NMs) are transformative for multiple purposes, from biomedical (diagnostics, therapeutics, and protection), energy, composites, electronics, and agri-environmental technologies, to consumer products and packaging (Egwu et al., 2022; Intisar et al., 2022; Kuhn et al., 2022). Nanomaterials are natural, incidental, or engineered materials consisting of solid particles, present on their own or bound as constituent parts of aggregates or agglomerates, and in which 50% or more in the number-based size distribution fulfil at least one of these conditions: a) one external dimension is in size range from 1 to 100 nm; b) the particle has an elongated shape, such as tubes, where two dimensions are smaller than 1 nm and, the other is larger than 100 nm; c) the particle has a plate-like, which external dimension is smaller than 1 nm and the other dimension larger than 100 nm (European Commission, 2022).

Carbon nanotubes (CNTs) and graphene oxide (GO) comprise the class of carbon nanomaterials that has received great attention from the global market. GO is a two-dimensional carbon structure with a one-atom thickness. It is chemically produced from graphite oxidation and composed of sp^2 and sp^3 hybridized carbon atoms. These sp^3 atoms are bonded to oxygen functional groups, such as hydroxyl, epoxy, and carboxyl (Becerril et al., 2008). CNTs are one-dimensional cylindrical structures formed by one (i.e., single-walled CNT) or more rolled graphene sheets (i.e., multi-walled CNT) (Iijima, 1991). They are key players exploited as adsorbents for removing environmental pollutants from water, biosensors, and drug delivery (Ray, 2015).

In 2015, 120 t of graphene-based materials were produced, and the global market value of graphene-based products is expected to reach $1.3 billion in 2023 (Ahmed; Rodrigues, 2013). It is worth mentioning the main Brazilian initiatives toward expanding the production and application of graphene and carbon nanotubes. The construction of the CTNano at the Federal University of Minas Gerais, where a pilot plant was installed in 2011 to produce carbon nanotubes on a large scale; The creation of Gerdau Graphene, a company to transform graphene into new solutions for the market; And the recent governmental call to support the development of new technologies with graphene. Therefore, the national market has been opened to the great opportunities that carbon nanomaterials represent. Brazil would become one of the most graphene manufacturers in the world since it has one of the largest graphite deposits together with China and Canada (Brasil, 2020).

If on the one hand, carbon nanomaterials represent a massive business, on the other hand, their risks to the environment and human health also require attention (Schwirn et al., 2020). Over the last three decades, it has been demonstrated that their properties, behaviour, and fate differ considerably from conventional materials (i.e., at bulk scale) or soluble substances (Klaessig et al., 2015). Thus, specific recommendations should be taken during their production, application, and disposal (Bundschuh et al., 2018). Even toxicity tests with carbon nanomaterials have specificities that have been discussed and the protocols adapted (Petersen et al., 2014). Laws and regulations must be revisited and developed to accurately classify these materials regarding potential human health and environmental risks (Godwin et al., 2015).

In vitro, in vivo, and in silico models have been applied to provide pivotal insights into our understanding of nanomaterial-mediated toxicity mechanisms. The ethical ambition to conduct experiments without using animals has resulted in intense efforts over the past few decades from industry, academia, and regulatory bodies to develop new methodologies. The expansion of new in vitro approaches (e.g., 3D cells culture, organs-on-chips, and organoids), together with the establishment of alternative model organisms, play a crucial role in substituting rodents for human health protection and explaining the fate and dynamic of NMs in the ecosystem (Pimtong et al., 2021).

Caenorhabditis elegans is one of the biological models that can be exploited to study the biological effects of NMs, considering a One-Health perspective towards protecting animal, human and environmental health (Gao, 2021). Indeed, its characteristics permit addressing indirect effects beyond simple toxicological effects, such as neurotoxicology and molecular pathways of neurodegeneration (Von Mikecz, 2022).

The great majority of studies published so far tend to focus on assessing carbon nanomaterials' behaviour, fate and toxicity in their pristine state. With the growth in volume production and application, carbon nanomaterials would unintentionally enter the natural environment (i.e., air, aquatic environments and soil) over the different stages of their life cycle (i.e., production, use and disposal) (Ding et al., 2022). In this system, NMs will be subject to a series of physical, chemical and biological transformations, besides interacting with organisms at different levels of the food chain, including humans (Ding et al., 2022). Therefore, to fully understand the potential risks of these materials to human and environmental health, it is crucial to identify how these transformations will impact on their toxicological response instead of just evaluating the effects of NMs' pristine counterparts (Lowry et al., 2012). Biocorona formation is one of these phenomena that alter the fate and behaviour of NMs; therefore, understanding this aspect is of fundamental relevance for nanotoxicology.

1.1. Biocorona effect on nanomaterials toxicity and interface with pre-existing contaminants

In the environment or in contact with biological fluids or organisms, NMs tend to undergo a series of physical, chemical and biological transformations, such as degradation, aggregation, redox reaction and dissolution (Figure 1A) (Ding et al., 2022). NMs will also never be alone; The natural environmental matrix is a complex mixture of natural organic matter, proteins, polysaccharides, extracellular polymeric substances or metabolites from cellular activity. These components contain a broad range of functional groups with a strong binding ability for the reactive surface of NMs. Likewise, when NMs enter in systemic circulation in the human body, they will be exposed to several biological components such as blood, cells and plasma protein (Palmieri et al., 2019). Therefore, in both environments, NMs will interface with these several biomolecules that will be spontaneously adsorbed by the highly reactive NMs' surfaces (Lundqvist et al., 2008). Their surface soon becomes covered with a layer of biomolecules, forming a coating, designated biocorona from a biomedical perspective, or environmental corona/eco-corona in an ecological context (Figure 1B).

Figure 1. Overview of the potential transformations that NMs are subject to undergo in the environment, including the protein corona effect (A). Overview of the nanomaterial surface after interacting with proteins (protein corona), natural organic matter and humic acids (environmental corona), or portions of environmental corona together with proteins, exopolymeric substances and metabolites from multiple organisms (B).

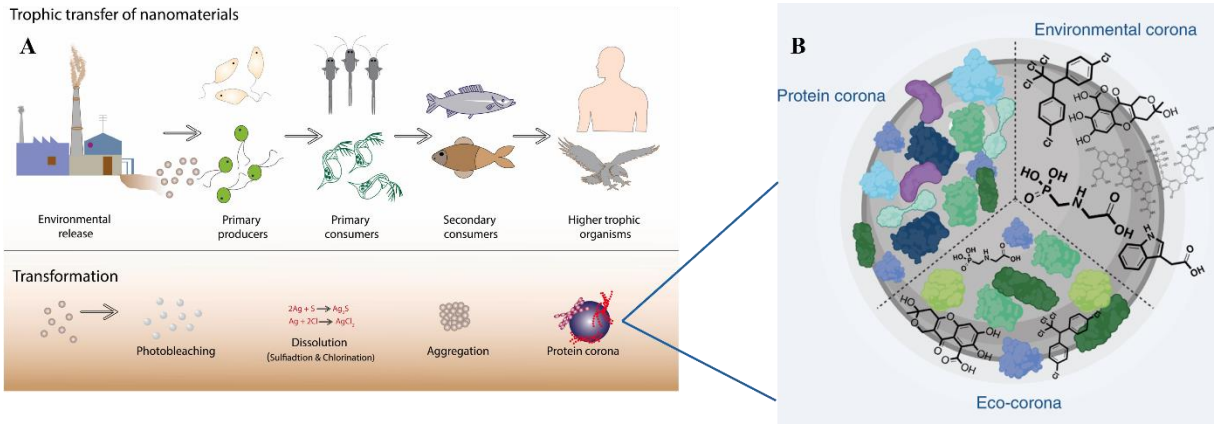

Adapted from Vineeth Kumar et al. (2022) and Wheeler et al. (2021).

Biocorona formation is a highly complex phenomenon dependent on a) intrinsic NMs properties (e.g., surface charge, size, shape, topography), b) biofluid characteristics (i.e., chemical composition) and c) ambient medium conditions (e.g., pH, temperature, light and ionic strength) (Foroozandeh; Aziz, 2015). The kinetics of biocorona adsorption is a dynamic process in which biomolecules are continuously adsorbed and desorb from NMs surfaces

(Wheeler et al., 2021). Some tools can be utilised to characterize the biocorona composition and nature, such as transmission electron microscopy (TEM) and cryomicroscopy (cryo-TEM), sodium dodecyl sulphate-polyacrylamide gel electrophoresis (SDS-PAGE), liquid-chromatography-mass spectrometry (LC-MS/MS), isothermal titration calorimetry (ITC) and Fourier transform infrared spectroscopy (FTIR) (Capriotti et al., 2014).

Studies exploring the biocorona implications on nanotoxicity have steadily grown over the past decade (Natarajan et al., 2021). The biocorona formation has been found to confers a new biological identity to the NMs, because alters nanoparticle characteristics properties, functionality, behaviour, biodistribuion and toxicity (Xu et al., 2020; Monopoli et al., 2012). There is no doubt that biocorona governs the in vivo fate and biological effects of NMs, such as translocation, distribution, metabolism, and immune response (Bhattacharya et al., 2016; Monopoli et al., 2012). However, our knowledge about this topic is still in its infancy.

In most cases, coronas were reported to alleviate the bioavailability and biological effects of NMs because it increases or decreases their colloidal stability in biological media. In other instances, the enhancing colloidal stability promoted by biocorona extends the NMs' toxicity because it facilitates their mobility and exposure of organisms to NMs (Markiewicz et al., 2018; Xu et al., 2020). Ultimately, biocorona formation can cause unknown ecological risks, which may impact human health through food chain transport (Wheeler et al., 2021).

It is also becoming evident that biocorona could change the fate and behaviour of pre-existing environmental pollutants or their interaction with each other, resulting in complex additive, synergic, and antagonist toxicity effects (Martinez et al., 2022; Zhang; Goss, 2021). Indeed, NMs, by themselves, may interact with these co-contaminants leading to an increased transport into the organism (known as the “trojan horse effect”) and elevated toxicity (Batista de Melo et al., 2019; Medeiros et al., 2020); On the other hand, NMs may decrease the free concentration of these pollutants and mobility through strong adsorption altering their colloidal behaviour and fate in the environment and, subsequently, toxicity (Liu et al., 2018; Naasz et al., 2018).

Hence, biocorona formation could add even more complexity to these interactions between NMs and pollutants. It has been discussed that a pollutant with a high binding affinity to NMs surface could displace macromolecules in the corona with weak affinity. In contrast, these molecules could act as binding sites for pollutants without being replaced (Reilly et al., 2022). These variabilities in the chemical interaction between corona-coated NMs and a pollutant display a key role in toxicity because they change the uptake efficiency of a pollutant by an organism and the exposure pathways. Hence, understanding the biocorona effect is crucial

to better interpret and assess the biological impacts of NMs and the modulation of the adverse effects of pre-existing pollutants in the environment.

1.2. *Caenorhabditis elegans* as a model organism

C. elegans is a free-living nematode of the *Rhabditidae* family. It was isolated from rich nutrient soil and described for the first time by Maupas (Maupas, 1900). But only in 1965, it was established as a model to study animal development and behaviour by Sydney Brenner (Brenner, 1974).

C. elegans was the first organism sequenced at the multicellular level (The *C. elegans* Sequencing Consortium, 1998). Nowadays, its utility has been expanded to diverse areas of modern biology (Koopman et al., 2016; Nguyen et al., 2016; Van Assche et al., 2015). Several regions of *C elegans* genes are similar to human genes, as well it exhibits high conservative levels compared to other vertebrates in terms of gene functions and metabolic pathways (Hastings et al., 2019). Due to these characteristics, *C elegans* has been applied to study the pathogenicity of several organisms in humans (e.g., viruses, bacteria) (Ewbank and Zugasti, 2011), as sensors for human and canine cancer (Namgong et al., 2022), for discovering new treatments for parasitic nematodes in agriculture (Schleker et al., 2022) or vaccines development (Roberts et al., 2013).

C. elegans is a platform for nanomaterials toxicity studies since it is a multicellular organism highly sensitive to environmental pollutants (Li et al., 2022). In addition, it is globally distributed, including in parts of America, Africa, Europa and the United States (Frézal and Félix, 2015). Most human neurotransmitter systems are present in this nematode, such as acetylcholine (ACh), glutamate, γ-aminobutyric acid (GABA), serotonin and dopamine, making *C elegans* an interesting animal to study neurotoxicology. In transgenic strains, specific genes are modified to express fluorescent proteins (e.g., green fluorescence protein, GFP) in an oxidative stress scenario, for example, and can be easily analysed by fluorescence microscopy due to the transparent body of *C. elegans* (Fajardo et al., 2022). On the other hand, the lack of a respiratory and circulatory system impedes the elucidation of the potential toxicity of pollutants and investigation of all human diseases (Gonzalez-Moragas et al., 2015a). Moreover, nematodes have no blood-brain barrier; thus, pollutants directly interact with their nervous system (Hunt, 2017).

C. elegans has a complete and well-described digestive, nervous and reproductive system protected by a collagenous cuticle (Figure 2). Besides protecting the body by blocking

the entry of some molecules from the environment, the cuticle is responsible for nematode locomotion and maintaining body morphology and integrity (Gonzalez-Moragas et al., 2015a).

The nervous system of *C. elegans* controls all the essential functions such as feeding, development, movement, metabolism and reproduction (Altun; Hall, 2005). It is formed by a nerve ring, a ventral and a dorsal nerve cord, and a complex head sensory system (Figure 2).

C. elegans was the first eukaryote in which neuronal cells were identified and characterized (Hall et al., 2005). Hermaphrodite nematodes have 302 nerve cells, which are identified by a name with two or three letters, or sometimes, by one number followed by one letter that specifies its anatomy position, such as L (left), R (right), D (dorsal) and V(ventral). The nerve ring in the head contains almost all the interneurons interconnected with axons from most sensory neurons; therefore, it is the brain of worms where most nematode sensory neurons are located. Ventral and dorsal nerves extend from the nerve ring until the end of the tail. The dorsal nerve contains a variety of motor neurons, and the ventral cord has several sensory motors and interneurons. Sensory receptors are concentrated in the head and sensitive to temperature variations, mechanical stimuli, chemical attractants, and repellents (Takeishi et al., 2020). 40 classes of *C. elegans* neurons are sensory, while 30 are motor neurons. Each neuron is invariantly positioned; therefore, it is easily recognised in vivo. In addition, all families of genes responsible for neuron function in mammals are present in *C. elegans.* A complete diagram of the chemical and electrical connections present in *C. elegans* neurons is available (Hall et al., 2005). In addition, connectomes that encompass the *C. elegans* body were recently entirely characterized (Cook et al., 2019).

The alimentary system of *C. elegans* (Figure 2) comprises the mouth, pharynx, intestine, rectum, and anus. It is is involved in adsorption, metabolism, storage and distribution of nutrients, which can be exploited to mimic the human intestinal system. Its pharynx presents 20 muscle cells, 20 nerve cells and 18 epithelial cells. In this region, a coordinated muscular contraction permits the bacteria ingestion that is crushed in the grinder in the terminal bulb and transferred to the intestine through the pharyngeal-intestinal valve. While its excretory system is responsible for osmoregulation and residue elimination (Hope, 1999). The digestion of bacteria in *C. elegans* intestine is rapid; bacteria stay inside the gut only for fewer than 2 min, but all the bacteria are digested over this 2 min. 47% of the total intestinal volume (i.e., waste material) is discarded through the anus every 50 seconds (Avery; You, 2012).

Figure 2 – Overview of *Caenorhabditis elegans* adult hermaphrodite anatomy.

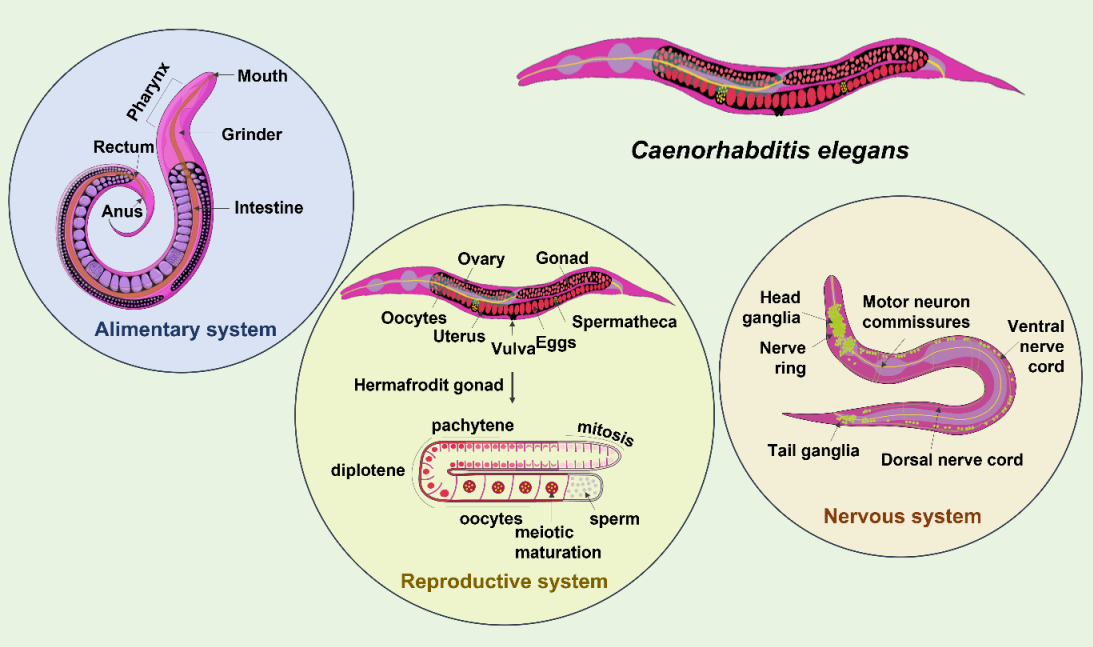

In the *C. elegans* germline (Figure 2), a common uterus connects two U-shaped gonad symmetric tubes, where stem cells are in mitotic proliferation at their distal ends. During this process, these cells move to the proximal region and stop dividing, initiating meiosis, where they are subject to undergo apoptosis. 50% of germ cells can suffer physiological apoptosis (Gumienny et al., 1999). However, stress-induced apoptosis can also occur in the loop of gonad when nematodes are exposed to DNA-damaging agents (Pazdernik; Schedl, 2013). In this sense, transgenic strains (e.g., MD701 strain in which CED-1::GFP fluorescence protein is expressed around the apoptotic germline cells) or the acridine orange dye can be useful for evaluating the mechanisms that trigger apoptosis during oogenesis.

In laboratories, *C. elegans* has been cultivated on Petri dishes with a lawn of bacteria, generally *Escherichia coli*. *C. elegans* is highly sensitive to a reference substance (Benzyldimethylhexadecylammonium, BAC-C16) that is useful for verifying the quality of *C. elegans* cultivating before the toxicity assays. This nematode can be exposed to several environmental conditions with or without a food source (bacteria) and in liquid or solid media with different ionic strengths. Lethal and sublethal endpoints can be assessed in toxicity studies, such as lethality, reproduction, lifespan, behaviour, growth, intestinal damage and gene expression. Its translucent body permits evaluating the uptake, translocation and excretion of pollutants in vivo.

1.3. Motivation

Carbon nanomaterials are a class of nanomaterials incorporated into new technologies and explored in biosensors, targeted therapies, energy generation and storage. However, the increasing use of nano-based products has raised concern about their release in the environment and potential risks to organisms and human health. To solve these issues, it is crucial to understand whether the carbon nanomaterials toxicity will be modified by the transformations that these materials will undergo in the environment or human body.

Nanomaterials will never be alone in the environment. It is estimated by the European Environment Agency the occurrence of more than 100 000 chemicals in the market. Co-exposure scenarios between pre-existing pollutants are expected to occur in the environment considering the complexity of this system. Consequently, it is critical to evaluate whether and how nanomaterials will modulate the toxicity of these pollutants to predict a more realistic environmental impact.

Biocorona formation is a phenomenon that spontaneously occurs when nanomaterials interface with biomolecules presents in environmental systems or biological fluids. The nano-bio-interface formed by this interaction results in this coating named biocorona, which governs the nanomaterials behaviour and fate, besides mediating their interactions with cells, tissues and organisms. Although several studies and regulatory agencies have confirmed the importance of evaluating the biocorona effect to predict the nanomaterials toxicity accurately, most of these researches were performed just considering the toxicity exerted by their pristine counterparts. Therefore, biocorona effect on nanomaterials toxicity remains to be better explained.

Despite *C. elegans* has been successfully exploited in nanotoxicity studies (Gonzalez-Moragas et al., 2015a), several factors influence the exposure of *C. elegans* to nanomaterials. One of them is related to the fact that NMs can be ingested with bacteria, and the biomolecules released from bacteria lysis can be absorbed on NMs' surface. As previously mentioned, this adsorption results in the biocorona effect (herein called *E. coli* corona formation) that changes the NMs' physicochemical properties, behaviour and toxicity. This relevant aspect, therefore, can not be overlooked by the *C. elegans* research community because it can lead to misinterpretations about NMs toxicity considering environmentally relevant exposure scenarios. Nevertheless, to the best of our knowledge, it was not studied before. Taking into account this, the toxicological implications of the biocorona effect from *E. coli* lysis was also

the focus of this thesis towards supporting further studies and the development of standardized protocols.

As demonstrated, there is a long way to go to fully understand the implications of biocorona formation in complex environmental scenarios. The interaction of biocorona-coated materials with pre-existing pollutants is poorly understood until this date. In addition, the possibility of a biocorona being formed in nanotoxicity studies with *C. elegans* or into the environment after NMs be uptake by *C. elegans* was not assumed before. Hence, in this thesis, two experimental articles were carried out to investigate these opening questions. First, the biocorona effect on carbon nanomaterials toxicity was investigated by using a protein model (bovine serum albumin). Then, the second paper focused on the specific biocorona formed by the interaction of graphene oxide with biomolecules collected from *E. coli* lysis and its implications for the toxicity outcomes, in single and co-exposure scenarios with a metal pollutant. Hence, this thesis aimed to study the effects of biocorona on the toxicity of carbon nanomaterials in the *C. elegans* model, considering both single and co-exposure testing.

1.4. Outline of this thesis

This thesis studied the toxicity of carbon nanomaterials in the *C. elegans* model with a particular focus on biocorona effects and co-exposure scenarios. These studies are presented as the following structure:

Chapter 1 contextualizes the main topic of the thesis and introduces the research gaps.

Chapter 2 is a literature review of the application of *C. elegans* model to study the toxicity of carbon nanomaterials, as well as the useful techniques for this evaluation and experimental challenges involved in these assays.

Chapter 3 contains a detailed study of the impact of albumin corona formation on the toxicity of graphene oxide and carbon nanotubes on *C. elegans*.

Chapter 4 includes a comprehensive study of the influence of biocorona formation from *E. coli* lysis on graphene oxide toxicity to *C. elegans*, and its toxicological implications to graphene oxide interaction with a model metal/pollutant (silver) on *C. elegans*.

Chapter 5 summarizes the main findings in this thesis and shows future perspectives to highlight topics of a future interest that remain to be investigated.

Supplementary materials for each chapter are available in the Appendix section.

Scientific publications include a list of publications resulting from this thesis and collaborations.

References[1]

Ahmed, F., Rodrigues, D.F., 2013. Investigation of acute effects of graphene oxide on wastewater microbial community: A case study. J Hazard Mater 256–257, 33–39. https://doi.org/10.1016/j.jhazmat.2013.03.064

Altun, Z.F., Hall, D.H., 2005. WormAtlas Hermaphrodite Handbook - Nervous System - General Description. WormAtlas. https://doi.org/10.3908/wormatlas.1.18

Avery, L., You, Y.J., 2012. C. elegans feeding, in: Erik M. Jorgensen (Ed.), The C. Elegans Research Community, WormBook. p. 23. https://doi.org/10.1895/wormbook.1.150.1

Batista de Melo, C., Côa, F., Alves, O.L., Martinez, D.S.T., Barbieri, E., 2019. Co-exposure of graphene oxide with trace elements: Effects on acute ecotoxicity and routine metabolism in Palaemon pandaliformis (shrimp). Chemosphere 223. https://doi.org/10.1016/j.chemosphere.2019.02.017

Becerril, H.A., Mao, J., Liu, Z., Stoltenberg, R.M., Bao, Z., Chen, Y., 2008. Evaluation of Solution-Processed Reduced Graphene Oxide Films as Transparent Conductors. ACS Nano 2, 463–470. https://doi.org/10.1021/cm060258+

Bhattacharya, K., Mukherjee, S. P., Gallud, A., Burkert, S. C., Bistarelli, S., Bellucci, S., Bottini, M., Star, A., & Fadeel, B., 2016. Biological interactions of carbon-based nanomaterials: From coronation to degradation. Nanomedicine: Nanotechnology, Biology, and Medicine, 12, 333–351. https://doi.org/10.1016/j.nano.2015.11.011

Brasil. Ministério de Minas e Energia, 2020. Projeto avaliação do potencial da grafita no Brasil - Fase 1. Brasília, DF. (Série Minerais Estratégicos, 5).

Brenner, S., 1974. The genetic of Caenorhabditis elegans. Genetics 77, 71–94. https://doi.org/10.1093/genetics/77.1.71

Bundschuh, M., Filser, J., Lüderwald, S., McKee, M.S., Metreveli, G., Schaumann, G.E., Schulz, R., Wagner, S., 2018. Nanoparticles in the environment: where do we come from, where do we go to? Environ Sci Eur 30. https://doi.org/10.1186/s12302-018-0132-6

Capriotti, A.L., Caracciolo, G., Cavaliere, C., Colapicchioni, V., Piovesana, S., Pozzi, D., Laganà, A., 2014. Analytical Methods for Characterizing the Nanoparticle–Protein Corona. Chromatographia 77, 755–769. https://doi.org/10.1007/s10337-014-2677-x

[1] Prepared according to Elsevier guide.

Côa, F., Delite, F. de S., Strauss, M., Martinez, D.S.T., 2022. Toxicity mitigation and biodistribution of albumin corona coated graphene oxide and carbon nanotubes in Caenorhabditis elegans. NanoImpact 27, 100413. https://doi.org/10.1016/j.impact.2022.100413

Cook, S.J., Jarrell, T.A., Brittin, C.A. et al., 2019. Whole-animal connectomes of both Caenorhabditis elegans sexes. Nature 571, 63–71. https://doi.org/10.1038/s41586-019-1352-7

Ding, X., Pu, Y., Tang, M., & Zhang, T., 2022. Environmental and health effects of graphene-family nanomaterials: Potential release pathways, transformation, environmental fate and health risks. Nano Today, 42, 101379. https://doi.org/10.1016/j.nantod.2022.101379

Egwu, C.N., Babalola, R., Udoh, T.H., Esio, O.O., 2022. Nanotechnology: Applications, Challenges, and Prospects. pp. 3–15. https://doi.org/10.1007/978-3-030-95820-6_1

European Comission, 2022. Commission Recommendation 2011/696/EU.

Ewbank, J.J., Zugasti, O., 2011. *C. elegans*: model host and tool for antimicrobial drug discovery. Dis Model Mech 4, 300–304. https://doi.org/10.1242/dmm.006684

Fajardo, C., Martín, C., Garrido, E., Sánchez-Fortún, S., Nande, M., Martín, M., Costa, G., 2022. Copper and Chromium toxicity is mediated by oxidative stress in Caenorhabditis elegans: The use of nanoparticles as an immobilization strategy. Environ Toxicol Pharmacol 92, 103846. https://doi.org/10.1016/j.etap.2022.103846

Foroozandeh, P., & Aziz, A. A., 2015. Merging Worlds of Nanomaterials and Biological Environment: Factors Governing Protein Corona Formation on Nanoparticles and Its Biological Consequences. Nanoscale Research Letters, 10(1), 221. https://doi.org/10.1186/s11671-015-0922-3

Frézal, L., Félix, M.-A., 2015. C. elegans outside the Petri dish. Elife 4. https://doi.org/10.7554/eLife.05849

Gao, P., 2021. The Exposome in the Era of One Health. Environmental Science & Technology, 55(5), 2790–2799. https://doi.org/10.1021/acs.est.0c07033

Godwin, H., Nameth, C., Avery, D., Bergeson, L.L., Bernard, D., Beryt, E., Boyes, W., Brown, S., Clippinger, A.J., Cohen, Y., Doa, M., Hendren, C.O., Holden, P., Houck, K., Kane, A.B., Klaessig, F., Kodas, T.; Landsiedel, R.; Lynch, I., Malloy, T., Miller, M.B., Muller, J., Oberdorster, G., Petersen, E. J., Pleus, R.C., Sayre, P., Stone, V., Sullivan, K.M., Tentschert, J., Wallis, P., Nel, A.E., 2015. Nanomaterial categorization for assessing risk potencial to facilitate regulatory decision-making. ACS Nano, 9(4), 3409-3417. https://doi.org/10.1021/acsnano.5b00941

Gonzalez-Moragas, L., Roig, A., Laromaine, A., 2015a. C. elegans as a tool for in vivo nanoparticle assessment. Adv Colloid Interface Sci 219, 10–26. https://doi.org/10.1016/j.cis.2015.02.001

Gonzalez-Moragas, Laura, Yu, S.-M., Carenza, E., Laromaine, A., Roig, A., 2015b. Protective Effects of Bovine Serum Albumin on Superparamagnetic Iron Oxide Nanoparticles Evaluated in the Nematode Caenorhabditis elegans. ACS Biomater Sci Eng 1, 1129–1138. https://doi.org/10.1021/acsbiomaterials.5b00253

Gumienny, T.L., Lambie, E., Hartwieg, E., Horvitz, H.R., Hengartner, M.O., 1999. Genetic control of programmed cell death in the Caenorhabditis elegans hermaphrodite germline. Development 126, 1011–1022. https://doi.org/10.1242/dev.126.5.1011

Hall, D.H., Lints, R., Altun, Z., 2005a. Nematode Neurons: Anatomy and Anatomical Methods in Caenorhabditis elegans. Int. Rev. Neuro 69, 1-35. https://doi.org/10.1016/S0074-7742(05)69001-0

Hastings, J., Mains, A., Virk, B., Rodriguez, N., Murdoch, S., Pearce, J., Bergmann, S., le Novère, N., Casanueva, O., 2019. Multi-Omics and Genome-Scale Modeling Reveal a Metabolic Shift During C. elegans Aging. Front Mol Biosci, 6, 15-50. https://doi.org/10.3389/fmolb.2019.00002

Hope, I.A., 1999. C. elegans: a practical approach. Oxford University Press, Oxford.

Hunt, P.R., 2017. The *C. elegans* model in toxicity testing. Journal of Applied Toxicology 37, 50–59. https://doi.org/10.1002/jat.3357

Iijima, S., 1991. Helical microtubules of graphitic carbon. Nature 354, 56–58. https://doi.org/10.1038/354056a0

Intisar, A., Ramzan, A., Sawaira, T., Kareem, A.T., Hussain, N., Din, M.I., Bilal, M., Iqbal, H.M.N., 2022. Occurrence, toxic effects, and mitigation of pesticides as emerging environmental pollutants using robust nanomaterials – A review. Chemosphere 293, 133538. https://doi.org/10.1016/j.chemosphere.2022.133538

Klaessig, F., Kodas, T., Landsiedel, R., Lynch, I., Malloy, T., Miller, M.B., Muller, J., Oberdorster, G., Petersen, E.J., Pleus, R.C., Sayre, P., Stone, V., Sullivan, K.M., Tentschert, J., Wallis, P., Nel, A.E., 2015. Nanomaterial Categorization for Assessing Risk Potential To Facilitate Regulatory Decision-Making. ACS Nano 9, 3409–3417. https://doi.org/10.1021/acsnano.5b00941

Kleiven, M., Oughton, D., 2015. Standard Operating Procedure Toxicity test with the nematode Caenorhabiditis elegans for the NANoREG core nanomaterials.

Koopman, M., Michels, H., Dancy, B.M., Kamble, R., Mouchiroud, L., Auwerx, J., Nollen, E.A.A., Houtkooper, R.H., 2016. A screening-based platform for the assessment of cellular respiration in Caenorhabditis elegans. Nat Protoc 11, 1798–1816. https://doi.org/10.1038/nprot.2016.106

Kuhn, R., Bryant, I.M., Jensch, R., Böllmann, J., 2022. Applications of Environmental Nanotechnologies in Remediation, Wastewater Treatment, Drinking Water Treatment, and Agriculture. Applied Nano 3, 54–90. https://doi.org/10.3390/applnano3010005

Li, H., Zeng, L., Wang, C., Shi, C., Li, Y., Peng, Y., Chen, H., Zhang, J., Cheng, B., Chen, C., Xiang, M., Huang, Y., 2022. Review of the toxicity and potential molecular mechanisms of parental or successive exposure to environmental pollutants in the model organism Caenorhabditis elegans. Environmental Pollution 311, 119927. https://doi.org/10.1016/j.envpol.2022.119927

Liu, Y., Nie, Y., Wang, J., Wang, J., Wang, X., Chen, S., Zhao, G., Wu, L., & Xu, A., 2018. Mechanisms involved in the impact of engineered nanomaterials on the joint toxicity with environmental pollutants. Ecotoxicology and Environmental Safety, 162, 92–102. https://doi.org/10.1016/j.ecoenv.2018.06.079

Li, J., He, Z., Guo, C., Wang, L., & Xu, S., 2014. Synthesis of carbon nanohorns/chitosan/quantum dots nanocomposite and its applications in cells labeling and in vivo imaging. Journal of Luminescence, 145, 74–80. https://doi.org/10.1016/j.jlumin.2013.06.036

Lowry, G. V., Gregory, K. B., Apte, S. C., & Lead, J. R., 2012. Transformations of Nanomaterials in the Environment. Environmental Science & Technology, 46(13), 6893–6899. https://doi.org/10.1021/es300839e

Lundqvist, M., Stigler, J., Elia, G., Lynch, I., Cedervall, T., & Dawson, K. A., 2008. Nanoparticle size and surface properties determine the protein corona with possible implications for biological impacts. Proceedings of the National Academy of Sciences, 105(38), 14265–14270. https://doi.org/10.1073/pnas.0805135105

Markiewicz, M., Kumirska, J., Lynch, I., Matzke, M., Köser, J., Bemowsky, S., Docter, D., Stauber, R., Westmeier, D., & Stolte, S., 2018. Changing environments and biomolecule coronas: consequences and challenges for the design of environmentally acceptable engineered nanoparticles. Green Chemistry, 20(18), 4133–4168. https://doi.org/10.1039/C8GC01171K

Martinez, D. S. T., Ellis, L.-J. A., da Silva, G. H., Petry, R., Medeiros, A. M. Z., Davoudi, H. H., Papadiamantis, A. G., Fazzio, A., Afantitis, A., Melagraki, G., & Lynch, I., 2022. Daphnia magna and mixture toxicity with nanomaterials – Current status and perspectives in data-driven risk prediction. Nano Today, 43, 101430. https://doi.org/10.1016/j.nantod.2022.101430

Maupas, E., 1900. Modes et formes de reproduction des nématodes. Archives de zoologie expérimentale et générale 8, 463–624.

Medeiros, A.M.Z. de, Côa, F., Alves, O.L., Teodoro Martinez, D.S., Barbieri, E., 2020. Metabolic effects in the freshwater fish Geophagus iporangensis in response to single and combined exposure to graphene oxide and trace elements. Chemosphere 243, 125316. https://doi.org/10.1016/j.chemosphere.2019.125316

Monopoli, M. P., Åberg, C., Salvati, A., & Dawson, K. A., 2012. Biomolecular coronas provide the biological identity of nanosized materials. Nature Nanotechnology, 7(12), 779–786. https://doi.org/10.1038/nnano.2012.207

Namgong, C., Kim, J.H., Lee, M.H., Midkiff, D., 2022. Non-invasive cancer detection in canine urine through Caenorhabditis elegans chemotaxis. Front Vet Sci 9. https://doi.org/10.3389/fvets.2022.932474

Naasz, S., Altenburger, R., & Kühnel, D., 2018. Environmental mixtures of nanomaterials and chemicals: The Trojan-horse phenomenon and its relevance for ecotoxicity. Science of The Total Environment, 635, 1170–1181. https://doi.org/10.1016/j.scitotenv.2018.04.180

Natarajan, L., Jenifer, M. A., & Mukherjee, A., 2021. Eco-corona formation on the nanomaterials in the aquatic systems lessens their toxic impact: A comprehensive review. Environmental Research, 194, 110669. https://doi.org/10.1016/j.envres.2020.110669

Nguyen, J.P., Shipley, F.B., Linder, A.N., Plummer, G.S., Liu, M., Setru, S.U., Shaevitz, J.W., Leifer, A.M., 2016. Whole-brain calcium imaging with cellular resolution in freely behaving *Caenorhabditis elegans*. Proceedings of the National Academy of Sciences 113. https://doi.org/10.1073/pnas.1507110112

Palmieri, V., Perini, G., de Spirito, M., & Papi, M., 2019. Graphene oxide touches blood: in vivo interactions of bio-coronated 2D materials. Nanoscale Horizons, 4(2), 273–290. https://doi.org/10.1039/C8NH00318A

Pazdernik, N., Schedl, T., 2013. Introduction to Germ Cell Development in Caenorhabditis elegans. pp. 1–16. https://doi.org/10.1007/978-1-4614-4015-4_1

Petersen, E.J., Henry, T.B., Zhao, J., MacCuspie, R.I., Kirschling, T.L., Dobrovolskaia, M.A., Hackley, V., Xing, B., White, J.C., 2014. Identification and Avoidance of Potential Artifacts and Misinterpretations in Nanomaterial Ecotoxicity Measurements. Environ Sci Technol 48, 4226–4246. https://doi.org/10.1021/es4052999

Pimtong, W., Samutrtai, P., Wongwanakul, R., Aueviriyavit, S., 2021. Predictive models for nanotoxicology: in vitro, in vivo, and computational models, in: Handbook of Nanotechnology Applications. Elsevier, pp. 683–710. https://doi.org/10.1016/B978-0-12-821506-7.00026-0

Ray, S. C., 2015. Application and Uses of Graphene Oxide and Reduced Graphene Oxide. In Applications of Graphene and Graphene-Oxide Based Nanomaterials. Elsevier. https://doi.org/10.1016/B978-0-323-37521-4.00002-9

Reilly, K., Davoudi, H., Guo, Z., Lynch, I., 2022. Chapter 6. The Composition of the Eco-corona Acquired by Micro- and Nanoscale Plastics Impacts on their Ecotoxicity and Interactions with Co-pollutants. pp. 132–155. https://doi.org/10.1039/9781839166570-00132

Roberts, B., Antonopoulos, A., Haslam, S.M., Dicker, A.J., McNeilly, T.N., Johnston, S.L., Dell, A., Knox, D.P., Britton, C., 2013. Novel expression of Haemonchus contortus vaccine candidate aminopeptidase H11 using the free-living nematode Caenorhabditis elegans. Vet Res 44, 111. https://doi.org/10.1186/1297-9716-44-111

Schleker, A.S.S., Rist, M., Matera, C., Damijonaitis, A., Collienne, U., Matsuoka, K., Habash, S.S., Twelker, K., Gutbrod, O., Saalwächter, C., Windau, M., Matthiesen, S., Stefanovska, T., Scharwey, M., Marx, M.T., Geibel, S., Grundler, F.M.W., 2022. Mode of action of fluopyram in plant-parasitic nematodes. Sci Rep 12, 11954. https://doi.org/10.1038/s41598-022-15782-7

Schwirn, K., Voelker, D., Galert, W., Quik, J., Tietjen, L., 2020. Environmental Risk Assessment of Nanomaterials in the Light of New Obligations Under the REACH Regulation: Which Challenges Remain and How to Approach Them? Integr Environ Assess Manag 16, 706–717. https://doi.org/10.1002/ieam.4267

Sivaselvam, S., Mohankumar, A., Thiruppathi, G., Sundararaj, P., Viswanathan, C., Ponpandian, N., 2020. Engineering the surface of graphene oxide with bovine serum albumin for improved biocompatibility in Caenorhabditis elegans. Nanoscale Adv 2, 5219–5230. https://doi.org/10.1039/D0NA00574F.

Takeishi, A., Takagaki, N., Kuhara, A., 2020. Temperature signaling underlying thermotaxis and cold tolerance in *Caenorhabditis elegans*. J Neurogenet 34, 351–362. https://doi.org/10.1080/01677063.2020.1734001

The *C. elegans* Sequencing Consortium, 1998. Genome Sequence of the Nematode C. elegans: A Platform for Investigating Biology. Science (1979) 282, 2012–2018. https://doi.org/10.1126/science.282.5396.2012

Tomak, A., Cesmeli, S., Hanoglu, B. D., Winkler, D., & Oksel Karakus, C., 2021. Nanoparticle-protein corona complex: understanding multiple interactions between environmental factors, corona formation, and biological activity. Nanotoxicology, 15(10), 1331–1357. https://doi.org/10.1080/17435390.2022.2025467

Van Assche, R., Broeckx, V., Boonen, K., Maes, E., de Haes, W., Schoofs, L., Temmerman, L., 2015. Integrating -Omics: Systems Biology as Explored Through C. elegans Research. J Mol Biol 427, 3441–3451. https://doi.org/10.1016/j.jmb.2015.03.015

Vineeth Kumar, C. M., Karthick, V., Kumar, V. G., Inbakandan, D., Rene, E. R., Suganya, K. S. U., Embrandiri, A., Dhas, T. S., Ravi, M., & Sowmiya, P., 2022. The impact of engineered nanomaterials on the environment: Release mechanism, toxicity, transformation, and remediation. Environmental Research, 212, 113202. https://doi.org/10.1016/j.envres.2022.113202

Von Mikecz, A., 2022. Exposome, Molecular Pathways and One Health: The Invertebrate Caenorhabditis elegans. International Journal of Molecular Sciences, 23(16), 9084. https://doi.org/10.3390/ijms23169084

Wheeler, K.E., Chetwynd, A.J., Fahy, K.M., Hong, B.S., Tochihuitl, J.A., Foster, L.A., Lynch, I., 2021. Environmental dimensions of the protein corona. Nat Nanotechnol 16, 617–629. https://doi.org/10.1038/s41565-021-00924-1

Wu, Q., Yin, L., Li, X., Tang, M., Zhang, T., & Wang, D., 2013. Contributions of altered permeability of intestinal barrier and defecation behavior to toxicity formation from graphene oxide in nematode Caenorhabditis elegans. Nanoscale, 5(20), 9934. https://doi.org/10.1039/c3nr02084c

Xu, L., Xu, M., Wang, R., Yin, Y., Lynch, I., & Liu, S., 2020. The Crucial Role of Environmental Coronas in Determining the Biological Effects of Engineered Nanomaterials. Small, 16(36), 2003691. https://doi.org/10.1002/smll.202003691

Zhang, F., Wang, Z., Peijnenburg, W. J. G. M., & Vijver, M. G., 2022. Review and Prospects on the Ecotoxicity of Mixtures of Nanoparticles and Hybrid Nanomaterials. Environmental Science & Technology, 56(22), 15238–15250. https://doi.org/10.1021/acs.est.2c03333

Zhang, Y., Goss, G.G., 2021. The "Trojan Horse" effect of nanoplastics: potentiation of polycyclic aromatic hydrocarbon uptake in rainbow trout and the mitigating effects of natural organic matter. Environ Sci Nano 8, 3685–3698. https://doi.org/10.1039/D1EN00738F

Zeng, L., Gao, J., Liu, Y., Gao, J., Yao, L., Yang, X., Liu, X., He, B., Hu, L., Shi, J., Song, M., Qu, G., & Jiang, G., 2019. Role of protein corona in the biological effect of nanomaterials: Investigating methods. TrAC Trends in Analytical Chemistry, 118, 303–314. https://doi.org/10.1016/j.trac.2019.05.039

2. CHAPTER 2. *Caenorhabditis elegans*: CURRENT STATUS AND PERSPECTIVES ON CARBON NANOTOXICITY RESEARCH [2]

Graphical abstract

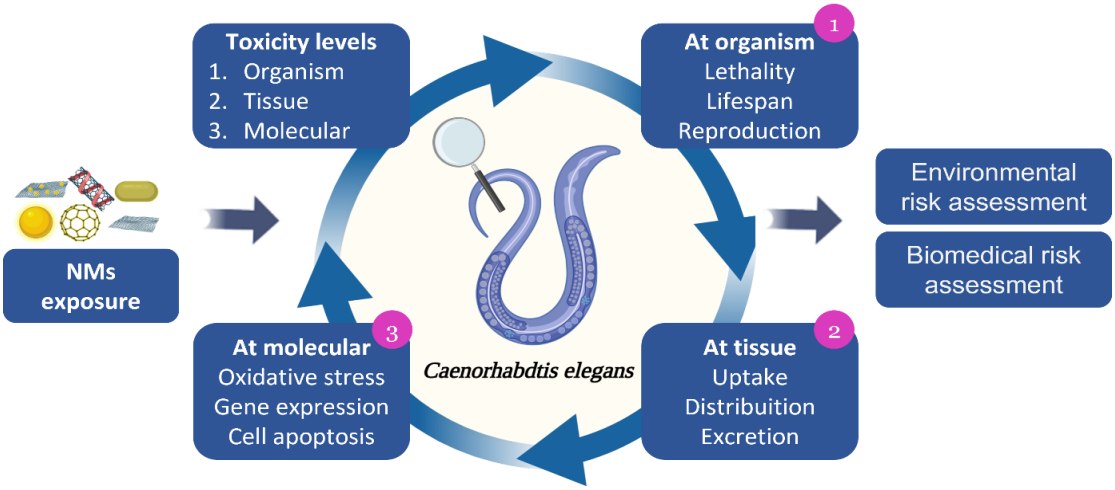

Abstract

Carbon nanomaterials are one of the most widely studied and exploited materials as they possess excellent optical, electrical and mechanical features. However, biosafety studies are compulsory to support their safe application and disposal. Relevant progress has already been made; however, traditional toxicological assays are typically expensive and time-consuming. Alternatively, *Caenorhabditis elegans* has emerged as a complete model organism for predictive toxicology as it has a transparent body, short reproductive and life cycles, and a fully sequenced genome with high homology with the human genome. This review discussed the advantages and limitations of *C. elegans* as a platform for nanotoxicology and nanosafety research. The current progress in nanotoxicity studies with this organism and carbon nanomaterials was summarized, and supportive tools for this evaluation were shown. The critical knowledge gaps and methodological challenges that influence nanomaterials toxicity were also raised. We believe this review will contribute to the scientists to discover and explore the possibilities offered by *C. elegans* to predict the nanomaterials risks and design safe and sustainable materials.

Keywords: model organism; nanotoxicology; nanotechnology; materials science techniques

[2] This review was elaborated in collaboration with other authors (Leandro de Sá Bortollozo, Daiana Ávila and Diego S.T. Martinez).

2.1. Introduction

Carbon nanomaterials (CNMs) are allotropes of carbon that have received significant attention because their unique properties improve the features of several products and technologies. They have been exploited in the biomedical field, for drug delivery, imaging, tissue engineering and target photothermal therapy (Maiti et al., 2019). However, this growing interest is becoming a relevant impasse as they can be released into the environment, reaching organisms and humans. Therefore, nanotechnology risks need to be well investigated towards a safe and responsible application.

Nanotoxicology is the field of science dedicated to elucidating the potential hazards of nanomaterials (NMs) to environmental compartments and human health. In vitro, in silico and in vivo models are part of the strategies to be adopted in this context. Experiments with cells are the first approach typically chosen to predict the biological response to nanomaterials. However, these assays demand complex facilities. On the other hand, model organisms are easily cultivated in laboratories and provide data from animals with active reproductive, digestive, endocrine and neuromuscular systems. *Danio rerio*, *Drosophila melanogaster*, and *Hydra vulgaris* are examples of valuable alternative models to assess the response to toxicants.

Since 1960, *C. elegans* has been considered a suitable model for carrying out simple and rapid screenings of the toxic effects of substances, both from an environmental and biomedical point of view. Its transparent body and its short life cycle permit rapid screening of several substances whereas applying in vivo vertebrate animals is expensive and time-consuming. *C. elegans* has digestive, reproductive, endocrine, sensory and neuromuscular systems with signaling pathways similar to humans. Several *C. elegans* transgenic strains are available to study the roles of specific genes in toxicological routes. Moreover, there are interesting tools to support nanotoxicity assessment with *C. elegans*. Due to its transparent body, optical and fluorescence microscopy techniques can be exploited to visualise fluorescent transgene expression, and nanomaterials uptake and biodistribution (Gonzalez-Moragas et al., 2015) Therefore, this nematode has opened the door to understanding NMs toxicity at the organism, tissue and molecular levels.

In recent years, a concerted effort has focused on investigating the effects of NMs in *C. elegans*. It has been discussed that carbon nanomaterials can affect the nematode lifespan, reproduction, fertility and functionality of its neurons. On the other hand, some scientific challenges and methodological particularities in assays with *C. elegans* have made it difficult to obtain and compare data. Therefore, this review intends to discuss the advantages

of *C. elegans* as a platform to assess the potential risks of NMs to human health and organisms and addresses the main techniques to support this evaluation. However, as some limitations need to be solved, they will also be discussed.

2.2. *Caenorhabditis elegans*: an alternative model to animal experimentation and nanotoxicity assessment

Using animals for scientific purposes is a practice from ancient Greece where medical experiments were carried out with animals. However, this practice has been intensely and globally discussed by researchers, society, and ethics committees in animal experimentation. Traditional experimental trials with rodents are questionable from an ethical point of view and a feasibility aspect. They are typically expensive, involve many animals and are time-consuming (Doke and Dhawale, 2015; Zemanova, 2020).

Applying alternative models is a strategic approach to replace the use of animals and reduce costs and time (Squiban and Kurz, 2011). Vertebrate models such as *Danio rerio* (known as zebrafish) have been widely explored in laboratories. Although they present high homology to humans than invertebrates, their life cycle is long, and manipulation is sometimes complex in comparison with the *C. elegans* model. On the other hand, zebrafish can be used for investigating the heart and vascular system, which are absent in *C. elegans*. Table 1.1 compares the features of two other model organisms (zebrafish and mice) to *C. elegans* characteristics. It is worth mentioning that the choice of approach will depend not only on costs and structure but especially on research purposes.

Adopting *C. elegans* for biological screening is advantageous because it can be cultivated in small laboratories at a lower cost than rodents. In addition, its development and life cycle are short (~3 days and 2 to 3 weeks, respectively). Other attributes of *C. elegans* can be highlighted: I) high reproductive capacity; II) multicellular complexity; III) fully sequenced genome; and IV) transparent cuticle (Gonzalez-Moragas et al., 2015; Hunt, 2017; Leung et al., 2008). Another advantage is the availability of transgenic strains to investigate mechanisms and molecular pathways involved in toxicity. These strains are typically produced by microinjection or gene bombardment, and over-express specific genes or express tagged proteins (Gonzalez-Moragas et al., 2015; Weinhouse et al., 2018).

Since its introduction into biological studies in the early 1960s by Sydney Brenner (O'Reilly et al., 2014), *C. elegans* has received attention for elucidating genetic pathways that control vital biological processes such as development, ageing and cell death. As 41% of the *C.*

elegans genome is homologous to the human genome, human diseases such as Alzheimer, Parkinson, diabetes, Duchenne muscular dystrophy and cancer have been studied with this organism (Gonzalez-Moragas et al., 2015; Hunt, 2017). Given the notoriety of these studies, three distinguished Nobel prizes were awarded in 2002, 2006 and 2008 to authors who used this nematode to understand in vivo molecular processes such as cellular apoptosis. It is noteworthy that the use of *C. elegans* in research laboratories is in accordance with accepted ethical principles (i.e., reduction, refinement and replacement) and it is not required special approval.

Due to its abundance in ecosystems and its key role in soil nutrient decomposition and cycling, *C. elegans* is a valuable indicator of environmental changes. It is highly sensitive to environmentally relevant concentrations (μg L^{-1} or ng L^{-1} range) and higher concentrations (1000 mg L^{-1}). These characteristics contribute to *C. elegans* has been emerged as a promising model for the assessment of NMs toxicity and other contaminants such as heavy metals, pesticides, hormones and microplastics (Chen et al., 2019; Goussen et al., 2015; Jiang et al., 2016; Lei et al., 2018; Mendonça et al., 2017; Soares et al., 2020; Squiban and Kurz, 2011; Wang et al., 2019). On the other hand, some limitations can be pointed out such as the lack of a circulatory system and specific organs (e.g., brain, heart, lungs or skeletal system) (Wu et al., 2019).

Nanotoxicological assays with *C. elegans* can be performed in liquid media (e.g., M9, S-basal, EPA), solid (e.g., NGM-agar), or in a medium that simulates the characteristics of sediments. Exposure regimes can be short (e.g., 3 h; 24 h) or prolonged (e.g., 96 h). Multiple parameters can be evaluated within the same experiment, especially by using automated systems such as microfluidic platforms to capture and process these data (Cornaglia et al., 2017). Some of the main biological parameters that have been assessed with *C. elegans* are survival, lifespan, growth, development, neurotoxicity and locomotory dysfunction, reproductive toxicity, and intestinal damage. In addition, molecular markers have also supported the toxicity evaluation, such as oxidative stress, DNA damage and repair, metabolomic profile and metabolites in *C. elegans*, such as glucose, lactic acid, and TCA cycle (Yao et al., 2022).

Table 1.1 – Comparison of key features between *Caenorhabditis elegans*, *Danio rerio* and mice.

		Animal model	
	Caenorhabditis elegans	***Danio rerio***	**Mice**
Habitat	Terrestrial (soil and sediments)	Aquatic	Terrestrial
Culture	Low cost	Low cost	High cost
Space	Hundreds of animals in a small 10 cm^3 petri dish	45 L aerated aquariums in a dedicated room	Isolated cages
Food	Bacteria	Dry flake food	Ration
Environmental conditions	20 °C	28 °C	18-23 °C 40-60% humidity
Adult size	~ 1 mm	~ 4.5 cm	~ 17 cm
Gender	Hermaphrodite	Male and female	Male and female
Life cycle	2-3 days	2-4 months	2-3 months
Embryogenesis	18 h, 20 °C	48-72 h, 28 °C	19-21 days
Lifetime	2-3 weeks	2-3 years	2-3 years
Offspring (per animal)	~ 300	100-200	40-100
Sequencing genome	In 1998	In 2013	In 2002
Homology with humans	41.7 % (20-71%)	70%	99%
Availability of automated tests	At all larval stages	Only at the embryo stage	It is not able
Other relevant features	Translucent body; stored in the freezer; several transgenic strains available	Transparent when embryo	Difficulty getting approved in ethics committees

Adapted from Gonzalez-Moragas et al. (2015).

The uptake of NMs by *C. elegans* occurs mainly through the mouth, which size is approximately 1 µm at the adult stage (Hunt, 2017; Leung et al., 2008). When internalized, NMs can be translocated from the gastrointestinal region to proximities of the nervous system, damaging neural signalling pathways (Chen et al., 2017). In addition, reproductive organs such as gonads and spermatheca are targeted tissues for NMs exposure. In this sense, imaging techniques such as X-ray fluorescence and hyperspectral darkfield microscopies are strategic tools to evaluate the pattern of nanomaterials distribution in *C. elegans*. Given their importance, a further topic discusses their principles, advantages, applications and limitations in nanotoxicity studies.

2.3. Scientific and methodological challenges in assays with *Caenorhabditis elegans* and nanomaterials

In the last three decades, relevant efforts have been made to understand NMs toxicity. However, difficulties inherent to toxicity tests, the lack of details of the adopted methodologies and the absence of standardized techniques complicate this process and lead to inconsistent, hardly comparable and reproducible results. Misinterpretation and generation of artefacts (inaccurate results) can occur at all stages during nanotoxicity tests, starting with the properties of NMs that may differ from those reported by the manufacturer to inaccurate sample preparation for biodistribution studies (Selck et al., 2016).

Figure 1 summarizes factors that can affect nano/bio interactions between *C. elegans* and NMs during biological assays. One of the main challenges is that some intrinsic NMs characteristics influence the toxic effect, such as size, morphology, surface chemical composition and surface charge. Differences in the synthesis method, variations between batches and impurities can also impact biological results (Martinez and Alves, 2013). The high energy applied in some procedures for preparing NMs dispersions can modify their properties, such as decreasing their size and increasing their structural defects (Chowdhury et al., 2014; Pradhan et al., 2016). The use of dispersing agents also adds a toxicological variable, and the low stability of stock dispersions leads to low reproducibility and uncertainties about the administered dose (Henry et al., 2007). Therefore, standardizing the NMs dispersion method is critical in biological experiments.

In tests carried out in liquid media, aggregation, agglomeration and sedimentation directly affect the interaction between NMs and *C. elegans* (Ellegaard-Jensen et al., 2012). Due to these factors, exposure to NMs is not constant and homogeneous during the tests. In solid media, the non-homogeneous exposure to NMs can be explained by the difficulty in uniformly mixing them in the agar during its preparation or over the prepared agar. Furthermore, high concentrations of phosphate that compose these media can interact with samples (Gonzalez-Moragas et al., 2017a). The media composition can also affect the dissolution and toxicity of metallic NMs or carbon NMs with metals on their surface (i.e., hybrids); incomplete or complete NMs dissolution can be observed in media with high concentrations of chloride ions (Starnes et al., 2015). These findings evidence why it is common to observe different levels of toxicity for the same material (Geitner et al., 2020).

Another variable is that NMs can undergo surface modifications when they come into contact with biological media and biomacromolecules, which can be excreted by the tested organism or generated by adding a food source. NMs will interact with these biomacromolecules and media components, forming a coating on their surface. This coating results in a new biological identity called biocorona that will impact their behaviour, fate and toxicity (Markiewicz et al., 2018). An equivalent phenomenon occurs when natural organic matter is added to the tests from an environmental perspective (Collin et al., 2014).

Figure 1 - Factors that may influence nano-bio interactions in assays with *C. elegans* biological model.

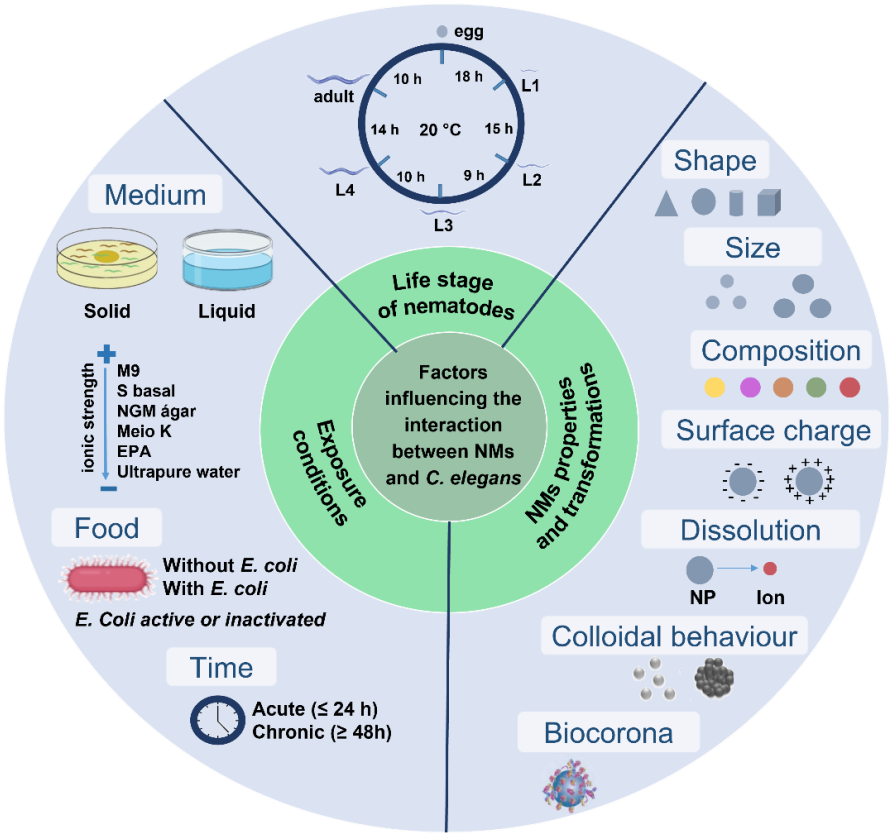

The addition of a food source can also lead to misinterpretation results. Positively charged NMs may form large aggregates with *E. coli*, decreasing food availability to *C. elegans*. With starvation, the nematode stops development and its reproduction is inhibited (Hanna et al., 2018). Bacterial density has been pointed out as an influencing aspect. By using the reference substance BAC-C16, it was observed that a minimum number of bacteria (500 FAU) is required for nematode development. A variation in bacterial density in 50 FAU occasioned inhibition of nematode growth at 19% (Hanna et al., 2016).

Moreover, some authors have reported that juveniles (L1 stage) are more sensitive to toxic effects than adults. In the study by Collin et al., the lethal concentration of cerium oxide nanoparticles (NPs) for L1 nematodes was 15.5 mg L^{-1}, while it was 272 mg L^{-1} at the L3 stage, demonstrating that adults were less affected (Collin et al., 2014). The duration of the tests is also related to toxicity. Longer exposures (≥48 h) can result in more significant impacts on *C. elegans*. In the study by Zhao et al., nematodes exposed for a long time to TiO_2 NPs (> 96 h) consumed more NPs than those exposed for 24 h, resulting in dysfunctions in pharyngeal pumping and locomotion behaviour, and reduction of defection capacity (Zhao et al., 2014).

Some methodological barriers in assays with *C. elegans* and NMs have also been discussed, such as the difficulty in accurately counting organisms. In an experiment, nematodes are quantified at least two times: I) at the beginning to determine the culture density for each treatment, and II) at the end when offspring number needs to be assessed to gain information on the impact of these substances on reproduction, for example. Although it sounds easy, it is a time-consuming, error-prone process and a challenge when researchers have many samples. The adopted methodologies are usually by approximation and are not properly reported in publications (Scanlan et al., 2018).

Another challenge is accurately measuring the NMs internalization by *C. elegans*. As demonstrated by Johnson et al., methods commonly adopted for sample preparation (i.e., rinsing with water or buffers are inefficient for removing some NMs adsorbed on nematode cuticles surface. Alternatively, these authors developed a protocol in which a sucrose gradient with different densities is applied (Johnson et al., 2017). Obviously, it needs to be adapted to carbon nanomaterials, but it is a starting point for discussions.

The factors previously raised evidence that a thorough investigation of the NMs physicochemical properties and colloidal behaviour is crucial to avoid artifacts in nanotoxicology studies. In this sense, the Organization for Economic Cooperation and Development (OECD) recently published a guideline (Guide No. 317) describing how nanotoxicity tests should be conducted in aquatic environments and sediments. This document defines the criteria for evaluation and what data should be reported in the studies (OECD, 2020).

The development of harmonized protocols is therefore a major issue towards producing experimental data comparable and minimising the production of artifacts. In addition, a rigorous posture is expected from nanotoxicology scientists in order to investigate not only toxicity but also to carefully examine the possibility of interfering during the tests. Special attention should be given to techniques that allow characterizing and quantifying NMs in experimental media. However, since these techniques are time-consuming, expensive, hard to be implemented and

require specialized equipment that sometimes is not available for complex matrices, an alternative is applying strategic experimental controls. National Institute of Standards and Technology (NIST) has published a list of experimental controls to be included in assays to improve their reliability (Petersen et al., 2015).

2.4. Toxicity of carbon nanomaterials on *Caenorhabditis elegans:* the state-of-the-art

Carbon nanomaterials family is composed of fullerenes, nanodiamonds, carbon nanotubes, graphene and its derivatives, such as graphene oxide, reduced graphene oxide and graphene quantum dots. These materials differ in structure, shape and size and are not necessarily confined at the nanoscale in all dimensions. Carbon nanomaterials have been exploited in various applications due to their excellent physicochemical properties, such as high mechanical strength, electrical conductivity and optical characteristics. They are promising materials for environmental remediation of contaminants, electronics and semiconductor industries, and biomedical applications, such as drug delivery and biosensors (Madima et al., 2020).

Graphene and its derivatives are one of the most commercially relevant carbon nanomaterials. The global market value of graphene-based products is expected to reach $1.3 billion in 2023, indicating a significant expansion of graphene production in the coming years (Ahmed and Rodrigues, 2013), consequently, the predicted graphene concentration in the environment is increasing from 0.001 to 1000 μg L^{-1} (Sun et al., 2016).

Graphene oxide (GO) is one of the most studied carbon nanomaterials from a toxicological point of view with *C. elegans*. Studies have reported the accumulation of GO in the nematode gut and its translocation to reproductive organs, neurons and eggs. It has been observed that concentrations higher than 5 mg L^{-1} cause a significant reduction in *C. elegans* reproductive capacity along with induction of germline apoptosis and interruption of its cell cycle (Nivedita et al., 2017; Zhao et al., 2016). While concentrations higher than 10 mg L^{-1}, affected its lifespan (Wu et al., 2013b). Prolonged exposure to GO significantly increases ROS production in *C. elegans* intestine and impairs its locomotion (Wu et al., 2014a). Disturbances in its defecation behaviour and immune response have also been observed (Wu et al., 2014a, 2013b).

A potential neurotoxic effect of GO was noticed by Kim et al. (2020) who observed GO accumulation in the nematode head by Raman spectroscopy, as well as an increase in ROS production and a decrease in dopaminergic and glutamatergic neurotransmitter content. On the other hand, some strategies have been reported to reduce the toxicity of GO to *C. elegans*. Our group recently demonstrated that GO can be chemically degraded by sodium hypochlorite, mitigating its adverse effects on *C. elegans* (Bortolozzo et al., 2021). Sivaselvam et al. (2020) also observed that modifying the GO surface with bovine serum albumin (BSA) can suppress GO toxicity. Similar results were reported in a study performed by our group, where GO was coated by BSA and its toxic effects were partly mitigated (Côa et al., 2022).

Carbon nanotubes (CNTs) are tubular structures formed by one or more sheets of graphene rolled. CNTs vary in length, diameter, chirality and number of layers. The estimated production of CNTs per year is from 55 to 3300 tons (Sun et al., 2014), and their estimated concentration in the environment ranges from 0.001 to 1000 μg L^{-1} (Sun et al., 2016). Significant studies were carried out to investigate the possible toxic effects of CNTs on *C. elegans*. The translocation of multi-walled carbon nanotubes (MWCNT) in nematode body from the pharynx to the intestine and gonad was described by Wu et al. (2013a). They observed alterations in nematode behaviour and brood size.

Recently, our group also confirmed that MWCNT could be translocated to the reproductive organs of *C. elegans*, affecting its survival, reproduction, fertility and growth (Côa et al., 2022). The pharynx has been pointed out as a key barrier in preventing the CNTs translocation to secondary organs (Zhuang et al., 2016a). Adverse effects of MWCNT (from 1 to 100 mg L^{-1}) on *C. elegans* lifespan and induction of oxidative stress have also been described. In addition, the expression patterns of some genes required for intestinal development and the defecation cycle have been affected by MWNCT exposure (Shu et al., 2015).

Carbon quantum dots (C-QDs) are carbon amorphous nanoparticles with diameters smaller than 10 nm (Li et al., 2020). C-QDs are majority important in the health field, as they have been applied as markers for in vivo bioimaging, drug administration, diagnosis and early treatment of diseases (Lee et al., 2019; Liu et al., 2013). Although few studies have been carried out with these materials and *C. elegans*, it has been demonstrated that C-QDs do not present potential toxicity to this organism (Atchudan et al., 2019; Han et al., 2019; Singh et al., 2018). The uptake of C-QDs via oral ingestion and accumulation in *C. elegans* tissues (gonad and germ cells) has been observed. However, since C-QDs are fluorescent and apparently biocompatible, they would be safely applied in bioimaging (Li et al., 2020).

As previously mentioned, biological effects of carbon-based are dependent on the physicochemical properties of the NM in question (e.g., morphology, size, surface charge) as well as its dispersion state, concentrations and conditions of exposure (e.g., the period of duration, the life stage of nematode and strain). Considering these aspects, Table 1.2 summarizes the studies published with *C. elegans* and carbon nanomaterials and details the experimental conditions under which were performed.

Although crucial studies have provided valuable insights into carbon nanomaterials toxicity, some aspects still required to be evaluated during these experiments: 1) It is a consensus that these materials can reach the nematode reproductive system causing reprotoxicity, but it is not well-defined how they are translocated between the tissues reaching this organ (Yao et al., 2022); 2) Most of the investigations are performed at short-term exposures; multigenerational exposure is not prioritized although this predicts how several generations will be impacted by NMs; 3) Characteristics of NMs can change over time in a toxicity assay with *C. elegans*, mainly in the presence of food (bacteria); however, to date, this has not been deeply studied; and 4) The products excreted by *C. elegans* after NMs ingestion have not yet been assessed.

Moreover, since *C. elegans* survives in soil, sediments and water, some knowledge gaps about the carbon nanomaterials transformations in the environment and toxicity could be filled with this model: 1) Transport of carbon nanomaterials in the food chain; 2) Interactions of those materials with pre-existing environmental pollutants and their implications to the environment; 3) Biogeochemical transformations of carbon nanomaterials in the environment (photodegradation, homo or heteroaggregation, coating with biomacromolecules – biocorona formation). Finally, the generation of data and no compilation of that with the physicochemical characterisation of carbon nanomaterials do not contribute to the generation of mathematical models to predict the toxicological effects; therefore, scientific publications in this field need to improve this aspect.

Table 1.2 – Summary of studies performed with carbon nanomaterials and *Caenorhabditis elegans* nematode.

Nanomaterial	Features	Exposure conditions	Endpoints	*Strain* Life stage	Key biological outcomes	References
GO	Synthesized by the group Diameter: 40–50 nm Zeta potential: -20.3 mV	K^+ 1 to 1000 μg L^{-1}	Growth, lifespan, locomotion behaviour, defecation and ROS	*N2, EG1285 and CF1553* L1 to adult Multi-generational exposure	Multi-generational exposure to GO affected neurons and the reproductive system, in addition to increase cell apoptosis and ROS production	Jin et al. (2022)
GO and GO coated by bovine serum albumin (BSA)	Synthesized by Hummers' method	EPA medium 0.001 to 10 mg L^{-1}	Lethality, growth, ROS, fertility and reproduction	*N2* L1 to adult, and L4 stage	GO was translocated from the intestinal barrier to gonads, eggs and head. It was toxic in acute and chronic assays. However, BSA-coating partially mitigated the GO adverse effects	Côa et al. (2022)
GO and chemical-degraded GO (NaClO–GO)	Synthesized by the group Size: GO ~156 nm and NaClO–GO ~29 nm.	EPA medium 0.01; 1, 10, 50 and 100 mg L^{-1}	Survival, growth, reproduction and fertility	*N2* L1 to adult	GO and NaClO-GO were uptake by nematodes. GO was toxic for all the evaluated endpoints, but degraded GO presented lower toxicity	Bortolozzo et al. (2021)
GO	Synthesized by Hummers' method Length: 40-50 nm Thickness: ±1 nm Zeta potential: −20.3 mV	K^+ medium 0.001 to 1 mg L^{-1}	Intestinal permeability (0-192 h)	*N2 and VP303* L1 to adult	GO dysregulated the physiological and functional state of the intestinal barrier with the induction of toxicity in *C. elegans*	Liu et al. (2020)
GO	UniNanoTech Thickness: 6 nm Height: 20 nm Lateral size: 40 nm Zeta potential: -20.5 mV	K^+ medium 10 mg L^{-1}	Biodistribution, oxidative stress, neurotoxicity and locomotive behaviour	*N2 and DA1267* L4 stage	GO caused damages in locomotion, decreased dopaminergic and glutamatergic neurons and increased ROS	Kim et al. (2020)
GO	UniNanoTech Thickness: 6 nm; Height: 20 nm; Lateral distribution: 40 nm Zeta potential: -20.5 mV	K^+ medium 10 mg L^{-1}	Reproduction and fatty acid metabolism (2-48 h)	*N2, BX107 fat-5, BX106 fat-6, BX153 fat-7, BX110 fat-6; fat- 5, BX160 fat-7, fat-5, BX156 fat-6, fat-7 and STE68 nhr-49* L4 stage	GO caused alteration in fatty acid metabolism and spermatogenesis suppression	Kim et al. (2018)

(continuation)

Nanomaterial	Features	Exposure conditions	Endpoints	*Strain* *Life stage*	Key biological outcomes	References
GO	Synthesized by Hummers' method Thickness: 1 nm Height: 40-50 nm Zeta potential: −22.5 mV	K^+ medium 10 mg L^{-1}	Biodistribution and molecular mechanisms	*N2, NR222/rde-1(ne219);kzIs9 and Is(Pmlt-7-mlt-7::GFP)* L1 to adult	Accumulation of GO in *C. elegans* gut as a result of functional disruption of the epidermal barrier	Ding et al. (2018a)
GO	Synthesized by modified Hummers' method Thickness: 1 nm Length: 40 to 50 nm Zeta potential: -21.5 mV	K^+ medium and NGM 50-200 mg L^{-1}	Molecular mechanisms of behaviour and neurotoxicity (96 h)	*N2, nlg-1(tm474) e nlg-1(ok259), of nlg-1(ok259)Ex(Pttx-3-nlg-1), nlg-1(ok259) Ex(Pgcy-28.d-nlg-1),nlg-1(ok259)Ex Pnpr- 9-nlg-1), nlg-1(ok259)Ex(Punc-86-nlg-1), nlg-1(tm474) and nlg-1(ok259)* L1 to adult	Significant aversive behaviour of nematodes to GO at concentrations higher than 50 mg L^{-1}. Nlg-1 in AIY or AIB interneurons regulated GO toxicity	Xiao et al. (2018)
GO	Synthesized by Hummers' method Length: 40 to 50 nm Zeta potential: -21.9 mV	K^+ medium 1; 10 and 100 mg L^{-1}	Molecular mechanisms, ROS production and biodistribution	*N2, VP303* L4 stage	PK3-3 might regulate intestinal permeability promoted by GO exposure. In addition, two proteins (ISP-1 and SOD-3) were identified which may have controlled the nematode oxidative stress	Ren et al. (2018)
GO interacted with humic acid (HA)	Purchased from Sigma Aldrich (lot MKBV1192V) Diameter: 225.1 ±105.4 nm	EPA medium GO- 0.1 to 100 mg L^{-1} HA - 20 mg L^{-1}	Recovery, growth, reproduction and fertility	*N2* L1 to adult and second generation	HA improved the GO colloidal stability; however, it increased the toxicity on fertility and reproduction	Castro et al. (2018)
GO	Synthesized by Hummers' method Thickness: 1 nm Height: 40-50 nm Zeta potential: -21.3 mV	K^+ medium 1, 10 and 100 mg L^{-1}	Biodistribution, oxidative stress and neural molecular mechanisms	*N2, mutants of nlg-1, pkc-1, abi-1, lin-45, and transgenic strains of Ex(Pnlg-1-nlg-1::GFP), nlg-1,pkc-1, lin-45, VP303, Is(Pttx-3-nlg-1), and daf-16(intestinalRNAi);Is(Pttx-3-nlg-1)* L1 to adult	GO may dysregulate NLG-1-mediated molecular signaling in the interneurons, and a neuronal signaling cascade of NLG-1-PKC-1-LIN-45 was raised to control the adverse effects of GO	Chen et al. (2017)

(continuation)

Nanomaterial	Features	Exposure conditions	Endpoints	*Strain* *Life stage*	Key biological outcomes	References
GO	Synthesized by Hummers' method Height: 40 to 50 nm Zeta potential: -22.2 mV	K^+ medium 1 mg L^{-1}	Molecular mechanisms of embryonic development	*N2, bar-1(ga80), apr-1(ok2970), gsk-3(tm1020), dsh- 1(ok1445), dsh-2(ok2164), mom-5(gk812), cfz-2(ok1201), daf- 16(mu86), pmk-1(km25), egl-5(n945), egl-5(n945), and bar-1(ga80)* L1 to adult	Exposure to GO caused damage to the functions of primary and secondary target organs of *C. elegans*, in addition to dysregulation of embryonic development	Zhi et al. (2017)
GO	Synthesized by Hummers' method Thickness: 1 nm Height: 40 to 50 nm Zeta potential: −21.8 mV	K^+ medium 0.1; 1; 10 and 100 mg L^{-1}	Germline apoptosis, fertility, DNA damage and bioinformatics analysis	*N2, MT1522, MT2547, MT8735, MT4770, WS2277, TJ1, SP506, MT15018, MT12969, MT13954, MD701, WS1433, and Ex(Pmir-360-mir-360)* L1 to adult	GO damaged the gonad development, reducing the reproductive capacity of *C. elegans*. A miRNA regulatory mechanism was activated to suppress the reproductive toxicity	Zhao et al. (2016)
GO and GO reduced (rGO)	Purchased from UniNanoTech Thickness GO: 6 nm; rGO: 7 nm Height GO: 20 nm rGO: 23 nm. Lateral size: 40 nm Zeta potential: GO: -20.5 mV; rGO: -9.2 mV	K^+ medium 5 – 100 mg L^{-1}	Uptake, gene expression profile, survival and reproduction	*N2, lin-44(n1792), egl-20(n585), mom-2 (or77), cwn- 1(ok546), cwn-2(ok895), pop-1(q645), mom-4(ne1539), lit-1(ne1991), egl-5(n486)POPTOP(syIs187), and POPFOP(sy974)* L3 and L4 stage	GO was accumulated in germline, while rGO not. GO caused higher reproductive toxicity than rGO. Wnt-MAPK signaling cascade was identified as the possible underlying mechanism induced by GO	Chatterjee et al. (2017)
GO	Synthesized by Hummers' method Size: ~40-60 nm Zeta potential: −22.5 mV	K^+ medium 0.1; 1; 10 and 100 mg L^{-1}	Biodistribution, survival, locomotion, molecular mechanisms	*N2, MT14768, MT17997, MT16696, MT13078, MT16309, MT15020, VT1503, MT15018, MT12969* L1 to adult	GO was found in the pharynx, intestine spermatheca and gonad of *C. elegans*. It may reduce the nematode lifespan and influence the functions of insulin/IGF signaling pathways and germline signaling	Wu et al. (2014b)

(continuation)

Nanomaterial	Features	Exposure conditions	Endpoints	*Strain* *Life stage*	Key biological outcomes	References
GO	Synthesized by modified Hummers' method Length: 72 ± 11 nm Zeta potential: -20.2 mV	K^+ medium 0.1; 0.5; 1; 10 and 100 mg L^{-1}	Growth, reproduction, lifespan, locomotion, biodistribution, ROS, and defecation	*N2* L1 to adult and L4 stage	Prolonged exposure to GO increased the permeable state of the intestinal barrier and the defecation cycle. Moreover, genes involved in nematode development and defecation were altered	Wu et al. (2013b)
Thiolated graphene oxide (GO-SH)	Purchased from JCNANO Thickness: 1 nm Height: 40-50 nm Zeta potential: −18.7 mV	K^+ medium 1,10 and 100 mg L^{-1}	Oxidative stress, locomotion, size, offspring and biodistribution	*N2 e gas-1(fc21)* L1 to adult	GO-SH was accumulated in the nematode body, affecting its intestinal barrier and primary and secondary targeted organs. Prolonged exposure to GO-SH decreased the expression of gas-1 that encodes a subunit of mitochondrial complex I	Ding et al. (2018b)
GO, Graphene Nanoplates (G) and Graphene Quantum Dots (GQDs)	Purchased from Nanjing XFNANO Materials Tech. Co., Ltd. (Jiangsu, China)	K^+ medium 1-100 mg L^{-1}	Lethality, biodistribution, neural damage assessment	*N2, BZ555 (dat-1p::GFP), EG1285 (unc-47p::GFP+ lin-15(+); and DA1240 (eat-4::GFP+ lin-15(+)* L1 to adult	GO reduced the nematode survival, but G and GQDs were not lethal. Three materials declined the body bends, head trashing and pharynx pumping. A down-expression of dat-2::GFP and eat-4::GFP was also observed, indicating that materials can damage the dopaminergic and glutamatergic neurons	Li et al. (2017)
Graphene exfoliated with fetal bovine serum (BSA-G) and sodium cholate (C-G)	Synthesized by the group Zeta potential: BSA-G: −25 mV, Graphene: −25 mV Size: ~500 nm	K^+ medium and NGM 50 – 500 μg mL^{-1}	Survival in acute and chronic study, body size and reproduction	*N2* L1 to adult	Ingestion of graphene flakes at concentrations ranging from 50 to 500 μg mL^{-1} did not reduce the population or survival rate. But GO prolonged (> 10 days) decreased the nematode survival	Pattammattel et al. (2017)
GO coated with polyethylene glycol (GO-PEG)	Synthesized by modified Hummers' method Diameter: 30-40 nm Zeta potential: -10.5 mV	K^+ medium 1 mg mL^{-1}	Molecular mechanisms of the epidermal barrier	*N2, NR222, mlt-7(RNAi)* L1/L2 to adult	In nematodes N2 or NR222, exposure to GO-PEG affected the expression of genes related to epidermal development	Eom et al. (2015)

(continuation)

Nanomaterial	Features	Exposure conditions	Endpoints	*Strain* Life stage	Key biological outcomes	References
Single-walled carbon nanotubes (SWCNT) combined with L-Cysteine	Purchased from NanoLab Diameter: 1.5 nm 95% purity	M9 medium 50; 100 and 250 µg mL^{-1}	Biodistribution, survival rate and body size	*N2* L1 to adult	SWCNTs associated with L-cysteine did not cause toxicity in short and long-term assays	Goodwin et al. (2014)
Pristine SWCNT and amide-modified SWCNT (a-SWCNTs)	Purchased from Sigma Aldrich. SWCNTs (cat no: 652512, length 0.5: 2 mm) and a-SWCNTs (cat no: 685380, length: 0.7-1 mm)	NGM 100; 250 and 500 mg mL^{-1}	Molecular mechanisms, biodistribution, size, survival	*N2* L1 to adult	a-SWCNTs caused significant growth inhibition and reduced *C. elegans* lifespan at the highest doses	Chen et al. (2013)
Multi-walled carbon nanotubes (MWCNT)	Diameter: 10-20 nm Length: 0.5-10 µm Zeta potential: -33.4 mV	K^+ medium 0.1–10 µg L^{-1}	Locomotion behaviour, brood size and germline lncRNAs	*N2* L1 to adult	MWCNT affected the brood size and locomotion behaviour. Expression of 5 lncRNAs was dysregulated by MWCNT	Zhao et al. (2022)
MWCNT and coated MWCNT with BSA	Purchased from CNT Co Diameter: 40-40 nm Length: 1-25 µm Zeta potential: -50.9 mV, and -36.7 mV (BSA)	EPA medium	Lethality, growth, ROS, fertility, reproduction and bioaccumulation	*N2* L1 to adult, and L4 stage	MWCNT was translocated from the intestine to *C. elegans'* secondary targeted organs, causing oxidative stress and affecting reproduction and fertility. However, BSA coating prevented the adverse effects of MWCNT	Côa et al. (2022)
MWCNT	Purchased from Shenzhen Nanotech Port Diameter: 10-20 nm Length: 0.4-4 µm Zeta potential: −32.4 mV	K^+ medium 1 mg mL^{-1}	Insulin signaling pathway	N2, mutant of mir-35(gk262), and transgenic strains of mir-35 and VP303/rde-1(ne219); kbIs7 L1-larvae to adult day-1	MWCNT exposure potentially dysregulates intestinal mir-35 and its direct target MAB-3, which may activate a protective intestinal response of nematodes against the MWCNTs toxicity	Zhao et al. (2019)

(continuation)

Nanomaterial	Features	Exposure conditions	Endpoints	*Strain* Life stage	Key biological outcomes	References
MWCNT	Purchased from Shenzhen Nanotech Diameter: 10 to 20 nm Length: 6-15 µm Zeta potential: -33.4 mV	K^+ medium 1 mg mL^{-1}	Lifespan, locomotion behaviour and molecular mechanisms	*N2* L1 to adult	MWCNT reduced the nematode lifespan and locomotion behaviour. MWCNT also induced an increase in mir-259:GFP in the intestine, pharynx and reproductive organs	Zhuang et al. (2016)
MWCNT oxygenation by hydroxylation (O+), amination (NH2) and carboxylation (COOH)	Purchased from Cheaptubes They have the same diameter (13-18 nm) and length (1-15 µm)	K^+ medium 50 and 100 mg L^{-1}	Survival and reproduction	*N2* L1 – L3 stage, and L1 to adult	Only pristine MWCNT reduced the reproductive capacity of *C. elegans*	Chatterjee et al. (2014)
MWCNT and MWCNT-COOH	Both diameters: ~10-20 nm Zeta potential: MWCNT: -33.2 mV MWCNT-COOH: -23.4 mV	K^+ medium 0.001-1000 µg L^{-1}	Lethality, reproduction, behaviour, ROS, biodistribution and molecular mechanisms	*N2* L1 to adult	MWCNT could damage the intestine and the function of neurons and reproductive organs. However, functionalization with COOH groups decreased their toxicity	Nouara et al. (2013)
Carbon nitride quantum dots (CNQDs)	Synthesized by the solid phase method Diameter: ~ 5 nm	M9 medium and NGM 1; 10 and 100 mg mL^{-1}	Size, pharyngeal pumping, reproduction, lifespan, frequency of body curvature and biodistribution	*N2* L4 stage	CNQDs did not cause toxicity *to C. elegans*. In addition, they showed fluorescence, proving that this material can be applied as a promising in vivo fluorescent imaging reagent	Li et al. (2020)
Nitrogen-doped carbon dots (N-CDs)	Synthesized from the *Malus floribunda* fruit Diameter: 4 nm	S-Basal 25 to 200 µg mL^{-1}	Biodistribution and cell viability	*N2* L1 to adult	N-CDs showed low toxicity and high biocompatibility	Atchudan et al. (2020)
N-CDs	Synthesized from *P. acidus* fruit Diameter: 5 nm	S-Basal 25-200 µg mL^{-1}	Biodistribution and cell viability	- L1 to adult	N-CDs exhibited biocompatibility and were successfully used for high-contrast imaging in *C. elegans*	Atchudan et al. (2019)
Carbon quantum dots (C-QDs)	Prepared from a zeolite precursor modelled with N-methylpiperazine by treatment with calcination and NaOH. Diameter: 2.5 nm	NGM 0.68; 0.22 and 0.04 g L^{-1}	Biodistribution, growth, reproduction, locomotion, pharyngeal pumping	*N2* L1 to adult	C-QDs entered the body via oral pathways and accumulated mainly in tissues, although a small portion could be attributed to internalization due to permeability	Xu et al. (2018)

(continuation)

Nanomaterial	Features	Exposure conditions	Endpoints	*Strain* Life stage	Key biological outcomes	References
C-QDs	Synthesized from aqueous beet extract Diameter: 5-8 nm	NGM 1.5 mg mL^{-1}	Biodistribution	*N2* L1 to adult	NMs showed a fluorescence signal in the intestinal tissues of worms without exerting toxic effects	Singh et al. (2018)
Fullerene of polyhydroxy	Synthesized by the group Diameter: ~ 100 nm	M9 medium and NGM 0.01; 0.1; 1; 10 and 100 µM	Biodistribution, survival, size, pharyngeal pump rate, ROS and molecular mechanisms of ageing	*N2, CF1553, CL2070, TK22, and CF1038* L1 to adult	Fullerene did not inhibit the growth and development of *C. elegans*. Besides, it delayed the ageing process in the nematodes, by regulating the activity of DAF-16 gene	Cong et al. (2015)
Fullerene	Synthesized by the group Diameter: ~100 nm Hydrodynamic size: ~40.1 nm	S-Basal 1; 10 and 100 µg mL^{-1}	Lifespan, reproduction, length, biodistribution and cell apoptosis	*N2, MT1522, MT3002, MT2547, MT5287, and JR1130* L4 to the second generation	Nematode survival was affected by fullerene exposure, as well as its lifespan, reproduction, growth and the functionality of its intestine	Jeong et al. (2012)
Gadolinium-doped fullerene $Gd@C_{82}(OH)_{22}$	Synthesized by the group Diameter: ~22,4 nm	Ultrapure water 0.01; 0.1; 1 and 10 mg mL^{-1}	Lifespan, growth, pharyngeal pump, thermotaxis and reproduction	*N2* L1 to adult	$Gd@C_{82}(OH)_{22}$ was well tolerated by *C. elegans* and has no apparent toxic effects in both adult and juvenile nematodes	Zhang et al. (2011)
Fluorescent nanodiamonds (FND) coated with BSA (BSA-FND) and dextran (Dextran-FND)	Synthesized by the group Diameters: FNDs: ~120 nm BSA-FNDs: ~170 nm Dextran-FNDs: ~290 nm	NGM 1 mg mL^{-1}	Offspring, lifespan, oxidative stress and biodistribution	*N2* L4 stage	Lifespan, offspring and ROS parameters demonstrated that FNDs did not cause any change in the organisms' longevity and reproduction	Mohan et al. (2010)
Graphite nanoplates (GNPs)	Synthesized by the group Thickness: ~9nm	Ultrapure water 50; 100 and 250 µg mL^{-1}	Mortality, size, genotoxicity and biodistribution	*N2 L1 to adult*	GNPs did not cause mortality and genotoxicity, although they have accumulated in the intestinal and reproductive region of nematode	Zanni et al. (2012)

2.5. Tools for evaluating nanomaterials internalization and biodistribution in *Caenorhabditis elegans*

Evaluating the uptake and biodistribution of NMs in the organisms is not only important for our understanding of their potential adverse effects but also for assessing their behaviour in the environment and ecosystem. Some robust techniques to investigate the NMs uptake by *C. elegans* will be presented; They have advantages and limitations that were raised and discussed in Table 1.3. Although some of them are unsuitable for specifically analysing carbon nanomaterials, they can be explored using markers such as fluorescent probes and dyes. Therefore, they were also shown in this topic.

Confocal Raman spectroscopy is one of the promising instruments to non-destructively evaluate the spatial distribution of NMs in *C. elegans* (Eliášová Sohová et al., 2018; Iannarelli et al., 2016; Kim et al., 2020; Tian et al., 2017). It does not require labels because carbon nanomaterials exhibit exclusive spectral signatures that are analysed by laser light focused onto the sample by a microscope objective. On the other hand, it provides semi-quantitative information, and mappings are time-consuming.

Figure 2 shows an example where GO accumulation in *C. elegans* was mapped. GO was found in all parts of the nematode body after 2 h of exposure, while after 48 h, the reproductive organs were the most affected region by GO accumulation (Kim et al., 2018). In another study, confocal Raman spectroscopy results indicated the presence of GO in the pharynx and intestine. In addition, even after nematodes were transferred to a medium without GO, this material remained accumulated in these tissues (Kim et al., 2020).

Confocal Raman spectroscopy was also helpful to identify the translocation of GO and MWCNT in a study of our research group. GO and MWCNT were uptake and transferred from the *C. elegans* intestine to the gonads. They also reached the nematode head and eggs. After 2 h of food resumption, GO and MWCNT still remained in the intestine. This NM translocation and long-time of retention were associated with the negative effect of both materials exerted on nematode fertility, reproduction and growth (Côa et al., 2022). Iannarelli et al. (2016) also investigated the behaviour of TiO_2 NPs in *C. elegans* by confocal Raman spectroscopy. They described that these NPs accumulated in its terminal bulb and were transferred to the reproductive system (vulval region and eggs).

Table 1.3 - Summary of promising tools to study carbon nanomaterials fate, uptake and biodistribution in *C. elegans.*

Detection method or technique	Obtained information	Advantages	Limitations	Previous studies performed with these tools
Optical microscopy	Internalization and biodistribution	Easy sample preparation, fast and simple analysis	Low spatial resolution (>300 nm), only qualitative, limited to carbon nanomaterials marked with dyes or that significantly accumulate inside the nematode	Han et al. (2019); Li et al. (2017); Yang et al. (2015)
Fluorescence microscopy	Internalization and biodistribution	Easy sample preparation, low cost, high contrast and straightforward operation	Low spatial resolution (>300 nm), non-quantitative and organisms can be affected by the exposure light from the fluorescence microscopy. In addition, it is restricted to fluorescent CNMs or CNMs labelled with fluorophores	Atchudan et al. (2019); Cong et al. (2019); Goodwin et al. (2014); Hendler-Neumark et al. (2021); Li et al. (2020); Li et al. (2014); Li et al. (2017); Mohan et al. (2010); Singh et al. (2018); Sonkar et al. (2012); Wu et al. (2016); Wu et al. (2013); Xu et al. (2018)
Laser scanning confocal microscopy (LSCM)	Uptake and biodistribution	Easy sample preparation, tomographic capacity (reconstruction of 3-D images), ability to track dynamic events	Limited depth (200 µm), expensive in relation to conventional microscopy, complex and slow image processing. Limited to fluorescent carbon nanomaterials or marked with fluorophores. Photodamage and requires a high number of images for robust statistical analysis	Goodwin et al. (2014); Guo et al. (2020) Lu et al. (2022); Pramanik et al. (2016); Qu et al. (2011); Singh et al. (2018); Sivaselvam et al. (2020); Sonkar et al. (2012); Xu et al. (2018); Yang et al. (2015); Zhang et al. (2012); Zhao et al. (2018)
Enhanced dark-field hyperspectral microscopy (EDFM-HSI)	Biodistribution (in the nematode cuticle, and tissues in some cases)	Minimal sample preparation, non-destructive, simple personnel training, and ability to combine imaging with spectroscopy	Lack of spatial resolution, time-consuming, computer of the equipment must be fast, the image acquisition is not automated, and the analysis requires ultraclean glass slides. The spectrum of analyzed material needs to be distinct from the *C. elegans* spectrum. There is not a standard spectrum library. And there are many potential artifacts of analysis	Fakhrullina et al. (2015); Bortolozzo et al. (2021); Stavitskaya et al. (2021)
Scanning electron microscopy (SEM)	Interaction of CNMs with nematode cuticle	It is successful applied when CNMs are visible on exterior surfaces, and it can be combined with energy dispersive X-ray spectrometer (EDS) to analyze the elemental composition	Low spatial resolution, only qualitative information, and it is not accurate to identify carbon nanomaterials	-

Detection method or technique	Obtained information	Advantages	Limitations	Previous studies performed with these tools
Transmission electronic microscopy (TEM)	Biodistribution (cellular level)	High resolution (> 1 nm), intracellular location and translocation routes	Non-quantitative, low contrast for carbon nanomaterials and requires complex sample preparation as ultrathin sections need to be prepared (50-100 nm) and cellular structures need to be contrasted	Wu et al. (2013b); Yang et al. (2015)
Confocal Raman spectroscopy	Internalization and biodistribution (in organs and tissues)	Easy sample preparation, simple analysis, it does not require labels, and enables CNMs characterization	Time-consuming, semi-quantitative information or requires calibration for quantitative analysis, and limited ability to detect trace quantities	Côa et al. (2022); Kim et al. (2020); Kim et al. (2018); Singh et al. (2018)
Inductively coupled plasma-mass-spectroscopy (ICP-MS)	CNMs internalization (whole body)	Allows the detection and quantification of CNMs coordinated or incorporated with metal ion, in a high level of accuracy (ppt levels)	Requires coordination or incorporation of metal ion into CNMs structure, which involves choosing metals that are not natural constituents of *C. elegans.* Necessary to apply acid digestion before the analysis in which contaminations could lead to interfering signals. Coordinated metal can be released from CNMs structure during the exposure or inside the nematode gut leading to misinterpretations	-
Autoradiograph	Biodistribution of 14^C labelling after tissue biological oxidation	Allows analyzing and quantifying the spatial distribution of CNMs by the radioactivity signal at low detection limits (ppb to ppt levels). And it is valuable to identify degradation products	Requires a special, expensive and dangerous synthesis. Most CNMs are not radiolabeled in the real world, therefore, sometimes the analysis are outside of reality. This technique can lead to misinterpretation because radioactive isotope can become separated from CNMs through nematode body	-
Liquid scintillation counting (LSC)	Biodistribution of 14^C labelling after tissue biological oxidation	Quantitative (ppt to ppb levels) and permits the detection of biotransformed CNMs in the tissues	Expensive and dangerous CNMs synthesis. Requires calibrating the instrument with radioactive carbon-14 chemicals and a minimal amount of sample is required to release enough gas for the analysis	-
Microwave-induced heating system	Carbon nanotubes detection and quantification in the organisms	Low cost, applicable for MWCNT quantification as it absorbs the microwave radiation, and the CNT concentration is proportional to the increase temperature observed	Non-commercially available, not very suitable for graphene materials family and requires calibrating the instrument	-

Figure 2 - Raman spectroscopy to assess graphene oxide internalization by *C. elegans*: A) Nematodes exposed to GO for 3 h and B) for 48 h and respective Raman spectrum at different points along the body.

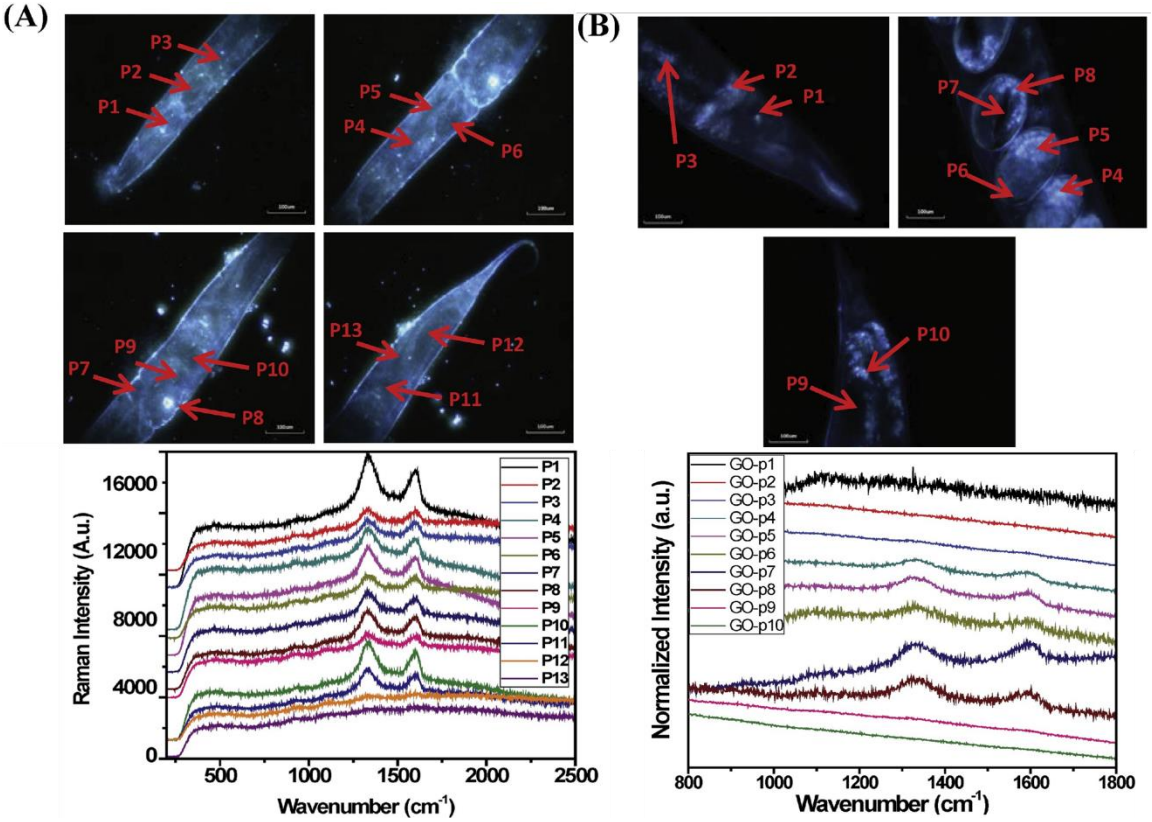

Reproduced from Kim et al., 2018.

Enhanced darkfield hyperspectral microscopy (EDHM) is an instrument that combines hyperspectral imaging with state-of-the-art optics and computer software (Roth et al., 2015). It is ideal for locating individual NPs and aggregates in complex samples through optical and spectroscopic identification in a fast, easy, cheap and non-destructive way. Moreover, compared to other microscopy techniques, EDHM can be performed without extensive personnel training. Nonetheless, the spectrum of *C. elegans* needs to be different from the analysed NM; In addition, there is no standard reference spectral library to support the analysis, and ultraclean glass slides should be used for sample preparation (Fakhrullin et al., 2021).

Some studies have employed EDHM to investigate the interaction of NMs and *C. elegans* (Arnold et al., 2013; Jeong et al., 2018; Luo et al., 2016; Nigamatzyanova and Fakhrullin, 2021). Stavitskaya et al. (2021) confirmed that EDHM was suitable to observe that halloysite nanotubes decorated with quantum dots were uptake by *C. elegans* and accumulated in the pharynx and gut. Our research group recently demonstrated that EDHM is also valuable to assess the uptake of GO and sodium hypochlorite-degraded GO (NaClO-GO) in *C. elegans*.

Our EDHM results (Figure 3) revealed that both were adsorbed in the nematode cuticle and mouth and accumulated in the pharynx and intestine (Bortolozzo et al., 2021).

Figure 3 - Darkfield hyperspectral microscopy images: a) Unexposed *C. elegans* (control group), b) *C. elegans* exposed to GO and c) *C. elegans* exposed to NaClO-GO. Red regions indicate the accumulated nanomaterials.

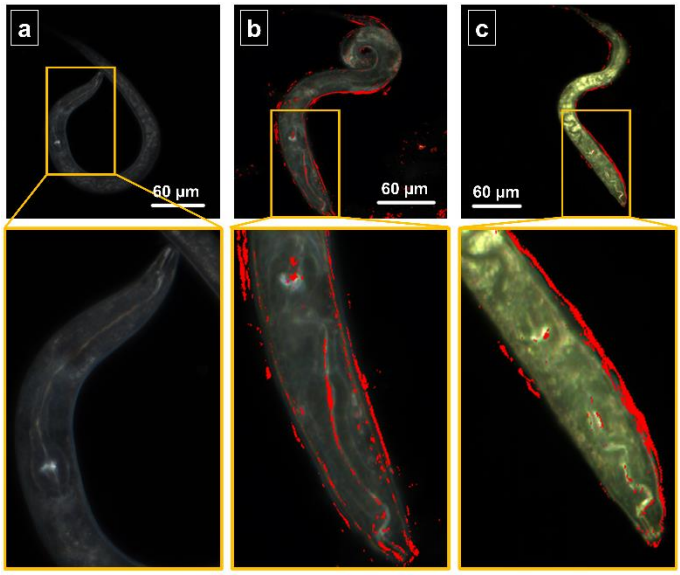

Reproduced from Bortolozzo et al. (2021).

Transmission electron microscopy (TEM) has been also applied to investigate NMs uptake, translocation and accumulation in *C. elegans* with high resolution (Fabig et al., 2019; Gonzalez-Moragas et al., 2015; Yu et al., 2016). It is a non-quantitative technique that requires complex sample preparation as cellular structures need to be contrasted and ultrathin sections prepared (50-100 nm). However, it can contribute to understand the NMs intracellular location and translocation routes, such as endocytosis. By TEM, Yu et al. (2016) noticed that iron oxide NPs (SPIONS) and BSA-coated SPIONS were internalized and remained monodisperse in *C. elegans* lumen for 6 days. Figure 4 demonstrates that TEM can be applied to locate cube-like iron nitride magnetic NPs inside the nematode gut cells (cytosol) (Gubert et al., 2022).

Other microscopy techniques have been advantageous. Scanning electron microscopy has allowed assessing the damages to the morphology of *C. elegans* cuticle, which is a significant barrier against NMs exposure (Angelstorf et al., 2014; Johnson et al., 2021; Kim et al., 2012). Likewise, confocal and fluorescence microscopy has supported several studies with fluorescent NMs or marked with fluorescent staining (Goodwin et al., 2014; Hendler-Neumark et al., 2021; Scharf et al., 2013). However, one negative point is that these fluorescent probes can come loose from the NMs surface, leading to misinterpretations.

Figure 4 – Transmission electron microscopy images of longitudinal and transversal cuts of *C. elegans* at the L1 stage (A, B, C) and L4 (D, E, F). The cuticle is represented by red arrows, lumen by yellow asterisks, inner gut cell by pink asterisks and cube-like iron nitride magnetic NPs by blue arrows.

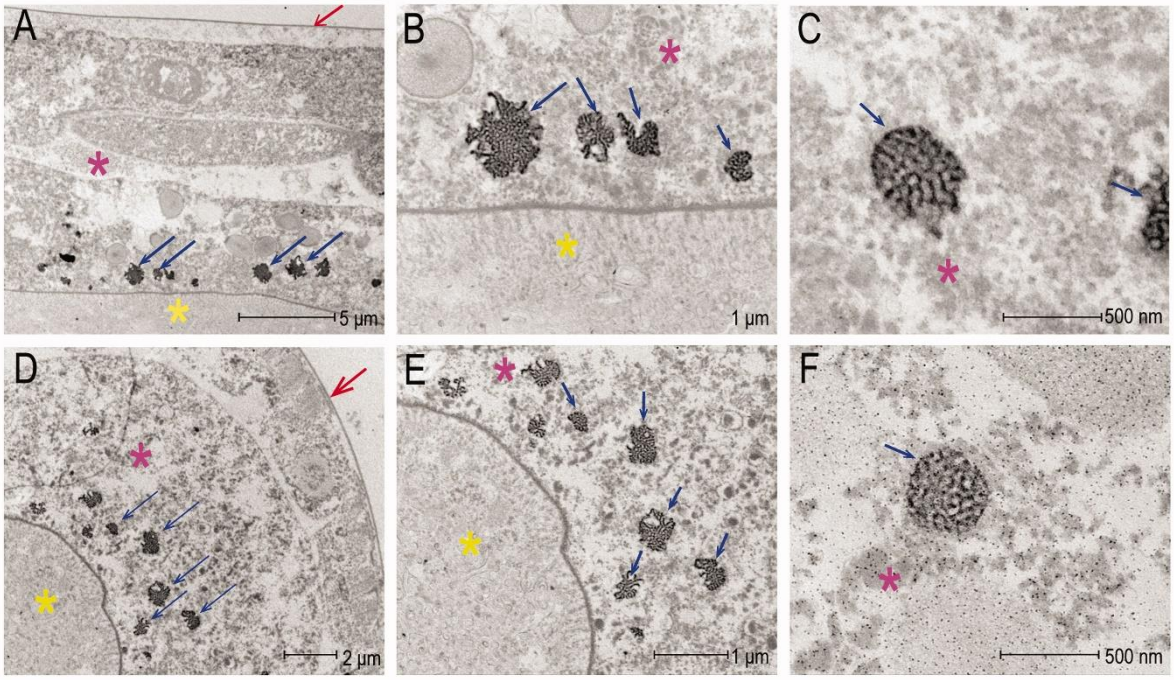

Reproduced from Gubert et al. (2022).

X-ray fluorescence (µ-XRF) is an advanced non-destructive technique for multi-elemental analysis with a high spatial resolution (Majumdar et al., 2012). Due to the high sensitivity, µ-XRF has been used to elucidate the NMs distribution within several organisms (Khan et al., 2019; Li et al., 2015). At synchrotron sources, µ-XRF can be also combined with other methods, such as X-ray absorption spectroscopy (XAS) or X-ray diffraction (XRD), providing speciation information, such as element oxidation state.

Figure 5 shows an example where µ-XRF was applied to study the biodistribution of CeO_2 NPs in *C. elegans*. Although a high abundance of Ce has been found in the intestinal lumen, Ce was not translocated across the intestinal barrier to other tissues (Figure 5A), and a low Ce retention was observed after the depuration process (Figure 5B). In another work, µ-XRF analysis indicated that QDs were uptake and accumulated in the alimentary system of nematodes. At prolonged exposure, QDs were translocated to the reproductive system (uterus and vulva), accumulated and expelled from the vulva. Due to this, damaged eggs and difficulties in egg laying were observed (Qu et al, 2011).

Figure 5 – XRF elemental distribution maps of a) undepurated *C. elegans* exposed to CeO_2 NPs and b) depurated nematode. Red is indicative of Ce accumulation, blue of Zn and green of Fe.

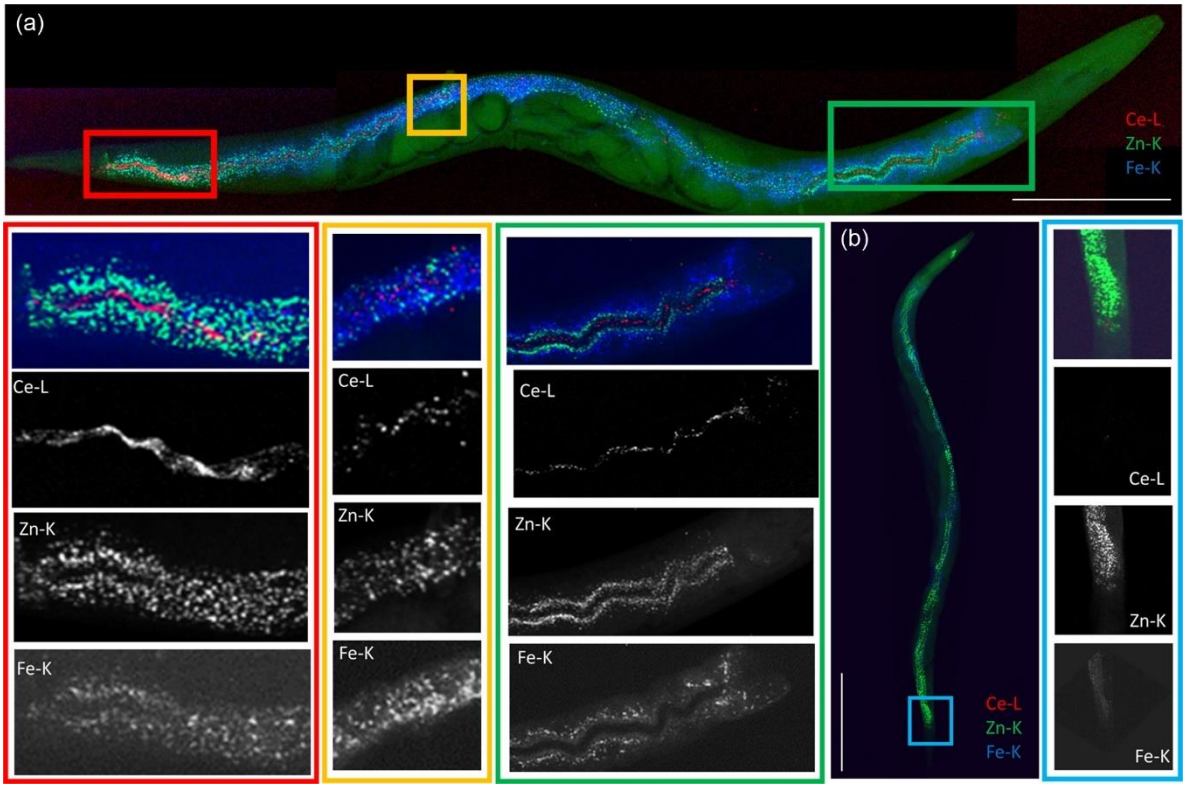

Reproduced from Rossbach et al. (2022).

It is worth remembering that each of these tools has strengths and limitations. The most suitable technique depends on the type of NM studied, the information aimed, and the equipment availability. Adopting a multi-analytical approach from the materials and biological sciences is recommended because, generally, just one technique is not enough to fully comprehend NMs fate in organisms.

2.6. Conclusion and perspectives

As a model system, *C. elegans* is a suitable organism to perform nanotoxicity assays because it presents a small size, a transparent body, two or three weeks of lifespan, genome sequenced, high homology with humans and availability of several transgenic strains. In addition, some toxicity pathways are conserved between this nematode and humans. These advantages make *C. elegans* a valuable animal to elucidate the adverse effects of NMs and toxicity mechanisms, offering practical benefits concerning other animals.

Significant advances have been made towards understanding carbon nanomaterials toxicity. Overall, graphene-based materials, carbon nanotubes and fullerene are toxic to *C. elegans* as they can affect its survival, reproduction, growth, fertility, germline cells, the functionality of the intestinal barrier and neurons, as well as deregulate the expression of some genes. Although, strategies to reduce their toxicity have been presented in the literature and should be considered towards a responsible and safe application.

Some aspects still require to be investigated: i) the transgenerational effects of carbon NMs; ii) the possible transformations that these materials may suffer inside the nematode with emphasis on chemical and physical analyses and toxicological responses; iii) the influence of *E. coli* on carbon NMs behaviour, fate and toxicity; iii) the excreted products after carbon NMs ingestion; iv) their transport in the food chain; vi) a lack of data compilation and raw data disclosure. Furthermore, the current gaps in methodologies demonstrate that some aspects need to be revisited, considering new facets that have been described; The available tools to assess the NMs translocation and accumulation in *C. elegans* should be better exploited.

We hope these outstanding questions can encourage scientists to take advantage of the possibilities offered by *C. elegans* to continue elevating the studies to a higher level of knowledge in the coming decades. In addition, these perspectives open the door for new studies that would help toxicologists, society and regulation agencies to further predict and understand the effects of NMs on organisms.

References[3]

Ahmed, F., Rodrigues, D.F., 2013. Investigation of acute effects of graphene oxide on wastewater microbial community: A case study. J Hazard Mater 256–257, 33–39. https://doi.org/10.1016/j.jhazmat.2013.03.064.

Angelstorf, J.S., Ahlf, W., von der Kammer, F., Heise, S., 2014. Impact of particle size and light exposure on the effects of TiO_2 nanoparticles on Caenorhabditis elegans. Environ Toxicol Chem 33, 2288–2296. https://doi.org/10.1002/etc.2674.

Arnold, M.C., Badireddy, A.R., Wiesner, M.R., di Giulio, R.T., Meyer, J.N., 2013. Cerium oxide nanoparticles are more toxic than equimolar bulk cerium oxide in Caenorhabditis elegans. Arch Environ Contam Toxicol 65, 224–233. https://doi.org/10.1007/s00244-013-9905-5.

Atchudan, R., Edison, T.N.J.I., Perumal, S., Clament Sagaya Selvam, N., Lee, Y.R., 2019. Green synthesized multiple fluorescent nitrogen-doped carbon quantum dots as an efficient label-free optical nanoprobe for in vivo live-cell imaging. J Photochem Photobiol A Chem 372, 99–107. https://doi.org/10.1016/j.jphotochem.2018.12.011.

[3] Prepared according to Elsevier guide.

Atchudan, R., Jebakumar Immanuel Edison, T.N., Perumal, S., Vinodh, R., Lee, Y.R., 2020. Multicolor-emitting carbon dots from Malus floribunda and their interaction with Caenorhabditis elegans. Mater Lett 261, 127153. https://doi.org/10.1016/j.matlet.2019.127153.

Bortolozzo, L.S., Côa, F., Khan, L.U., Medeiros, A.M.Z., Da Silva, G.H., Delite, F.S., Strauss, M., Martinez, D.S.T., 2021. Mitigation of graphene oxide toxicity in *C. elegans* after chemical degradation with sodium hypochlorite. Chemosphere 278, 130421. https://doi.org/10.1016/j.chemosphere.2021.130421.

Bosch, S., Botha, T.L., Jordaan, A., Maboeta, M., Wepener, V., 2018. Sublethal effects of ionic and nanogold on the nematode Caenorhabditis elegans. J Toxicol, 2018. https://doi.org/10.1155/2018/6218193.

Castro, V.L., Clemente, Z., Jonsson, C., Silva, M., Vallim, J.H., de Medeiros, A.M.Z., Martinez, D.S.T., 2018. Nanoecotoxicity assessment of graphene oxide and its relationship with humic acid. Environ Toxicol Chem 37, 1998–2012. https://doi.org/10.1002/etc.4145.

Charan, S., Chien, F.C., Singh, N., Kuo, C.W., Chen, P., 2011. Development of lipid targeting Raman probes for in vivo imaging of Caenorhabditis elegans. Chemistry - A European Journal 17, 5165–5170. https://doi.org/10.1002/chem.201002896.

Chatterjee, N., Yang, J., Kim, H.M., Jo, E., Kim, P.J., Choi, K., Choi, J., 2014. Potential toxicity of differential functionalized multiwalled carbon nanotubes (MWCNT) in human cell line (BEAS2B) and caenorhabditis elegans. Journal of Toxicology and Environmental Health - Part A: Current Issues 77, 1399–1408. https://doi.org/10.1080/15287394.2014.951756.

Chatterjee, N., Young-ho, K., Jisu, Y., P, R.C., Woo, J.S., Jinhee, C., 2017. A systems toxicology approach reveals the Wnt-MAPK crosstalk pathway mediated reproductive failure in Caenorhabditis elegans exposed to graphene oxide (GO) but not to reduced graphene oxide (rGO). Nanotoxicology 11, 76–86. https://doi.org/10.1080/17435390.2016.1267273.

Chen, H., Li, H., Wang, D., 2017. Graphene Oxide Dysregulates Neuroligin / NLG-1-Mediated Molecular Signaling in Interneurons in Caenorhabditis elegans. Scientific Reports 7, 1–14. https://doi.org/10.1038/srep41655.

Chen, H., Wang, C., Li, H., Ma, R., Yu, Z., Li, L., Xiang, M., Chen, X., Hua, X., Yu, Y., 2019. A review of toxicity induced by persistent organic pollutants (POPs) and endocrine-disrupting chemicals (EDCs) in the nematode Caenorhabditis elegans. J Environ Manage 237, 519–525. https://doi.org/10.1016/j.jenvman.2019.02.102.

Chen, P.H., Hsiao, K.M., Chou, C.C., 2013. Molecular characterization of toxicity mechanism of single-walled carbon nanotubes. Biomaterials 34, 5661–5669. https://doi.org/10.1016/j.biomaterials.2013.03.093.

Chowdhury, S.M., Dasgupta, S., McElroy, A.E., Sitharaman, B., 2014. Structural disruption increases toxicity of graphene nanoribbons. Journal of Applied Toxicology 34, 1235–1246. https://doi.org/10.1002/jat.3066.

Côa, F., Delite, F. de S., Strauss, M., Martinez, D.S.T., 2022. Toxicity mitigation and biodistribution of albumin corona coated graphene oxide and carbon nanotubes in Caenorhabditis elegans. NanoImpact 27, 100413. https://doi.org/10.1016/j.impact.2022.100413.

Collin, B., Oostveen, E., Tsyusko, O. v., Unrine, J.M., 2014. Influence of Natural Organic Matter and Surface Charge on the Toxicity and Bioaccumulation of Functionalized Ceria Nanoparticles in Caenorhabditis elegans. Environ Sci Technol 48, 1280–1289. https://doi.org/10.1021/es404503c.

Cong, S., Liu, K., Qiao, F., Song, Y., & Tan, M. (2019). Biocompatible fluorescent carbon dots derived from roast duck for in vitro cellular and in vivo C. elegans bio-imaging. Methods, 168, 76–83. https://doi.org/10.1016/j.ymeth.2019.07.007

Cong, W., Wang, P., Qu, Y., Tang, J., Bai, R., Zhao, Y., Chen, C., Bi, X., 2015. Biomaterials Evaluation of the influence of fullerenol on aging and stress resistance using Caenorhabditis elegans. Biomaterials 42, 78–86. https://doi.org/10.1016/j.biomaterials.2014.11.048.

Cornaglia, M., Lehnert, T., Gijs, M.A.M., 2017. Microfluidic systems for high-throughput and high-content screening using the nematode Caenorhabditis elegans. Lab Chip 17, 3736–3759. https://doi.org/10.1039/C7LC00509A.

Ding, X., Rui, Q., Wang, D., 2018a. Functional disruption in epidermal barrier enhances toxicity and accumulation of graphene oxide. Ecotoxicol Environ Saf 163, 456–464. https://doi.org/10.1016/j.ecoenv.2018.07.102.

Ding, X., Wang, J., Rui, Q., Wang, D., 2018b. Long-term exposure to thiolated graphene oxide in the range of μg/L induces toxicity in nematode Caenorhabditis elegans. Science of the Total Environment 616–617, 29–37. https://doi.org/10.1016/j.scitotenv.2017.10.307.

Doke, S.K., Dhawale, S.C., 2015. Alternatives to animal testing: A review. Saudi Pharmaceutical Journal 23, 223–229. https://doi.org/10.1016/j.jsps.2013.11.002.

Eliášová Sohová, M., Bodík, M., Siffalovic, P., Bugárová, N., Labudová, M., Zaťovičová, M., Hianik, T., Omastová, M., Majková, E., Jergel, M., Pastoreková, S., 2018. Label-free tracking of nanosized graphene oxide cellular uptake by confocal Raman microscopy. Analyst 143, 3686–3692. https://doi.org/10.1039/c8an00225h.

Ellegaard-Jensen, L., Jensen, K.A., Johansen, A., 2012. Nano-silver induces dose-response effects on the nematode Caenorhabditis elegans. Ecotoxicol Environ Saf 80, 216–223. https://doi.org/10.1016/j.ecoenv.2012.03.003.

Eom, H.J., Roca, C.P., Roh, J.Y., Chatterjee, N., Jeong, J.S., Shim, I., Kim, H.M., Kim, P.J., Choi, K., Giralt, F., Choi, J., 2015. A systems toxicology approach on the mechanism of uptake and toxicity of MWCNT in Caenorhabditis elegans. Chem Biol Interact 239, 153–163. https://doi.org/10.1016/j.cbi.2015.06.031.

Fabig, G., Schwarz, A., Striese, C., Laue, M., Müller-Reichert, T., 2019. In situ analysis of male meiosis in *C. elegans*. Methods Cell Biol 152, 119–134. https://doi.org/10.1016/bs.mcb.2019.03.013.

Fakhrullina, G. I., Akhatova, F. S., Lvov, Y. M., & Fakhrullin, R. F., 2015. Toxicity of halloysite clay nanotubes in vivo: a Caenorhabditis elegans study. Environmental Science: Nano, 2(1), 54–59. https://doi.org/10.1039/C4EN00135D

Fakhrullin, R., Nigamatzyanova, L., Fakhrullina, G., 2021. Dark-field/hyperspectral microscopy for detecting nanoscale particles in environmental nanotoxicology research. Sci Total Environ 772, 145478. https://doi.org/10.1016/j.scitotenv.2021.145478.

Gao, Y., Liu, N., Chen, C., Luo, Y., Li, Y., Zhang, Z., Zhao, Y., 2008. Mapping technique for biodistribution of elements in a model organism, Caenorhabditis elegans, after exposure to copper nanoparticles with microbeam synchrotron radiation X-ray fluorescence. J Anal Atom Spectrom 1121–1124. https://doi.org/10.1039/b802338g.

Geitner, N.K., Ogilvie Hendren, C., Cornelis, G., Kaegi, R., Lead, J.R., Lowry, G. V., Lynch, I., Nowack, B., Petersen, E., Bernhardt, E., Brown, S., Chen, W., de Garidel-Thoron, C., Hanson, J., Harper, S., Jones, K., von der Kammer, F., Kennedy, A., Kidd, J., Matson, C., Metcalfe, C.D., Pedersen, J., Peijnenburg, W.J.G.M., Quik, J.T.K., Rodrigues, S.M., Rose, J., Sayre, P., Simonin, M., Svendsen, C., Tanguay, R., Tefenkji, N., van Teunenbroek, T., Thies, G., Tian, Y., Rice, J., Turner, A., Liu, J., Unrine, J., Vance, M., White, J.C., Wiesner, M.R., 2020. Harmonizing across environmental nanomaterial testing media for increased comparability of nanomaterial datasets. Environ Sci Nano 7, 13–36. https://doi.org/10.1039/C9EN00448C.

Gonzalez-Moragas, L., Maurer, L.L., Harms, V.M., Meyer, J.N., Laromaine, A., Roig, A., 2017. Materials and toxicological approaches to study metal and metal-oxide nanoparticles in the model organism: Caenorhabditis elegans. Mater Horiz 4, 719–746. https://doi.org/10.1039/c7mh00166e.

Gonzalez-Moragas, L., Roig, A., Laromaine, A., 2015a. *C. elegans* as a tool for in vivo nanoparticle assessment. Adv Colloid Interface Sci 219, 10–26. https://doi.org/10.1016/j.cis.2015.02.001.

Gonzalez-Moragas, Laura, Yu, S.-M., Carenza, E., Laromaine, A., Roig, A., 2015b. Protective Effects of Bovine Serum Albumin on Superparamagnetic Iron Oxide Nanoparticles Evaluated in the Nematode Caenorhabditis elegans. ACS Biomater Sci Eng 1, 1129–1138. https://doi.org/10.1021/acsbiomaterials.5b00253.

Guo, T., Cheng, L., Zhao, H., Liu, Y., Yang, Y., Liu, J., & Wu, Q., 2020. The C. elegans miR-235 regulates the toxicity of graphene oxide via targeting the nuclear hormone receptor DAF-12 in the intestine. Scientific Reports, 10(1), 16933. https://doi.org/10.1038/s41598-020-73712-x

Goodwin, C.M., Lewis, G.G., Fiorella, A., Ellison, M.D., Kohn, R., 2014. Synthesis and toxicity testing of cysteine-functionalized single-walled carbon nanotubes with Caenorhabditis elegans. RSC Adv 4, 5893–5900. https://doi.org/10.1039/c3ra44888f.

Goussen, B., Péry, A.R.R., Bonzom, J.M., Beaudouin, R., 2015. Transgenerational Adaptation to Pollution Changes Energy Allocation in Populations of Nematodes. Environ Sci Technol 49, 12500–12508. https://doi.org/10.1021/acs.est.5b03405.

Gubert, G., Gubert, P., Sandes, J.M., Bornhorst, J., Alves, L.C., Quines, C.B., Mosca, D.H., 2022. The nanotoxicity assessment of cube-like iron nitride magnetic nanoparticles at the organismal level of nematode Caenorhabditis elegans. Nanotoxicology 16, 472–483. https://doi.org/10.1080/17435390.2022.2099768.

Han, G., Zhao, J., Zhang, R., Tian, X., Liu, Z., Wang, A., Liu, R., Liu, B., Han, M.Y., Gao, X., Zhang, Z., 2019. Membrane-Penetrating Carbon Quantum Dots for Imaging Nucleic Acid Structures in Live Organisms. Angewandte Chemie - International Edition 58, 7087–7091. https://doi.org/10.1002/anie.201903005.

Hanna, S.K., Bustos, A.M., Peterson, A.W., Reipa, V., Scanlan, D., Coskun, S.H., Cho, T.J., Johnson, M.E., Vincent, A., Nelson, B.C., Winchester, M.R., Elliott, J.T., Petersen, E.J., 2018. Agglomeration of Escherichia coli with positively charged nanoparticles can lead to artifacts in a standard Caenorhabditis elegans toxicity assay 52, 5968–5978. https://doi.org/10.1021/acs.est.7b06099.

Hanna, S.K., Cooksey, G.A., Dong, S., Nelson, B.C., Mao, L., Elliott, J.T., Petersen, E.J., 2016. Feasibility of using a standardized: Caenorhabditis elegans toxicity test to assess nanomaterial toxicity. Environ Sci Nano 3, 1080–1089. https://doi.org/10.1039/c6en00105j.

Hendler-Neumark, A., Wulf, V., Bisker, G., 2021. In vivo imaging of fluorescent single-walled carbon nanotubes within *C. elegans* nematodes in the near-infrared window. Mater Today Bio 12, 100175. https://doi.org/10.1016/j.mtbio.2021.100175.

Henry, T.B., Menn, F.-M., Fleming, J.T., Wilgus, J., Compton, R.N., Sayler, G.S., 2007. Attributing Effects of Aqueous C60 Nano-Aggregates to Tetrahydrofuran Decomposition Products in Larval Zebrafish by Assessment of Gene Expression. Environ Health Perspect 115, 1059–1065. https://doi.org/10.1289/ehp.9757.

Hu, C.C., Wu, G.H., Lai, S.F., Muthaiyan Shanmugam, M., Hwu, Y., Wagner, O.I., Yen, T.J., 2018. Toxic Effects of Size-tunable Gold Nanoparticles on Caenorhabditis elegans Development and Gene Regulation. Sci Rep 8, 1–10. https://doi.org/10.1038/s41598-018-33585-7.

Hunt, P.R., 2017. The *C. elegans* model in toxicity testing. Journal of Applied Toxicology 37, 50–59. https://doi.org/10.1002/jat.3357.

Iannarelli, L., Giovannozzi, A.M., Morelli, F., Viscotti, F., Bigini, P., Maurino, V., Spoto, G., Martra, G., Ortel, E., Hodoroaba, V.-D., Rossi, A.M., Diomede, L., 2016. Shape engineered TiO_2 nanoparticles in Caenorhabditis elegans: a Raman imaging-based approach to assist tissue-specific toxicological studies. RSC Adv 6, 70501–70509. https://doi.org/10.1039/C6RA09686G.

Jeong, J., Song, T., Chatterjee, N., Choi, I., Cha, Y.K., Choi, J., 2018. Developing adverse outcome pathways on silver nanoparticle-induced reproductive toxicity via oxidative stress in the nematode Caenorhabditis elegans using a Bayesian network model. Nanotoxicology 12, 1182–1197. https://doi.org/10.1080/17435390.2018.1529835.

Jeong, Y., Lee, J., Sik, S., 2012. Apoptosis-mediated in vivo toxicity of hydroxylated fullerene nanoparticles in soil nematode Caenorhabditis elegans. Chemosphere 87, 49–54. https://doi.org/10.1016/j.chemosphere.2011.11.054.

Jiang, Y., Chen, J., Wu, Y., Wang, Q., Li, H., 2016. Sublethal toxicity endpoints of heavy metals to the nematode Caenorhabditis elegans. PLoS One 11, 1–12. https://doi.org/10.1371/journal.pone.0148014.

Jin, L., Dou, T.-T., Chen, J.-Y., Duan, M.-X., Zhen, Q., Wu, H.-Z., Zhao, Y.-L., 2022. Sublethal toxicity of graphene oxide in Caenorhabditis elegans under multi-generational exposure. Ecotoxicol Environ Saf 229, 113064. https://doi.org/10.1016/j.ecoenv.2021.113064.

Johnson, M. E., Hanna, S. K., Montoro, A.R.B., Sims, C. M., Elliott, L. C. C., Lingayat, A., Johnston, A. C., Nikoobakht, B., Elliott, J. T., Holbrook, R. D., Scott, K. C. K., Murphy, K. E., Petersen, E. J., Yu, L. L., Nelson, B. C., 2017. Separation, Sizing, and Quantitation of Engineered Nanoparticles in an Organism Model Using Inductively Coupled Plasma Mass Spectrometry and Image Analysis. ACS Nano 11, 526–540. https://doi.org/10.1021/acsnano.6b06582.

Johnson, M.E., Bennett, J., Montoro Bustos, A.R., Hanna, S.K., Kolmakov, A., Sharp, N., Petersen, E.J., Lapasset, P.E., Sims, C.M., Murphy, K.E., Nelson, B.C., 2021. Combining secondary ion mass spectrometry image depth profiling and single particle inductively coupled plasma mass spectrometry to investigate the uptake and biodistribution of gold nanoparticles in Caenorhabditis elegans. Anal Chim Acta 1175, 338671. https://doi.org/10.1016/j.aca.2021.338671.

Johnson, M.E., Montoro Bustos, A.R., Hanna, S.K., Petersen, E.J., Murphy, K.E., Yu, L.L., Nelson, B.C., Winchester, M.R., 2017. Sucrose density gradient centrifugation for efficient separation of engineered nanoparticles from a model organism, *Caenorhabditis elegans*. Gaithersburg, MD. https://doi.org/10.6028/NIST.SP.1200-24.

Khan, L.U., Da Silva, G.H., De Medeiros, A.M.Z., Khan, Z.U., Gidlund, M., Brito, H.F., Moscoso-Londoño, O., Muraca, D., Knobel, M., Pérez, C.A., Martinez, D.S.T., 2019. Fe3O4@SiO2 Nanoparticles Concurrently Coated with Chitosan and GdOF:Ce3+,Tb3+ Luminophore for Bioimaging: Toxicity Evaluation in the Zebrafish Model. ACS Appl Nano Mater 2, 3414–3425. https://doi.org/10.1021/acsanm.9b00339.

Kim, J., Shirasawa, T., Miyamoto, Y., 2010. The effect of TAT conjugated platinum nanoparticles on lifespan in a nematode Caenorhabditis elegans model. Biomaterials 31, 5849–5854. https://doi.org/10.1016/j.biomaterials.2010.03.077.

Kim, M., Eom, H.J., Choi, I., Hong, J., Choi, J., 2020. Graphene oxide-induced neurotoxicity on neurotransmitters, AFD neurons and locomotive behavior in Caenorhabditis elegans. Neurotoxicology 77, 30–39. https://doi.org/10.1016/j.neuro.2019.12.011.

Kim, Y., Jeong, J., Yang, J., Joo, S., Hong, J., Choi, J., 2018. Graphene oxide nano-bio interaction induces inhibition of spermatogenesis and disturbance of fatty acid metabolism in the nematode Caenorhabditis elegans. Toxicology 410, 83–95. https://doi.org/10.1016/j.tox.2018.09.006.

Kim, S.W., Nam, S.H., An, Y.J., 2012. Interaction of Silver Nanoparticles with Biological Surfaces of Caenorhabditis elegans. Ecotoxicol Environ Saf 77, 64–70. https://doi.org/10.1016/j.ecoenv.2011.10.023.

Lee, S.H., Kim, D.Y., Lee, J., Lee, S.B., Han, H., Kim, Y.Y., Mun, S.C., Im, S.H., Kim, T.-H., Park, O.O., 2019. Synthesis of Single-Crystalline Hexagonal Graphene Quantum Dots from Solution Chemistry. Nano Lett 19, 5437-5442 https://doi.org/10.1021/acs.nanolett.9b01940.

Lei, L., Liu, M., Song, Y., Lu, S., Hu, J., Cao, C., Xie, B., Shi, H., He, D., 2018. Polystyrene (nano)microplastics cause size-dependent neurotoxicity, oxidative damage and other adverse effects in Caenorhabditis elegans. Environ Sci Nano 5, 2009–2020. https://doi.org/10.1039/C8EN00412A.

Leung, M.C.K., Williams, P.L., Benedetto, A., Au, C., Helmcke, K.J., Aschner, M., Meyer, J.N., 2008. Caenorhabditis elegans: An emerging model in biomedical and environmental toxicology. Toxicological Sciences 106, 5–28. https://doi.org/10.1093/toxsci/kfn121.

Li, H., Fei, C., Yang, D., Tan, C., Chen, Z., Wang, J., Wang, G., Fan, H., Yao, H., Wang, C., Chong, H., 2020. Synthesis of carbon nitride quantum dots and biocompatibility evaluation using C. elegans as a model organism. Mater Today Commun 25, 101383. https://doi.org/10.1016/j.mtcomm.2020.101383.

Li, P., Xu, T., Wu, S., Lei, L., He, D., 2017. Chronic exposure to graphene-based nanomaterials induces behavioral deficits and neural damage in Caenorhabditis elegans 1140–1150. https://doi.org/10.1002/jat.3468.

Li, Y., Li, Y.-F., Zhao, J., Gao, Y., Chen, C., 2015. Accumulation and transformation of nanomaterials in ecological model organisms investigated by using synchrotron radiation techniques. J Anal Atom Spectrom 30, 2038–2047. https://doi.org/10.1039/C5JA00235D.

Liu, F., Jang, M.H., Ha, H.D., Kim, J.H., Cho, Y.H., Seo, T.S., 2013. Facile synthetic method for pristine graphene quantum dots and graphene oxide quantum dots: Origin of blue and green luminescence. Advanced Materials 25, 3657–3662. https://doi.org/10.1002/adma.201300233.

Liu, P., Shao, H., Kong, Y., Wang, D., 2020. Effect of graphene oxide exposure on intestinal Wnt signaling in nematode Caenorhabditis elegans. J Environ Sci (China) 88, 200–208. https://doi.org/10.1016/j.jes.2019.09.002.

Lu, J.-H., Hou, W.-C., Tsai, M.-H., Chang, Y.-T., & Chao, H.-R., 2022. The Impact of Background-Level Carboxylated Single-Walled Carbon Nanotubes (SWCNTs−COOH) on Induced Toxicity in Caenorhabditis elegans and Human Cells. International Journal of Environmental Research and Public Health, 19(3), 1218. https://doi.org/10.3390/ijerph19031218

Luo, X., Xu, S., Yang, Y., Li, L., Chen, S., Xu, A., Wu, L., 2016. Insights into the Ecotoxicity of Silver Nanoparticles Transferred from Escherichia coli to Caenorhabditis elegans. Sci Rep 6, 36465. https://doi.org/10.1038/srep36465.

Madima, N., Mishra, S.B., Inamuddin, I., Mishra, A.K., 2020. Carbon-based nanomaterials for remediation of organic and inorganic pollutants from wastewater. A review. Environ Chem Lett 18, 1169–1191. https://doi.org/10.1007/s10311-020-01001-0.

Maiti, D., Tong, X., Mou, X., Yang, K., 2019. Carbon-Based Nanomaterials for Biomedical Applications: A Recent Study. Front Pharmacol 9. https://doi.org/10.3389/fphar.2018.01401.

Majumdar, S., Peralta-Videa, J.R., Castillo-Michel, H., Hong, J., Rico, C.M., Gardea-Torresdey, J.L., 2012. Applications of synchrotron μ-XRF to study the distribution of biologically important elements in different environmental matrices: A review. Anal Chim Acta 755, 1–16. https://doi.org/10.1016/j.aca.2012.09.050.

Markiewicz, M., Kumirska, J., Lynch, I., Matzke, M., Köser, J., Bemowsky, S., Docter, D., Stauber, R., Westmeier, D., Stolte, S., 2018. Changing environments and biomolecule coronas: consequences and challenges for the design of environmentally acceptable engineered nanoparticles. Green Chemistry 20, 4133–4168. https://doi.org/10.1039/C8GC01171K.

Martinez, D.S.T. e, Alves, O.L., 2013. Interação de nanomateriais com biossistemas e a nanotoxicologia: na direção de uma regulamentação. Revista da Sociedade Brasileira para o Progresso da Ciência 65, 32–36.

Mendonça, M.C.P., Rizoli, C., Ávila, D.S., Amorim, M.J.B., de Jesus, M.B., 2017. Nanomaterials in the Environment: Perspectives on in Vivo Terrestrial Toxicity Testing. Front Environ Sci 5, 1–6. https://doi.org/10.3389/fenvs.2017.00071.

Mohan, N., Chen, C.S., Hsieh, H.H., Wu, Y.C., Chang, H.C., 2010. In vivo imaging and toxicity assessments of fluorescent nanodiamonds in Caenorhabditis elegans. Nano Lett 10, 3692–3699. https://doi.org/10.1021/nl1021909.

Nigamatzyanova, L., Fakhrullin, R., 2021. Dark-field hyperspectral microscopy for label-free microplastics and nanoplastics detection and identification in vivo: A Caenorhabditis elegans study. Environmental Pollution 271, 116337. https://doi.org/10.1016/j.envpol.2020.116337.

Nivedita, C., Young-ho, K., Jisu, Y., P, R.C., Woo, J.S., Jinhee, C., 2017. A systems toxicology approach reveals the Wnt-MAPK crosstalk pathway mediated reproductive failure in Caenorhabditis elegans exposed to graphene oxide (GO) but not to reduced graphene oxide (rGO). Nanotoxicology 0, 000. https://doi.org/10.1080/17435390.2016.1267273.

Nouara, A., Wu, Q., Li, Y., Tang, M., Wang, H., Zhao, Y., Wang, D., 2013. Carboxylic acid functionalization prevents the translocation of multi-walled carbon nanotubes at predicted environmentally relevant concentrations into targeted organs of nematode Caenorhabditis elegans. Nanoscale 5, 6088. https://doi.org/10.1039/c3nr00847a.

O'Reilly, L.P., Luke, C.J., Perlmutter, D.H., Silverman, G.A., Pak, S.C., 2014. *C. elegans* in high-throughput drug discovery. Adv Drug Deliv Rev 69–70, 247–253. https://doi.org/10.1016/j.addr.2013.12.001.

Organisation for Economic Co-operation and Development, 2020. Guidance document on aquatic and sediment toxicological Testing of nanomaterials.

Pattammattel, A., Pande, P., Kuttappan, D., Puglia, M., Basu, A.K., Amalaradjou, M.A., Kumar, C. V., 2017. Controlling the Graphene-Bio Interface: Dispersions in Animal Sera for Enhanced Stability and Reduced Toxicity. Langmuir 33, 14184–14194. https://doi.org/10.1021/acs.langmuir.7b02854.

Petersen, E.J., Diamond, S.A., Kennedy, A.J., Goss, G.G., Ho, K., Lead, J., Hanna, S.K., Hartmann, N.B., Hund-Rinke, K., Mader, B., Manier, N., Pandard, P., Salinas, E.R., Sayre, P., 2015. Adapting OECD Aquatic Toxicity Tests for Use with Manufactured Nanomaterials: Key Issues and Consensus Recommendations. Environ Sci Technol 49, 9532–9547. https://doi.org/10.1021/acs.est.5b00997.

Piechulek, A., von Mikecz, A., 2018. Life span-resolved nanotoxicology enables identification of age-associated neuromuscular vulnerabilities in the nematode Caenorhabditis elegans. Environmental Pollution 233, 1095–1103. https://doi.org/10.1016/j.envpol.2017.10.012.

Pradhan, S., Hedberg, J., Blomberg, E., Wold, S., Odnevall Wallinder, I., 2016. Effect of sonication on particle dispersion, administered dose and metal release of non-functionalized, non-inert metal nanoparticles. Journal of Nanoparticle Research 18, 285. https://doi.org/10.1007/s11051-016-3597-5.

Pramanik, A., Kole, A. K., Krishnaraj, R. N., Biswas, S., Tiwary, C. S., Varalakshmi, P., Rai, S. K., Kumar, B. A., & Kumbhakar, P., 2016. A Novel Technique of Synthesis of Highly Fluorescent Carbon Nanoparticles from Broth Constituent and In-vivo Bioimaging of C. elegans. Journal of Fluorescence, 26, 1541–1548. https://doi.org/10.1007/s10895-016-1854-8

Qu, M., Li, Y., Wu, Q., Xia, Y., Wang, D., 2017. Neuronal ERK signaling in response to graphene oxide in nematode Caenorhabditis elegans. Nanotoxicology 11, 520–533. https://doi.org/10.1080/17435390.2017.1315190.

Qu, Y., Li, W., Zhou, Y., Liu, X., Zhang, L., Wang, L., Li, Y., Iida, A., Tang, Z., Zhao, Y., Chai, Z., Chen, C., 2011. Full Assessment of Fate and Physiological Behavior of Quantum Dots Utilizing Caenorhabditis elegans as a Model Organism. Nano Lett 11, 3174–3183. https://doi.org/10.1021/nl201391e.

Ren, M., Zhao, L., Ding, X., Krasteva, N., Rui, Q., Wang, D., 2018. Developmental basis for intestinal barrier against the toxicity of graphene oxide. Part Fibre Toxicol 15, 1–16. https://doi.org/10.1186/s12989-018-0262-4.

Rossbach, L.M., Brede, D.A., Nuyts, G., Cagno, S., Olsson, R.M.S., Oughton, D.H., Falkenberg, G., Janssens, K., Lind, O.C., 2022. Synchrotron XRF Analysis Identifies Cerium Accumulation Colocalized with Pharyngeal Deformities in CeO_2 NP-Exposed Caenorhabditis elegans. Environ Sci Technol 56, 5081–5089. https://doi.org/10.1021/acs.est.1c08509.

Roth, G.A., Tahiliani, S., Neu-Baker, N.M., Brenner, S.A., 2015. Hyperspectral microscopy as an analytical tool for nanomaterials. Wiley Interdiscip Rev Nanomed Nanobiotechnol 7, 565–579. https://doi.org/10.1002/wnan.1330.

Scanlan, L.D., Lund, S.P., Coskun, S.H., Hanna, S.K., Johnson, M.E., Sims, C.M., Brignoni, K., Lapasset, P., Petersen, E.J., Elliott, J.T., Nelson, B.C., 2018. Counting Caenorhabditis elegans: Protocol Optimization and Applications for Population Growth and Toxicity Studies in Liquid Medium. Sci Rep 8, 904. https://doi.org/10.1038/s41598-018-19187-3.

Scharf, A., Piechulek, A., von Mikecz, A., 2013. Effect of nanoparticles on the biochemical and behavioral aging phenotype of the nematode Caenorhabditis elegans. ACS Nano 7, 10695–10703. https://doi.org/10.1021/nn403443r.

Selck, H., Handy, R.D., Fernandes, T.F., Klaine, S.J., Petersen, E.J., 2016. Nanomaterials in the aquatic environment: A European Union–United States perspective on the status of ecotoxicity testing, research priorities, and challenges ahead. Environ Toxicol Chem 35, 1055–1067. https://doi.org/10.1002/etc.3385.

Shu, C., Yu, X., Wu, Q., Zhuang, Z., Zhang, W., Wang, D., 2015. Pretreatment with paeonol prevents the adverse effects and alters the translocation of multi-walled carbon nanotubes in nematode Caenorhabditis elegans. RSC Adv 5, 8942–8951. https://doi.org/10.1039/C4RA14377A.

Singh, V., Rawat, K.S., Mishra, S., Baghel, T., Fatima, S., John, A.A., Kalleti, N., Singh, D., Nazir, A., Rath, S.K., Goel, A., 2018. Biocompatible fluorescent carbon quantum dots prepared from beetroot extract for in vivo live imaging in *C. elegans* and BALB/c mice. J Mater Chem B 6, 3366–3371. https://doi.org/10.1039/c8tb00503f.

Sivaselvam, S., Mohankumar, A., Thiruppathi, G., Sundararaj, P., Viswanathan, C., Ponpandian, N., 2020. Engineering the surface of graphene oxide with bovine serum albumin for improved biocompatibility in Caenorhabditis elegans. Nanoscale Adv 2, 5219–5230. https://doi.org/10.1039/D0NA00574F.

Soares, M.V., Charão, M.F., Jacques, M.T., dos Santos, A.L.A., Luchese, C., Pinton, S., Ávila, D.S., 2020. Airborne toluene exposure causes germline apoptosis and neuronal damage that promotes neurobehavioural changes in Caenorhabditis elegans. Environmental Pollution 256, 113406. https://doi.org/10.1016/j.envpol.2019.113406.

Sonkar, S. K., Ghosh, M., Roy, M., Begum, A., & Sarkar, S., 2012. Carbon Nano-Onions as Nontoxic and High-Fluorescence Bioimaging Agent in Food Chain—An In Vivo Study from Unicellular E. coli to Multicellular C. elegans. Materials Express, 2(2), 105–114. https://doi.org/10.1166/mex.2012.1064.

Squiban, B., Kurz, C.L., 2011. *C. elegans*: an all in one model for antimicrobial drug discovery. Curr Drug Targets 12, 967–77. https://doi.org/10.2174/138945011795677854.

Starnes, D.L., Unrine, J.M., Starnes, C.P., Collin, B.E., Oostveen, E.K., Ma, R., Lowry, G. V., Bertsch, P.M., Tsyusko, O. V., 2015. Impact of sulfidation on the bioavailability and toxicity of silver nanoparticles to Caenorhabditis elegans. Environmental Pollution 196, 239–246. https://doi.org/10.1016/j.envpol.2014.10.009.

Stavitskaya, A., Fakhrullina, G., Nigamatzyanova, L., Sitmukhanova, E., Khusnetdenova, E., Fakhrullin, R., Vinokurov, V., 2021. Biodistribution of Quantum Dots-Labelled Halloysite Nanotubes: A Caenorhabditis elegans In Vivo Study. Materials 14, 5469. https://doi.org/10.3390/ma14195469.

Sun, T.Y., Bornhöft, N.A., Hungerbühler, K., Nowack, B., 2016. Dynamic Probabilistic Modeling of Environmental Emissions of Engineered Nanomaterials. Environ Sci Technol 50, 4701–4711. https://doi.org/10.1021/acs.est.5b05828.

Sun, T.Y., Gottschalk, F., Hungerbühler, K., Nowack, B., 2014. Comprehensive probabilistic modelling of environmental emissions of engineered nanomaterials. Environmental Pollution 185, 69–76. https://doi.org/10.1016/j.envpol.2013.10.004.

Tian, L.J., Peng, Y., Chen, D.L., Ma, J.Y., Yu, H.Q., Li, W.W., 2017. Spectral insights into the transformation and distribution of CdSe quantum dots in microorganisms during food-chain transport. Sci Rep 7, 1–7. https://doi.org/10.1038/s41598-017-04694-6.

Wang, M., Nie, Y., Liu, Ying, Dai, H., Wang, J., Si, B., Yang, Z., Cheng, L., Liu, Yun, Chen, S., Xu, A., 2019. Transgenerational effects of diesel particulate matter on Caenorhabditis elegans through maternal and multigenerational exposure. Ecotoxicol Environ Saf 170, 635–643. https://doi.org/10.1016/j.ecoenv.2018.12.027.

Weinhouse, C., Truong, L., Meyer, J.N., Allard, P., 2018. Caenorhabditis elegans as an emerging model system in environmental epigenetics. Environ Mol Mutagen 59, 560–575. https://doi.org/10.1002/em.22203.

Wu, Q., Li, Yinxia, Li, Yiping, Zhao, Y., Ge, L., Wang, H., Wang, D., 2013a. Crucial role of the biological barrier at the primary targeted organs in controlling the translocation and toxicity of multi-walled carbon nanotubes in the nematode Caenorhabditis elegans. Nanoscale 5, 11166. https://doi.org/10.1039/c3nr03917j.

Wu, Q., Yin, L., Li, X., Tang, M., Zhang, T., Wang, D., 2013b. Contributions of altered permeability of intestinal barrier and defecation behavior to toxicity formation from graphene oxide in nematode Caenorhabditis elegans. Nanoscale 5, 9934. https://doi.org/10.1039/c3nr02084c.

Wu, Q., Zhao, Y., Fang, J., Wang, D., 2014a. Immune response is required for the control of in vivo translocation and chronic toxicity of graphene oxide. Nanoscale 6, 5894–5906. https://doi.org/10.1039/c4nr00699b.

Wu, Q., Zhao, Y., Zhao, G., Wang, D., 2014b. MicroRNAs control of in vivo toxicity from graphene oxide in Caenorhabditis elegans. Nanomedicine 10, 1401–1410. https://doi.org/10.1016/j.nano.2014.04.005.

Wu, T., Xu, H., Liang, X., Tang, M., 2019. Caenorhabditis elegans as a complete model organism for biosafety assessments of nanoparticles. Chemosphere 221, 708–726. https://doi.org/10.1016/j.chemosphere.2019.01.021.

Xiao, G., Chen, H., Krasteva, N., Liu, Q., Wang, D., 2018. Identification of interneurons required for the aversive response of Caenorhabditis elegans to graphene oxide. J Nanobiotechnology 16, 1–8. https://doi.org/10.1186/s12951-018-0373-y.

Xiong, H., Pears, C., Woollard, A., 2017. An enhanced *C. elegans* based platform for toxicity assessment. Sci Rep 7, 1–11. https://doi.org/10.1038/s41598-017-10454-3.

Xu, J., Wang, Liping, Mu, Y., Zhang, Y., Wang, M., Wang, Q., Wang, K., Guan, S., Li, J., Wang, Licheng, 2018. Carbon quantum dots as fluorescent probes for imaging and detecting free radicals in *C. elegans*. J Nanosci Nanotechnol 18, 763–771. https://doi.org/10.1166/jnn.2018.15190.

Yang, X., Jiang, C., Hsu-Kim, H., Badireddy, A.R., Dykstra, M., Wiesner, M., Hinton, D.E., Meyer, J.N., 2014. Silver nanoparticle behavior, uptake, and toxicity in Caenorhabditis elegans: Effects of natural organic matter. Environ Sci Technol 48, 3486–3495. https://doi.org/10.1021/es404444n.

Yang, Y., Xu, G., Xu, S., Chen, S., Xu, A., Wu, L., 2018. Effect of ionic strength on bioaccumulation and toxicity of silver nanoparticles in Caenorhabditis elegans. Ecotoxicol Environ Saf 165, 291–298. https://doi.org/10.1016/j.ecoenv.2018.09.008.

Yang, J., Zhao, Y., Wang, Y., Wang, H., & Wang, D., 2015. Toxicity evaluation and translocation of carboxyl functionalized graphene in Caenorhabditis elegans. Toxicology Research, 4(6), 1498–1510. https://doi.org/10.1039/C5TX00137D

Yao, Y., Zhang, T., Tang, M., 2022. A critical review of advances in reproductive toxicity of common nanomaterials to Caenorhabditis elegans and influencing factors. Environmental Pollution 306, 119270. https://doi.org/10.1016/j.envpol.2022.119270.

Yu, S.M., Gonzalez-Moragas, L., Milla, M., Kolovou, A., Santarella-Mellwig, R., Schwab, Y., 2016. Bio-identity and fate of albumin-coated SPIONs evaluated in cells and by the *C. elegans* model. Acta Biomater 43, 348–357. https://doi.org/10.1016/j.actbio.2016.07.024.

Zanni, E., De Bellis, G., Bracciale, M.P., Broggi, A., Santarelli, M.L., Sarto, M.S., Palleschi, C., Uccelletti, D., 2012. Graphite nanoplatelets and Caenorhabditis elegans: Insights from an in vivo model. Nano Lett 12, 2740–2744. https://doi.org/10.1021/nl204388p.

Zemanova, M.A., 2020. Towards more compassionate wildlife research through the 3Rs principles: moving from invasive to non-invasive methods. Wildlife Biol 2020. https://doi.org/10.2981/wlb.00607.

Zhang, W., Wang, C., Li, Z., Lu, Z., Li, Y., Yin, J.-J., Zhou, Y.-T., Gao, X., Fang, Y., Nie, G., & Zhao, Y., 2012. Unraveling Stress-Induced Toxicity Properties of Graphene Oxide and the Underlying Mechanism. Advanced Materials, 24(39), 5391–5397. https://doi.org/10.1002/adma.201202678

Zhang, W., Sun, B., Zhang, L., Zhao, B., Nie, G., Zhao, Y., 2011. Biosafety assessment of Gd@C82(OH)22 nanoparticles on Caenorhabditis elegans. Nanoscale 3, 2636–2641. https://doi.org/10.1039/c1nr10239g.

Zhao, L., Kong, J., Krasteva, N., Wang, D., 2018. Deficit in the epidermal barrier induces toxicity and translocation of PEG modified graphene oxide in nematodes. Toxicol Res (Camb) 7, 1061–1070. https://doi.org/10.1039/C8TX00136G.

Zhao, Y., Jin, L., Wang, Y., Kong, Y., Wang, D., 2019. Prolonged exposure to multi-walled carbon nanotubes dysregulates intestinal mir-35 and its direct target MAB-3 in nematode Caenorhabditis elegans. Sci Rep 9, 1–9. https://doi.org/10.1038/s41598-019-48646-8.

Zhao, Y., Wu, Q., Tang, M., Wang, D., 2014. The in vivo underlying mechanism for recovery response formation in nano-titanium dioxide exposed Caenorhabditis elegans after transfer to the normal condition. Nanomedicine 10, 89–98. https://doi.org/10.1016/j.nano.2013.07.004.

Zhao, Y., Wu, Q., Wang, D., 2016. An epigenetic signal encoded protection mechanism is activated by graphene oxide to inhibit its induced reproductive toxicity in Caenorhabditis elegans. Biomaterials 79, 15–24. https://doi.org/10.1016/j.biomaterials.2015.11.052.

Zhao, Y., Xu, R., Hua, X., Rui, Q., Wang, D., 2022. Multi-walled carbon nanotubes induce transgenerational toxicity associated with activation of germline long non-coding RNA linc-7 in *C. elegans*. Chemosphere 301, 134687. https://doi.org/10.1016/j.chemosphere.2022.134687.

Zhi, L., Qu, M., Ren, M., Zhao, L., Li, Y., Wang, D., 2017. Graphene oxide induces canonical Wnt/β-catenin signaling-dependent toxicity in Caenorhabditis elegans. Carbon N Y 113, 122–131. https://doi.org/10.1016/j.carbon.2016.11.041.

Zhuang, Z., Li, M., Liu, H., Luo, L., Gu, W., Wu, Q., Wang, D., 2016. Function of RSKS-1-AAK-2-DAF-16 signaling cascade in enhancing toxicity of multi-walled carbon nanotubes can be suppressed by mir-259 activation in Caenorhabditis elegans. Sci Rep 6, 1–13. https://doi.org/10.1038/srep32409.

3. CHAPTER 3. TOXICITY MITIGATION AND BIODISTRIBUTION OF ALBUMIN CORONA COATED GRAPHENE OXIDE AND CARBON NANOTUBES IN *Caenorhabditis elegans* [4]

Highlights

- Albumin corona changed surface and colloidal properties of carbon nanomaterials.
- Acute toxicity of carbon nanomaterials to *C. elegans* was mitigated by albumin corona.
- Albumin corona mitigated chronic toxicity only for carbon nanotubes in *C. elegans*.
- Biodistribution is dependent on carbon nanomaterial structures and corona formation.
- Confocal Raman spectroscopy is very useful to monitor nanomaterials biodistribution.

Graphical abstract

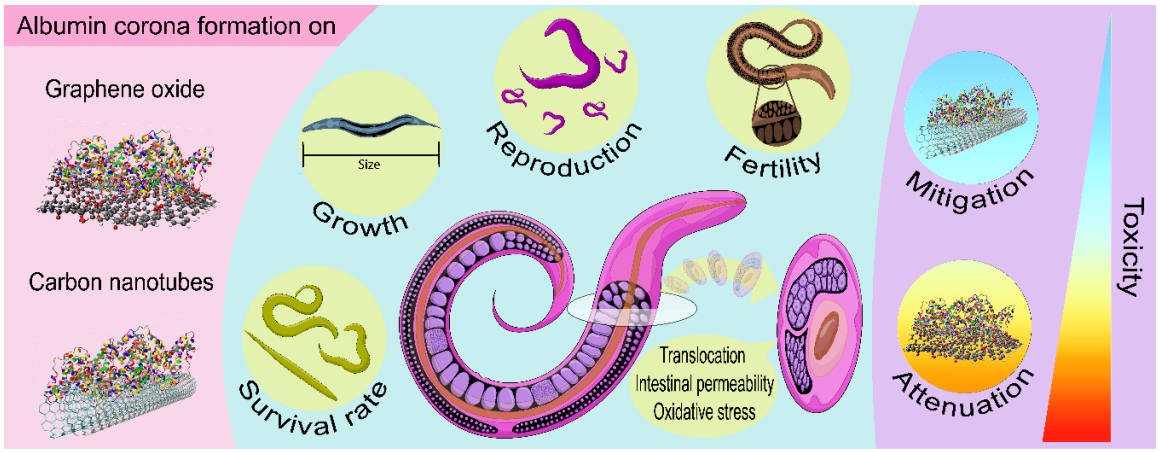

Abstract

In this work, the toxicity and biodistribution of graphene oxide (GO) and oxidized multi-walled carbon nanotubes (MWCNT) were investigated in *Caenorhabditis elegans*. Bovine serum albumin (BSA) was selected as a model protein to evaluate the influence of protein corona formation on materials physicochemical properties, colloidal stability, and toxicity. Biological assays were performed to assess the effects of bare and albumin corona coated materials on survival, oxidative stress, intestinal barrier permeability, growth, reproduction, and fertility. Critical alterations in topography, surface roughness, and chemistry of GO and MWCNT were observed due to albumin corona formation. These modifications were associated with changes

[4]This chapter has already been published as a scientific paper in the NanoImpact Journal. Côa et al. Toxicity mitigation and biodistribution of albumin corona coated graphene oxide and carbon nanotubes in *C. elegans*. (2022) DOI: 10.1016/j.impact.2022.100413.

in colloidal stability of materials and prevention of their aggregation and sedimentation in nematode testing medium. Both GO and MWCNT caused damage to nematode survival, growth, reproduction, and fertility, as well as enhanced oxidative stress and permeability of the intestinal barrier. But GO was more toxic than MWCNT to *C. elegans*, especially at long-term assays. Albumin corona mitigated 100% of the acute and chronic effects of MWCNT. In contrast, the negative effects of GO were not completely mitigated; GO inhibited 16.2% of nematode growth, 86.5% of reproduction, and 32.0% of fertility at the highest concentration evaluated (10 mg L^{-1}), while corona-coated GO mitigated 50% of reproduction inhibition and 100% of fertility and growth. Confocal Raman spectroscopy imaging was crucial to point out that bare and albumin corona coated GO and MWCNT crossed the *C. elegans* intestinal barrier reaching its reproductive organs. However, BSA corona protected the nematode targeted organs from negative effects from MWCNT and blocked its translocation to other tissues, while coated GO was translocated inside the nematode affecting the functionality of crucial organs. In addition, coated MWCNT was excreted after 2 h of food resumption, whereas coated GO still accumulated in the nematode intestine. Our results demonstrate that materials' different translocation and excretion patterns in *C. elegans* had a relation to the impaired physiological functions of primary and secondary organs. This work is a contribution toward a better understanding of the impacts of protein corona on the toxicity of graphene oxide and carbon nanotubes; essential information for biological applications and nanosafety.

Keywords: nanomaterials; biocorona; nanotoxicity; Raman spectroscopy

3.1. Introduction

Nanomaterials are prone to interact with biomolecules, due to their high free surface energy, leading to the formation of a molecular coating commonly called biocorona, which alters nanomaterials characteristics, modulates their colloidal stability, biological effects and environmental fate (Chetwynd and Lynch, 2020; Markiewicz et al., 2018;). Understanding the effect of biocoronas has become essential for advances in nanomedicine, nanobiotechnology, environmental nanoscience and nanosafety, once biocorona modifies the surface of materials changing their nano-bio interfaces and consequently their effects on cells, organisms and ecosystems (Natarajan et al., 2021; Cai and Chen, 2019). However, the influence of biocoronas on the toxicological response of nanomaterials is still under debate (Singh et al., 2021).

Graphene oxide (GO) and carbon nanotubes (CNTs) are some of the most attractive nanomaterials explored in a wide range of commercial products such as composites, energy devices and construction materials (StatNano, 2018). They are widely used in drug delivery systems, biosensors and tissue engineering (Maiti et al., 2019). However, regulatory authorities and the scientific community have raised uncertainties over potential environmental and human health risks of these nanoscale materials; for example, CNTs were recently added to the SIN list ("Substitute it now") as a material that should not be used unless risk assessment can prove safe use (Hansen and Lennquist, 2020). The toxicological risks of GO and CNTs are dependent on their physico-chemical properties such as size, chemical composition, surface chemistry, and defects (De Marchi et al., 2018; Kumar Babele et al., 2021; Ma et al., 2015; Ou et al., 2016; Rodrigues et al., 2020; Sydlik et al., 2015). However, not only the intrinsic properties of these materials should be considered in the nanotoxicology evaluation, but also the extrinsic; it is, therefore, essential to comprehend the influence of biocorona on biodistribution and toxicity of GO and CNTs under different biological and environmental systems (Canesi et al., 2017). In addition, the adoption of standard protocols to address the nanomaterials toxicity is a critical factor because the lack of standardization of method of dispersion of nanomaterials, exposure medium, and biological endpoints make inter-laboratory comparisons often difficult, sometimes even leading to contradictory results, which are not useful to support the nanomaterials risk assessment.

Due to its high abundance, solubility, low cost, and similar structural morphology to human serum albumin, bovine serum albumin (BSA) has been commonly used as a protein model to understand the protein-nanomaterial interactions at the interface with biological and environmental systems (Akhuli et al., 2021; Sopotnik et al., 2015). Several groups have

experimentally studied or modelled the adsorption of BSA on nanomaterials to investigate their fate in aquatic and terrestrial environments where other biomolecules may co-exist (i.e., humic acid, lipids) (Sun et al., 2018). BSA-coating can also be used to improve the metallic ion removal from aqueous solutions by nanomaterials (Martinez et al., 2020; Yu et al., 2019) and for the delivery of several nanoparticles and molecules that, when freely administered, could present side effects (Aires et al., 2017; Mariam et al., 2016).

Caenorhabditis elegans (nematode) is one of the most used model organisms in studies about the toxicity of nanomaterials, drugs and environmental contaminants (Gonzalez-Moragas et al., 2015; Mueller et al., 2020; Soares et al., 2020). This organism is an appropriate model for these studies because of its optical transparency, short-life cycle, short lifespan and high sensibility to environmental toxicants. In addition, it is useful to investigate basic physiological processes, such as oxidative stress response (Höss et al., 2020; Wu et al., 2019). Studies have shown that GO and MWCNT may damage the intestinal barrier of *C. elegans* and be translocated from its primary to secondary targeted organs (Nouara et al., 2013; Wu et al., 2014; Zhi et al., 2016b). Negative effects on nematode reproduction have also been observed, such as reduction of sperm and progeny number, induction of apoptosis in the germline and inhibition of fertility rate. GO and carbon nanotubes exposure may affect the *C. elegans* locomotion and dysregulate its neuronal system (Kim et al., 2020a; Li et al., 2017). On the other hand, recent studies have pointed out that toxicity of graphene oxide to *C. elegans* could be attenuated by coating the GO surface with proteins (Sivaselvam et al., 2020a; Wu et al., 2016) or by chemically degrading its carbon structure with sodium hypochlorite (Bortolozzo et al., 2021).

Translocation and accumulation of nanomaterials within nematodes could impact the functionality of their crucial organs. Carbon nanomaterials biodistribution inside cells and organisms is commonly probed using fluorescent dyes (Sivaselvam et al., 2020b; Zhi et al., 2016a). However, these probes can be released (non-intentional) from nanomaterials, and then the observed distribution does not necessarily represent the presence of nanomaterials in the biological tissues (Dorney et al., 2012). Confocal Raman spectroscopy has been successfully applied to investigate the internalization of nanomaterials in cells (Efeoglu et al., 2015; Lázaro et al., 2021) and mice (Newman et al., 2020). Since graphene oxide and carbon nanotubes exhibit unique spectral signatures, this technique can easily identify these materials in *C. elegans* (Kim et al., 2020b, 2018). Despite this, no study has employed Confocal Raman spectroscopy to assess the biodistribution and excretion of albumin corona coated nanomaterials in *C. elegans.*

In this work, the adoption of standard and validated protocols was prioritized to investigate acute and chronic toxicity and biodistribution of bare and albumin corona coated GO and oxidized MWCNT in the *C. elegans* model. The main physico-chemical properties of materials were accessed by an integrated characterization approach and colloidal stability studies. Biological endpoints such as survival, oxidative stress, growth, reproduction and fertility were monitored to evaluate their toxicity. Raman spectroscopy imaging was used as a non-invasive and label-free method to study the biodistribution and excretion of these materials. Finally, it was observed that albumin corona mitigated 100% the acute toxicity (survival) of both GO and oxidized MWCNT, while the inhibition of reproduction promoted by GO was mitigated only in 50% by albumin corona.

3.2. Material and methods

GO was prepared from flake graphite (Lot MKBW0432V, Sigma Aldrich) by a modified Hummers' method (Becerril et al., 2008). 370 mL of sulphuric acid (A.R., Lot 2087915, Synth) was added into a flask with flake graphite (5.0 g) and $NaNO_3$ (3.75 g, 3MKBS2180V, Sigma Aldrich) in bath ice under continuous stirring. After 20 min, potassium permanganate (22.5 g, Lot #SZBE1620, Sigma Aldrich) was slowly added to the mixture for 60 min. Then, the reaction was maintained under agitation for 72 h at room temperature and posteriorly diluted in 300 mL ultrapure water (UPW, Milli-Q water filtration system, Millipore). At this moment, the reaction released bubbles and gases. The mixture was further agitated for one hour at 95 °C. Oxygen peroxide (15 mL, 30.0%, Lot 48541F, Synth) was added dropwise to eliminate the unreacted $KMnO_4$. The mixture turned yellow, and it was allowed to stand overnight. It was centrifuged (3,800 g, 15 min, 20 °C) and rinsed with sulphuric acid (3.0%) and oxygen peroxide (0.5%) to remove impurities. The final mixture was centrifuged at 3,800 g for 15 min and washed with UPW (300 mL). Then, it was dialyzed with continuous water exchange for three days. Graphene oxide dispersion was freeze-dried for 72 h and stored in a desiccator.

Oxidized MWCNT were prepared from raw multi-walled carbon nanotubes produced by chemical vapour deposition (CVD), with a diameter of 10-40 nm and length of 1-25 µm purchased from CNT Co. Ltd. (Incheon, Korea). 1.0 g of raw multi-walled carbon nanotubes were oxidized with nitric acid (9.0 mol L^{-1}, 200 mL, Lot 228294, Synth) under reflux at 150 °C for 24 h. Then, they were washed with UPW by filtration (0.22 µm PTFE membrane) to remove

the excess acid until neutral pH. Lastly, the MWCNT sample was freeze-dried for 72 h and stored in a desiccator.

3.2.1. Preparation and characterization of GO and MWCNT stock dispersions

It is currently a consensus that preparing stable stock dispersions of nanomaterials is a pivotal issue to obtain reliable results in nanoecotoxicity studies (Cerrillo et al., 2015; OECD, 2020). Therefore, some steps were taken to reach stable stock dispersions to dilute them in sub-stocks for toxicity assays besides applying them in BSA interaction.

Stock dispersions (500 mg L^{-1}) were prepared as recommended in the OECD Guideline No. 318 (OECD, 2017) and their colloidal stabilities were posteriorly evaluated. Powder GO and MWCNT samples (10 mg) were pre-wetted with UPW (0.2 mL) and left as a wet paste for 24 h. Then, UPW (19.8 mL) was added, and dispersions were sonicated in an ultrasonic bath (Cole-Parmer, model 08895-43, USA) which temperature was controlled (20-30 ^{o}C). Dispersion aliquots were collected every 20 min, and hydrodynamic diameters (HD) were analyzed by dynamic light scattering (DLS) in a ZetaSizer Nano ZS instrument (Malvern). For each sample, three consecutive replicates were evaluated. Sonication was performed until there were no changes in HD values. Moreover, quality criteria were considered, such as count rate and variation between measures, which indicate aggregation/agglomeration within the same measurement. In addition, the presence of agglomerates/aggregates was also estimated by observing the exponential decay and baseline of correlograms. Stock-dispersions were used within three hours and not stored for longer than two weeks, as recommended in the OECD Guideline No. 318 (OECD, 2017).

Colloidal stability of stock dispersions of bare GO and MWCNT was evaluated by two methods (i.e., static and non-static). In both, stock dispersions (500 mg L^{-1}) were diluted in UPW at 100 mg L^{-1} for GO and 25 mg L^{-1} for MWCNT and put in Eppendorf tubes. In the static experiment, aliquots (1 mL) were remained static over 6 h. Each hour, 100 µL from the top of supernatants were collected. Absorbance values were measured by UV-Vis spectroscopy in a microplate reader UV-Vis spectrophotometer (Multiskan TM GO, Thermo Scientific) at 500 and 400 nm wavelength for GO and MWCNT, respectively. In the non-static test, aliquots were prepared and directly centrifuged (Centrifuge 5810R, Eppendorf) during 10 min under different rotation speeds (from 26.5 to 2,150 g). 100 µL of the supernatant top was collected at each step, and absorbance values were obtained by UV-Vis spectroscopy at the same wavelengths as

mentioned above. The parameter evaluated in both methods was absorbance because it is directly proportional to the amount of suspended materials after procedures.

3.2.2. Albumin corona formation on GO and MWCNT

Before experiments, 10 mg bovine serum albumin (98% purity, Sigma Aldrich, Lot #SLBD5326) was freshly prepared in 10 mL phosphate-buffered saline (PBS, pH 7.4, Lot 75150661B, Life technologies) by gentle agitation.

GO and MWCNT were interacted with BSA incubating 200 µL of materials stock dispersions (500 mg L^{-1}) with 800 µL of BSA solution (1 mg mL^{-1}) in Eppendorf tubes (1.5 mL), during 1 h at 37 °C in a thermoblock system (Thermomixer C, Eppendorf). After incubation, samples were washed by centrifugation to remove unbound or weakly bound proteins (soft corona). The first centrifugation step was carried out at 20,800 g for 1 h at 4 ºC. Supernatants were removed, and pellets were dispersed in 1 mL of PBS. Three more steps of centrifugation (30 min) and washing with PBS were performed. After the third washing procedure, obtained samples consisting of hard corona coated nanomaterials complexes in colloidal form (i.e., pellet) were stored at 10 ºC for further analyses and designated by coated GO and MWCNT or specifically as BSA@GO and BSA@MWCNT.

To analyze the adsorption capacity of GO and MWCNT, a volume of 500 µL of stock dispersions (1 mg mL^{-1}) was individually incubated with 500 µL BSA solution (1.0 mg mL^{-1}) for 1 h, at 37 °C in a thermoblock system. One step of centrifugation was performed at 20,800 g for 1 h at 4 ºC and BSA amount in the supernatant was quantified by the Bradford assay (Lot #SLBV5669, Sigma-Aldrich) by UV-Vis spectroscopy at 595 nm. The protein adsorption capacity was calculated by subtracting initial and final amounts of proteins in the supernatant, which value was divided by the amount of materials added in the test.

3.2.3. Physico-chemical characterization of nanomaterials

Physicochemical properties of nanomaterials govern their colloidal behaviour in aqueous solution and biological media, biocorona formation and toxicity (Garcia-Bennett et al., 2019). In this sense, we used an integrated approach to understand the structural, morphological and chemical properties of GO and MWCNT before and after biocorona formation. Bare samples were analysed without additional treatments. Biocorona-coated samples were washed

three times with ultrapure water to remove buffer salts that could interfere in atomic force microscopy (AFM) and thermogravimetric analyses (TGA).

The topography of bare and coated materials was analysed by AFM. 5 µL of materials dispersions (10 mg L^{-1}) were deposited onto freshly cleaved mica substrates (2 x 2 cm). Images were acquired in tapping mode on MultiMode VIII microscope with NanoScope V controller model (Bruker), using a silicon tip (NCHR, Budget Sensors) with a nominal resonance frequency of 300 kHz and a nominal force constant of 40 N/m. Images were treated in Gwyddion software (2.5 version). Average height profiles were obtained from 20 different GO flakes and 10 different regions of MWCNT. GO and BSA@GO surface roughness were calculated from an equal area on the flakes (2500 nm^2).

TGA was carried out with bare and coated materials to study the materials composition on a Simultaneous Thermal Analyzer (TGA; STA 449 F3 Jupiter; NETZSCH, Germany). Samples were analysed from room temperature (25 ºC) to 900 ºC, in an atmosphere of synthetic air flowing at 50 mL min^{-1} at heating rates of 10 ºC min^{-1} for GO and 5 ºC min^{-1} for MWCNT, once 10 ºC min^{-1} is not suitable to perform TGA analysis for MWCNT because it presents fast degradation.

Materials surface elemental composition was assessed by X-ray photoelectron spectroscopy (XPS) in a K-Alpha System (Thermofischer Scientific, USA) using Al Kα X-rays and charge compensation during analyses. Pass energies of 50 eV were employed to obtain survey spectra collected at four different areas per sample with a spatial resolution of 400 µm. Data were analysed with Thermo Avantage software (version 5.957).

Materials surface charges were assessed in Zetasizer NanoZS equipment by electrophoretic light scattering. Measurements were performed at 50 mg L^{-1} for GO and 25 mg L^{-1} for MWCNT in UPW and the medium utilized for biological assays.

3.2.4. Biological assays with *Caenorhabditis elegans*

3.2.4.1. Preparation of sub-stocks of bare and coated materials for toxicity assays

Sub-stocks of bare and coated GO and MWCNT were prepared before toxicity assays. They were prepared in ultrapure water at concentrations ten times higher than the nominal concentration intended in biological tests (0.001; 0.01; 0.1; 1.0; 5.0 and 10.0 mg L^{-1}). A serial dilution was adopted to dilute dispersions as recommended in Guidance No. 317 for stable stock

dispersions (OECD, 2020). The same volume of nanomaterials was added to each well (100 µL) of toxicity assays.

For bare materials, stock dispersions (500 mg L^{-1}) were diluted in ultrapure water after bath sonication as previously described. However, in the case of coated materials, it was observed loss of materials during the procedure of biocorona formation. Therefore, it was required that final concentrations of GO and MWCNT in pellets be evaluated before preparing sub-stocks for toxicity assays. With this proposal, calibration curves of GO and MWCNT were prepared to measure the concentration of GO and MWCNT by UV-Vis spectroscopy, following the protocol developed by Cerrillo et al. (2015). First, absorbance spectra were obtained from GO, MWCNT and BSA samples (Figure S1-A and B). The most appropriate wavelength to elaborate calibration curves was selected considering the point where BSA absorbance did not interfere in the absorbance of GO and MWCNT. The selected wavelength was 400 nm for both materials. Calibration curves were elaborated by diluting GO stock dispersion in ultrapure water at 30.0; 60.0; 90.0, 120.0 and 150.0 mg L^{-1} (Figure S2-A) and MWCNT at 10.0; 30.0; 60.0; 90.0 and 120.0 mg L^{-1} (Figure S2-B). Every time that coated materials were freshly prepared, pellets were resuspended in UPW, and final concentrations of GO and MWCNT were assessed by correlation of absorbance values in calibration curves. Then, sub-stocks were prepared in UPW for toxicity assays.

3.2.4.2. Characterization of colloidal stability

Biological assays were performed in a moderately hard reconstituted water defined by the U.S. Environmental Protection Agency, herein named EPA medium. It is constituted by 60.0 mg L^{-1} $CaSO_4.2H_2O$, 60.0 mg L^{-1} $MgSO_4$, 96.0 mg L^{-1} $NaHCO_3$ and 4.0 mg L^{-1} KCl, and it is recommended in a Standard Operating Procedure developed by EU NanoReg (Kleiven and Oughton, 2015) because presents fewer chloride salts than the commonly used media (e.g., K^+ medium or M9-buffer) which hinder nanomaterials colloidal stability.

Aggregation/agglomeration and sedimentation of materials were studied in EPA medium to verify their colloidal behaviour in toxicity assays. A similar study was performed in UPW to clarify the influence of salts of EPA medium on materials' stability.

Bare and coated GO and MWCNT stock dispersions were prepared in UPW and diluted in EPA medium or UPW at 50 and 25 mg L^{-1}, respectively. Aggregation and deposition behaviour were monitored by DLS and UV-Vis spectroscopy, respectively. By DLS, variation in HD was monitored each 24 h for a 96-h period. Experiments were carried out in 3 mL

cuvettes (model DTS0012), and the evaluated suspension volume was 1 mL. For each sample, three consecutive replicates were measured. Moreover, quality criteria (correlogram, count rate and variation between measurements) were considered. For UV-Vis measurements, dispersions were put into the same vessel where biological assays were performed (24-well plate) following the recommendations of Guidance No. 317 (OECD, 2020). Over 96 h and every 24 h, aliquots (100 µL) of the supernatant top were collected and absorbance was measured at 400 nm on a microplate reader UV-Vis spectrophotometer (Multiskan TM GO, Thermo Scientific). Digital pictures of dispersions in Eppendorf tubes (1.5 mL) were also recorded over time.

Microscopy images were also obtained from wells where long-term experiments were performed to identify whether there was the formation of aggregates and bacteria during the tests.

3.2.4.3. *Caenorhabditis elegans* maintenance and strain preparation for toxicity assays

Wild-type nematodes (N2 Bristol) were obtained from *Caenorhabditis* Genetics Center (CGC, Minnesota) and maintained at 20 ºC on nematode growth medium (NGM) plates seeded with *Escherichia coli* OP50 strain as a feed source, following the protocol of Stiernagle (2006). Besides, worms were cultured on 8P agar seeded with *E. coli* NA22 strain to reach a large number of gravid nematodes required for performing toxicity tests.

Before each test, a synchronization procedure was carried out to obtain worms at L1 or L3 larval stage. The adopted protocol was elaborated by Porta-de-la-Riva et al. (2012), and it was detailed in the supplementary material.

3.2.4.4. Acute assays

Acute toxicity assays were conducted following the protocol developed by Maurer et al. (2015). Experiments were performed in 24 well plates with a total test volume of 1 mL per well. Each well contained ~20 *C. elegans* young adults (10 µL), 100 µL of tested material and EPA medium (890 µL). Nematodes were exposed to bare and coated nanomaterials at 0.01; 0.1; 1.0; 5.0 and 10.0 mg L^{-1} concentrations during 24 h at 20 ºC, without food. For each test, negative controls were carried out using UPW because stock dispersions were prepared in this medium. After 24 h, live organisms were counted in a stereomicroscope (Stemi 508, Zeiss), and then the survival rate was calculated. Organisms were considered dead when they did not respond to a

stimulus with an aluminum wire. Six replicates for each concentration and at least three independent assays were realized.

3.2.4.5. Oxidative stress measurement

To analyze the oxidative stress in nematodes, the production of reactive oxygen species (ROS) was measured by using the CM-H2DCFDA probe (Lot 1942272, Invitrogen, Thermofischer). 40 *C. elegans* L3-stage were exposed to 0.01; 0.1 and 1.0 mg L^{-1} of bare and coated nanomaterials in EPA medium, in 24-well plates for 24 h. A positive control was applied (hydrogen peroxide, 5.0 mM, Lot K45302610416, Merck) to verify the sensibility of the CM- H2DCFDA probe and *C. elegans* to respond to oxidative stress. In the case of H_2O_2 exposure, worms were exposed just for one hour.

At the end of exposure, worms were transferred to microtubes and centrifuged for 3 min at 774 g and 20 ^oC. Afterwards, they were washed with EPA medium twice by centrifugation to remove the materials and H_2O_2. After the last centrifugation, 84 µL of CM-H2DCFDA (250.0 µM) was added to 200 µL of EPA containing worms at a final concentration of 75.0 µM CM-H2DCFDA. After 2 h, worms were washed twice by centrifugation with EPA medium to remove the probe. They were transferred to a black polystyrene plate, and fluorescence intensity was measured under a microplate reader (Infinite 200 Pro, Tecan) using 488 and 510 nm as excitation and emission wavelength, respectively. Five replicates were performed per treatment. ROS was expressed as the relative fluorescent unit per live worms. A parallel experiment was carried out employing the same conditions used to measure the ROS production by a microplate reader. However, the applied concentration of CM-H2DCFDA was 25.0 µM, and fluorescence images were obtained in an inverted microscope (Axio Vert.A1, Zeiss) with an Axion 203 camera using the FITC/GFP channel. Levamisole (4.0 mM, Sigma Aldrich) was used to immobilize the worms.

The sensitivity of *C. elegans* to ROS production was proved because ROS production significantly increased in nematodes exposed to H_2O_2 in relation to unexposed nematodes (control) (Figure S3).

3.2.4.6. Nile red staining

Nile red staining assay was performed according to Escorcia et al. (2018) to investigate the influence of bare and coated materials on the permeability of the *C. elegans* intestinal

barrier. 60 L3-stage worms were exposed to bare and coated nanomaterials at 1.0 mg L^{-1} in EPA medium in a 24-well plate. After 48 h, worms were transferred to Eppendorf tubes (1.5 mL) and centrifuged at 774 g for 3 min and 20 ºC. Supernatants were discarded, and pellets (100 µL) were washed with PBST (PBS 1x and 0.01% triton x-100, Lot #SLBM7930V, Sigma Aldrich). Worms were again centrifuged, supernatants were discarded, and 100 µL of isopropanol 40% (Lot #SHBF4874V, Sigma Aldrich) was added to the worm's pellet, which was incubated for 3 min. They were centrifuged, supernatants removed and 150 µL Nile red (NR) solution was added. NR stock solution was prepared by dissolving 10 mg Nile red (Lot #SLBP9326V, Sigma Aldrich) in acetone 100%, afterwards, for each 1 mL of isopropanol 40%, 6 µL NR stock solution was added. Worms were exposed to Nile red for 2 h in dark. After that, they were washed with PBST for 30 min to remove NR excess. Fluorescence microscopy images were acquired in an inverted microscope (Axio Vert.A1, Zeiss) with an Axion 203 camera using the FITC/GFP channel. Fluorescence intensity was obtained using the ImageJ software, and relative fluorescence intensity was calculated from the fluorescence intensity of the control group (unexposed).

3.2.4.7. Long-term assay

Chronic assays were performed from L1-larvae to adult nematodes (L4) as described in the ISO 10872:2010 protocol (ISO, 2010a). Before tests, *E. coli* suspensions were prepared in EPA medium, and bacterial density was adjusted to the appropriate amount (1000±50 FAU). Detailed information is provided in the supplementary material (Figure S4).

Experiments were carried out in 24-well plates, each well containing 10-15 juvenile nematodes (L1), 100 µL test suspension, 500 µL suspension *E. coli* OP50 (at 1000 FAU) and 400 µL EPA medium. Evaluated concentrations of bare and coated nanomaterials were 0.001; 0.01; 0.1; 1.0 and 10.0 mg L^{-1}. In addition, as recommended in the ISO 10872:2010, the sensibility of strain to the chemical reference substance benzycetyldimethylammonium chloride (BAC-C16, Lot #FLVB65259, Sigma Aldrich) on *C. elegans* growth was evaluated. BAC-C16 was prepared in UPW, and worms were exposed to 7.61; 10.67; 16.0; 24.0; 36.0; 54.0 and 81.0 mg L^{-1}. Exposures were performed at 20 ºC with continuous gentle shaking to promote oxygenation.

After 96 h, 100 µL of Rose Bengal solution (300 mg L^{-1}) was added per well, and plates were incubated at 80 ºC for 10 min to kill the worms. Images of nematodes were recorded in an inverted microscope (Axio Vert.A1, Zeiss) equipped with an Axion 203 camera and

analyzed using ImageJ software. Results were expressed as inhibition rates of reproduction, fertility and growth, calculated from the number of offspring, fertile nematodes and length of organisms at L4-stage, respectively. Six independent replicates were tested by treatment, and three independent experiments were carried out. Validity criteria were considered as required by the ISO 10872:2010. The recovery of organisms in negative controls was ≥ 80 and ≤120%; average percentage of males was ≤10%; average fertility was ≥80%, and reproduction ≥ 30 juveniles per exposed organism. Therefore, experiments that did not meet these criteria were disregarded. In addition, inhibition rates below 10% were considered negligible, according to recommendations by Höss et al. (2012).

It was found that the concentration of BAC-C16 that inhibited 50% of growth was 15.6 (14.9-16.4) mg L^{-1} (Figure S5). Since the standard guideline (ISO 10872:2010) recommends that EC_{50} values range between 8.0-22.0 mg L^{-1}, the *C. elegans* strain was suitable for performing assays (ISO, 2010b).

3.2.5. Raman spectroscopy imaging for biodistribution studies

Accumulation of bare and coated materials inside the nematodes was investigated by Raman confocal spectroscopy. 40 L3-stage worms were exposed to bare and coated samples at 10.0 mg L^{-1} in EPA medium. After 48 h, a group of nematodes (1/3) was separated, washed twice with EPA, and fixed with 4% paraformaldehyde (Lot #SLBF2268V, Sigma-Aldrich). The remaining nematodes were transferred to NGM medium with food or without food where they were maintained for 2 h or 12 h, respectively, following the protocol of Gonzalez-Moragas et al (2015b), in order to verify the accumulation of materials upon excretion by Raman confocal spectroscopy. Afterwards, they were washed twice with EPA, and fixed with 4% paraformaldehyde for further analysis. Raman spectra were obtained at several positions of nematodes bodies (head, intestine, gonad, egg and rectum) at depth profiles from -30 to 120 µm (assuming 0 µm as the upper cuticle) with steps of 10 µm. Spectra were acquired with a Confocal Raman spectrometer (XploRA PLUS, Horiba) equipped with an optical confocal microscope (50x objective). The excitation wavelength was 532 nm, and spectra were acquired with 6 accumulations of 3 s each, slit 200 µm and hole 500 µm.

3.2.6. Data analysis

Data were expressed as means with standard deviation (SD) and analyzed by one or two-way analysis of variance (ANOVA) with a Tukey´s multiple comparison test using GraphPad Prism (5.0 version). Results with $p<0.05$ were considered statically different.

3.3. Results and Discussion

3.3.1. Physico-chemical properties of nanomaterials

Nanosafety reports and guidelines have notably highlighted the importance of properly characterizing the physico-chemical properties of nanomaterials to provide the basis for understanding their biological effects in nanotoxicology studies (OECD, 2020). Figure 1 shows GO and MWCNT properties before and after BSA corona formation, investigated by a multi-technique approach.

Concerning morphological aspects, it has been demonstrated for graphene oxide that lateral size plays a significant role in nano-bio interactions with proteins. Kenry et al. (2016), for example, reported that albumin adsorption increases along with graphene oxide flakes lateral size increase. While for MWCNT, their diameters exert a pivotal influence on protein adsorption (X. Zhao et al., 2015). AFM images (Figure 1A to 1D and Figure 1G to 1J) reveal that BSA@GO presents a higher surface roughness (1.33±0.4 nm) than bare GO (0.23±0.04 nm. In addition, GO thickness increased from 1.0±0.1 nm to 4.0±0.33 nm after interaction with BSA according to the height profiles data. These findings demonstrate that BSA has coated most of the surface of GO sheets, as also observed in other studies about protein complexes on graphene oxide using AFM (Franqui et al., 2019; Martinez et al., 2020). AFM has also been a powerful technique to characterize the interaction of proteins and MWCNT (Du et al., 2011). It is noteworthy that BSA@MWCNT shows more superficial irregularities and broader diameters than MWCNT, indicating that nanotubes were coated by BSA. For example, Figure 1H and 1J show a height increase from 10.9 nm to 51.0 nm.

Thermal decomposition profiles (Figure 1E and 1K) of materials also confirm the albumin corona formation. TGA curve of GO sample shows a first mass loss at temperatures lower than 130 ºC is related to water desorption from the material surface. The second weight loss occurred between 160 to 300 ºC and is attributed to elimination of labile and stable oxygen-containing functional groups. Lastly, decomposition of graphitic regions of GO is observed

between 520 to 680 ºC (Kavinkumar and Manivannan, 2016). For MWCNT, volatilization of water occurred at temperatures below 130 ºC. Then, decomposition of oxygenated groups occurred between 200 and 400 ºC (Datsyuk et al., 2008). Finally, the last weight loss is noted at temperatures over 460 ºC when the carbon structure is degraded. Thermal profiles of BSA@GO and BSA@MWCNT are a combination of the BSA curve with GO or MWCNT curves. At temperatures lower than 150 ºC, adsorbed water present at the samples is evaporated and BSA is denaturated (Michnik, 2003). Then, two simultaneous events occur at 160-525 ºC for BSA@GO and 215-375 ºC for BSA@MWCNT. At these temperature ranges, decomposition of BSA is observed together with the degradation of oxygenated functional groups of the carbon materials (Datsyuk et al., 2008; Michnik, 2003). At temperatures higher than 510 ºC and 460 ºC for GO and MWCNT respectively, decomposition of the carbon structures is observed and thermally stable carbonaceous product formed during BSA degradation (Gebregeorgis et al., 2013).

X-ray photoelectron spectroscopy was performed to analyze materials surfaces chemical composition. XPS survey data (Figure 1F) suggest that GO is composed of carbon (65.8±0.9%), oxygen (32.1±0.6%) and nitrogen (2.1±0.1%), whereas BSA@GO shows 67.1±0.3% of carbon, 21.5±0.4% of oxygen and 11.4±0.2% of nitrogen. Analysis of MWCNT (Figure 1L) shows that the bare material has only carbon (90.3±1.9%) and oxygen (9.7±1.9%) atoms, while BSA@MWCNT is composed of carbon (77.4±1.2%), oxygen (14.1±0.7%) and nitrogen (8.9±0.5%). Considering that BSA is a nitrogen-rich compound due to its amino groups (Peng et al., 2004), an increase in nitrogen abundance for the BSA corona coated GO and MWCNT evidences the attachment of this protein on both materials surfaces.

Raman spectroscopy analyses were performed to offer further evidence of BSA interaction with the carbon nanomaterials (Figure S6-A and B). After protein corona formation, the D and G-bands of GO were shifted toward lower wavelengths at 1334 and 1533 cm^{-1}. Besides, characteristic bands of MWCNT (D, G, D' and G') were shifted to higher wavelengths at 1330, 1583, 1614 and 2655 cm^{-1}, respectively. According to Sivaselvam et al. (2020), protein interactions through nitrogen atoms bonding on nanomaterials surfaces lead to vibrational disturbances responsible for peak shifts in Raman spectra.

Figure 1 - Characterization of bare and albumin corona coated materials. AFM image of GO (A) and height profile of GO flake (B); AFM image of BSA@GO (C) and height profile of BSA@GO (D); TGA and DSC curves of GO, BSA@GO and BSA (E); Elemental composition surface of GO and BSA@GO (F); AFM images of MWCNT (G) and a height profile of a single region of MWCNT (H); AFM image of BSA@MWCNT (I) and height profile of a single region of BSA@MWCNT (J); TGA and DSC curves of MWCNT, BSA@MWCNT and BSA (K) and elemental composition surface of MWCNT and BSA@MWCNT (L).White boxes and lines represent the selected region to elaborate height profiles.

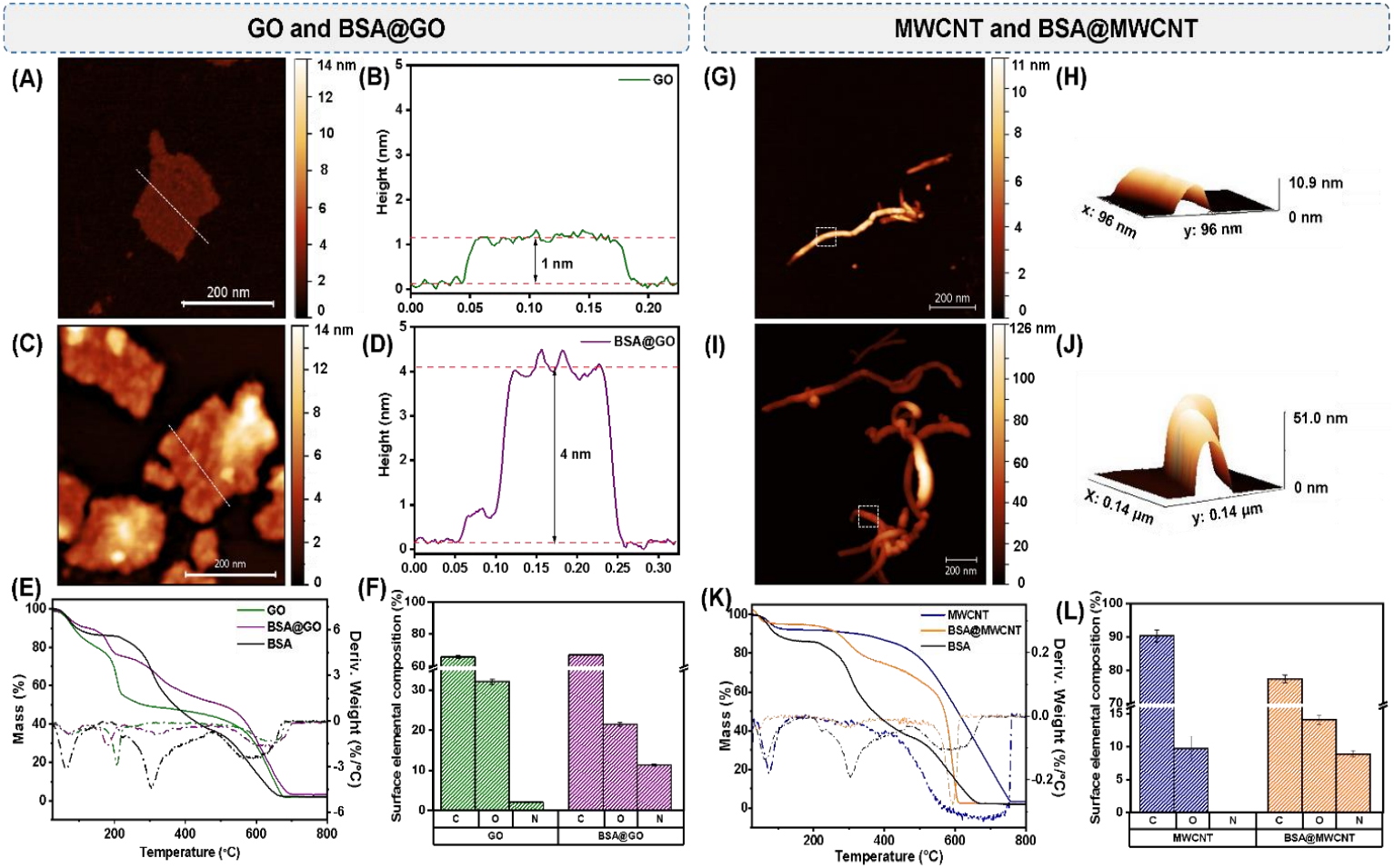

GO presented a 21.7% higher adsorption capacity of BSA than MWCNT. GO was able to adsorb about 0.28±0.01 mg_{BSA}/mg_{GO}, while MWCNT adsorbed 0.23±0.01 mg_{BSA}/mg_{MWCNT}. Nanomaterials may adsorb proteins via hydrogen bonding, electrostatic interactions, and/or van der Waals forces (hydrophobic interaction, π-π interaction) (Marchesan and Prato, 2015; Nel et al., 2009). XPS survey data (Figure 1F and 1L) showed that GO presents approximately two times more oxygen groups than MWCNT. High-resolution C1s XPS spectra (Figure S7), evidenced that more epoxy/hydroxyl groups are present in GO than MWCNT; however, an equivalent amount of carboxyl/ester groups were observed in both samples. Since proteins can be adsorbed through electrostatic interactions, the highest amount and variety of oxygenated groups of GO surface can be associated with its highest adsorption capacity. Although the specific surface area can also influence the BSA adsorption capacity of those materials.

So far, our results indicate that materials surfaces were successfully coated by BSA, leading to the formation of a protein corona on both. AFM analysis showed that thickness and surface roughness were altered due to BSA-adsorption, as also material thermal decomposition showed different behaviour. BSA interactions at GO and MWCNT surfaces were verified by vibrational disturbances observed at Raman spectra. Those results evidence that both materials present a new identity after BSA coating (hard corona), and therefore distinct colloidal behaviour and toxicological profiles are expected.

3.3.2. Dispersion stability of materials in ultrapure water and EPA medium

Preparation of stable and reproducible stock dispersions plays an important role in the reliability and accuracy of nanotoxicity results (Cerrillo et al., 2015; OECD, 2017). To optimize the dispersion conditions, first, the hydrodynamic diameters of materials in the stock dispersions were measured by DLS in function of sonication time. After 80 min of sonication, hydrodynamic values of GO and MWCNT were reduced from 408.0±3.4 nm to 189.7±2.5 nm and 123.9±0.2 nm to 104.8±0.4 nm (Figure S8), respectively, and the baseline of correlograms became flat; indicating that there were no aggregates in stock dispersion after this time. Therefore, 80 min of sonication was selected as a suitable time to achieve well-dispersed stocks for both nanomaterials.

Static and non-static experiments were carried out to further evaluate the colloidal stability of GO and MWCNT stock dispersions. Over 90% of GO and MWCNT remained suspended in UPW evaluated by UV-Vis absorption at 400 nm (Figure S9-A and B). These results have shown that sonication of nanomaterials stock dispersions led to highly dispersed

suspensions, as categorized in the OECD guideline No. 318, and being suitable for toxicity testing (OECD, 2017).

Assessing nanomaterials colloidal behaviour in the biological medium of toxicity tests is also necessary because it is one of the most critical factors that impact nanobio-interactions and toxicological outcomes of nanomaterials (Laux et al., 2018; Petersen et al., 2014). Dispersion stability of bare and albumin corona-coated GO and MWCNT in UPW and EPA medium was assessed.

In Figure 2A and 2B is notable that hydrodynamic diameter of bare GO and MWCNT in UPW remained constant over 96 h. However, the exponential decay and correlograms' baselines suggest aggregate formation for GO, while flat correlogram baselines indicate good colloidal stability of MWCNT (Figure S10). In EPA medium, hydrodynamic diameter values of bare GO and MWCNT increased after 96 h from 242.0±5.6 nm to 1432.0±46.3 nm, and 112.1±0.2 nm to 1006.1±42.3 nm respectively. Correlograms of samples were disturbed over 96 h due to the formation of aggregates, demonstrating that GO and MWCNT were not stable in EPA medium. On the other hand, BSA@GO and BSA@MWNCT hydrodynamic diameter values in EPA medium did not increase over 96 h. Besides, good correlograms were obtained for BSA@MWCNT over 96 h, but the baseline of the BSA@GO correlogram suggests the presence of some aggregates in its sample after 24 h of analysis (Figure S10).

Visual inspection (Figure 2C) and UV-vis absorption measurements (Figure 2D), showed that 90% of bare materials remained in suspension in UPW up to 96 h. In EPA medium, the percentage of suspended materials rapidly decreased in the first 24 h of incubation, indicating drastic particle sedimentation. Nonetheless, BSA-corona improved dispersion stabilities of GO and MWCNT in EPA medium. During the first 24 h only 10% of coated materials suffered sedimentation, and 60% and 90% of BSA@GO and BSA@WMCNT, respectively, remained in suspension after 96 h. These results are in accordance with DLS data, which point out that albumin corona improved the GO and MWCNT dispersion stabilities in EPA medium.

Figure 2 - Colloidal stability evaluation of GO and BSA@GO at 50 mg L^{-1} (A), and MWCNT and BSA@MWCNT at 25 mg L^{-1} (B) by DLS. Digital pictures of dispersion stability study with samples in ultrapure water (UPW) and EPA medium from 0 to 96 h (C). Deposition behaviour over 96 h incubation in UPW and EPA medium measured by UV-Vis spectroscopy (D).

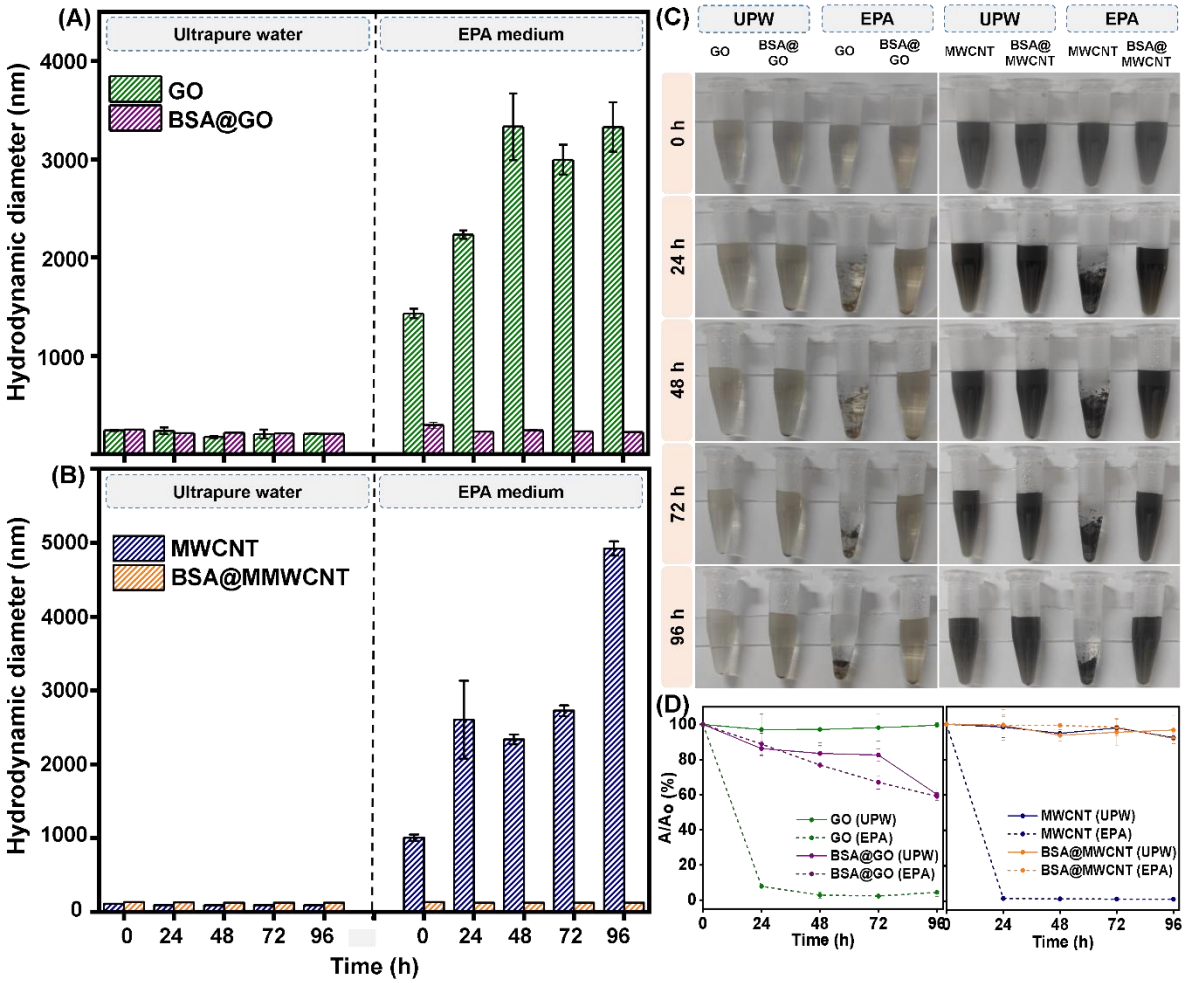

Furthermore, albumin corona formation was also accompanied by variations in materials surface charges. Zeta potential values changed from -49.9±0.7 to -32.7±1.4 mV for GO, and from -50.9± 0.4 to -36.7±1.6 mV for MWCNT, after BSA corona formation (Table S1). Proteins contain positively charged fragments of arginine and lysine that, when interacted with negatively charged oxygenated groups present in nanomaterial´s surface, lead to an increase in zeta potential values, as also verified in other works (Treuel et al., 2015; Zhang et al., 2019).

Several studies have ascribed high colloidal stabilities of GO and oxidized MWCNT to oxygenated groups existing in their surfaces (Chowdhury et al., 2015; de Medeiros et al., 2021; Deline et al., 2020). These negatively charged groups promote strong electrostatic repulsion among particles preventing aggregation, for this reason, GO and MWCNT have remained stable in UPW. However, high ionic strength and presence of cations in biological media are known

for disturbing nanomaterials colloidal stability (Baalousha et al., 2013; Baun et al., 2017; Côa et al., 2017). Monovalent cations (Na^+ and K^+) can compress the electrical double layer formed by functional groups on GO and MWCNT, reducing repulsive energy between particles and leading to destabilization of systems (Gao et al., 2017). Furthermore, multivalent cations (Mg^{2+} and Ca^{2+}) may act as a "bridge" between two individual GO sheets through complexation with functional groups (Park et al., 2008). Therefore, a decrease of colloidal stabilities of GO and MWCNT in EPA medium was observed in our experiments. It is noteworthy that biocorona improved the colloidal stabilities of both materials in EPA medium. Increase of steric hindrance can explain this as a consequence of protein coating on GO and MWCNT surfaces preventing the electrical double layer compression effect caused by cations dissolved in EPA medium (Du et al., 2014; Sun et al., 2018).

3.3.3. Influence of albumin corona on toxicity and internalization of materials in *Caenorhabditis elegans*

Taking into account that BSA-coating has modified the physiochemical properties and colloidal behaviours of GO and MWCNT, short and prolonged-term assays were performed to analyze these aspects on the toxicity towards the *C. elegans* model.

Short-term assays were carried out with young adult nematodes (L3 stage) to investigate the effects of nanomaterials on *C. elegans* survival. Figure 3A shows that GO caused a reduction of survival rate at concentrations from 0.1 to 10.0 mg L^{-1}. At 10.0 mg L^{-1}, only 41.0±12.1% of nematodes remained alive. Likewise, survival of nematodes exposed to bare MWCNT decreased along with concentrations increased from 0.01 to 10.0 mg $L^{-1,}$ reaching 49.5±11.5% at the highest concentration (Figure 3B). Conversely, BSA@GO and BSA@MWCNT did not show any effects on the survival of nematodes. Therefore, our results demonstrated that bare GO and MWCNT hampered nematode survival, whereas albumin corona mitigated the lethal effects of GO and MWCNT on *C. elegans*.

Figure 3 - Effects of GO and BSA@GO (A) and MWCNT and BSA@MWCNT (B) on *C. elegans* survival. Bars with ** are significantly different ($p \leq 0.05$) from the control or different between from one another.

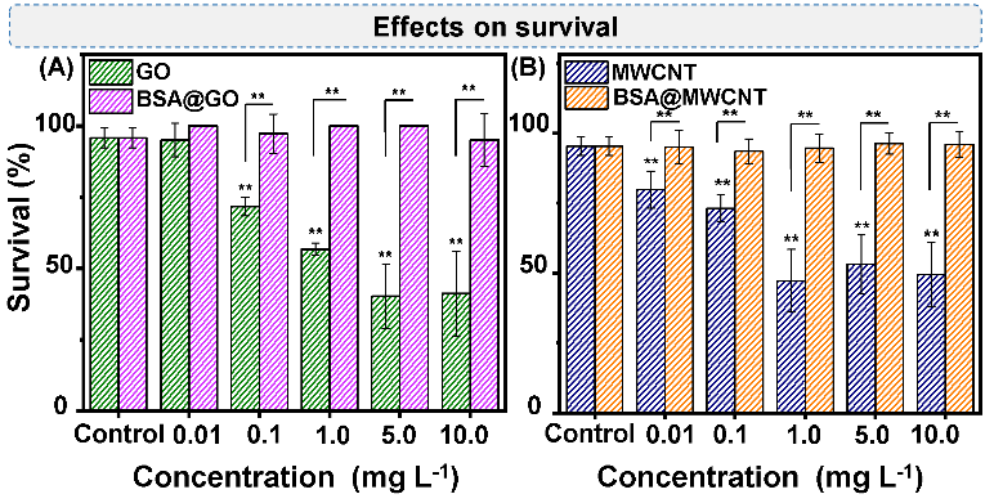

Consistent with our findings, other authors have described that GO exposure may affect *C. elegans* survival. However, only this study and another performed by our research group reported this effect at this nominal concentration range (0.1-10.0 mg L^{-1}) (Bortolozzo et al., 2021). Exposure at low doses of GO (0.001 to 1.0 μg L^{-1}) was investigated by Tsai et al. (2021), who observed that nematode lifespan was significantly reduced, even though GO has not been lethal to nematodes. Nivedita et al. (2017) and Li et al. (2017a) confirmed that GO caused lethality of worms, though at high concentrations (over 50.0 mg L^{-1}). Similarly, our study is the first indication that bare MWCNT can be toxic at these concentrations in short-term exposures. Despite this, negative effects of MWCNT (1.0-100.0 mg L^{-1}) on *C. elegans* lifespan and induction of oxidative stress were noticed by Shu et al. (2015). Regarding the albumin-coated materials, no comparative studies have assessed the influence of BSA@GO and BSA@MWCNT on nematode survival. Nevertheless, Sivaselvam et al. (2020) also demonstrated that albumin corona formation mitigated the damages of GO (0.5-100.0 mg L^{-1}) in acute toxicity assays.

Our data have revealed that albumin corona suppressed the acute toxicity of GO and MWCNT on the *C. elegans* model. Therefore, further experiments were performed to analyze whether nematodes were affected by the overproduction of reactive oxygen species. ROS are naturally produced in normal metabolism conditions by mitochondria respiration and are essential to homeostasis maintenance. However, when stimulated by pollutants, the production of ROS is the primary factor that impairs different organisms because an excessive amount of these species may result on oxidation and structural damage of proteins, lipids and DNA.

Thus, enhancement of ROS production is a common mechanism in toxicology because it is linked to the process of cell death (Finkel and Holbrook, 2000). Figure 4A evidences ROS overproduction in nematodes exposed to GO at 0.01; 0.1 and 1.0 mg L^{-1}. Likewise, exposure to BSA@GO increased the ROS level in nematodes, although it was less prominently since ROS generation was significantly higher in nematodes exposed to GO than BSA@GO at 0.1 and 1.0 mg L^{-1}. Exposure to MWCNT at 1.0 mg L^{-1} led to ROS overproduction, whereas BSA@MWCNT did not stimulate activation of stress on nematodes (Figure 4B). Therefore, our data indicate that GO was the material that more stimulated the ROS production, while MWCNT affected nematode only at 1.0 mg L^{-1} dose. Albumin corona reduced ROS overproduction induced by MWCNT exposure, and this same effect was observed in nematodes exposed to BSA@GO (0.1-10.0 mg L^{-1}), but the induction of stress was not totally suppressed in this case.

Figure 4 - Oxidative stress in nematodes exposed to bare and coated GO (A) and bare and coated MWCNT (B). Fluorescent microscope images of non-exposed nematodes (C), exposed to positive control - H_2O_2 at 5.0 mM (D), and exposed to GO (E), BSA@GO (F), MWCNT (G) and BSA@MWCNT (H) at 1.0 mg L^{-1}. Bars with ** are significantly different ($p \leq 0.05$) from the control or different between from one another.

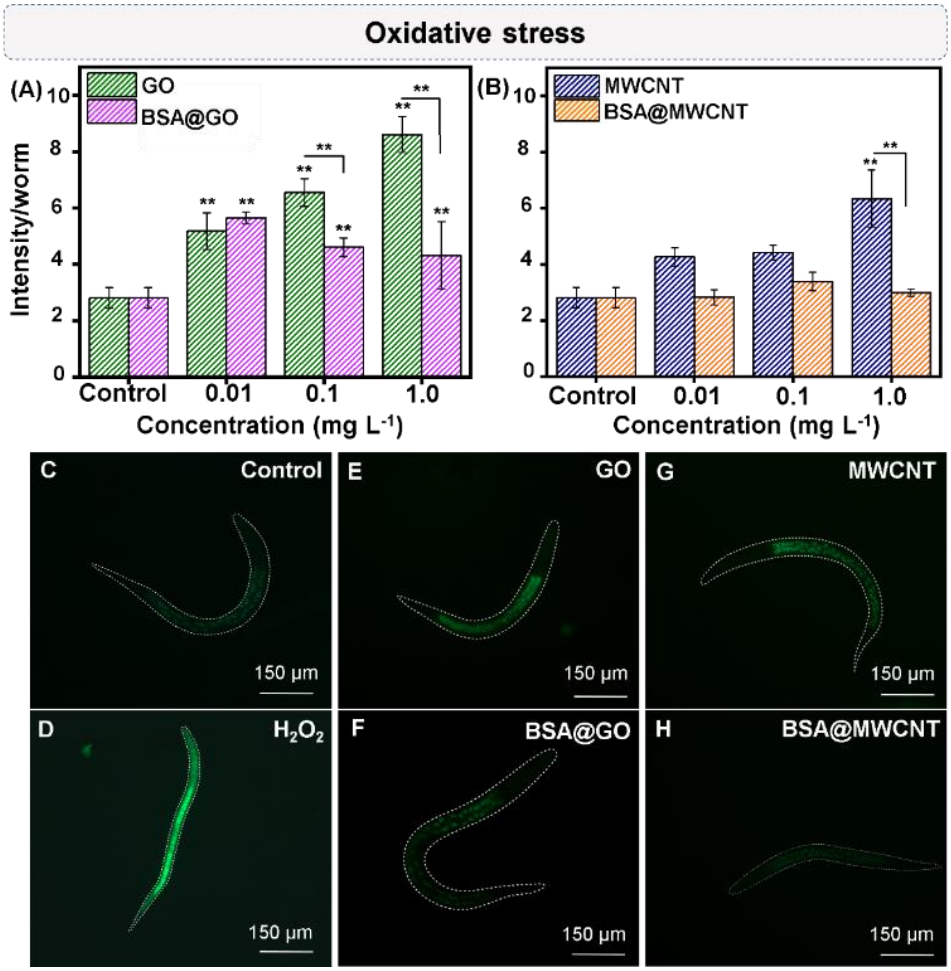

As mentioned, oxidative stress is a common mechanism that affects organisms when are exposed to environmental pollutants. In *C. elegans*, the intestine is a major stress response site, as it is one of the first lines of defense against toxicants (McGhee, 2007). Thus, excessive ROS production has been related to injuries in the *C. elegans* intestine (Kim et al., 2020b; Shu et al., 2015; Wu et al., 2014). In addition, a hyper-permeable state of the intestinal barrier has been observed in consequence of pollutants exposure. Influence of bare and coated materials on the physiological state of *C. elegans* intestine was investigated using a lipophilic fluorescent dye (i.e., Nile red) **(**Figure 5**).** Our result suggests that BSA@MWCNT did not negatively affect the nematode intestine, while the other materials impair this tissue. The relative fluorescence intensity of Nile red signal enhanced in worms exposed to GO, BSA@GO and MWCNT; however, it was similar to control for worms exposed to BSA@MWCNT (Figure 5A). For that reason, our results imply that GO, BSA@GO and MWCNT may contribute to disruption of the intestinal barrier, while BSA@MWCNT may not impair its functionality. GO was the material that more increased the permeability of the worm´s intestine, which was reduced because of albumin coating.

Figure 5 - Effects of bare and albumin-coated GO and MWCNT at 1.0 mg L^{-1} on *C. elegans* intestinal permeability (A) and fluorescent microscopy images of non-exposed nematodes (B) and exposed to GO (C), BSA@GO (D), MWCNT (E) and BSA@MWCNT (F). Bars with ** are significantly different ($p \leq 0.05$) from the control or different between from one another.

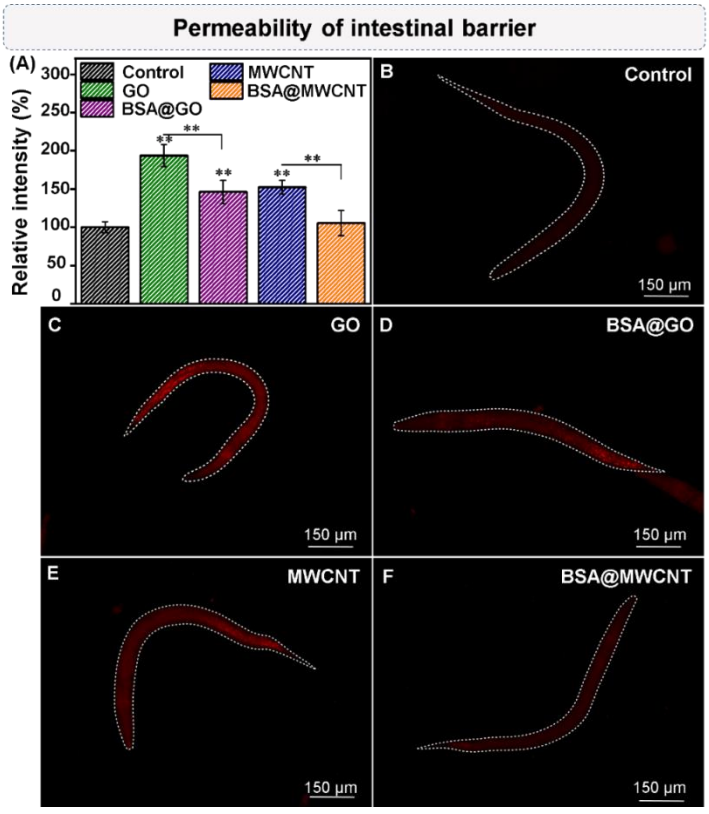

Other studies have noticed the hyper-permeable state of the *C. elegans* intestine due to GO and MWCNT exposures (Wu et al., 2013b; Y. Zhao et al., 2015; Zhi et al., 2016b). It was observed that MWCNT (100.0 mg L^{-1}) altered expression patterns of some genes required for intestinal development and affected mean defecation cycle length (Shu et al., 2015). Similar effects were noticed in worms exposed to GO (Wu et al., 2013b; Zhi et al., 2016b). Nevertheless, it is the first indication that corona-coated GO affected intestinal permeability. Intestine plays a crucial role in avoiding pollutants translocation within *C. elegans* (Wu et al., 2013a). Therefore, because of its hyper-permeable state, it is expected that materials have crossed this barrier reaching the secondary targeted organs, where they may cause damages to the functions of reproductive organs (Kim et al., 2020b, 2018). In this sense, the biodistribution of bare and corona coated materials within nematodes was evaluated in our study and its consequence on *C. elegans* development and reproduction.

Nanomaterials biodistribution was evaluated by Raman confocal spectroscopy to understand further the toxic effects of bare and coated samples on *C. elegans*. Both carbon materials exhibit characteristic Raman spectral signatures (D and G-bands, Figure S6) that permit their easy localization and identification inside organisms. Depth profile measurements were performed in strategic regions/points of *C. elegans* (head, intestine, gonad, egg and rectum). For this, nematode cuticle was considered the point zero, and then Raman spectra were acquired from -30 (i.e., above to the cuticle/out of organism) to 120 µm in-depth (i.e., within the organism) (Figure 6). Intensity of the D-band was choosed to be recorded, and maximum intensity was used to build the depth profiles shown in Figure 6. Profiles intensity and asymmetry were used to infer the presence of carbon materials and conclude about their internalization. Below two examples are discussed to detail how these conclusions were obtained. The first example is the graphic for GO in the nematode intestine. It is possible to observe a signal of GO outside the nematode (before point 0) that dropped and then increased after the cuticle (after point 0), indicating the presence of GO inside the nematode. The second example consists in observing the MWCNT internalization in the nematode head. In this graphic, there is a signal of MWCNT outside of *C. elegans*, which achieved the maximum intensity at -10 µm depth. But an asymmetry on the profile is observed between 10 and 40 µm depth indicating the occurrence of MWCNT in the nematode head.

Figure 6 and Figure S11 reveal that GO and BSA@GO were internalized and accumulated in the nematode head, intestine, gonad, eggs and rectum. MWCNT was also found in all regions, except in eggs. The internalization of BSA@MWCNT was not found in eggs and head but was observed in the intestine, gonad and rectum.

Figure 6 - Scheme of Raman spectroscopy experiment used to evaluate nanomaterials internalization in *C. elegans* (top). D-band intensity depth profiles (from -30 to 120 µm) used to monitor biodistribution of GO, BSA@GO, MWCNT and BSA@MWCNT in different tissues of nematodes. The laser power applied on a sampling point was 1.2 mW.

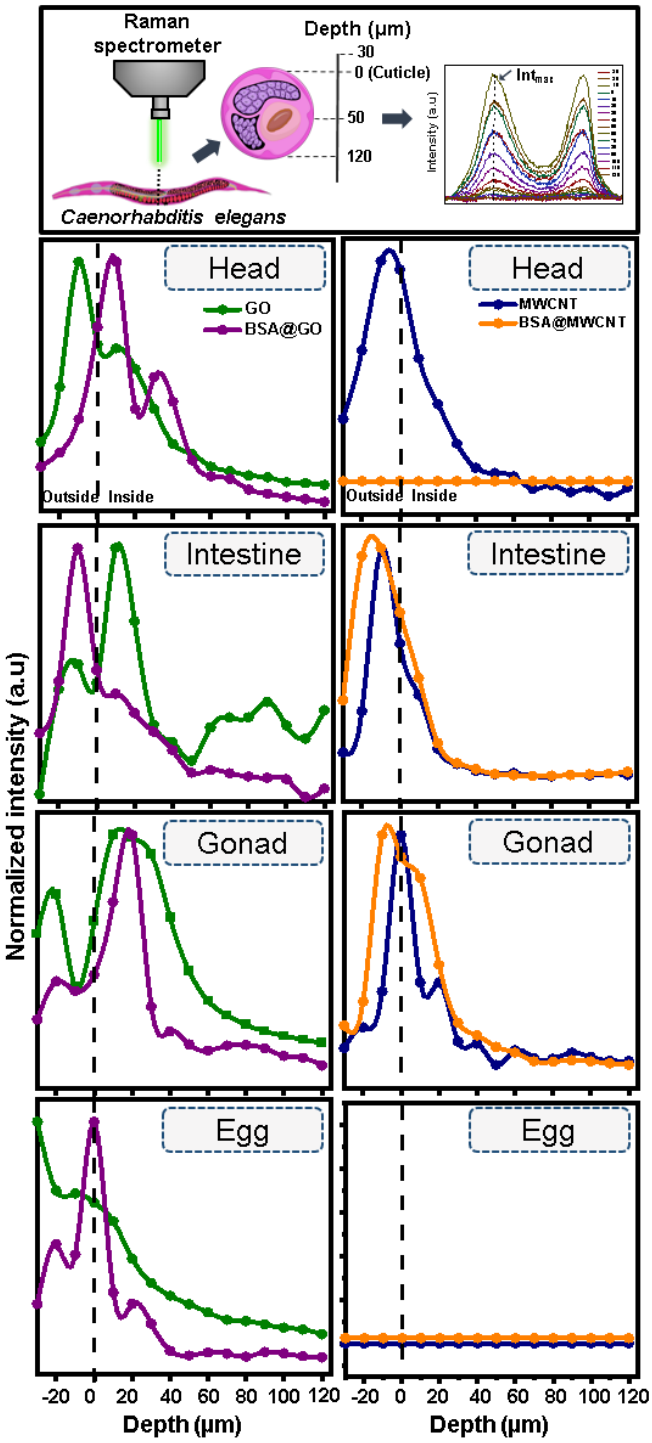

C. elegans presents a size-selective filtering mechanism in its buccal cavity that affects nanomaterials uptake in liquid media (Avery and You, 2012; Fang-Yen et al., 2009). However, once uptake by the *C. elegans* pharyngeal muscle movement, they can be transferred towards

its digestive system (i.e., pharynx, intestinal lumen and rectum), muscular and neuronal tissues. By crossing the intestinal barrier, they can distribute on the distal gonad and uterus, where embryos are matured before being released from the vulva (Hubbard and Reenstein, 2005). Therefore, nanomaterials translocation to reproductive organs may result in immature eggs and egg-laying difficulties, affecting the progeny number. Our results reveal that materials were found in the gonad, which evidences that they were translocated from the alimentary to reproductive system. However, only GO and BSA@GO were located inside nematode eggs. Three eggs shells usually wrap embryos; thus, the penetration of substances into them is hampered by these three layers (Qu et al., 2011). The occurrence of GO and BSA@GO in eggs demonstrates the possibility that they achieved embryos and be transferred from exposed nematodes to offspring. In addition, the existence of GO, BSA@GO and MWCNT in the nematode head region is an alarming signal because it is where most of the neurons are located, as well as muscles, glands and structural cells (Avery and You, 2012).

In addition to the translocation of nanomaterials inside the *C. elegans*, their accumulation or excretion by the nematodes is an important aspect to toxicological effects. Therefore, this dynamic was studied by Confocal Raman spectroscopy. Nematodes were exposed to materials for 48 h without food and transferred to NGM plates where they were maintained unfed for 12 h or fed with bacteria for 2 h. Our results (Figure S12) suggest that GO, BSA@GO, MWCNT and BSA@MWCNT could remain accumulated in the intestine of unfed nematodes even after 12 h. However, when food was restored, spectral signatures of BSA@MWCNT was not observed in the nematode intestine, indicating it was excreted. In addition, the signal of BSA@MWCNT inside the other nematode tissues became extremely low, suggesting that the amount of material in the targeted organs was reduced. Intestines of nematodes exposed to GO, BSA@GO and MWCNT showed spectral signatures even when they were feed for 2 h, indicating a longer retention time of these materials in *C. elegans* lumen. It is worth mentioning that the signal of GO, BSA@GO and MWCNT inside the nematode tissues also became worse due to the excretion. Therefore, it is not possible to conclude that the materials were fully eliminated from these tissues. In any case, non-excretion of these materials from the intestine indicate that it may cause other toxicity events in the nematodes.

In *C. elegans*, defection is a process controlled by the nervous system and performed through the rhythmic activation of a cycle of muscle contractions. Undigested materials are discarded by anus of nematodes in 50-second cycles, which can become more slowly (80-second cycles) or ceased, as food is not available (Gonzalez-Moragas et al., 2015b). Our data indicate that during the translocation of materials, only BSA@MWCNT did not

reached the nematode head, where most of the neurons are located. In contrast, other materials were translocated to this region and were not excreted, suggesting a correlation between the impaired nervous system and the defecation/excretion process.

Translocation and accumulation of bare and albumin corona coated GO and MWCNT within nematodes could negatively influence the functionality of their crucial organs. To observe these aspects, long-term exposure experiments were carried out monitoring the inhibition of nematode growth, reproduction and fertility as endpoints. Figure 7A and 7B show that 10.0 mg L^{-1} of GO or MWCNT disturbed nematode development because growth inhibition rates were 16.2±2.1% and 13.9±2.6%, respectively. On the other hand, BSA@GO and BSA@MWCNT did not affect *C. elegans* growth because the inhibition rates did not reach 10% (i.e., threshold). GO caused inhibition of reproduction at 1.0 mg L^{-1} (30.6±8.4%) and 10.0 mg L^{-1} (86.5±2.9%) (Figure 7C), as well as MWCNT at 10.0 mg L^{-1} (40.4±7.6%) (Figure 7D). BSA@GO was reprotoxic in all tested concentrations. GO was significantly more harmful to reproduction than BSA@GO at 10.0 mg L^{-1}. Conversely, nematode reproduction was not affected by BSA@MWCNT. Fertility was inhibited in nematodes exposed to GO at 1.0 mg L^{-1} (14.8±1.5%) and 10.0 mg L^{-1} (32.0±9.3%) (Figure 7E), besides to MWCNT at 10.0 mg L^{-1} (14.3±2.7%) (Figure 7F). Therefore, GO and MWCNT affected nematode growth, reproduction and fertility, while BSA@GO only impaired reproduction, and BSA@MWCNT did not induce chronic effects to *C. elegans.*

Figure 7 - Long-term effects of GO and BSA@GO on *C. elegans* growth (A), reproduction (B) and fertility (C), and MWCNT and BSA@MWCNT on growth (D), reproduction (E) and fertility (F). Bars with ** are significantly different ($p \leq 0.05$) from the control or different between from one another. The segmented red line represents the threshold (10%).

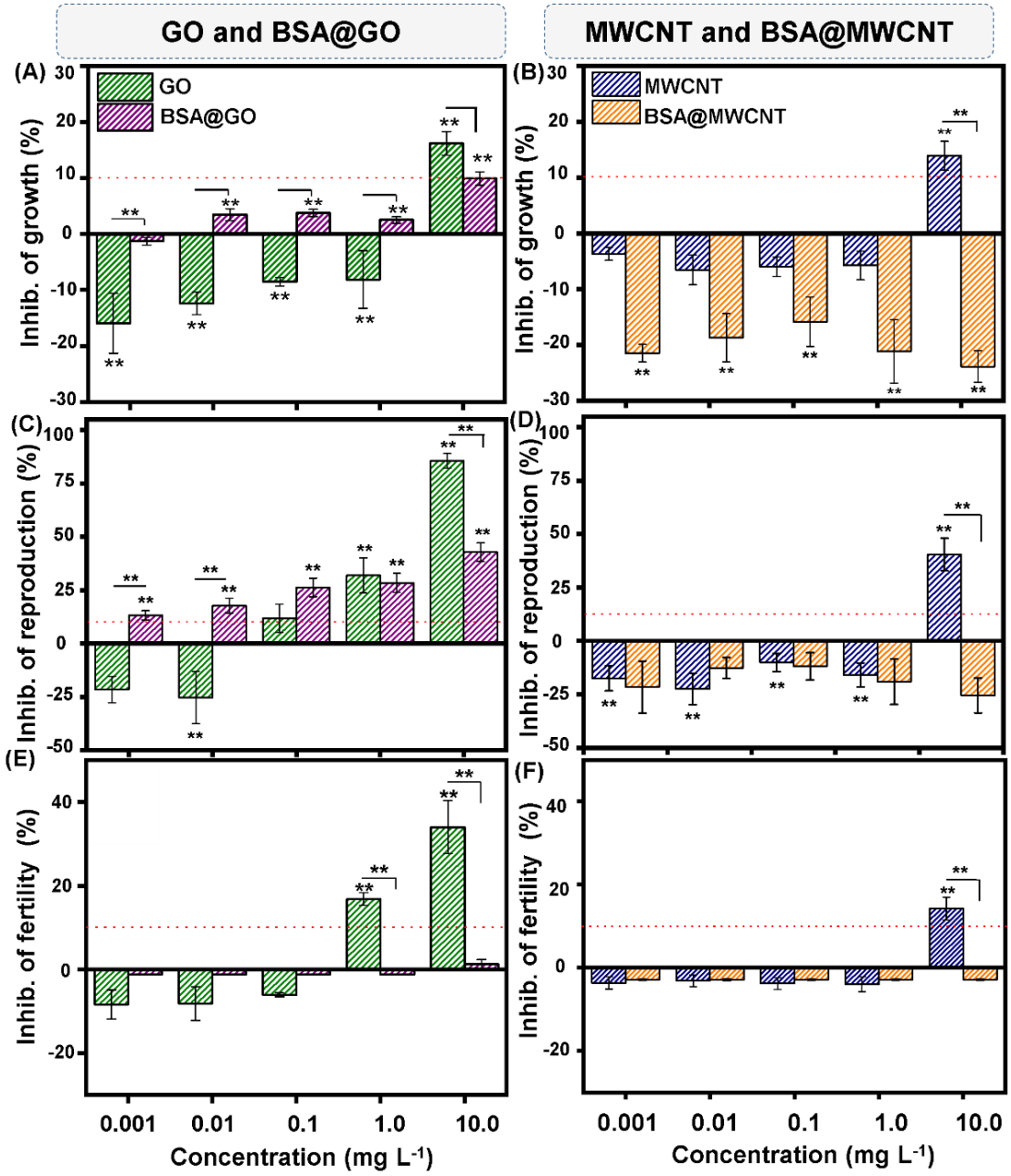

When worms face stress levels at the early exposure stage, they save energy typically used for their development, thus, the nematode growth is inhibited (Höss et al., 2020). Here, GO and MWCNT exposures affected nematodes growth, corroborating with the fact that exposure to these materials led to an oxidative stress scenario as observed at ROS assays (Figure 4). The potential of GO and MWCNT to be translocated inside *C. elegans* and induce reproductive toxicity agrees with the findings previously reported. GO, BSA@GO and

MWCNT were translocated from the intestine to the nematode gonad and hampered nematode reproduction, suggesting that these materials affected the functionality of this crucial organ, compromising the next generation of nematodes. However, only GO and MWCNT inhibited fertility, suggesting that their reprotoxic effects may be accumulative. Kim et al. (2018) also reported that GO was translocated to *C. elegans* gonads using Raman spectroscopy. Consequently, reduction of sperm and progeny numbers were observed, as well disruption of nematode fat metabolism. Nivedita et al. (2017) identified GO around germline and embryos and described that the Wnt-MAPK crosstalk pathway was related to reproductive failure promoted by GO exposure. Wu et al. (2013a) found MWCNT in *C. elegans* intestine, pharynx and gonad. In addition, damages on the reproductive system and neuronal tissues were observed in view of the fact that brood size was reduced, and nematode behaviour was affected after exposure to 0.1-1000 mg L^{-1} MWCNT. Similarly, Shu et al. (2015) proved that MWCNT (1.0-100 mg L^{-1}) decreased the offspring number and affected worm's locomotion, demonstrating potential repro- and neurotoxic effect of MWCNT. Therefore, our study confirms the evidence that GO and MWCNT are toxic for *C. elegans*. At short-term exposure, the effect of both on nematode survival was similar. However, oxidative stress activation and intestinal permeability enhancement were more significant in nematodes exposed to GO. Besides, GO was translocated to all *C. elegans* tissues, and its long-term effects were more pronounced than for MWCNT. However, GO and MWCNT present several physicochemical differences that may lead to different and complex biological responses (De Marchi et al., 2018; Kumar Babele et al., 2021; Ma et al., 2015; Ou et al., 2016; Rodrigues et al., 2020; Sydlik et al., 2015). Toxicity and the different patterns translocation of GO and MWCNT may be related to the physico-chemical properties of these materials, especially the different morphology features that GO and MWCNT showed (i.e., size, topography and surface roughness).

It has been shown before that biocorona reduces nanomaterials toxicity in vitro assays (Chong et al., 2015; Ge et al., 2011; Hu et al., 2011; Tenzer et al., 2013; X. Zhao et al., 2015). However, limited studies have been performed to understand the influence of biocorona-coated nanomaterials in in vivo assays, especially with *C. elegans* model. Until now, no study has compared the toxicity of bare and albumin-coated GO and MWCNT to *C. elegans*.

In our study, albumin corona reduced 100% the acute and chronic effects of MWCNT to *C. elegans* model, but the long-term effects of GO and its impacts on the intestinal barrier of nematodes were not totally mitigated. Among other factors, this result may be related to the fact that toxicity was governed by the differences found in the colloidal stability of bare and coated materials. As bare materials tended to deposit during short-term assays (Figure 2), it is expected

that worms have been exposed to higher concentration of GO and MWCNT than for albumin corona coated materials. In addition to the deposition, bare GO and MWCNT aggregated during the acute toxicity assays, which could hinder their internalization by the nematodes. Nevertheless, the worm's mouth at the L3 stage has ~ 4 μm (Mueller et al., 2020), suggesting that nematodes could easily ingest even the aggregated materials (Figure S13). Therefore, it is hypothesized that the higher delivery dose that nematodes were exposed to GO and MWCNT explain why nematodes were more affected by bare materials than coated ones in acute assays. At long-term biological tests, 100% of GO and MWCNT and 40% of BSA@GO suffered deposition, whereas BSA@MWCNT remained stable. BSA@MWCNT was the only one with no effects over nematodes during 96 h of experiment; thus, the low doses of exposure to this material may partially explain this result. On the other side, low doses of BSA@GO inhibited nematode reproduction. In fact, in the first 24 h, GO settled and aggregated, while BSA@GO did not aggregate. As *C. elegans* at the L1 stage presents a buccal cavity size of ~1 μm (Mueller et al., 2020), worms may have initially uptake more BSA@GO than GO. However, as GO was 100% deposited, nematodes began to ingest more GO as their mouth increased. At 10.0 mg L^{-1}, the availability of GO was higher than BSA@GO. Consequently, nematodes exposed to GO were more affected. Our results, therefore, evidence that differences in stability of bare and coated materials governed the dynamic of nematode exposure to materials and, subsequently, the toxicity. These findings point out that it is crucial to consider these differences in dispersion stability in our biological tests in terms of the bioavailability of tested material to *C. elegans*.

Despite there is not a dosimetry method developed for measuring the dose that reaches nematodes during tests (i.e., "bioavailable dose"), such as is calculated in in vitro dosimetry for cells (DeLoid et al., 2017, 2015), this influences biological response. In addition, the formation of aggregates and bacteria in chronic assays needs to be considered because it may make food unavailable, causing artefacts on toxicity (Hanna et al., 2018). Although materials have aggregated in our long-term tests, it was not observed clusters of bacteria and materials by visual inspection analyses (Figure S14), cancelling the supposition that lack of food for nematodes has caused toxicity.

The effects of protein-coated GO were also previously investigated by Sivaselvam et al. (2020), who reported that this coating mitigated the GO toxicity and hindered its translocation to secondary organs of *C. elegans*. However, we reported that, whereas albumin corona hindered the translocation of MWCNT on the nematode head and spermatheca region, BSA@GO was translocated to all the nematode tissues affecting their functionality. BSA@MWCNT was excreted by the nematodes when food was restored, indicating that the

amount of deposited BSA@MWCNT in the intestine and gonad of nematodes may not have been enough to affect the development and function of their intestinal barrier and reproductive organ in the long-term assays. In contrast, since BSA@GO remain accumulated in nematode intestine even after 2 h of food resumption, the higher bioavailability of BSA@GO in comparison to BSA@MWCNT could be responsible for the fact that the toxicity of BSA@GO was not totally mitigated.

Indeed, *C. elegans* intestine is a complex biological environment where nanomaterials and protein coatings may be degraded by the mild acidic conditions and enzymes of digestive system (Qu et al., 2011; Tan et al., 2020), therefore, the long-time of retention of BSA@GO in nematode could have led to partial degradation of albumin corona inside its intestine, reestablishing the adverse effects of GO, especially at long-term assays. It may elucidate why BSA@GO exposure enhanced intestinal barrier permeability and oxidative stress, causing inhibition of nematode reproduction. Although, further investigations are required to establish a detailed mechanism of albumin corona degradation. It is challenging due to the lack of accurate and reliable analytical methods to recover the corona-coated materials from biological tissues without disturbing their characteristics (Wheeler et al., 2021).

Finally, our results shed light on the fact that albumin coating suppressed the toxic effects of GO and MWCNT to *C. elegans* at short-term exposures; while mitigation of chronic toxic effects was more evident for MWCNT when compared to GO. GO, MWCNT and BSA@GO was translocated from intestinal barrier to secondary organs of *C. elegans*, remaining accumulated in nematode intestine, suggesting that it is mandatory considering the long-term impact of these nanomaterials, specially in studies that propose engineering the surface of the nanomaterials with protein coatings towards protecting organisms of their potential risks.

3.4. Conclusions

Graphene oxide and multi-walled carbon nanotubes were coronated with bovine serum albumin; altering the materials' thickness, roughness, surface charge, and chemical composition. Albumin corona increased materials' colloidal stability in the nematode testing medium; displaying an important role in toxicological assays. Pristine GO and MWCNT caused damage to nematode survival, growth, reproduction, and fertility, as well as enhanced oxidative stress and intestinal barrier permeability. However, the negative effects of GO and MWCNT on *C. elegans* survival were suppressed by albumin corona. Bare GO and MWCNT were

translocated from the intestine to secondary organs of *C. elegans*, but albumin coated hindered the translocation of MWCNT and protected the intestine and reproductive organ from the MWCNT damages. Long-term effects of GO were not entirely mitigated, and activation of stress and enhancement of intestinal permeability were observed for nematodes exposed to albumin-coated GO. In addition, albumin-coated GO remained accumulated in the nematode intestine even after food resumption. In this sense, we hypothesize that albumin corona on GO could be partially degraded inside *C. elegans*, re-establishing its adverse effects on the reproduction system and intestinal cells. Confocal Raman spectroscopy was confirmed as a powerful technique to probe the biodistribution of carbon nanomaterials inside *C. elegans*, without labelling or histological preparations.

References[5]

Aires, A., Cadenas, J.F., Guantes, R., Cortajarena, A.L., 2017. An experimental and computational framework for engineering multifunctional nanoparticles: designing selective anticancer therapies. Nanoscale 9, 13760–13771. https://doi.org/10.1039/C7NR04475E

Akhuli, A., Chakraborty, D., Agrawal, A.K., Sarkar, M., 2021. Probing the Interaction of Bovine Serum Albumin with Copper Nanoclusters: Realization of Binding Pathway Different from Protein Corona. Langmuir 37, 1823–1837. https://doi.org/10.1021/acs.langmuir.0c03176

Avery, L., You, Y.., 2012. *C. elegans* feeding, in: Erik M. Jorgensen (Ed.), The *C. elegans* Research Community, WormBook. p. 23. https://doi.org/10.1895/wormbook.1.150.1

Baalousha, M., Nur, Y., Römer, I., Tejamaya, M., Lead, J.R., 2013. Effect of monovalent and divalent cations, anions and fulvic acid on aggregation of citrate-coated silver nanoparticles. Sci. Total Environ. 454–455, 119–131. https://doi.org/10.1016/j.scitotenv.2013.02.093

Baun, A., Sayre, P., Steinhäuser, K.G., Rose, J., 2017. Regulatory relevant and reliable methods and data for determining the environmental fate of manufactured nanomaterials. NanoImpact. https://doi.org/10.1016/j.impact.2017.06.004

Becerril, H.A., Mao, J., Liu, Z., Stoltenberg, R.M., Bao, Z., Chen, Y., 2008. Evaluation of Solution-Processed Reduced Graphene Oxide Films as Transparent Conductors. ACS Nano 2, 463–470. https://doi.org/10.1021/cm060258+

Bortolozzo, L.S., Côa, F., Khan, L.U., Medeiros, A.M.Z., Silva, G.H., Delite, F.S., Strauss, M., Martinez, D.S.T., 2021. Mitigation of graphene oxide toxicity in *C. elegans* after chemical degradation with sodium hypochlorite. Chemosphere 130421. https://doi.org/10.1016/j.chemosphere.2021.130421

[5] Prepared according to Elsevier guide (NanoImpact Journal).

Cai, R., Chen, C., 2019. The Crown and the Scepter: Roles of the Protein Corona in Nanomedicine. Adv. Mater. 31, 1805740. https://doi.org/10.1002/adma.201805740

Canesi, L., Balbi, T., Fabbri, R., Salis, A., Damonte, G., Volland, M., Blasco, J., 2017. Biomolecular coronas in invertebrate species: Implications in the environmental impact of nanoparticles. NanoImpact 8, 89–98. https://doi.org/10.1016/j.impact.2017.08.001

Cerrillo, C., Barandika, G., Igartua, A., Areitioaurtena, O., Marcaide, A., Mendoza, G., 2015. Ecotoxicity of multiwalled carbon nanotubes: Standardization of the dispersion methods and concentration measurements. Environ. Toxicol. Chem. 34, 1854–1862. https://doi.org/10.1002/etc.2999

Chetwynd, A.J., Lynch, I., 2020. The rise of the nanomaterial metabolite corona, and emergence of the complete corona. Environ. Sci. Nano 7, 1041–1060. https://doi.org/10.1039/C9EN00938H

Chong, Y., Ge, C., Yang, Z., Garate, J.A., Gu, Z., Weber, J.K., Liu, J., Zhou, R., 2015. Reduced Cytotoxicity of Graphene Nanosheets Mediated by Blood-Protein Coating. ACS Nano 9, 5713–5724. https://doi.org/10.1021/nn5066606

Chowdhury, I., Mansukhani, N.D., Guiney, L.M., Hersam, M.C., Bouchard, D., 2015. Aggregation and Stability of Reduced Graphene Oxide: Complex Roles of Divalent Cations, pH, and Natural Organic Matter. Environ. Sci. Technol. 49, 10886–10893. https://doi.org/10.1021/acs.est.5b01866

Côa, F., Strauss, M., Clemente, Z., Rodrigues Neto, L.L., Lopes, J.R., Alencar, R.S., Souza Filho, A.G., Alves, O.L., Castro, V.L.S.S., Barbieri, E., Martinez, D.S.T., 2017. Coating carbon nanotubes with humic acid using an eco-friendly mechanochemical method: Application for Cu(II) ions removal from water and aquatic ecotoxicity. Sci. Total Environ. 607–608. https://doi.org/10.1016/j.scitotenv.2017.07.045

Datsyuk, V., Kalyva, M., Papagelis, K., Parthenios, J., Tasis, D., Siokou, A., Kallitsis, I., Galiotis, C., 2008. Chemical oxidation of multiwalled carbon nanotubes. Carbon N. Y. 46, 833–840. https://doi.org/10.1016/j.carbon.2008.02.012

De Marchi, L., Neto, V., Pretti, C., Figueira, E., Chiellini, F., Morelli, A., Soares, A.M.V.M., Freitas, R., 2018. Toxic effects of multi-walled carbon nanotubes on bivalves: Comparison between functionalized and nonfunctionalized nanoparticles. Sci. Total Environ. 622–623, 1532–1542. https://doi.org/10.1016/j.scitotenv.2017.10.031

De Medeiros, A.M.Z., Khan, L.U., da Silva, G.H., Ospina, C.A., Alves, O.L., de Castro, V.L., Martinez, D.S.T., 2021. Graphene oxide-silver nanoparticle hybrid material: an integrated nanosafety study in zebrafish embryos. Ecotoxicol. Environ. Saf. 209, 111776. https://doi.org/10.1016/j.ecoenv.2020.111776

Deline, A.R., Frank, B.P., Smith, C.L., Sigmon, L.R., Wallace, A.N., Gallagher, M.J., Goodwin, D.G., Durkin, D.P., Fairbrother, D.H., 2020. Influence of Oxygen-Containing Functional Groups on the Environmental Properties, Transformations, and Toxicity of Carbon Nanotubes. Chem. Rev. 120, 11651–11697. https://doi.org/10.1021/acs.chemrev.0c00351

DeLoid, G.M., Cohen, J.M., Pyrgiotakis, G., Demokritou, P., 2017. Preparation, characterization, and in vitro dosimetry of dispersed, engineered nanomaterials. Nat. Protoc. 12, 355–371. https://doi.org/10.1038/nprot.2016.172

Dorney, J., Bonnier, F., Garcia, A., Casey, A., Chambers, G., Byrne, H.J., 2012. Identifying and localizing intracellular nanoparticles using Raman spectroscopy. Analyst 137, 1111. https://doi.org/10.1039/c2an15977e

Du, J., Ge, C., Liu, Y., Bai, R., Li, D., Yang, Y., Liao, L., Chen, C., 2011. The Interaction of Serum Proteins with Carbon Nanotubes Depend on the Physicochemical Properties of Nanotubes. J. Nanosci. Nanotechnol. 11, 10102–10110. https://doi.org/10.1166/jnn.2011.4976

Du, P., Zhao, J., Mashayekhi, H., Xing, B., 2014. Adsorption of Bovine Serum Albumin and Lysozyme on Functionalized Carbon Nanotubes. J. Phys. Chem. C 118, 22249–22257. https://doi.org/10.1021/jp5044943

Efeoglu, E., Keating, M., McIntyre, J., Casey, A., Byrne, H.J., 2015. Determination of nanoparticle localisation within subcellular organelles in vitro using Raman spectroscopy. Anal. Methods 7, 10000–10017. https://doi.org/10.1039/C5AY02661J

Escorcia, W., Ruter, D.L., Nhan, J., Curran, S.P., 2018. Quantification of Lipid Abundance and Evaluation of Lipid Distribution in Caenorhabditis elegans by Nile Red and Oil Red O Staining. J. Vis. Exp. https://doi.org/10.3791/57352

Fang-Yen, C., Avery, L., Samuel, A.D.T., 2009. Two size-selective mechanisms specifically trap bacteria-sized food particles in Caenorhabditis elegans. Proc. Natl. Acad. Sci. 106, 20093–20096. https://doi.org/10.1073/pnas.0904036106

Finkel, T., Holbrook, N.J., 2000. Oxidants, oxidative stress and the biology of ageing. Nature 408, 239–247. https://doi.org/10.1038/35041687

Franqui, L.S., De Farias, M.A., Portugal, R. V., Costa, C.A.R., Domingues, R.R., Souza Filho, A.G., Coluci, V.R., Leme, A.F.P., Martinez, D.S.T., 2019. Interaction of graphene oxide with cell culture medium: Evaluating the fetal bovine serum protein corona formation towards in vitro nanotoxicity assessment and nanobiointeractions. Mater. Sci. Eng. C 100, 363–377. https://doi.org/10.1016/J.MSEC.2019.02.066

Gao, Y., Ren, X., Tan, X., Hayat, T., Alsaedi, A., Chen, C., 2017. Insights into key factors controlling GO stability in natural surface waters. J. Hazard. Mater. 335, 56–65. https://doi.org/10.1016/j.jhazmat.2017.04.027

Garcia-Bennett, A.E., Everest-Dass, A., Moroni, I., Rastogi, I. Das, Parker, L.M., Packer, N.H., Brown, L.J., 2019. Influence of surface chemistry on the formation of a protein corona on nanodiamonds. J. Mater. Chem. B 7, 3383–3389. https://doi.org/10.1039/C9TB00445A

Ge, C., Du, J., Zhao, L., Wang, L., Liu, Y., Li, D., Yang, Y., Zhou, R., Zhao, Y., Chai, Z., Chen, C., 2011. Binding of blood proteins to carbon nanotubes reduces cytotoxicity. Proc. Natl. Acad. Sci. 108, 16968–16973. https://doi.org/10.1073/pnas.1105270108

Gebregeorgis, A., Bhan, C., Wilson, O., Raghavan, D., 2013. Characterization of Silver/ Bovine Serum Albumin (Ag/BSA) nanoparticles structure: Morphological, compositional, and interaction studies. J. Colloid Interface Sci. 389, 31–41. https://doi.org/10.1016/j.jcis.2012.08.041

Gonzalez-Moragas, L., Yu, S.-M., Carenza, E., Laromaine, A., Roig, A., 2015. Protective Effects of Bovine Serum Albumin on Superparamagnetic Iron Oxide Nanoparticles Evaluated in the Nematode Caenorhabditis elegans. ACS Biomater. Sci. Eng. 1, 1129–1138. https://doi.org/10.1021/acsbiomaterials.5b00253

Hanna, S.K., Bustos, A.R.M., Peterson, A.W., Reipa, V., Scanlan, L.D., Coskun, S.H., Cho, T.J., Johnson, M.E., Hackley, V.A., Nelson, B.C., Winchester, M.R., Elliott, J.T., Petersen, E.J., 2018. Agglomeration of Escherichia coli with Positively Charged Nanoparticles Can Lead to Artifacts in a Standard Caenorhabditis elegans Toxicity Assay. Environ. Sci. Technol. 52, 5968–5978. https://doi.org/10.1021/acs.est.7b06099

Hansen, S.F., Lennquist, A., 2020. Carbon nanotubes added to the SIN List as a nanomaterial of Very High Concern. Nat. Nanotechnol. 15, 3–4. https://doi.org/10.1038/s41565-019-0613-9

Höss, S., Ahlf, W., Bergtold, M., Bluebaum-Gronau, E., Brinke, M., Donnevert, G., Menzel, R., Möhlenkamp, C., Ratte, H.-T., Traunspurger, W., Danwitz, B. von, Pluta, H.-J., 2012. Interlaboratory comparison of a standardized toxicity test using the nematode Caenorhabditis elegans (ISO 10872). Environ. Toxicol. Chem. 31, 1525–1535. https://doi.org/10.1002/etc.1843

Höss, S., Roessink, I., Brock, T.C.M., Traunspurger, W., 2020. Response of a nematode community to the fungicide fludioxonil in sediments of outdoor freshwater microcosms compared to a single species toxicity test. Sci. Total Environ. 710, 135627. https://doi.org/10.1016/j.scitotenv.2019.135627

Hu, W., Peng, C., Lv, M., Li, X., Zhang, Y., Chen, N., Fan, C., Huang, Q., 2011. Protein Corona-Mediated Mitigation of Cytotoxicity of Graphene Oxide. ACS Nano 5, 3693–3700. https://doi.org/10.1021/nn200021j

Hubbard, E.J.A., Reenstein, D., 2005. Introduction to the germ line. WormBook. https://doi.org/10.1895/wormbook.1.18.1

ISO, 2010. Water quality - Determination of the toxic effect of sediment and soil samples on growth, fertility and reproduction of Caenorhabditis elegans (Nematoda). Geneva, Switzerland.

Kavinkumar, T., Manivannan, S., 2016. Synthesis, Characterization and Gas Sensing Properties of Graphene Oxide-Multiwalled Carbon Nanotube Composite. J. Mater. Sci. Technol. 32, 626–632. https://doi.org/10.1016/j.jmst.2016.03.017

Kenry, K., Loh, K.P., Lim, C.T., 2016. Molecular interactions of graphene oxide with human blood plasma proteins. Nanoscale 8, 9425–9441. https://doi.org/10.1039/C6NR01697A

Kim, M., Eom, H.-J., Choi, I., Hong, J., Choi, J., 2020a. Graphene oxide-induced neurotoxicity on neurotransmitters, AFD neurons and locomotive behavior in Caenorhabditis elegans. Neurotoxicology 77, 30–39. https://doi.org/10.1016/j.neuro.2019.12.011

Kim, M., Eom, H.J., Choi, I., Hong, J., Choi, J., 2020b. Graphene oxide-induced neurotoxicity on neurotransmitters, AFD neurons and locomotive behavior in Caenorhabditis elegans. Neurotoxicology 77, 30–39. https://doi.org/10.1016/j.neuro.2019.12.011

Kim, Y., Jeong, J., Yang, J., Joo, S.-W., Hong, J., Choi, J., 2018. Graphene oxide nano-bio interaction induces inhibition of spermatogenesis and disturbance of fatty acid metabolism in the nematode Caenorhabditis elegans. Toxicology 410, 83–95. https://doi.org/10.1016/j.tox.2018.09.006

Kleiven, M., Oughton, D., 2015. Standard Operating Procedure Toxicity test with the nematode Caenorhabiditis elegans for the NANoREG core nanomaterials.

Kumar Babele, P., Kumar Verma, M., Kant Bhatia, R., 2021. Carbon nanotubes: A review on risks assessment, mechanism of toxicity and future directives to prevent health implication. Biocell 45, 267–279. https://doi.org/10.32604/biocell.2021.013409

Laux, P., Riebeling, C., Booth, A.M., Brain, J.D., Brunner, J., Cerrillo, C., Creutzenberg, O., Estrela-Lopis, I., Gebel, T., Johanson, G., Jungnickel, H., Kock, H., Tentschert, J., Tlili, A., Schäffer, A., Sips, A.J.A.M., Yokel, R.A., Luch, A., 2018. Challenges in characterizing the environmental fate and effects of carbon nanotubes and inorganic nanomaterials in aquatic systems. Environ. Sci. Nano 5, 48–63. https://doi.org/10.1039/C7EN00594F

Lázaro, I., Sharp, P., Gurcan, C., Ceylan, A., Stylianou, M., Kisby, T., Chen, Y., Vranic, S., Barr, K., Taheri, H., Ozen, A., Bussy, C., Yilmazer, A., Kostarelos, K., 2021. Deep Tissue Translocation of Graphene Oxide Sheets in Human Glioblastoma 3D Spheroids and an Orthotopic Xenograft Model. Adv. Ther. 4, 2000109. https://doi.org/10.1002/adtp.202000109

Li, P., Xu, T., Wu, S., Lei, L., He, D., 2017. Chronic exposure to graphene-based nanomaterials induces behavioral deficits and neural damage in Caenorhabditis elegans. J. Appl. Toxicol. 37, 1140–1150. https://doi.org/10.1002/jat.3468

Ma, J., Liu, R., Wang, X., Liu, Q., Chen, Y., Valle, R.P., Zuo, Y.Y., Xia, T., Liu, S., 2015. Crucial Role of Lateral Size for Graphene Oxide in Activating Macrophages and Stimulating Pro-inflammatory Responses in Cells and Animals. ACS Nano 9, 10498–10515. https://doi.org/10.1021/acsnano.5b04751

Maiti, D., Tong, X., Mou, X., Yang, K., 2019. Carbon-Based Nanomaterials for Biomedical Applications: A Recent Study. Front. Pharmacol. 9. https://doi.org/10.3389/fphar.2018.01401

Marchesan, S., Prato, M., 2015. Under the lens: carbon nanotube and protein interaction at the nanoscale. Chem. Commun. 51, 4347–4359. https://doi.org/10.1039/C4CC09173F

Mariam, J., Sivakami, S., Dongre, P.M., 2016. Albumin corona on nanoparticles – a strategic approach in drug delivery. Drug Deliv. 23, 2668–2676. https://doi.org/10.3109/10717544.2015.1048488

Markiewicz, M., Kumirska, J., Lynch, I., Matzke, M., Köser, J., Bemowsky, S., Docter, D., Stauber, R., Westmeier, D., Stolte, S., 2018. Changing environments and biomolecule coronas: Consequences and challenges for the design of environmentally acceptable engineered nanoparticles. Green Chem. 20, 4133–4168. https://doi.org/10.1039/c8gc01171k

Martinez, D.S.T., Da Silva, G.H., de Medeiros, A.M.Z., Khan, L.U., Papadiamantis, A.G., Lynch, I., 2020. Effect of the Albumin Corona on the Toxicity of Combined Graphene Oxide and Cadmium to Daphnia magna and Integration of the Datasets into the NanoCommons Knowledge Base. Nanomaterials 10, 1936. https://doi.org/10.3390/nano10101936

Maurer, L.L., Ryde, I.T., Yang, X., Meyer, J.N., 2015. Caenorhabditis elegans as a Model for Toxic Effects of Nanoparticles: Lethality, Growth, and Reproduction. Curr. Protoc. Toxicol. 66, 20.10.1-20.10.25. https://doi.org/10.1002/0471140856.tx2010s66

McGhee, J., 2007. The *C. elegans* intestine. WormBook. https://doi.org/10.1895/wormbook.1.133.1

Michnik, A., 2003. Thermal stability of bovine serum albumin DSC study. J. Therm. Anal. Calorim. 71, 509–519. https://doi.org/10.1023/A:1022851809481

Mueller, M.-T., Fueser, H., Trac, L.N., Mayer, P., Traunspurger, W., Höss, S., 2020. Surface-Related Toxicity of Polystyrene Beads to Nematodes and the Role of Food Availability. Environ. Sci. Technol. 54, 1790–1798. https://doi.org/10.1021/acs.est.9b06583

Natarajan, L., Jenifer, M.A., Mukherjee, A., 2021. Eco-corona formation on the nanomaterials in the aquatic systems lessens their toxic impact: A comprehensive review. Environ. Res. 194, 110669. https://doi.org/10.1016/j.envres.2020.110669

Nel, A.E., Mädler, L., Velegol, D., Xia, T., Hoek, E.M. V, Somasundaran, P., Klaessig, F., Castranova, V., Thompson, M., 2009. Understanding biophysicochemical interactions at the nano–bio interface. Nat. Mater. 8, 543–557. https://doi.org/10.1038/nmat2442

Newman, L., Rodrigues, A.F., Jasim, D.A., Vacchi, I.A., Ménard-Moyon, C., Bianco, A., Bussy, C., Kostarelos, K., 2020. Nose-to-Brain Translocation and Cerebral Biodegradation of Thin Graphene Oxide Nanosheets. Cell Reports Phys. Sci. 1, 100176. https://doi.org/10.1016/j.xcrp.2020.100176

Nivedita, C., Young-ho, K., Jisu, Y., P, R.C., Woo, J.S., Jinhee, C., 2017. A systems toxicology approach reveals the Wnt-MAPK crosstalk pathway mediated reproductive failure in Caenorhabditis elegans exposed to graphene oxide (GO) but not to reduced graphene oxide (rGO). Nanotoxicology 0, 000. https://doi.org/10.1080/17435390.2016.1267273

Nouara, A., Wu, Q., Li, Y., Tang, M., Wang, H., Zhao, Y., Wang, D., 2013. Carboxylic acid functionalization prevents the translocation of multi-walled carbon nanotubes at predicted environmentally relevant concentrations into targeted organs of nematode Caenorhabditis elegans. Nanoscale 5, 6088. https://doi.org/10.1039/c3nr00847a

OECD, 2020. Guidance document on aquatic and sediment toxicological testing of nanomaterials, OECD Publishing.

OECD, 2017. Test No. 318: Dispersion Stability of Nanomaterials in Simulated Environmental Media, OECD Guidelines for the Testing of Chemicals, Section 3. OECD. https://doi.org/10.1787/9789264284142-en

Ou, L., Song, B., Liang, H., Liu, J., Feng, X., Deng, B., Sun, T., Shao, L., 2016. Toxicity of graphene-family nanoparticles: a general review of the origins and mechanisms. Part. Fibre Toxicol. 13, 57. https://doi.org/10.1186/s12989-016-0168-y

Park, S., Lee, K.-S., Bozoklu, G., Cai, W., Nguyen, S.T., Ruoff, R.S., 2008. Graphene Oxide Papers Modified by Divalent Ions—Enhancing Mechanical Properties via Chemical Cross-Linking. ACS Nano 2, 572–578. https://doi.org/10.1021/nn700349a

Peng, Z.G., Hidajat, K., Uddin, M.S., 2004. Adsorption of bovine serum albumin on nanosized magnetic particles. J. Colloid Interface Sci. 271, 277–283. https://doi.org/10.1016/j.jcis.2003.12.022

Petersen, E.J., Henry, T.B., Zhao, J., MacCuspie, R.I., Kirschling, T.L., Dobrovolskaia, M.A., Hackley, V., Xing, B., White, J.C., 2014. Identification and Avoidance of Potential Artifacts and Misinterpretations in Nanomaterial Ecotoxicity Measurements. Environ. Sci. Technol. 48, 4226–4246. https://doi.org/10.1021/es4052999

Porta-de-la-Riva, M., Fontrodona, L., Villanueva, A., Cerón, J., 2012. Basic Caenorhabditis elegans Methods: Synchronization and Observation. J. Vis. Exp. https://doi.org/10.3791/4019

Qu, Y., Li, W., Zhou, Y., Liu, X., Zhang, L., Wang, L., Li, Y.F., Iida, A., Tang, Z., Zhao, Y., Chai, Z., Chen, C., 2011. Full assessment of fate and physiological behavior of quantum dots utilizing Caenorhabditis elegans as a model organism. Nano Lett. 11, 3174–3183. https://doi.org/10.1021/nl201391e

Rodrigues, A.F., Newman, L., Jasim, D., Mukherjee, S.P., Wang, J., Vacchi, I.A., Ménard-Moyon, C., Bianco, A., Fadeel, B., Kostarelos, K., Bussy, C., 2020. Size-Dependent Pulmonary Impact of Thin Graphene Oxide Sheets in Mice: Toward Safe-by-Design. Adv. Sci. 7, 1903200. https://doi.org/10.1002/advs.201903200

Shu, C., Yu, X., Wu, Q., Zhuang, Z., Zhang, W., Wang, D., 2015. Pretreatment with paeonol prevents the adverse effects and alters the translocation of multi-walled carbon nanotubes in nematode Caenorhabditis elegans. RSC Adv. 5, 8942–8951. https://doi.org/10.1039/C4RA14377A

Singh, N., Marets, C., Boudon, J., Millot, N., Saviot, L., Maurizi, L., 2021. In vivo protein corona on nanoparticles: does the control of all material parameters orient the biological behavior? Nanoscale Adv. 3, 1209–1229. https://doi.org/10.1039/D0NA00863J

Sivaselvam, S., Mohankumar, A., Thiruppathi, G., Sundararaj, P., Viswanathan, C., Ponpandian, N., 2020. Engineering the surface of graphene oxide with bovine serum albumin for improved biocompatibility in Caenorhabditis elegans. Nanoscale Adv. 2, 5219–5230. https://doi.org/10.1039/D0NA00574F

Soares, M.V., Charão, M.F., Jacques, M.T., dos Santos, A.L.A., Luchese, C., Pinton, S., Ávila, D.S., 2020. Airborne toluene exposure causes germline apoptosis and neuronal damage that promotes neurobehavioural changes in Caenorhabditis elegans. Environ. Pollut. 256, 113406. https://doi.org/10.1016/j.envpol.2019.113406

Sopotnik, M., Leonardi, A., Križaj, I., Dušak, P., Makovec, D., Mesarič, T., Ulrih, N.P., Junkar, I., Sepčić, K., Drobne, D., 2015. Comparative study of serum protein binding to three different carbon-based nanomaterials. Carbon 95, 560-572. https://doi.org/10.1016/j.carbon.2015.08.018

StatNano, 2018. StatNano Annual report 2017. https://doi.org/10.22631/sar.2018.03

Stiernagle, T., 2006. Maintenance of *C. elegans*. WormBook 1-11. https://doi.org/10.1895/wormbook.1.101.1

Sun, B., Zhang, Y., Chen, W., Wang, K., Zhu, L., 2018. Concentration Dependent Effects of Bovine Serum Albumin on Graphene Oxide Colloidal Stability in Aquatic Environment. Environ. Sci. Technol. 52, 7212–7219. https://doi.org/10.1021/acs.est.7b06218

Sydlik, S.A., Jhunjhunwala, S., Webber, M.J., Anderson, D.G., Langer, R., 2015. In Vivo Compatibility of Graphene Oxide with Differing Oxidation States. ACS Nano 9, 3866–3874. https://doi.org/10.1021/acsnano.5b01290

Tan, Y., Zhu, X., Wu, D., Song, E., Song, Y., 2020. Compromised Autophagic Effect of Polystyrene Nanoplastics Mediated by Protein Corona Was Recovered after Lysosomal Degradation of Corona. Environ. Sci. Technol. 54, 11485–11493. https://doi.org/10.1021/acs.est.0c04097

Tenzer, S., Docter, D., Kuharev, J., Musyanovych, A., Fetz, V., Hecht, R., Schlenk, F., Fischer, D., Kiouptsi, K., Reinhardt, C., Landfester, K., Schild, H., Maskos, M., Knauer, S.K., Stauber, R.H., 2013. Rapid formation of plasma protein corona critically affects nanoparticle pathophysiology. Nat. Nanotechnol. 8, 772–781. https://doi.org/10.1038/nnano.2013.181

Treuel, L., Docter, D., Maskos, M., Stauber, R.H., 2015. Protein corona – from molecular adsorption to physiological complexity. Beilstein J. Nanotechnol. 6, 857–873. https://doi.org/10.3762/bjnano.6.88

Tsai, M.-H., Chao, H.-R., Jiang, J.-J., Su, Y.-H., Cortez, M.P., Tayo, L.L., Lu, I.-C., Hsieh, H., Lin, C.-C., Lin, S.-L., Wan Mansor, W.N., Su, C.-K., Huang, S.-T., Hsu, W.-L., 2021. Toxicity of Low-dose Graphene Oxide Nanoparticles in an in-vivo Wild Type of Caenorhabditis elegans Model. Aerosol Air Qual. Res. 21. https://doi.org/10.4209/aaqr.200559

Wheeler, K.E., Chetwynd, A.J., Fahy, K.M., Hong, B.S., Tochihuitl, J.A., Foster, L.A., Lynch, I., 2021. Environmental dimensions of the protein corona. Nat. Nanotechnol. 16, 617–629. https://doi.org/10.1038/s41565-021-00924-1

Wu, Q., Li, Yinxia, Li, Yiping, Zhao, Y., Ge, L., Wang, H., Wang, D., 2013a. Crucial role of the biological barrier at the primary targeted organs in controlling the translocation and toxicity of multi-walled carbon nanotubes in the nematode Caenorhabditis elegans. Nanoscale 5, 11166. https://doi.org/10.1039/c3nr03917j

Wu, Q., Yin, L., Li, X., Tang, M., Zhang, T., Wang, D., 2013b. Contributions of altered permeability of intestinal barrier and defecation behavior to toxicity formation from graphene oxide in nematode Caenorhabditis elegans. Nanoscale 5, 9934. https://doi.org/10.1039/c3nr02084c

Wu, Q., Zhao, Y., Fang, J., Wang, D., 2014. Immune response is required for the control of in vivo translocation and chronic toxicity of graphene oxide. Nanoscale 6, 5894. https://doi.org/10.1039/c4nr00699b

Wu, Q., Zhou, X., Han, X., Zhuo, Y., Zhu, S., Zhao, Y., Wang, D., 2016. Genome-wide identification and functional analysis of long noncoding RNAs involved in the response to graphene oxide. Biomaterials 102, 277–291. https://doi.org/10.1016/j.biomaterials.2016.06.041

Wu, T., Xu, H., Liang, X., Tang, M., 2019. Caenorhabditis elegans as a complete model organism for biosafety assessments of nanoparticles. Chemosphere 221, 708–726. https://doi.org/10.1016/j.chemosphere.2019.01.021

Yang, J., Zhao, Y., Wang, Y., Wang, H., & Wang, D. (2015). Toxicity evaluation and translocation of carboxyl functionalized graphene in Caenorhabditis elegans. Toxicology Research, 4(6), 1498–1510. https://doi.org/10.1039/C5TX00137D

Yu, X., Sun, S., Zhou, L., Miao, Z., Zhang, X., Su, Z., Wei, G., 2019. Removing Metal Ions from Water with Graphene–Bovine Serum Albumin Hybrid Membrane. Nanomaterials 9, 276. https://doi.org/10.3390/nano9020276

Zhang, T., Tang, M., Yao, Y., Ma, Y., Pu, Y., 2019. MWCNT interactions with protein: surface-induced changes in protein adsorption and the impact of protein corona on cellular uptake and cytotoxicity. Int. J. Nanomedicine Volume 14, 993–1009. https://doi.org/10.2147/IJN.S191689

Zhao, X., Lu, D., Hao, F., Liu, R., 2015a. Exploring the diameter and surface dependent conformational changes in carbon nanotube-protein corona and the related cytotoxicity. J. Hazard. Mater. 292, 98–107. https://doi.org/10.1016/j.jhazmat.2015.03.023

Zhao, Y., Yu, X., Jia, R., Yang, R., Rui, Q., Wang, D., 2015b. Lactic Acid Bacteria Protects Caenorhabditis elegans from Toxicity of Graphene Oxide by Maintaining Normal Intestinal Permeability under different Genetic Backgrounds. Sci. Rep. 5, 17233. https://doi.org/10.1038/srep17233

Zhi, L., Fu, W., Wang, X., Wang, D., 2016a. ACS-22, a protein homologous to mammalian fatty acid transport protein 4, is essential for the control of the toxicity and translocation of multi-walled carbon nanotubes in Caenorhabditis elegans. RSC Adv. 6, 4151–4159. https://doi.org/10.1039/C5RA23543J

Zhi, L., Ren, M., Qu, M., Zhang, H., Wang, D., 2016b. Wnt Ligands Differentially Regulate Toxicity and Translocation of Graphene Oxide through Different Mechanisms in Caenorhabditis elegans. Sci. Rep. 6, 39261. https://doi.org/10.1038/srep39261

4. CHAPTER 4. INFLUENCE OF *Escherichia coli* CORONA FORMATION ON COMBINED TOXICITY OF GRAPHENE OXIDE WITH SILVER IONS IN *Caenorhabditis elegans*[6]

Graphical Abstract

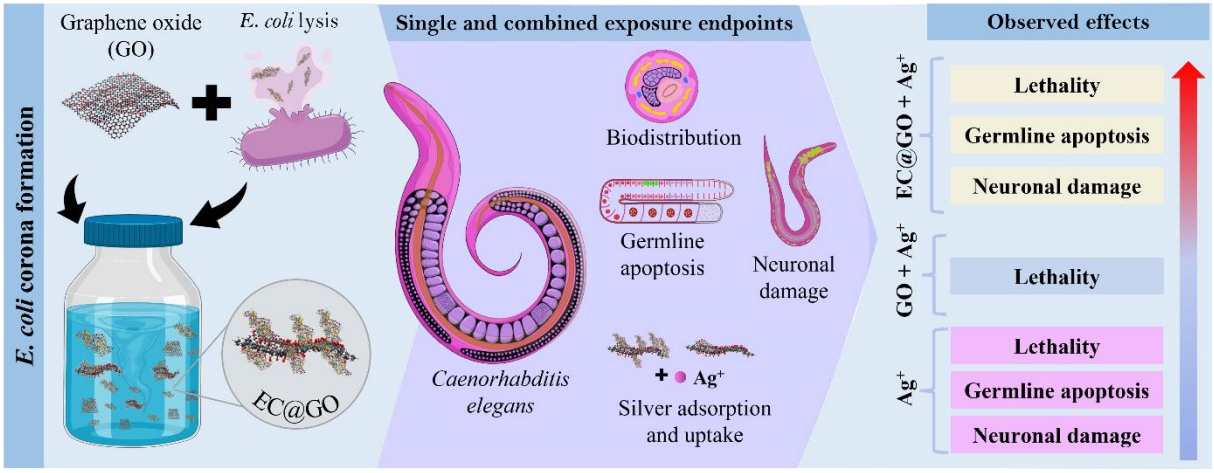

Abstract

Although adding bacteria as a food source for *Caenorhabditis elegans* is crucial to avoid starvation during nanotoxicity studies, the effect of *Escherichia coli* corona formation on biological response is still unknown. This study aimed to investigate how *E. coli* corona formation affects behaviour and the combined toxicity of graphene oxide (GO) with silver ions to *C. elegans*. Critical alterations were observed in the physicochemical properties of GO due to the biocorona formation. The surface modification with biocorona increased the potential of GO to adsorb silver ions by three times and improved its colloidal stability in EPA (tested medium). *E. coli* corona mitigated GO adverse effects on nematode survival; however, bare and coated GO crossed the nematode intestinal barrier, reaching its secondary target organs. Both damaged the germline of the nematodes, while only bare GO induced neural injuries. Combined exposure of GO and Ag^+ enhanced the silver lethality to nematode survival by 210%, while this effect was 460% higher for coated GO. Both GO+Ag^+ and EC@GO+Ag^+ were translocated to secondary organs of *C. elegans*, where they induced apoptotic corpses in the germline and potential injuries to neurons. Silver ions were internalized by the nematodes, but nematodes exposed to EC@GO+Ag^+ internalized 200% more silver than nematodes exposed to GO+Ag^+.

[6] This article was elaborated in collaboration with other authors (Mathias Strauss, Fabricio Delite, Daiana Ávila, Carlos A. Pérez, Cássio H. Abreu-Junior, Iseult Lynch and Diego S.T. Martinez).

Consequently, the adverse effects of EC@GO+Ag^{+} on *C. elegans* germline and neurons were higher than the combined effects of GO+Ag^{+}. Therefore, this study indicates that biocorona formation plays a crucial influence on nanotoxicity assays with *C. elegans*; interactions between biomolecules derived from bacteria and nanomaterials must be considered an integral part of toxicity assessment.

Keywords: joint toxicity; germline apoptosis; neuronal damage; uptake

4.1. Introduction

Caenorhabditis elegans is a free-living nematode exploited as a model organism in multiple biomedical and environmental toxicology fields. It exhibits 41.7% genome homology with humans and shares numerous biological characteristics with humans regarding physiology, anatomy, and metabolism. Most of its neurotransmitters correspond to human neurotransmitter system components, which is a crucial aspect to study human neurological diseases and the impacts of pollutants on the neural system. *C. elegans* also presents a translucent body, small size, and short life cycle, which permits quick investigation of the uptake and biodistribution of substances inside its body and their short-time adverse effects (Brenner, 1974; Hunt, 2017; Schafer, 2005).

Several studies have demonstrated the feasibility and advantages of using *C. elegans* to identify the potential therapeutic of new drugs or to evaluate the safety of nanomaterials (NMs) (Rossbach et al., 2022; Yao et al., 2022). However, some factors can modulate nanomaterial exposure in *C. elegans*, leading sometimes to misrepresentative results (Gonzalez-Moragas et al., 2017). The standard bacteria food source (*Escherichia coli*) is crucial to avoid starvation effects, however, adds considerable drawbacks to biological assays (Hanna et al., 2018). NMs and bacteria can not only interact in solid or liquid media but also because they can be concomitantly internalised, ground into the pharynx, and transferred to the intestine. Then, NMs will come into contact with *E. coli* lysed content and other secreted macromolecules, which may coat their highly reactive surface. This coating, known as biocorona, commonly modifies the NMs surface and physicochemical characteristics (e.g., shape, surface composition), determining their colloidal stability in biological media and impacts on the organisms. Although the biocorona concept has been widely studied in the blood and environmental matrices (Canesi et al., 2017), it has not been addressed thus far in *C. elegans* assays.

Graphene oxide (GO) is a carbon nanomaterial extensively exploited in biomedical areas, batteries, and sensors (Maiti et al., 2019). However, it can negatively affect *C. elegans* survival and damage its primary and secondary targeted organs (Kim et al., 2020; Zhao et al., 2020; Zhi et al., 2016). Our previous study reported that GO was translocated from the nematode intestine to secondary organs, affecting the intestinal barrier and reducing nematode survival, reproduction, fertility, and growth (Côa et al., 2022). In addition, it has been demonstrated the potential of GO act as carrier transferring pollutants among different environmental matrices for several organisms (Cao et al., 2021; Martinez et al., 2022). Nonetheless, it is a not clear whether graphene oxide can modulate the toxicity of environmental pollutants to *C. elegans*.

In addition to carbon nanomaterials, heavy metal pollutants are largely distributed in the environment due to natural sources (geological background) and industrial activities (Zhang and Wang, 2020). Although some metals are essential to maintain the functionality of biological systems, they can also be introduced as very harmful pollutants in the environment, causing undesirable effects on the organisms, such as neurotoxicity, hepatotoxicity, and nephrotoxicity (Ali et al., 2019). Mercury, nickel, lead, copper and silver are some of the heavy metals that have been reported as toxic for *C. elegans* and implicated in reduced survival, life span, reproduction and locomotion behaviour (Du and Wang, 2009; Wang and Wang, 2008a; Wu et al., 2011).

Release of NMs into the environment has raised great concern in terms of toxicology because they can interact with these pre-existing pollutants, causing unexpected effects (Liu et al., 2018). It was reported that TiO_2 nanoparticles interacted with arsenic, cadmium, and nickel, increasing their bioaccumulation and reproductive toxicity for *C. elegans* (Wang et al., 2018). Similar toxicity results were observed in a co-exposure scenario between polystyrene nanoparticles and organochlorine pesticides (Li et al., 2020), suggesting that the association of different pollutant effects needs to be further addressed to predict a more realistic environmental impact.

Although it is widely discussed that biocorona formation can interfere in the toxicological response to NMs, the effect of *E. coli* corona formation on *C. elegans* assays is still unclear. In this regard, we proposed assessing the *E. coli* corona formation on the GO surface and its influence in a co-exposure scenario with a heavy metal pollutant (silver ions). Physicochemical properties of GO were evaluated before and after biocorona formation, as well as its colloidal stability. The effects of single and co-exposure were assessed by nematode survival, germline apoptosis, and neuronal damage endpoints. In addition, the uptake,

distribution and accumulation of uncoated and coated GO without and with silver ions were investigated by confocal Raman spectroscopy, and the total silver concentration internalised by nematodes was quantitatively assessed by ICP-MS. Our findings provide the very first evidence that biocorona formation influence on nanotoxicity assays with *C. elegans* in single and co-exposure testing.

4.2. Material and methods

4.2.1. Materials

Graphene oxide was prepared according to a modified Hummers' method, as detailed before by Côa et al. (2022). Briefly, GO was obtained from oxidative exfoliation of graphite flakes with sulfuric acid and potassium permanganate. After synthesis, GO was freeze-dried and stored. Before experiments, GO stock-dispersion (0.5 mg mL^{-1}) was prepared according to the OECD Guideline No. 318 (OECD, 2017) and as standardized in Côa et al. (2022). In brief, 10 mg GO was pre-wetted with 200 µL ultrapure water. After 24 h, 19.8 mL of ultrapure water was added, and bath sonication (Cole-Parmer, model 08895-43, USA) was carried out for 80 min at a controlled temperature (15-20 ^{o}C). Ultrapure water from a Milli-Q Millipore system was used to prepare all solutions.

Silver nitrate (Lot 46624, 99.93% purity, Neon Company) was selected to prepare the metal stock solution in ultrapure water at 200 mg L^{-1} of silver ions and stored at 4 °C in the dark until usage.

4.2.2. *Escherichia coli* lysis and biocorona formation

OP50 *E. coli* lysis as described in the supplementary material. Briefly, OP50 *E. coli* was cultivated in Luria-Bertani (LB) liquid medium at 37 °C for 14 h. Bacteria suspension was centrifuged, the supernatant discarded, and the pellet rinsed in phosphate buffer saline (PBS). This solution was sonicated in an ultrasonic tip processor, centrifuged, and supernatant was filtered to get only soluble proteins. The total amount of protein was quantified by the Bradford assay (Figure S1) and adjusted to 1 mg mL^{-1} for further use. *E. coli* proteins were maintained frozen.

To promote the formation of an *E. coli* corona on GO, 200 µL of GO stock dispersion (0.5 mg mL^{-1}) was incubated with 500 µL of soluble proteins (1 mg mL^{-1}) and 300 µL PBS in Eppendorf tubes (1.5 mL) at 37 °C for 60 min in a thermoblock (Thermomixer C, Eppendorf). Steps of centrifugation and washing were performed to remove the softly adsorbed proteins. Tubes were centrifuged at 10,000 rpm, 4 °C for 60 min. Supernatants were discarded, and pellets were resuspended in 10x diluted PBS. Three washing steps were carried out to obtain the GO-protein complex (i.e., pellet form), which was named corona-coated GO or EC@GO, and maintained at 10 °C until use for a maximum of two days. Therefore, corona-coated GO was always prepared freshly before each experiment. Since the steps of washing and centrifugation could reduce the GO concentration in the complex EC@GO, GO concentration in the pellets was always checked before preparing the sub stocks for experiments. A calibration curve was prepared in our previous article (Côa et al., 2022) according to the protocol of Cerrillo et al. (2015) in which NM concentration in the pellets is checked by UV-Vis spectroscopy at 400 nm.

4.2.3. Characterization of graphene oxide with and without corona

A multi-analytical approach was applied to study the physicochemical properties of GO before and after biocorona formation. All the details relating to these analyses were described in supplementary material. Briefly, surface roughness and thickness of GO and EC@GO were evaluated by atomic force microscopy (AFM). Surface elemental composition and chemistry was studied by X-ray photoelectron spectroscopy (XPS), and determination of functional groups by attenuated total reflection Fourier-transform infrared spectroscopy (ATR-FTIR). Proteins adsorbed on the GO surface were eluted and separated by sodium dodecyl sulphate-polyacrylamide gel electrophoresis (SDS-PAGE).

4.2.4. Adsorption experiments

To understand the dynamic of silver ions adsorption on GO and EC@GO, an experiment was performed with a fixed concentration of materials (10 mg L^{-1}) and two concentrations of Ag^{+} (5 and 15 mg L^{-1}). Samples were incubated at 20 ºC in EPA medium for 30 min in a rotatory shaker (Luferco Phoenix, model AP-22). Then, they were centrifuged at 14,000 rpm, 20 ºC for 1 h. Supernatants were collected and acidified in 5% HNO_3. The amount of silver in the samples was quantified on an Agilent Technologies 7500ce ICP-MS. The adsorption capacity of GO

and EC@GO for silver ions removal was calculated by the difference between the initial and final concentration of Ag^+ in the solution.

4.2.5. Biological experiments

4.2.5.1. Dispersion characterization and colloidal stability studies

In biological assays with nanomaterials, some crucial aspects must be investigated to understand the nanomaterials toxicity accurately. The available dose to nematodes is not necessarily the same as the administered dose because NMs tend to sediment during the assays. And aggregation and agglomeration phenomena are directly related to the nanomaterials' uptake by the organisms because they reduce the total surface area of the suspended NM available to interact with the organisms (DeLoid et al., 2017). Although there is no specific standardised protocol to deeper investigates and rationalize these issues, some adapted guidelines can be applied to explore their behaviour in biological media. Absorbance is a valuable parameter because it is proportional to the amount of material in suspension (OECD, 2017).

As EU NanoReg recommended (Kleiven and Oughton, 2015), moderately hard reconstituted water (herein named EPA medium) was utilised as a low ionic strength exposure medium. The amount of GO with and without corona in suspension over 24 h in EPA and ultrapure water (UW) was measured by ultraviolet-visible spectrophotometry (UV-Vis). Dispersions of 10 mg L^{-1} GO and EC@GO were prepared in UW and EPA and disposed on a 24-well plate to simulate the same conditions of biological assays, as suggested in Guidance No. 317 (Organisation for Economic Co-operation and Development, 2020). Aliquots (100 µL) from the top of the well were removed, and absorbance at 400 nm wavelength after 1, 3, 6, and 24 h in a microplate reader (Multiskan TM GO, Thermo Scientific). Data were expressed as A/A_o, where A is the value obtained each time and A_o is the initial measured absorbance (0 h). Digital pictures were also obtained to visually compare the stability of materials.

Moreover, silver speciation in the exposure conditions was calculated by chemical equilibrium diagrams with the Spana software.

4.2.5.2. *Caenorhabditis elegans* culturing and synchronization

Wild-type (N2 Bristol) and transgenic strains (MD701 -[*lin-7p::ced-1*::GFP + *lin-15*(+)] and AML175 -[*wtfIs3* [*rab-3p*::NLS::GFP + *rab-3p*::NLS::tagRFP]) were obtained from the *Caenorhabditis* Genetics Center (CGC), as well as the bacteria strains. Worms were maintained on nematode growth medium (NGM) plates seeded with OP50 *E. coli* at 20 °C as described by Stiernagle (2006). Nematodes were also cultivated in an 8P-agar medium with a NA22 *E. coli* lawn for synchronization procedure. Age-synchronized worms were obtained as recommended by Porta-de-la-Riva et al. (2012) by isolating eggs from mature adults with a bleaching solution (1 mL NaOH 10 M, 4 mL NaClO 3% and 5 mL ultrapure water), followed by rinsing in EPA medium and filtration in a 40 µm cell strainer to remove worm debris. Eggs were placed on NGM seed with *E. coli* OP50 and incubated at 20 °C for 48 h to obtain young nematodes (L4 stage).

4.2.5.3. Preparation of sub-stocks for toxicity assays

For single exposures, sub-stocks of GO, EC@GO or $AgNO_3$ were prepared by diluting the stock dispersions in UW at concentrations ten times higher than the nominal concentration. Then, 100 µL of these suspensions were applied in toxicity tests.

For co-exposure assays, a fixed and non-toxic concentration of GO or EC@GO (0.1 µg L^{-1}) was incubated with increasing concentrations of Ag^{+} at concentrations ten times higher than the nominal concentration. Incubation was carried out for 30 minutes in a rotatory shaker. Then, nematodes were exposed to 100 µL of this mixture.

4.2.5.4. Lethality assays

Lethality assays were carried out according to the protocol of Maurer et al. (2015). Young adult worms were exposed to silver ions and materials in 24-well plates for 24 h. In the single exposure, ~15 worms (15 µL) were added per well with 100 µL test-solution and 885 µL EPA medium; while in co-exposure, 200 µL test-solution with ~15 worms (15 µL) and 785 µL EPA medium were added. In the single toxicity assays, nematodes were exposed to a silver concentration range from 1.8 to 35.8 µg L^{-1}, and to GO and EC@GO at concentrations ranging from 0.0001 to 10 mg L^{-1}. In co-exposure tests, the first non-toxic tested concentration of GO

or EC@GO (0.1 µg L^{-1}) was combined with silver at concentrations ranging from 1.8 to 13 µg L^{-1}.

Mortality was measured after 24 h by counting the living worms under a stereomicroscope (Stemi 508, Zeiss). Worms were considered dead when they had no response to a stimulus with a metal wire. Survival rates were calculated and utilized to elaborate dose-response curves. Experiments were repeated at least three times.

4.2.5.5. Biodistribution studies by Raman confocal spectroscopy

Internalization and biodistribution of GO, EC@GO, GO+Ag^{+}, and EC@GO+Ag^{+} by nematodes were investigated by Raman confocal spectroscopy. 60 L4-stage organisms were exposed to 10 mg L^{-1} GO or EC@GO, which was also combined with the effective silver concentration inhibiting the *C. elegans* survival by 50% (LC_{50}). After 48 h exposure, nematodes were washed with EPA twice by centrifugation and preserved in 2% paraformaldehyde (Lot #SLBF2268V, Sigma-Aldrich). Experiments were twice repeated. Four nematodes per treatment and per assay were randomly chosen to be analysed in a Confocal Raman spectrometer (XploRA PLUS, Horiba) equipped with an optical confocal microscope (50 x objective). Spectra were acquired over z-depth from -30 to 120 µm (upper cuticle is considered as the 0 µm reference) using a 5 µm as acquisition steps. Each spectrum was obtained from 800 to 2000 cm^{-1} with 6 accumulations of 3 s and at excitation wavelength of 532 nm. The laser power applied on a sampling point was 1.2 mW.

4.2.5.6. Silver internalization by nematodes

Total silver concentration in *C. elegans* was evaluated by inductively coupled plasma mass spectrometry (ICP-MS). For this purpose, 2,700 worms (1 mL of worms suspension) were transferred to 50 mL centrifuge tubes containing 5 mL test solution and 44 mL EPA medium. Worms were exposed to 12.4 µg L^{-1} Ag^{+}, 0.1 µg L^{-1} GO+5.7µg L^{-1} Ag^{+} and 0.1 µg L^{-1} EC@GO+2.7 µg L^{-1} Ag^{+}, which corresponded to LC_{50} values of each treatment. Six independent replicates per treatment were prepared. After 24 h, worms were immobilized in a fridge (5 °C) and pellet obtained by centrifugation at 5,000 rpm, 4 °C for 5 min. Supernatants were discarded to remove excess exposure media, and pellets (1 mL) were transferred to Eppendorf tubes. Three steps of centrifugation and washing with ultrapure water were carried

out to remove residual Ag^+. Pelleted worms (200 µL) were frozen at -20 °C, then transferred to 15 mL centrifuge tubes, and completely digested with HNO_3 50% by adding 800 µL 62.5% HNO_3 (Lot 385212, Sigma Aldrich, previously purified in a sub-boiling distillation system SubClean from Milestone). This procedure was performed overnight at room temperature, and after that, samples were diluted in 10 mL with ultrapure water to achieve 5 vol % HNO_3. Ten procedural blanks (with and without nematodes – only reagents) were included during sample preparation.

ICP-MS measurements were carried out on an Agilent Technologies 7500ce ICP-MS. A calibration curve was prepared at 0.1; 1, 10; 100, and 200 µg L^{-1} Ag^+ from an environmental calibration standard (Lot 13-166JB, 5% HNO_3, Agilent Technologies) composed of Ag, Al, As, Ba, Be, Co, Cr, Mn, Nb, and Ni. Calibration curve exhibited a suitable coefficient for analyses (r2=0.9999). Amount of silver internalized by worms was calculated by the mass of total silver divided by the total number of organisms used for digestion. For that, alive worms were newly counted before digestion according to a standardized protocol developed by Scanlan et al. (2018). Experiments were twice repeated.

To avoid undesired silver contaminants, all borosilicate glasses used in these experiments were acid cleaned by a soak in an aqua regia solution (three parts hydrochloric acid and one-part nitric acid) followed by one rinse with tap water and five rinses with ultrapure water. Metal-free plastics were acquired from SSIbio and BioClean companies.

4.2.5.7. Neuronal effects assessment

L4 stage worms of the AML175 strain were exposed to single and co-exposure scenarios. After exposure, they were transferred to Eppendorf tubes and centrifuged at 2,100 rpm, 20 ºC for 3 min. Then, they were mounted onto microscope slides, anaesthetized with levamisole (6 mM, Lot 05-096/03, Noxon) and capped with coverslips. Images were captured using an inverted stereomicroscope (Axio Vert.A1, Zeiss equipped with an Axion 203 camera) outfitted with a fluorescence module and an FTIC filter set (excitation/emission: 495 nm/519 nm). Before, images were standardized by programming the Zeiss software to ensure that pictures were obtained using the same exposure time, gain, saturation, and colour gain levels. Experiments were twice repeated. At least 60 random worms from each treatment were analysed. Relative fluorescence intensity of the body was quantified using the ImageJ software (1.52a version), and results were expressed as a percentage compared to the control group (nonexposed).

4.2.5.8. Germline cell apoptosis evaluation

Apoptotic cells were measured using MD701 transgenic worms, in which the CED-1::GFP is expressed in the nuclei of gonadal sheath cells (Lant and Derry, 2013). In this assay, L4 worms of the MD701 strain were exposed to GO, EC@GO, Ag^+, GO+Ag^+, and EC@GO+Ag^+ for 24 h in a 24-well plate, at the same concentrations used in assays performed for ICP-MS analysis. They were transferred to Eppendorf tubes (1.5 mL), rinsed with EPA medium, picked onto microscope slides containing 10 µL levamisole (2 mM) and sealed with cover glass. Samples were analysed in a 60x objective in an Olympus microscope (BX-53, Japan) outfitted with a camera, fluorescence module, and an FTIC filter set. The number of apoptotic cells was scored in the gonad loop region of at least 10 worms per group (Anton Gartner et al., 2008). Each treatment consisted of four independent replicates, and experiments were twice repeated.

4.2.6. Data analysis and statistics

Data were expressed as means with standard error of the mean (SEM) and analysed by one or two-way analysis of variance (ANOVA) with a Tukey´s multiple comparison test using GraphPad Prism (5.0 version). Results with $p<0.05$ were considered statically significant. A sigmoidal dose-response model was used to draw the dose-response curves and obtain the LC_{50} values and 95% confidence interval (CI) with Graphpad Prism.

4.3. Results and discussion

4.3.1. Characterization of *Escherichia coli* corona formation

The formation of coatings with biomolecules, like proteins, on NMs surfaces substantially affects their physicochemical properties, colloidal stability, and toxicological profile. Therefore, characterization is an essential step for understanding the NMs behaviour in nanotoxicity assays (Cedervall et al., 2007; Ge et al., 2015; Tomak et al., 2021). In this work, AFM, XPS, FTIR, and SDS-PAGE were explored as complementary techniques to investigate the physicochemical properties of GO and modifications promoted on it after the biocorona interaction.

Atomic force microscopy is a powerful technique to study the nano-protein interfaces because it allows direct measurements of topographic alterations at nanomaterials surfaces (Chong et al., 2015; Dobrovolskaia et al., 2009; Franqui et al., 2019). In our study, height profiles obtained from AFM images (Figure 1B and D) indicate that the thickness of GO flakes increased from 0.9±0.1 nm, typical of single layer GO, to 2.6±0.3 nm after its interaction with *E. coli* proteins. In addition, the surface of EC@GO became rougher (1.02±0.4 nm) than that of the pristine GO (0.25±0.3 nm). These results suggest that *E. coli* proteins have coated most of the GO surface forming a protein layer on its sheets.

X-ray photoelectron spectroscopy is another useful tool to understand protein corona formation since is one of the most sensitive methods for analysing the NMs surface elemental composition (Baldovino et al., 2016; Zhang et al., 2013a). Our XPS survey data demonstrate that GO is composed of 66.4±1.2% carbon, 31.4±0.9% oxygen and 1.7±0.1% nitrogen atoms, whereas EC@GO presents 66.3±0.6% carbon, 19.4±0.2% oxygen and 14.1±0.1% nitrogen (Figure 1E). The increase in nitrogen abundance observed for EC@GO sample can be ascribed to the protein adsorption on GO surface since proteins are rich-nitrogen compounds (Peng et al., 2004).

Previous studies have demonstrated that protein attachment on NMs can be identified by attenuated total reflectance-Fourier transform infrared spectroscopy (ATR-FTIR) (Liu et al., 2010; Martins et al., 2022). ATR-FTIR is useful because allows to identify and characterize the functional groups present on NMs surfaces. Comparing the FTIR spectra of GO and EC@GO (Figure 1F), it is possible observing an increase in the diversity of functional groups on the GO surface after protein interaction, which has been also confirmed in other studies of protein corona formation (Martinez et al., 2020; Vanea and Simon, 2011). In the GO spectrum, peaks at 1045, 1215, 1613, 1719, and a broad band at 3400 cm^{-1} correspond to C-O (primary alcohol) stretching vibration, C-O (epoxy) and C-OH (phenol), C=C (aromatic carbon bonds), C=O (carboxylic acid and carbonyl moieties), and O-H stretch vibration, respectively (Wang et al., 2011; Yu et al., 2010). While the FTIR spectrum of EC@GO shows a decrease in intensities of oxygen-related peaks (at 1718 and 1045 cm^{-1}), and the emergence of nitrogen-related peaks. Two strong signals associated with amide groups (N-C=O) are observed at 1645 and 1523 cm^{-1}, suggesting that carboxylic groups reacted with NH_2 groups from *E. coli* proteins forming amide linkage (Emadi et al., 2017; Krimm and Bandekar, 1986). Moreover, a peak corresponding to the aromatic amide group (C-N) is observed at 1243 cm^{-1} (Baldovino et al., 2016; Zhang et al., 2013b). -CH_3 and -CH_2 stretching vibrations at 2853 and 2926 cm^{-1} related to the amino acids that compose proteins were also detected (Ullah et al., 2020), in addition to phosphate groups

at 1152 cm^{-1} (Choudhary et al., 2017). Therefore, the FTIR and XPS spectra suggest the formation of a GO-protein complex since they confirmed the attachment of nitrogen-related groups on the GO surface. It is worth mentioning that these observed functional groups will be mostly responsible for the interaction with pollutants because they work as active sites to adsorb for example heavy metal ions (X. Liu et al., 2019).

Figure 1 - Graphene oxide characterisation before and after corona formation. AFM image of GO (A) and EC@GO (C) and respective height profiles of GO and EC@GO flakes (B and D); Surface elemental composition of GO and EC@GO obtained by XPS analysis (E) and attenuated total reflectance-Fourier transform infrared spectroscopy (ATR-FTIR) data (F).

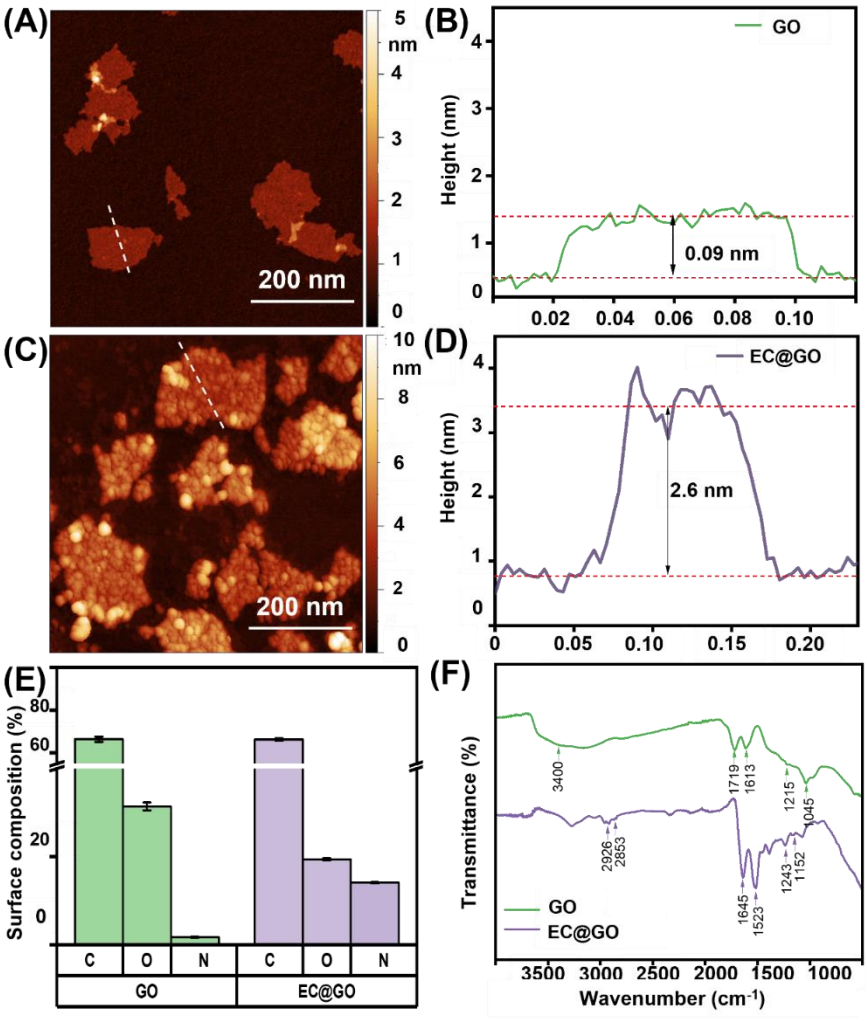

Different mechanisms are involved in the binding affinities between graphene oxide and proteins, such as the types of functional groups present at its surface, van der Walls interactions, covalent bonds, and π-π stacking (Li et al., 2014). These mechanisms may co-exist during the protein adsorption, but one may prevail over others, resulting in the preferential adsorption of some proteins from *E. coli* extract (Costa et al., 2021). SDS-PAGE analysis has been very

suitable in qualitatively identifying the proteins adsorbed on NMs based on their molecular weight (Baimanov et al., 2019). By this tool, the profile of total proteins that compose the extract from *E. coli* lysis was evaluated, as well as the pattern of proteins that were adsorbed by GO. In Figure 2, acrylamide gel demonstrates a selective adsorption of *E. coli* protein at the GO surface, evidenced by the fact that the protein pattern recovered from GO partially differs from total proteins. Some abundant proteins found in *E. coli* extract were not adsorbed by GO (such as that at 22 kDa) or displayed a weak affinity (such as between 25 and 32 kDa), while others are present in the total proteins and on the GO surface at the same intensity (for example, at 46 kDa).

Figure 2 - SDS-PAGE analysis of total soluble proteins from *E. coli* lysis and proteins recovered from graphene oxide surface after corona formation.

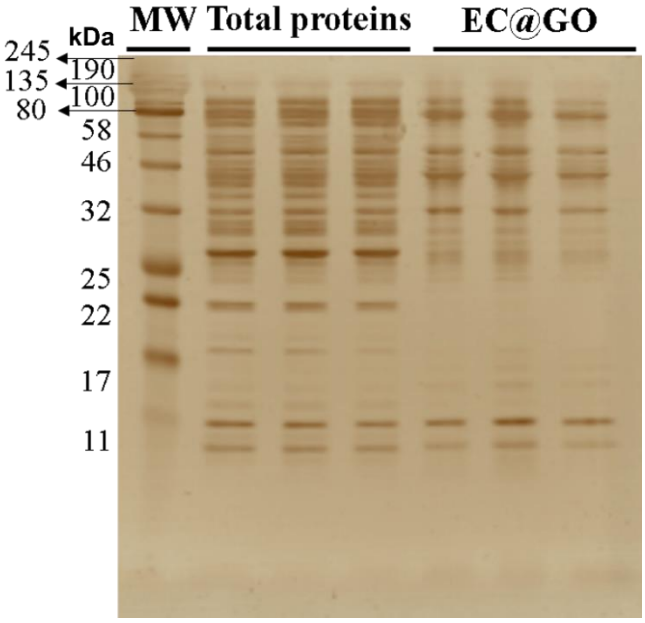

In short, the morphological, chemical, and biochemical analyses performed in this study demonstrate that a protein coating is formed on the GO surface as a result of its interaction with *E. coli* lysate. This coating led to the increase of surface roughness and GO thickness, as well as the nitrogen functional groups abundance on its surface. Selective adsorption of proteins from *E. coli* lysis was also observed. These results evidenced that the biocorona formation in nanotoxicity assays with *C. elegans* cannot be neglected. In view of this, we performed other assays to further explore how *E. coli* corona formation can affect the behaviour and the joint toxicity of GO with silver ions to *C. elegans*.

4.3.2. *Escherichia coli* corona influence on GO colloidal behaviour, internalization, and toxicity

Caenorhabditis elegans has been explored as a very useful organism for investigating the toxicity of environmental pollutants (Gonzalez-Moragas et al., 2015). However, our results suggest that toxicity assays performed with *C. elegans* and nanomaterials must consider the biocorona formation as it changed the GO physicochemical properties and colloidal stability, which can influence the exposure dynamic and toxicity. Considering these aspects, the implications of *E. coli* corona formation on GO toxicity were evaluated. Besides, its impacts on co-exposure testing were also assessed by applying a heavy metal model (i.e., silver ions).

Acute toxicity tests were carried out with young adult organisms to evaluate the survival of nematodes after 24 h exposure to GO and EC@GO (from 0.0001 to 10 mg L^{-1}). Our results show that only GO exposure affected nematode survival at concentrations over 0.1 mg L^{-1}. At 0.1 mg L^{-1} of GO, nematode survival was reduced to 71.7±3.9%, reaching 49.5±6.3% at 10 mg L^{-1}. While no negative effect was observed on the survival of nematodes exposed to EC@GO as more than 90% of organisms remained alive in the assays (Figure 3).

Figure 3 - Effects of GO and EC@GO (from 0.0001 to 10 mg L^{-1}) on nematode survival. Bars indicate average ± S.E.M. Significant differences between the control group and different treatments are indicated by α, and β indicated the differences between the treatments ($p<0.05$).

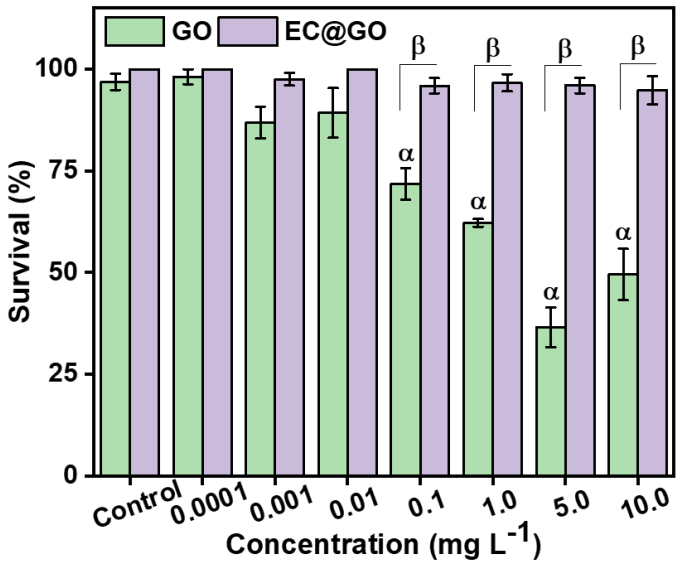

Unlike previously reported results (Nivedita et al., 2017; Tsai et al., 2021), our data evidenced that GO caused lethality at concentrations higher than 0.1 mg L^{-1}. However, biocorona mitigated the GO toxicity to nematode survival. Other researchers have reported the

mitigation effect on NMs toxicity by protein coatings (Côa et al., 2022; Gonzalez-Moragas et al., 2015; Sivaselvam et al., 2020). Gonzalez-Moragas et al. (2015) for example, observed that bovine serum albumin (BSA) exerted a protective role in preventing the direct interaction of superparamagnetic iron oxide nanoparticles with the *C. elegans* intestinal environment, reducing their negative effects.

The protective effect displayed by biocorona may not the only reason for the toxicity reduction. Another critical point is that coated NMs usually show different colloidal stabilities during biological assays (Moore et al., 2015). In the current study, GO was not stable for 24 h in the exposure medium (EPA). The amount of GO in suspension was reduced over the experiment, and at the end, 100% of GO was deposited at the bottom of the well. On the other hand, EC@GO was more stable in the EPA medium; despite it being also deposited, 40% of EC@GO remained suspended after 24 h (Figure S2). This result evidences that, although nematodes have been exposed to the same nominal concentration of GO and EC@GO, the available dose that reached the organisms differed. Hence, nematodes could have been exposed to higher concentrations of GO than EC@GO, which may be associated with the fact that they were more affected by GO. Similar results regarding this toxicological response were also observed in our earlier studies, which demonstrated that a BSA coating improved the colloidal stability of GO, reducing its toxic effects on nematode survival (Côa et al., 2022).

Even though exposure dose exerts a key role in toxicological response, the internalised fraction plays a huge role in toxicity because it is the portion that reaches the target organs and is toxicologically active (Escher and Hermens, 2004). In our study, confocal Raman spectroscopy was exploited to assess the uptake and biodistribution of GO and EC@GO in different tissues and organs of *C. elegans*. GO has characteristic Raman fingerprints (D and G-bands), which enables its easy localization inside the worms without using exogenous labels that can come off its surface, leading to misinterpretations (Dorney et al., 2012). Depth profiles were drafted from the intensity of characteristic D-band recorded to confirm that materials were inside nematodes, similar to what was proposed and explained in our previous study (Côa et al., 2022); The occurrence of asymmetric peaks and the increase of intensity signal after the laser penetrated the cuticle (point zero) were considered indicative that GO was uptake by the nematode. Our confocal Raman spectroscopy data indicate accumulation of GO and EC@GO in the nematode intestine, head, gonad, and spermatheca region (inside eggs) (Figure 4).

Figure 4 - Internalization of GO and EC@GO (at 10 mg L^{-1}) in *C. elegans* tissues analysed by confocal Raman spectroscopy from -25 to 120 µm depth. Point zero represents the nematode cuticle.

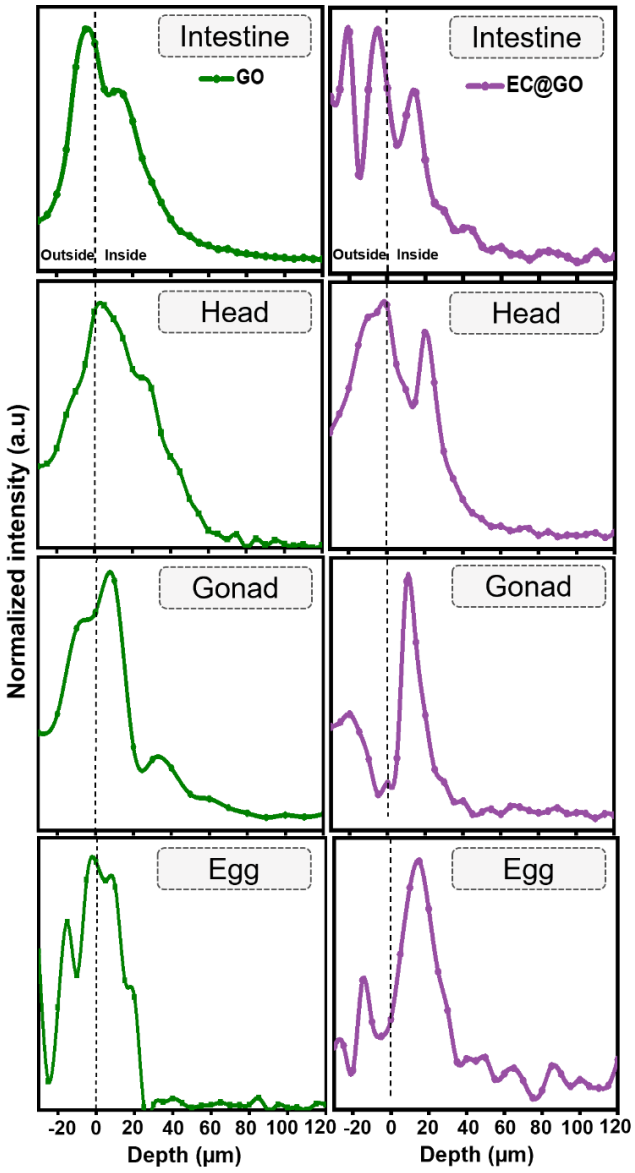

The alimentary system of *C. elegans* comprises the mouth, pharynx, intestine, rectum and anus. Through the activation of sensory neurons, *C. elegans* capture the food (bacteria) that is disrupted by the pharyngeal grinder and transported to the intestine. By a size-selective mechanism, excessively large particles (>3 µm) are excluded in the pharynx that filters and expels the remaining liquid. Therefore, nematodes can actively ingest NMs together with food, however, their internalization is size excluding. By crossing the intestinal barrier, NMs can be transported to other locations in the organism (Wu et al., 2014; Zhao et al., 2018; Zhi et al., 2016).

The observed presence of GO and EC@GO in the gonads and head implies that both materials crossed the intestinal barrier and were translocated to these tissues. In addition, both were distributed around the spermatheca region, reaching eggs, even though embryos are wrapped in three shells (Qu et al., 2011). The translocation of GO inside the nematode affects the functionality of its intestinal barrier, reproductive organs, and neurons (Kim et al., 2018; Li et al., 2017; Wu et al., 2014). When GO is transferred to the nematode gonad, it can suppress spermatogenesis and offspring production (Kim et al., 2018). The locomotor behaviour can also be hindered by GO which damages the *C. elegans* AFD sensory neurons as well as the dopaminergic and glutamatergic neurons (Kim et al., 2020). In addition, once GO crosses the intestinal barrier, it affects its permeable state (Côa et al., 2022), altering the genes required for intestinal development and suppressing the defecation behaviour (Wu et al., 2013). These outcomes demonstrate that the translocation of GO and EC@GO in the nematode body cannot be disregarded. Although the biocorona has mitigated the adverse effects of GO on nematode survival, it was translocated to its secondary organs.

Two transgenic *C. elegans* strains (MD701 and AML175) were exploited in our experiments to investigate whether the materials could have affected the physiological functions of nematodes. In AML175 strain [*wtfIs3* [*rab-3p*::NLS::GFP + *rab-3p*::NLS::tagRFP]), the decrease of fluorescence intensity is indicative of harmed neurons because their nuclei are marked with GFP and tagRFP fluorescence proteins. While, MD701 strain (*bcls39* [*lim-7p::ced-1*::gfp + *lin-15*(+)] is a useful tool to track the impairment of pollutants in the *C. elegans* reproductive system because the CED- 1::GFP fluorescence protein is expressed around germline apoptotic cells.

By exposing AML175 *C. elegans* strain to different concentrations of GO and EC@GO (from 0.0001 to 10 mg L^{-1}), our data reveal a moderately but significantly decrease in the fluorescence intensity of the neural system marked with GFP and tagRFP in nematodes exposed to 10 mg L^{-1} GO (92.7±1.4%), whereas the fluorescence intensity of worms exposed to EC@GO (98.4±1.7%) was similar to control (100±1.9%) (Figure 5).

Figure 5 – Diagram of *C. elegans* neuronal system (A), effects of GO and EC@GO (from 0.0001 to 10 mg L^{-1}) on *C. elegans* neuronal system (B), representative fluorescence images of unexposed nematode (control) and exposed to 10 mg L^{-1} of GO (D). α indicates the treatments that are statistically different from the control group ($p<0.05$).

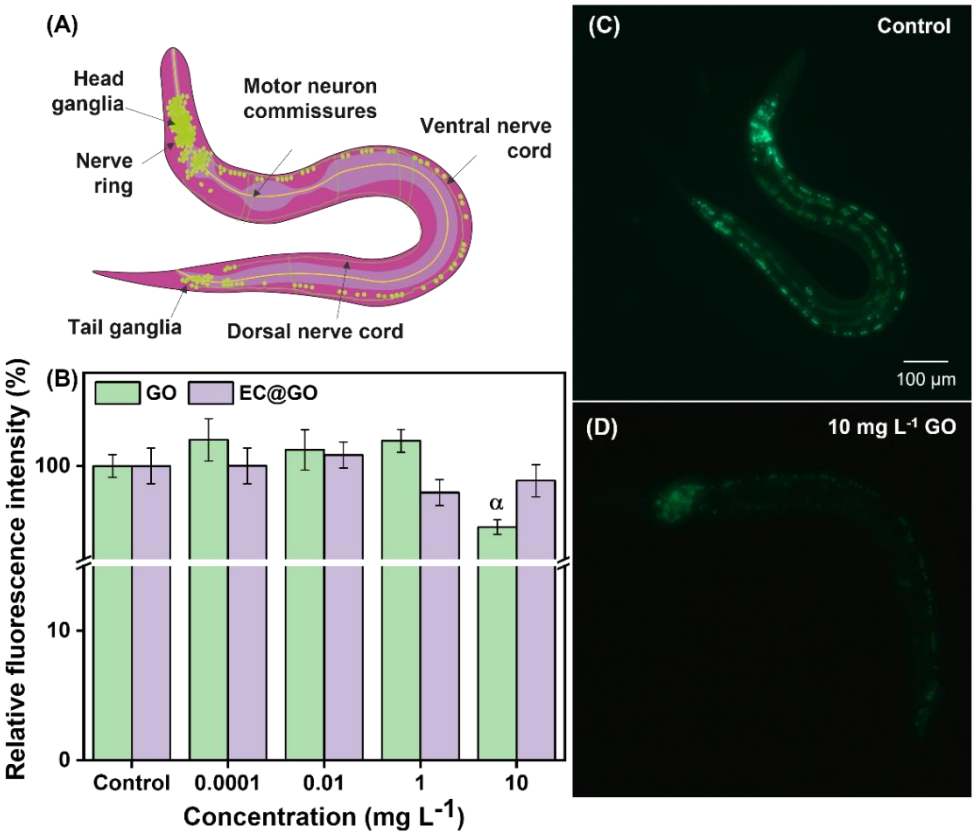

The nervous system is the most complex organ of *C. elegans* and is one of the targeted for NMs exposure (Zheng et al., 2022) as it controls all the nematode basic functions such as feeding, development, movement, metabolism, and reproduction (White et al., 1986). As well as in our work, Kim et al. (2020) exploited the confocal Raman spectroscopy tool and observed GO deposition in the head region of *C. elegans*. This was accompanied by a significant alteration in locomotor behaviour, such as stop time, and speed. The volume of neurotransmitters in dopaminergic and glutamatergic neurons was reduced, as well as the expression of genes required for the function of AFD neurons, demonstrating the potential neurotoxic effect of GO. In addition, GO has also been reported as a deregulator of the signalling cascade mir-247-GOA-1-DGK-1/PKC and MEK- 2/MEK in *C. elegans*, which are related to the neuronal Gαo signalling in response to GO (Liu et al., 2019; Qu et al., 2017).

There are still no other studies about the influence of *E. coli* corona formation on the neurotoxic effect of GO, but our results suggest that only GO may potentially affect the functionality of *C. elegans* neurons. Further studies are required to specifically identify the neurons affected by GO and confirm how the biocorona suppresses its neurotoxic effects.

Figure 6 shows the effect of GO and EC@GO on the induction of germline apoptosis in *C. elegans*. A significant increase in the expression of CED-1::GFP clusters around germline cells in relation to the control group (5.8±0.4) was observed for nematodes exposed to 1 and 10 mg L^{-1} of GO (9.2±0.5 and 10.9±0.6), and EC@GO (8.9±0.5 and 10.7±0.7) (Figure 5B). However, the magnitude of this rise (~1.5-2.0 fold) is not statically different between materials, demonstrating that the effect was similar for both. Therefore, our data suggest that GO and EC@GO affected similarly the nematode germline cells.

Figure 6 - Diagram of germline apoptosis in *C. elegans* (A); Effect of GO and EC@GO on the induction of apoptotic corpses in the germline of *C. elegans* (B). Representative fluorescence images of apoptotic induction using the MD701 strain (*bcls39* [*lim-7p*::*ced-1*::*gfp* + *lin-15*(+)] (C). White arrows point to the apoptotic cells, and α indicates significant differences between control and different treatments ($p<0.05$).

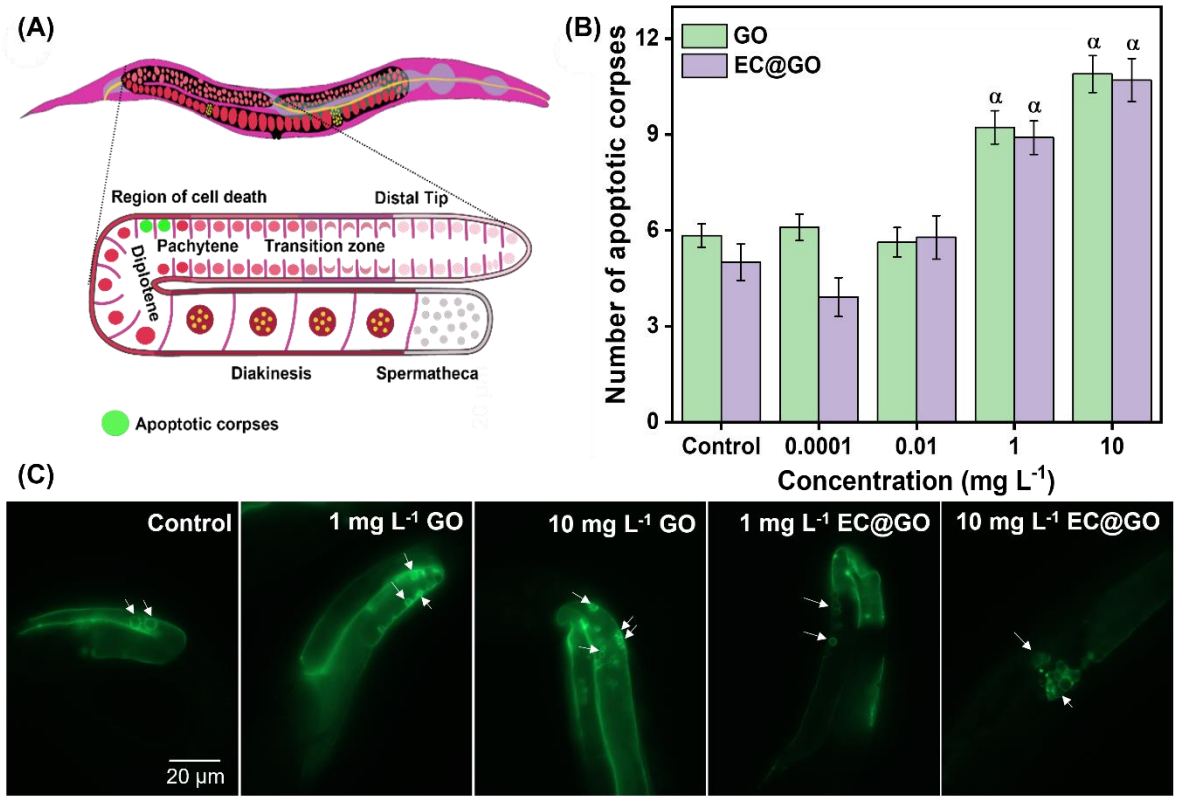

The germline mitotic region of a young adult nematode is composed of 100 cells which self-renew and produces differentiating gametes. Apoptosis is a programmed event, part of the oogenesis process, that regulates genomic stability, removes malfunctioning germ cells, and controls sperm production (Elmore, 2007). Environmental stressors can activate apoptosis, affecting germline functionality, decreasing the number of mature oocytes and retarding offspring development (Franco et al., 2009).

GO and heavy metals have been described as inductors of germline apoptosis in *C. elegans* (Jin et al., 2022; Wang et al., 2009, 2007; Zhao et al., 2016). Zhao et al. (2016) reported that GO promoted germline apoptosis, cell cycle arrest and DNA fragmentation, affecting gonad development and nematode reproduction. GO also activated a miRNA regulation mechanism (*mir-360*) to suppress its reprotoxicity to *C. elegans*. Moreover, consecutive exposure to GO reduced the number of offspring and oocytes in nematodes, enhanced germline apoptosis, and promoted the expression of reproductive-related genes *ced-3, ced-4, ced-9, egl- 1,* and *ced-13* (Jin et al., 2022). We hypothesize that GO and EC@GO could have affected the functionality of reproductive organs since they were translocated to the nematode gonad and spermatheca region, causing the death of germline cells crucial for nematode reproduction. This hypothesis is supported by our previous study, in which GO and albumin-corona GO were translocated to *C. elegans* gonads and affected its reproduction and fertility (Côa et al., 2022).

4.3.3. Influence of GO and *Escherichia coli* corona on silver toxicity

Heavy metals are broadly distributed pollutants that would co-exist with NMs in the environment. Once interacted, metal pollutants can be adsorbed on NMs surfaces that could act as carriers of them, modulating their behaviour, fate, and toxicity towards organisms (Batista de Melo et al., 2019; Medeiros et al., 2020).

In this study, a fixed non-toxic concentration of GO and EC@GO was mixed with different silver concentrations. The effects of single and combined exposure between uncoated or coated GO and Ag^{+} on *C. elegans* were investigated by observing its survival, induction of germline apoptosis and neuronal damages.

According to the dose-response curves of single and joint toxicity assays (Figure 7A), LC_{50} value (i.e., lethal concentration that kills 50% of organisms) for nematodes exposed to Ag^{+} was 12.5 µg L^{-1} (95% CI=11.8-13.1), while it was 5.7 µg L^{-1} (95% CI=5.4-6.0) for GO+Ag^{+}, and 2.7 µg L^{-1} (95% CI= 2.5-2.9) for EC@GO+Ag^{+}.

Figure 7 - Biological effects of single and co-exposure assays with GO and Ag^{+}. Dose-response curves CL_{50} (A), damages on germline cells (B) and neurons (C). Data are present as mean±SEM; α indicates the treatments different from the control, β suggests the differences between the treatments and ɵ represents data not applicable because no surviving nematodes at this dose ($p<0.05$).

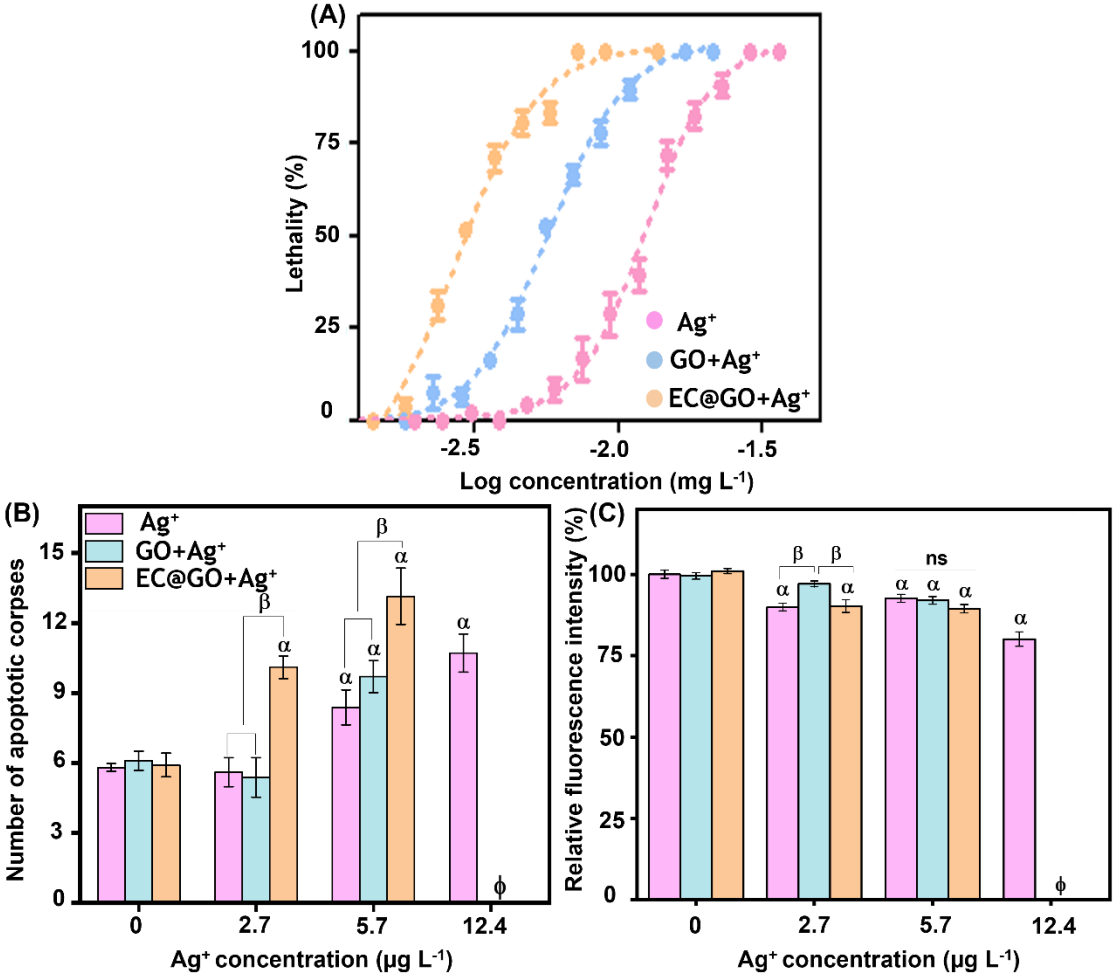

Previous studies have reported that some heavy metals may be toxic to *C. elegans* survival, such as iron (HU et al., 2008), lead and mercury (Xing et al., 2009; Zhang et al., 2010), copper, zinc, cadmium, chromium (Jiang et al., 2016), and nickel (Wang and Wang, 2008b). In agreement with the tendency observed in our study, Starnes et al. (2015) described that LC_{50} for nematodes exposed to Ag^{+} in moderated hard reconstituted water is 7.5 µg L^{-1} (95% CI= 7.01-7.89).

For the first time, we demonstrated that the co-exposure of silver ions with GO could affect nematode survival. The combination of GO with Ag^{+} increased the silver toxicity 2.1 times. Similarly, corona-coated GO increased the silver toxicity 4.6 times. This data indicates that the joint toxicity of uncoated or coated GO with silver ions requires to be further investigated.

As previously mentioned, the uptake and biodistribution of pollutants inside organisms can dysregulate the functionality of their crucial organs, cells and molecular processes (Hartman et al., 2021). In this way, uptake and distribution of GO+Ag^+ and EC@GO+Ag^+ in nematodes were investigated by confocal Raman spectroscopy. Our data (Figure S3) suggest internalization of GO and EC@GO combined with Ag^+ in all the nematode tissues (i.e., intestine, head, gonad and eggs).

GO+Ag^+ and EC@GO+Ag^+ were uptake and translocated from the primary (intestine) to the secondary organs of *C. elegans* (reproductive system and head). As such, germline apoptosis and neuronal damage were selected as endpoints to better understand whether the accumulation of these materials in nematode head and gonads could result in damage to *C. elegans*.

Figure 7B reveals an average of 5.8±0.2 apoptotic corpses in the germline of unexposed nematodes. EC@GO+Ag^+ at 2.7 µg L^{-1} caused the death of 10.1±0.5 germline cells, while no effect was observed at this dose for GO+Ag^+ and Ag^+. At 5.7 µg L^{-1}, nematodes exposed to Ag^+ and GO+Ag^+ showed a similar number of apoptotic corpses, 8.3±0.7 and 9.7±0.7, respectively, whereas the magnitude of this effect was significantly higher for EC@GO+Ag^+ (13.1±1.2). In addition, nematodes exposed to 12.4 µg L^{-1} of silver showed 10.7±0.8 germ cell corpses, but this concentration was not evaluated for EC@GO+Ag^+ and GO+Ag^+ because no nematodes survived. Therefore, our data indicate that EC@GO+Ag^+ induced germline apoptosis at lower concentrations than GO+Ag^+ and Ag^+; besides, it was more apoptosis-inductive than others at 5.7 µg L^{-1}, even in relation to the highest tested Ag^+ concentration (12.4 µg L^{-1}).

Concerning neuronal effect, Figure 7C demonstrates a decrease in GFP fluorescence intensity of nematodes exposed to 2.7 µg L^{-1} of EC@GO+Ag^+ and Ag^+, from 100.0±1.3 (unexposed) to 90.2±1.9 and 89.9±1.2%, respectively. At 5.7 µg L^{-1}, all the treatments induced a reduction of fluorescence intensity, but at the same magnitude that was observed at 2.7 µg L^{-1}. Nematodes were severely impaired by the single exposure to Ag^+ at 12.4 µg L^{-1}, which reduced GFP intensity to 80.1±2.2%. This data suggests that single toxicant only or joint toxicity caused alterations in neurons, but Ag^+ and EC@GO+Ag^+ were the most harmful at the lowest concentration.

Metal pollutants have been pointed out to cause reproductive toxicity to *C. elegans*, which can also be transferred to its progeny (Guo et al., 2009; Wang et al., 2007; Wu et al., 2011). Starnes et al. (2015) demonstrated the potential of silver ions to be reprotoxic. They reported that 15.3 µg L^{-1} of silver ions reduced offspring number per adult by 50%. Wang and Yang (2007) also confirmed that the offspring was affected by silver exposure (21 µg L^{-1}),

as well as the reproductive speed and nematode development. In agreement with these studies, our results suggest that silver ions can impair the functionality of *C. elegans* reproductive system as Ag^+ caused germline apoptosis in its gonads.

Although the effects of uncoated and coated GO combined with silver on *C. elegans* gonads have not been studied before, Wang et al. (2019) observed that Cd was adsorbed on TiO_2 NPs and translocated to nematode gonads and embryos, causing germline apoptosis. Therefore, the damages caused by GO+Ag^+ and EC@GO+Ag^+ on *C. elegans* germline may be ascribed to their translocation to the gonads. But it is worth mentioning that EC@GO+Ag^+ was the most apoptosis-inductive, therefore, this effect needs to be further deeply investigated.

Neurotoxic effects of heavy metals have been described in the literature (Du and Wang, 2009; Wang and Xing, 2008). A decrease in the relative intensity of cell bodies in AFD neurons was noticed in nematodes exposed to Ag^+ (Xiaojuan Xing et al., 2009). The morphology of these cells was altered due to metal exposure, and a reduction in relative transcript levels of *ttx- 1* was detected and ascribed to losses in the thermosensory signal. Moreover, silver ions may disrupt the morphology and development of AFD sensory neurons fundamental for worms' perception behaviour. Locomotion behaviour defects reflect the possible dysfunction of the nervous system. Zhang et al. (2010) described that 5 µg L^{-1} of Ag^+ reduced the nematode body bends, and its learning performance. These studies agree with our results that demonstrate that silver ions can damage the neurons. EC@GO+Ag^+ was more harmful to neurons than GO+Ag^+ and its toxicity was similar to Ag^+. However, the translocations of both to nematode head is a concern issue, because alterations in neurons would lead to dysregulations in nematode basic functions, such as movement, metabolism and reproduction.

To sum up, our results indicate that Ag^+ exposure affected *C. elegans* survival, neurons and germline cells. The co-exposure of GO with Ag^+ increased the silver toxicity 2.1 times, however, this effect was aggravated by *E. coli* corona coated GO 4.6 times. Although both materials with silver have been translocated to all the nematode tissues, the negative effects of EC@GO+Ag^+ on *C. elegans* germline and neurons were higher than the joint effects of GO with Ag^+. These findings suggest that uptake and behaviour of these materials and silver need to be investigated to understand why the *E. coli* corona aggravate the silver toxicity in a higher level when compared to GO with Ag^+.

4.3.4. Influence of GO and *Escherichia coli* corona on silver bioaccumulation

Internalization and biodistribution of pollutants inside organisms are critical factors that govern toxicity. Bioaccumulation involves the uptake of a chemical from the external environment into the organism. Understanding this process is the basis to obtain information about toxicity because different accumulation levels can result in different toxic effects (Hartman et al., 2021).

The total silver concentration internalized by nematodes was quantitatively assessed by ICP-MS. To compare the observed effects in these analyses, nematodes were exposed to LC_{50} values found in the single and co-exposure assays performed with Ag^+ (12.4 µg L^{-1}), GO+Ag^+ (5.7 µg L^{-1}) and EC@Ag^+ (2.7 µg L^{-1}).

Figure 8 indicates that nematodes exposed to Ag^+, GO+Ag^+ and EC@GO+Ag^+ accumulated 1171.6±193.9, 50.8±19.3 and 55.4±7.9 ng/organism of silver, respectively. In contrast, the background concentration of silver in unexposed worms was 1.1±0.7 ng/organism.

Figure 8 - Total silver concentration internalized by nematodes measured by ICP-MS.

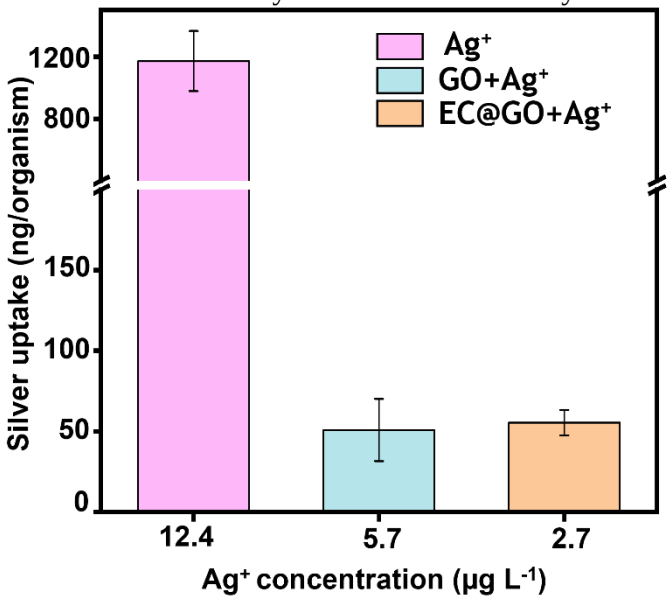

Considering the different initial concentrations at which organisms were exposed, each nematode accumulated 9%, 0.9%, and 2% of silver when exposed to Ag^+, GO+Ag^+ and EC@GO+Ag^+, respectively. Nematodes exposed to Ag^+ accumulated the most silver content. However, *C. elegans* exposed to EC@GO+Ag^+ accumulated twice as much silver than those exposed to GO+Ag^+, indicating that biocorona coating on GO could lead to an increase in silver internalization.

There are no previous attempts to study the effect of *E. coli* corona on the uptake and bioaccumulation of GO combined with heavy metals in the *C. elegans* model. However, previous research has reported that GO can adsorb heavy metals on its surface increasing their transport into the organisms and toxicity (Jurgelėnė et al., 2022). Understanding the adsorption of silver ions on GO is essential to comprehend their bioavailability to *C. elegans* and subsequent biological responses.

The adsorption of silver ions by GO and EC@GO was evaluated in a preliminary study by applying a fixed concentration of material (10 mg L^{-1}) with two different Ag^+ concentrations (5 and 15 mg L^{-1}). Our results demonstrate that GO adsorbed 28.7±1.9% and 47.8±2.8% of Ag^+, respectively, while corona-coated GO adsorbed 92.4±1.5% and 94.1±2.2% (Figure S4). Therefore, the adsorption capacity of GO to remove 5 and 15 mg L^{-1} Ag^+ was 2.8±0.2 mg Ag/g GO and 4.8±0.7 mg Ag/g GO, respectively, while for corona-coated GO, it was 5.5±0.1 mg Ag/g EC@GO and 15.7±0.1 mg Ag/g EC@GO. These results evidence that EC@GO shows the highest adsorption capacity for silver ions removal as the amount of silver adsorbed by EC@GO was higher than GO.

GO has a strong adsorption capacity for heavy metals due to the oxygenated functional groups present on its surface (carboxyl, hydroxyl and epoxy groups) that work as binding sites to metals (Liu et al., 2019). Nevertheless, functional groups from proteins (-SH, NH and - COOH) are also strong active adsorption sites for heavy metals (Van Tran et al., 2018). Our XPS and FTIR data demonstrated an increase in the diversity of functional groups at the GO surface after biocorona formation. Then, the addition of these functional groups from *E. coli* lysis on GO surface can be responsible for the highest adsorption capacity shown for EC@GO.

Our biological assays demonstrated that the amount of silver internalized by nematodes exposed to EC@GO+Ag^+ was twice higher than that of nematodes exposed to GO+Ag^+. Several aspects can be involved in this response. But firstly, it is expected that the amount of silver delivered by EC@GO+Ag^+ to the nematodes be higher than that offered by GO+Ag^+ because EC@GO+Ag^+ adsorbed more silver according to our adsorption studies.

Additionally, we cannot exclude the possibility that *E. coli* coating could turn GO more assimilable by nematodes because *E. coli* is its bacterial food source. Thus, the silver bonded on the EC@GO surface could have been partially or totally desorbed and released during digestion or internalization within the nematode tissues. This supposition was previously raised by Jones and Candido (1999), who reported that Cd may have attached to the *E. coli* surface and desorbed in *C. elegans* pharynx and gut, causing oxidative stress in these tissues. These

factors probably contributed for EC@GO+Ag^{+} be more toxic than the other treatments and affected the nematode survival, neurons and germline cells after being translocated to its secondary target organs.

We raise the hypothesis that GO could also act as a carrier agent for silver, because GO+Ag^{+} increased the lethality of Ag^{+} to *C. elegans*, similar what was observed for EC@GO. Silver was complexed with the functional groups of GO surface, and consequently, internalized and translocated within nematode tissues. However, the magnitude of the damages promoted by GO+Ag^{+} in the *C. elegans* secondary organs was similar to the effects observed in nematodes exposed to Ag^{+}. In our previous work, we demonstrated that GO could remain retained in the *C. elegans* intestine for at least 12 h (Côa et al., 2022). Other studies have indicated that *C. elegans* defecation behaviour is negatively affected by GO exposure (Sivaselvam et al., 2020; Wu et al., 2013). Therefore, the long-retention time of this material inside the nematodes could have also increased the silver retention, causing higher toxicity to nematode survival. On the other hand, the most part of GO+Ag^{+} could be remained retained in the nematode intestine. Because of this, its effects on secondary organs were similar to the observed for silver ions.

We cannot ignore the fact that Ag^{+} exposure was the least toxic for *C. elegans* survival, although organisms exposed to this treatment show the highest silver internalized content. Silver toxicity is dependent on silver species, that are modulated by the media composition (Hogstrand et al.,1996). As such, we modelled the speciation of silver species expected in the EPA medium considering the conditions of our experiments. At 12.4 µg L^{-1} (LC_{50} for Ag^{+} exposure), two species of silver were found, Ag^{+} (mostly) and AgCl (solid) (Figure S5). This suggest that silver toxicity was probably influenced by these two silver species (i.e., Ag^{+} and AgCl). As AgCl is a precipitated silver form, nematodes may have ingested a high amount of silver because they may have come into contact with that at the bottom of the well; This explains the highest silver content found in our ICP-MS results for nematodes exposed to Ag^{+}.

AgCl is known to be less toxic than Ag^{+} to the organisms (Ratte, 1999); This may clarify why nematodes internalized more silver when exposed to Ag^{+} but were less affected. Although, we suppose that two metallothioneins (i.e., *mtl-1* and *mtl-2*) also influenced on silver toxicity. *Mtl- 1* and *mtl-2* are a group of cytoplasmatic proteins associated with metal detoxification in organisms. These proteins play a key role in the organisms because they hinder the diffusion of heavy metals within cells, preventing these metals from binding to other important enzymes and proteins that are responsible for maintaining the biological functions in organisms (George Cherian and Goyer, 1978). *Mtl-1* and *mtl-2* show a high affinity for Hg^{2+}, Cu^{+}, Cd^{+2}, Zn^{+2}, and Ag^{+} (Hogstrand et al., 1996; Mayer et al., 2003). In view of this, we assumed that these two

metallothioneins could have controlled the silver toxicity in nematodes exposed to Ag^+, reducing or at least controlling its adverse effects.

Besides this critical relationship between toxicity and silver speciation, the colloidal stability of NMs and heavy metals during the toxicity assay cannot be overlooked. The behaviour of GO+Ag^+ and EC@GO+Ag^+ in EPA medium was investigated during 24 h. Our data suggest that after 6 h of exposure, the percentage of suspended GO+Ag^+ and EC@GO+Ag^+ decreased to 45.4±4.6% and 35.3±3.1%, respectively. At the end of the experiment (24 h), only 5% and 20% of GO+Ag^+ and EC@GO+Ag^+, respectively, still remained suspended (Figure S2). Indeed, Wang et al. (2018) have reported that interactions between heavy metals and NMs reduce the surface energy of NMs, leading to agglomeration/aggregation events. In their study, the adsorption of cadmium, arsenic or nickel on TiO_2 nanoparticles changed the vertical distribution of these pollutants in the liquid medium and induced prolonged exposure to *C. elegans*. These observations signal that toxicity and materials uptake may have also been influenced by the available dose of materials to nematodes.

4.4. Conclusions

Our results evidence that graphene oxide was coated by biomolecules extracted from *E. coli* (biocorona formation). This biomolecular coating altered its physico-chemical properties such as topography and surface chemical composition. Uncoated and biocorona-coated GO were internalized and translocated inside the *C. elegans* body. GO was toxic for survival, germline cells and neuronal system of *C. elegans*, while nematodes exposed to coated GO did not die and its neurons were preserved. Therefore, biocorona mitigated the adverse effects of GO to nematode survival and neurons, but it did not supress its adverse effects on germline cells. These findings indicate that evaluating the implication of biocorona formation on graphene oxide toxicity is compulsory to understand its risks to environmental and human health.

Heavy metals make part of vital biological processes, but non-essential metals may disrupt the biological functions of organisms. In short, our results demonstrate that silver exposure affected all the measured endpoints; namely, it reduced nematode survival, altered its nervous system and induced germline apoptosis. Combined exposure of GO and Ag^+ increased the silver lethality to nematode survival by 2.1 times, while this effect was 4.6 times higher for corona-coated GO. Both GO+Ag^+ and EC@GO+Ag^+ were translocated to all the nematode

tissues. However, nematodes exposed to EC@GO+Ag^+ internalized 2 times more silver than nematodes exposed to GO with Ag^+. Consequently, the negative effects of EC@GO+Ag^+ on *C. elegans* germline and neurons were higher than the combined effects of GO+Ag^+. Indeed, the surface modification with biocorona increased the potential of GO to adsorb silver ions, demonstrating that the silver dose delivered by EC@GO+Ag^+ to nematodes could be higher than GO+Ag^+, which explains why EC@GO+Ag^+ was more toxic. Furthermore, biocorona formation could turn GO more assimilable by nematodes because *E. coli* is its bacterial food source. Whereas uncoated GO could increase the retention timer of silver inside the nematode intestine. These results suggest for the first time the potential role of graphene oxide in enhancing the toxicity of silver ions to *C. elegans* model. And fills a gap in the literature by demonstrating that the *E. coli* corona has a critical impact on combined toxicity of graphene oxide with metals drawing attention for both environmental risks assessment and agricultural applications.

References[7]

Ali, H., Khan, E., Ilahi, I., 2019. Environmental Chemistry and Ecotoxicology of Hazardous Heavy Metals: Environmental Persistence, Toxicity, and Bioaccumulation. J Chem 2019, 1–14. https://doi.org/10.1155/2019/6730305

Altun, Z.F., Hall, D.H., 2005. WormAtlas Hermaphrodite Handbook - Nervous System - General Description. WormAtlas. https://doi.org/10.3908/wormatlas.1.18

Anton Gartner, Peter R Boag, T Keith Blackwell, 2008. Germline survival and apoptosis. https://doi.org/10.1895/wormbook.1.145.1

Baimanov, D., Cai, R., Chen, C., 2019. Understanding the Chemical Nature of Nanoparticle–Protein Interactions. Bioconjug Chem 30, 1923–1937. https://doi.org/10.1021/acs.bioconjchem.9b00348

Baldovino, F.H., Quitain, A.T., Dugos, N.P., Roces, S.A., Koinuma, M., Yuasa, M., Kida, T., 2016. Synthesis and characterization of nitrogen-functionalized graphene oxide in high-temperature and high-pressure ammonia. RSC Adv 6, 113924–113932. https://doi.org/10.1039/C6RA22885B

Batista de Melo, C., Côa, F., Alves, O.L., Martinez, D.S.T., Barbieri, E., 2019. Co-exposure of graphene oxide with trace elements: Effects on acute ecotoxicity and routine metabolism in Palaemon pandaliformis (shrimp). Chemosphere 223. https://doi.org/10.1016/j.chemosphere.2019.02.017

[7] Prepared according to Elsevier guide.

Bortolozzo, L.S., Côa, F., Khan, L.U., Medeiros, A.M.Z., Silva, G.H., Delite, F.S., Strauss, M., Martinez, D.S.T., 2021. Mitigation of graphene oxide toxicity in *C. elegans* after chemical degradation with sodium hypochlorite. Chemosphere 130421. https://doi.org/10.1016/j.chemosphere.2021.130421

Brenner, S., 1974. The genetic of Caenorhabditis elegans. Genetics 77, 71–94. https://doi.org/10.1093/genetics/77.1.71

Canesi, L., Balbi, T., Fabbri, R., Salis, A., Damonte, G., Volland, M., Blasco, J., 2017. Biomolecular coronas in invertebrate species: Implications in the environmental impact of nanoparticles. NanoImpact 8, 89–98. https://doi.org/10.1016/j.impact.2017.08.001

Cao, X., Ma, C., Chen, F., Luo, X., Musante, C., White, J.C., Zhao, X., Wang, Z., Xing, B., 2021. New insight into the mechanism of graphene oxide-enhanced phytotoxicity of arsenic species. J Hazard Mater 410, 124959. https://doi.org/10.1016/j.jhazmat.2020.124959

Cedervall, T., Lynch, I., Foy, M., Berggård, T., Donnelly, S.C., Cagney, G., Linse, S., Dawson, K.A., 2007. Detailed Identification of Plasma Proteins Adsorbed on Copolymer Nanoparticles. Angewandte Chemie International Edition 46, 5754–5756. https://doi.org/10.1002/anie.200700465

Cerrillo, C., Barandika, G., Igartua, A., Areitioaurtena, O., Marcaide, A., Mendoza, G., 2015. Ecotoxicity of multiwalled carbon nanotubes: Standardization of the dispersion methods and concentration measurements. Environ Toxicol Chem 34, 1854–1862. https://doi.org/10.1002/etc.2999

Chong, Y., Ge, C., Yang, Z., Garate, J.A., Gu, Z., Weber, J.K., Liu, J., Zhou, R., 2015. Reduced Cytotoxicity of Graphene Nanosheets Mediated by Blood-Protein Coating. ACS Nano 9, 5713–5724. https://doi.org/10.1021/nn5066606

Choudhary, P., Parandhaman, T., Ramalingam, B., Duraipandy, N., Kiran, M.S., Das, S.K., 2017. Fabrication of Nontoxic Reduced Graphene Oxide Protein Nanoframework as Sustained Antimicrobial Coating for Biomedical Application. ACS Appl Mater Interfaces 9, 38255–38269. https://doi.org/10.1021/acsami.7b11203

Côa, F., Delite, F. de S., Strauss, M., Martinez, D.S.T., 2022. Toxicity mitigation and biodistribution of albumin corona coated graphene oxide and carbon nanotubes in Caenorhabditis elegans. NanoImpact 27, 100413. https://doi.org/10.1016/j.impact.2022.100413

Costa, L.S. da, Khan, L.U., Franqui, L.S., Delite, F. de S., Muraca, D., Martinez, D.S.T., Knobel, M., 2021. Hybrid magneto-luminescent iron oxide nanocubes functionalized with europium complexes: synthesis, hemolytic properties and protein corona formation. J Mater Chem B 9, 428–439. https://doi.org/10.1039/D0TB02454F

DeLoid, G.M., Cohen, J.M., Pyrgiotakis, G., Demokritou, P., 2017. Preparation, characterization, and in vitro dosimetry of dispersed, engineered nanomaterials. Nat Protoc 12, 355–371. https://doi.org/10.1038/nprot.2016.172

Dobrovolskaia, M.A., Patri, A.K., Zheng, J., Clogston, J.D., Ayub, N., Aggarwal, P., Neun, B.W., Hall, J.B., McNeil, S.E., 2009. Interaction of colloidal gold nanoparticles with human blood: effects on particle size and analysis of plasma protein binding profiles. Nanomedicine 5, 106–117. https://doi.org/10.1016/j.nano.2008.08.001

Dorney, J., Bonnier, F., Garcia, A., Casey, A., Chambers, G., Byrne, H.J., 2012. Identifying and localizing intracellular nanoparticles using Raman spectroscopy. Analyst 137, 1111. https://doi.org/10.1039/c2an15977e

Du, M., Wang, D., 2009. The neurotoxic effects of heavy metal exposure on GABAergic nervous system in nematode Caenorhabditis elegans. Environ Toxicol Pharmacol 27, 314–320. https://doi.org/10.1016/j.etap.2008.11.011

Ellegaard-Jensen, L., Jensen, K.A., Johansen, A., 2012. Nano-silver induces dose-response effects on the nematode Caenorhabditis elegans. Ecotoxicol Environ Saf 80, 216–223. https://doi.org/10.1016/j.ecoenv.2012.03.003

Elmore, S., 2007. Apoptosis: A Review of Programmed Cell Death. Toxicol Pathol 35, 495–516. https://doi.org/10.1080/01926230701320337

Emadi, F., Amini, A., Gholami, A., Ghasemi, Y., 2017. Functionalized Graphene Oxide with Chitosan for Protein Nanocarriers to Protect against Enzymatic Cleavage and Retain Collagenase Activity. Sci Rep 7, 42258. https://doi.org/10.1038/srep42258

Escher, B.I., Hermens, J.L.M., 2004. Internal Exposure: Linking Bioavailability to Effects. Environ Sci Technol 38, 455A-462A. https://doi.org/10.1021/es0406740

Franco, R., Sánchez-Olea, R., Reyes-Reyes, E.M., Panayiotidis, M.I., 2009. Environmental toxicity, oxidative stress and apoptosis: Ménage à Trois. Mutation Research/Genetic Toxicology and Environmental Mutagenesis 674, 3–22. https://doi.org/10.1016/j.mrgentox.2008.11.012

Franqui, L.S., de Farias, M.A., Portugal, R. v., Costa, C.A.R., Domingues, R.R., Souza Filho, A.G., Coluci, V.R., Leme, A.F.P., Martinez, D.S.T., 2019. Interaction of graphene oxide with cell culture medium: Evaluating the fetal bovine serum protein corona formation towards in vitro nanotoxicity assessment and nanobiointeractions. Materials Science and Engineering: C 100, 363–377. https://doi.org/10.1016/j.msec.2019.02.066

Ge, C., Tian, J., Zhao, Y., Chen, C., Zhou, R., Chai, Z., 2015. Towards understanding of nanoparticle–protein corona. Arch Toxicol 89, 519–539. https://doi.org/10.1007/s00204-015-1458-0

George Cherian, M., Goyer, R.A., 1978. Metallothioneins and their role in the metabolism and toxicity of metals. Life Sci 23, 1–9. https://doi.org/10.1016/0024-3205(78)90317-X

Gonzalez-Moragas, L., Maurer, L.L., Harms, V.M., Meyer, J.N., Laromaine, A., Roig, A., 2017. Materials and toxicological approaches to study metal and metal-oxide nanoparticles in the model organism: Caenorhabditis elegans. Mater Horiz 4, 719–746. https://doi.org/10.1039/c7mh00166e

Gonzalez-Moragas, L., Roig, A., Laromaine, A., 2015. *C. elegans* as a tool for in vivo nanoparticle assessment. Adv Colloid Interface Sci 219, 10–26. https://doi.org/10.1016/j.cis.2015.02.001

Gonzalez-Moragas, Laura, Yu, S.-M., Carenza, E., Laromaine, A., Roig, A., 2015. Protective Effects of Bovine Serum Albumin on Superparamagnetic Iron Oxide Nanoparticles Evaluated in the Nematode Caenorhabditis elegans. ACS Biomater Sci Eng 1, 1129–1138. https://doi.org/10.1021/acsbiomaterials.5b00253

Guo, Y., Yang, Y., Wang, D., 2009. Induction of reproductive deficits in nematode Caenorhabditis elegans exposed to metals at different developmental stages. Reproductive Toxicology 28, 90–95. https://doi.org/10.1016/j.reprotox.2009.03.007

Hanna, S.K., Bustos, A.R.M., Peterson, A.W., Reipa, V., Scanlan, L.D., Coskun, S.H., Cho, T.J., Johnson, M.E., Hackley, V.A., Nelson, B.C., Winchester, M.R., Elliott, J.T., Petersen, E.J., 2018. Agglomeration of Escherichia coli with Positively Charged Nanoparticles Can Lead to Artifacts in a Standard Caenorhabditis elegans Toxicity Assay. Environ Sci Technol 52, 5968–5978. https://doi.org/10.1021/acs.est.7b06099

Hartman, J.H., Widmayer, S.J., Bergemann, C.M., King, D.E., Morton, K.S., Romersi, R.F., Jameson, L.E., Leung, M.C.K., Andersen, E.C., Taubert, S., Meyer, J.N., 2021. Xenobiotic metabolism and transport in Caenorhabditis elegans. Journal of Toxicology and Environmental Health, Part B 24, 51–94. https://doi.org/10.1080/10937404.2021.1884921

Hogstrand, C., Galvez, F., Wood, C.M., 1996. Toxicity, silver accumulation and metallothionein induction in freshwater rainbow trout during exposure to different silver salts. Environ Toxicol Chem 15, 1102–1108. https://doi.org/10.1002/etc.5620150713

Hu, Y.-O., Wang, Y., Ye, B.-P., Wang, D.-Y., 2008. Phenotypic and Behavioral Defects Induced by Iron Exposure Can Be Transferred to Progeny in Caenorhabditis elegans. Biomedical and Environmental Sciences 21, 467–473. https://doi.org/10.1016/S0895-3988(09)60004-0

Hunt, P.R., 2017. The *C. elegans* model in toxicity testing. Journal of Applied Toxicology. https://doi.org/10.1002/jat.3357

Jiang, Y., Chen, J., Wu, Y., Wang, Q., Li, H., 2016. Sublethal toxicity endpoints of heavy metals to the nematode Caenorhabditis elegans. PLoS One 11, 1–12. https://doi.org/10.1371/journal.pone.0148014

Jin, L., Dou, T.-T., Chen, J.-Y., Duan, M.-X., Zhen, Q., Wu, H.-Z., Zhao, Y.-L., 2022. Sublethal toxicity of graphene oxide in Caenorhabditis elegans under multi-generational exposure. Ecotoxicol Environ Saf 229, 113064. https://doi.org/10.1016/j.ecoenv.2021.113064

Jones, D., Candido, E.P.M., 1999. Feeding is inhibited by sublethal concentrations of toxicants and by heat stress in the nematode Caenorhabditis elegans: Relationship to the cellular stress response. Journal of Experimental Zoology 284, 147–157. https://doi.org/10.1002/(SICI)1097-010X(19990701)284:2<147::AID-JEZ4>3.0.CO;2-Z

Jurgelėnė, Ž., Montvydienė, D., Šemčuk, S., Stankevičiūtė, M., Sauliutė, G., Pažusienė, J., Morkvėnas, A., Butrimienė, R., Jokšas, K., Pakštas, V., Kazlauskienė, N., & Karabanovas, V. (2022). The impact of co-treatment with graphene oxide and metal mixture on Salmo trutta at early development stages: The sorption capacity and potential toxicity. Science of The Total Environment, 838, 156525. https://doi.org/10.1016/j.scitotenv.2022.156525

Kim, M., Eom, H.-J., Choi, I., Hong, J., Choi, J., 2020. Graphene oxide-induced neurotoxicity on neurotransmitters, AFD neurons and locomotive behavior in Caenorhabditis elegans. Neurotoxicology 77, 30–39. https://doi.org/10.1016/j.neuro.2019.12.011

Kim, Y., Jeong, J., Yang, J., Joo, S.-W., Hong, J., Choi, J., 2018. Graphene oxide nano-bio interaction induces inhibition of spermatogenesis and disturbance of fatty acid metabolism in the nematode Caenorhabditis elegans. Toxicology 410, 83–95. https://doi.org/10.1016/j.tox.2018.09.006

Kleiven, M., Oughton, D., 2015. Standard Operating Procedure Toxicity test with the nematode Caenorhabiditis elegans for the NANoREG core nanomaterials.

Krimm, S., Bandekar, J., 1986. Vibrational Spectroscopy and Conformation of Peptides, Polypeptides, and Proteins. pp. 181–364. https://doi.org/10.1016/S0065-3233(08)60528-8

Lant, B., Derry, W.B., 2013. Methods for detection and analysis of apoptosis signaling in the *C. elegans* germline. Methods 61, 174–182. https://doi.org/10.1016/j.ymeth.2013.04.022

Li, P., Xu, T., Wu, S., Lei, L., He, D., 2017. Chronic exposure to graphene-based nanomaterials induces behavioral deficits and neural damage in Caenorhabditis elegans. Journal of Applied Toxicology 37, 1140–1150. https://doi.org/10.1002/jat.3468

Li, S., Mulloor, J.J., Wang, L., Ji, Y., Mulloor, C.J., Micic, M., Orbulescu, J., Leblanc, R.M., 2014. Strong and Selective Adsorption of Lysozyme on Graphene Oxide. ACS Appl Mater Interfaces 6, 5704–5712. https://doi.org/10.1021/am500254e

Li, X., Hu, J., Qiu, R., Zhang, X., Chen, Y., He, D., 2020. Joint toxic effects of polystyrene nanoparticles and organochlorine pesticides (chlordane and hexachlorocyclohexane) on Caenorhabditis elegans. Environ Sci Nano. https://doi.org/10.1039/D0EN00654H

Liu, J., Fu, S., Yuan, B., Li, Y., Deng, Z., 2010. Toward a Universal "Adhesive Nanosheet" for the Assembly of Multiple Nanoparticles Based on a Protein-Induced Reduction/Decoration of Graphene Oxide. J Am Chem Soc 132, 7279–7281. https://doi.org/10.1021/ja100938r

Liu, P., Shao, H., Ding, X., Yang, R., Rui, Q., Wang, D., 2019. Dysregulation of Neuronal Gαo Signaling by Graphene Oxide in Nematode Caenorhabditis elegans. Sci Rep 9, 6026. https://doi.org/10.1038/s41598-019-42603-1

Liu, X., Ma, R., Wang, Xiangxue, Ma, Y., Yang, Y., Zhuang, L., Zhang, S., Jehan, R., Chen, J., Wang, Xiangke, 2019. Graphene oxide-based materials for efficient removal of heavy metal ions from aqueous solution: A review. Environmental Pollution 252, 62–73. https://doi.org/10.1016/j.envpol.2019.05.050

Liu, Y., Nie, Y., Wang, Jingjing, Wang, Juan, Wang, X., Chen, S., Zhao, G., Wu, L., Xu, A., 2018. Mechanisms involved in the impact of engineered nanomaterials on the joint toxicity with environmental pollutants. Ecotoxicol Environ Saf 162, 92–102. https://doi.org/10.1016/j.ecoenv.2018.06.079

Maiti, D., Tong, X., Mou, X., Yang, K., 2019. Carbon-Based Nanomaterials for Biomedical Applications: A Recent Study. Front Pharmacol 9. https://doi.org/10.3389/fphar.2018.01401

Martinez, D.S.T., da Silva, G.H., de Medeiros, A.M.Z., Khan, L.U., Papadiamantis, A.G., Lynch, I., 2020. Effect of the Albumin Corona on the Toxicity of Combined Graphene Oxide and Cadmium to Daphnia magna and Integration of the Datasets into the NanoCommons Knowledge Base. Nanomaterials 10, 1936. https://doi.org/10.3390/nano10101936

Martinez, D.S.T., Ellis, L.-J.A., da Silva, G.H., Petry, R., Medeiros, A.M.Z., Davoudi, H.H., Papadiamantis, A.G., Fazzio, A., Afantitis, A., Melagraki, G., Lynch, I., 2022. Daphnia magna and mixture toxicity with nanomaterials – Current status and perspectives in data-driven risk prediction. Nano Today 43, 101430. https://doi.org/10.1016/j.nantod.2022.101430

Martins, C.H.Z., Côa, F., da Silva, G.H., Bettini, J., de Farias, M.A., Portugal, R.V., Umbuzeiro, G. de A., Alves, O.L., Martinez, D.S.T., 2022. Functionalization of carbon nanotubes with bovine plasma biowaste by forming a protein corona enhances copper removal from water and ecotoxicity mitigation. Environ Sci Nano 9, 2887–2905. https://doi.org/10.1039/D2EN00145D

Maurer, L.L., Ryde, I.T., Yang, X., Meyer, J.N., 2015. Caenorhabditis elegans as a Model for Toxic Effects of Nanoparticles: Lethality, Growth, and Reproduction. Curr Protoc Toxicol 66, 20.10.1-20.10.25. https://doi.org/10.1002/0471140856.tx2010s66

Mayer, G.D., Leach, A., Kling, P., Olsson, P.-E., Hogstrand, C., 2003. Activation of the rainbow trout metallothionein-A promoter by silver and zinc. Comp Biochem Physiol B Biochem Mol Biol 134, 181–188. https://doi.org/10.1016/S1096-4959(02)00248-8

Medeiros, A.M.Z. de, Côa, F., Alves, O.L., Teodoro Martinez, D.S., Barbieri, E., 2020. Metabolic effects in the freshwater fish Geophagus iporangensis in response to single and combined exposure to graphene oxide and trace elements. Chemosphere 243, 125316. https://doi.org/10.1016/j.chemosphere.2019.125316

Moore, T.L., Rodriguez-Lorenzo, L., Hirsch, V., Balog, S., Urban, D., Jud, C., Rothen-Rutishauser, B., Lattuada, M., Petri-Fink, A., 2015. Nanoparticle colloidal stability in cell culture media and impact on cellular interactions. Chem Soc Rev 44, 6287–6305. https://doi.org/10.1039/C4CS00487F

Nivedita, C., Young-ho, K., Jisu, Y., P, R.C., Woo, J.S., Jinhee, C., 2017. A systems toxicology approach reveals the Wnt-MAPK crosstalk pathway mediated reproductive failure in Caenorhabditis elegans exposed to graphene oxide (GO) but not to reduced graphene oxide (rGO). Nanotoxicology 0, 000. https://doi.org/10.1080/17435390.2016.1267273

Organisation for Economic Co-operation and Development - OECD, 2017. Test No. 318: Dispersion Stability of Nanomaterials in Simulated Environmental Media, OECD Guidelines for the Testing of Chemicals, Section 3. https://doi.org/10.1787/9789264284142-en

Organisation for Economic Co-operation and Development - OECD, 2020. Guidance document on aquatic and sediment toxicological Testing of nanomaterials.

Peng, Z.G., Hidajat, K., Uddin, M.S., 2004. Adsorption of bovine serum albumin on nanosized magnetic particles. J Colloid Interface Sci 271, 277–283. https://doi.org/10.1016/j.jcis.2003.12.022

Porta-de-la-Riva, M., Fontrodona, L., Villanueva, A., Cerón, J., 2012. Basic Caenorhabditis elegans Methods: Synchronization and Observation. Journal of Visualized Experiments. https://doi.org/10.3791/4019

Qu, M., Li, Y., Wu, Q., Xia, Y., Wang, D., 2017. Neuronal ERK signaling in response to graphene oxide in nematode Caenorhabditis elegans. Nanotoxicology 11, 520–533. https://doi.org/10.1080/17435390.2017.1315190

Qu, Y., Li, W., Zhou, Y., Liu, X., Zhang, L., Wang, L., Li, Y., Iida, A., Tang, Z., Zhao, Y., Chai, Z., Chen, C., 2011. Full Assessment of Fate and Physiological Behavior of Quantum Dots Utilizing Caenorhabditis elegans as a Model Organism. Nano Lett 11, 3174–3183. https://doi.org/10.1021/nl201391e

Ratte, H. T., 1999. Bioaccumulation and toxicity of silver compounds: A review. Environmental Toxicology and Chemistry, 18(1), 89–108. https://doi.org/10.1002/etc.5620180112

Rossbach, L.M., Brede, D.A., Nuyts, G., Cagno, S., Olsson, R.M.S., Oughton, D.H., Falkenberg, G., Janssens, K., Lind, O.C., 2022. Synchrotron XRF Analysis Identifies Cerium Accumulation Colocalized with Pharyngeal Deformities in CeO 2 NP-Exposed Caenorhabditis elegans. Environ Sci Technol 56, 5081–5089. https://doi.org/10.1021/acs.est.1c08509

Scanlan, L.D., Lund, S.P., Coskun, S.H., Hanna, S.K., Johnson, M.E., Sims, C.M., Brignoni, K., Lapasset, P., Petersen, E.J., Elliott, J.T., Nelson, B.C., 2018. Counting Caenorhabditis elegans: Protocol Optimization and Applications for Population Growth and Toxicity Studies in Liquid Medium. Sci Rep 8, 904. https://doi.org/10.1038/s41598-018-19187-3

Schafer, W.R., 2005. Deciphering the Neural and Molecular Mechanisms of *C. elegans* Behavior. Current Biology 15, R723–R729. https://doi.org/10.1016/j.cub.2005.08.020

Sivaselvam, S., Mohankumar, A., Thiruppathi, G., Sundararaj, P., Viswanathan, C., Ponpandian, N., 2020. Engineering the surface of graphene oxide with bovine serum albumin for improved biocompatibility in Caenorhabditis elegans. Nanoscale Adv 2, 5219–5230. https://doi.org/10.1039/D0NA00574F

Starnes, D.L., Unrine, J.M., Starnes, C.P., Collin, B.E., Oostveen, E.K., Ma, R., Lowry, G. v., Bertsch, P.M., Tsyusko, O. v., 2015. Impact of sulfidation on the bioavailability and toxicity of silver nanoparticles to Caenorhabditis elegans. Environmental Pollution 196, 239–246. https://doi.org/10.1016/j.envpol.2014.10.009

Stiernagle, T., 2006. Maintenance of *C. elegans*. WormBook 1–11. https://doi.org/10.1895/wormbook.1.101.1

Tomak, A., Cesmeli, S., Hanoglu, B.D., Winkler, D., Oksel Karakus, C., 2021. Nanoparticle-protein corona complex: understanding multiple interactions between environmental factors, corona formation, and biological activity. Nanotoxicology 15, 1331–1357. https://doi.org/10.1080/17435390.2022.2025467

Tsai, M.-H., Chao, H.-R., Jiang, J.-J., Su, Y.-H., Cortez, M.P., Tayo, L.L., Lu, I.-C., Hsieh, H., Lin, C.-C., Lin, S.-L., Wan Mansor, W.N., Su, C.-K., Huang, S.-T., Hsu, W.-L., 2021. Toxicity of Low-dose Graphene Oxide Nanoparticles in an in-vivo Wild Type of Caenorhabditis elegans Model. Aerosol Air Qual Res 21. https://doi.org/10.4209/aaqr.200559

Ullah, R., Khan, S.A., Aladresi, A.A.M., Alharbi, S.A., Chinnathambi, A., 2020. Ovalbumin-mediated synthesis and simultaneous functionalization of graphene with increased protein stability. Green Chem Lett Rev 13, 60–67. https://doi.org/10.1080/17518253.2020.1725150

Van Tran, V., Park, D., Lee, Y.-C., 2018. Hydrogel applications for adsorption of contaminants in water and wastewater treatment. Environmental Science and Pollution Research 25, 24569–24599. https://doi.org/10.1007/s11356-018-2605-y

Vanea, E., Simon, V., 2011. XPS study of protein adsorption onto nanocrystalline aluminosilicate microparticles. Appl Surf Sci 257, 2346–2352. https://doi.org/10.1016/j.apsusc.2010.09.101

Wang, D., Wang, Y., 2008a. Nickel sulfate induces numerous defects in Caenorhabditis elegans that can also be transferred to progeny. Environmental Pollution 151, 585–592. https://doi.org/10.1016/j.envpol.2007.04.003

Wang, D., Wang, Y., 2008b. Nickel sulfate induces numerous defects in Caenorhabditis elegans that can also be transferred to progeny. Environmental Pollution 151, 585–592. https://doi.org/10.1016/j.envpol.2007.04.003

Wang, D., Xing, X., 2008. Assessment of locomotion behavioral defects induced by acute toxicity from heavy metal exposure in nematode Caenorhabditis elegans. Journal of Environmental Sciences 20, 1132–1137. https://doi.org/10.1016/S1001-0742(08)62160-9

Wang, D.-Y., Yang, P., 2007. Silver Exposure Causes Transferable Defects of Phenotypes and Behaviors in Nematode Caenorhabditis elegans. Environ Bioindic 2, 89–98. https://doi.org/10.1080/15555270701457695

Wang, J., Dai, H., Nie, Y., Wang, M., Yang, Z., Cheng, L., Liu, Y., Chen, S., Zhao, G., Wu, L., Guang, S., Xu, A., 2018. TiO_2 nanoparticles enhance bioaccumulation and toxicity of heavy metals in Caenorhabditis elegans via modification of local concentrations during the sedimentation process. Ecotoxicol Environ Saf 162, 160–169. https://doi.org/10.1016/j.ecoenv.2018.06.051

Wang, J., Nie, Y., Dai, H., Wang, M., Cheng, L., Yang, Z., Chen, S., Zhao, G., Wu, L., Guang, S., Xu, A., 2019. Parental exposure to TiO 2 NPs promotes the multigenerational reproductive toxicity of Cd in Caenorhabditis elegans via bioaccumulation of Cd in germ cells. Environ Sci Nano 6, 1332–1342. https://doi.org/10.1039/C8EN01042K

Wang, S., Wu, L., Wang, Y., Luo, X., Lu, Y., 2009. Copper-induced germline apoptosis in Caenorhabditis elegans: The independent roles of DNA damage response signaling and the dependent roles of MAPK cascades. Chem Biol Interact 180, 151–157. https://doi.org/10.1016/j.cbi.2009.03.012

Wang, S., Yu, D., Dai, L., Chang, D.W., Baek, J.-B., 2011. Polyelectrolyte-Functionalized Graphene as Metal-Free Electrocatalysts for Oxygen Reduction. ACS Nano 5, 6202–6209. https://doi.org/10.1021/nn200879h

Wang, S., Zhao, Y., Wu, L., Tang, M., Su, C., Hei, T.K., Yu, Z., 2007. Induction of Germline Cell Cycle Arrest and Apoptosis by Sodium Arsenite in Caenorhabditis elegans. Chem Res Toxicol 20, 181–186. https://doi.org/10.1021/tx0601962

White, J.G., Southgate, E., Thomson, J.N., Brenner, S., 1986. The structure of the nervous system of the nematode Caenorhabditis elegans. Philos Trans R Soc Lond B Biol Sci 314, 1–304.

Wu, Q., He, K., Liu, P., Li, Y., Wang, D., 2011. Association of oxidative stress with the formation of reproductive toxicity from mercury exposure on hermaphrodite nematode Caenorhabditis elegans. Environ Toxicol Pharmacol 32, 175–184. https://doi.org/10.1016/j.etap.2011.04.009

Wu, Q., Yin, L., Li, X., Tang, M., Zhang, T., Wang, D., 2013. Contributions of altered permeability of intestinal barrier and defecation behavior to toxicity formation from graphene oxide in nematode Caenorhabditis elegans. Nanoscale 5, 9934. https://doi.org/10.1039/c3nr02084c

Wu, Q., Zhao, Y., Fang, J., Wang, D., 2014. Immune response is required for the control of in vivo translocation and chronic toxicity of graphene oxide. Nanoscale 6, 5894. https://doi.org/10.1039/c4nr00699b

Xing, Xiaojuan, Du, M., Xu, X., Rui, Q., Wang, D., 2009. Exposure to metals induces morphological and functional alteration of AFD neurons in nematode Caenorhabditis elegans. Environ Toxicol Pharmacol 28, 104–110. https://doi.org/10.1016/j.etap.2009.03.006

Xing, X., Rui, Q., Wang, D., 2009. Lethality Toxicities Induced by Metal Exposure During Development in Nematode Caenorhabditis Elegans. Bull Environ Contam Toxicol 83, 530–536. https://doi.org/10.1007/s00128-009-9816-3

Yao, Y., Zhang, T., Tang, M., 2022. A critical review of advances in reproductive toxicity of common nanomaterials to Caenorhabditis elegans and influencing factors. Environmental Pollution 306, 119270. https://doi.org/10.1016/j.envpol.2022.119270

Yu, D., Yang, Y., Durstock, M., Baek, J.-B., Dai, L., 2010. Soluble P3HT-Grafted Graphene for Efficient Bilayer−Heterojunction Photovoltaic Devices. ACS Nano 4, 5633–5640. https://doi.org/10.1021/nn101671t

Zhang, C., Hao, R., Liao, H., Hou, Y., 2013. Synthesis of amino-functionalized graphene as metal-free catalyst and exploration of the roles of various nitrogen states in oxygen reduction reaction. Nano Energy 2, 88–97. https://doi.org/10.1016/j.nanoen.2012.07.021

Zhang, Q., Wang, C., 2020. Natural and Human Factors Affect the Distribution of Soil Heavy Metal Pollution: a review. Water Air Soil Pollut 231, 350. https://doi.org/10.1007/s11270-020-04728-2

Zhang, Y., Ye, B., Wang, D., 2010. Effects of Metal Exposure on Associative Learning Behavior in Nematode Caenorhabditis elegans. Arch Environ Contam Toxicol 59, 129–136. https://doi.org/10.1007/s00244-009-9456-y

Zhao, L., Kong, J., Krasteva, N., Wang, D., 2018. Deficit in the epidermal barrier induces toxicity and translocation of PEG modified graphene oxide in nematodes. Toxicol Res (Camb) 7, 1061–1070. https://doi.org/10.1039/C8TX00136G

Zhao, Y., Chen, H., Yang, Y., Wu, Q., Wang, D., 2020. Graphene oxide disrupts the protein-protein interaction between Neuroligin/NLG-1 and DLG-1 or MAGI-1 in nematode Caenorhabditis elegans. Science of The Total Environment 700, 134492. https://doi.org/10.1016/j.scitotenv.2019.134492

Zhao, Y., Wu, Q., Wang, D., 2016. An epigenetic signal encoded protection mechanism is activated by graphene oxide to inhibit its induced reproductive toxicity in Caenorhabditis elegans. Biomaterials 79, 15–24. https://doi.org/10.1016/j.biomaterials.2015.11.052

Zheng, F., Chen, C., Aschner, M., 2022. Neurotoxicity Evaluation of Nanomaterials Using *C. elegans*: Survival, Locomotion Behaviors, and Oxidative Stress. Curr Protoc 2. https://doi.org/10.1002/cpz1.496

Zhi, L., Ren, M., Qu, M., Zhang, H., Wang, D., 2016. Wnt Ligands Differentially Regulate Toxicity and Translocation of Graphene Oxide through Different Mechanisms in Caenorhabditis elegans. Sci Rep 6, 39261. https://doi.org/10.1038/srep39261

5. CHAPTER 5. GENERAL CONCLUSIONS AND FUTURE OUTLOOK

Due to the promising NMs to revolutionise many facets of technology, their benefits are unquestionable in our modern life. However, understanding their implications for environmental and human health is indispensable to protect the ecosystem and developing safe and sustainable products.

In the last two decades, NMs toxicity has become one of the topics of greatest concern in the literature and decision-making by regulatory agents. Consequently, public and governmental investments have been directed to suppress this gap. Countless relevant works have been published and have brought us closer of predicting the risks of nanotechnology. However, only in the last ten years, the biocorona formation effect has been the focus of many studies since it has been demonstrated that this aspect influences the biological response to NMs exposure. Until now, the influence of biocorona formation in studies with *C. elegans* was still poorly assessed. Moreover, in the environment, nanomaterials will never be alone; Pre-existing pollutants and biomolecules will be part of the transformation processes that these materials will undergo. Therefore, this current research goes in the direction of understanding the implications of the biocorona effect on the toxicity of carbon nanomaterials and co-exposure scenarios. Three chapters were prepared to cover these questions, and the main outputs were summarised below.

Chapter 2 demonstrated the potential of *C. elegans* to be exploited as an alternative model to animal experimentation and nanotoxicity assessment. The literature review revealed significant progress towards evaluating the potential adverse effects of carbon nanomaterials on *C. elegans,* indicating that, under certain conditions, these materials can affect the nematode survival and lifespan, and damage its secondary target organs (neurons and reproductive system); Nevertheless, some approaches can be applied to alleviate the carbon nanomaterials toxicity (e.g., coating with humic acid or proteins, treatment with bleach water). In addition, this review pointed out that scientific and methodological gaps must be considered towards harmonising the protocols and reducing misinterpretations concerning the nanotoxicity results. It also demonstrated that the available techniques to investigate the NMs internalization and biodistribution in *C. elegans* have been very useful but can still be better explored.

Chapter 3 aimed to evaluate the influence of biocorona formation on graphene oxide and multi-walled carbon nanotubes toxicity. A protein model (i.e., bovine serum albumin) was selected to perform these studies. In brief, it was demonstrated that both pristine carbon nanomaterials were toxic to nematode survival, reproduction, and fertility. In addition, they

were translocated from its intestinal barrier to secondary targeted organs, increasing oxidative stress and affecting their physiological functions (i.e., reproduction and fertility). Albumin corona prevented the translocation of carbon nanotubes inside nematode, mitigating their chronic adverse effects. On the other hand, GO was transferred to all the nematode tissues, even with protein coating. Moreover, this material with and without protein remained accumulated in the nematode intestine after 2 h of food resumption. Consequently, GO toxicity was only partially suppressed by albumin coating, which may have suffered degradation inside the nematode intestine due to the long-time of retention, re-establishing the negative effects of graphene oxide on nematode gonad. Therefore, this chapter contributes to the nanotoxicology field by demonstrating that the translocation and excretion of biocorona-coated materials must be studied before proposing their application, as they were related to the damage observed in *C. elegans*.

Chapter 4 explored the implications of *E. coli* lysis and the consequent biocorona formation on toxicity assays with *C. elegans*. The effects of this coating on the behaviour and combined toxicity of graphene oxide with silver ions were also evaluated. In short, it was observed a bicorona on the GO surface. Biocorona increased the colloidal stability of GO and reduced its adverse effects on nematode survival but did not eliminate the damage to the reproductive system (germline apoptosis). Silver exposure affected all the measured endpoints; namely, it reduced nematode survival, altered its nervous system and induced germline apoptosis. Combined exposure of GO and Ag^+ increased the silver lethality to nematode survival by 210%, while this effect was 460% higher for protein-coated GO. Both GO+Ag^+ and EC@GO+Ag^+ were translocated to all the nematode tissues. However, nematodes exposed to EC@GO+Ag^+ internalized 2 times more silver than nematodes exposed to GO with Ag^+. Consequently, the negative effects of EC@GO+Ag^+ on *C. elegans* germline and neurons were higher than the combined effects of GO+Ag^+. Indeed, the surface modification with biocorona increased the potential of GO to adsorb silver ions, demonstrating that the silver dose delivered by EC@GO+Ag^+ to nematodes could be higher than GO+Ag^+, which explains why EC@GO+Ag^+ was more toxic. Therefore, this chapter represents a key contribution to the research studies in *C. elegans*, because reveals that *E. coli* corona exerts a pivotal role in the toxicity of graphene oxide, both in single and co-exposure testing. This finding demonstrates that further works must consider the *E. coli* corona formation effect in their experimental drawings, as well as these aspects must be incorporated in the development of standardized protocols and be discussed towards understanding the NMs effects in environmentally complex scenarios.

To sum up, this thesis reveals that *C. elegans* is a suitable model to expand our understanding of biocorona implications on the toxicity of carbon nanomaterials and behaviour in vivo. In addition, it brings up that the biocorona effect cannot be overlooked specially in co-exposure scenarios. However, some issues remain to be elucidated to fully comprehend their impacts to the human and environmental health. Some considerations on future topics of importance in this field are detailed below.

Relating to the Chapter 3:

1) This chapter shows that albumin corona exerts a protective effect against carbon nanomaterials toxicity (especially in the nanotubes case); Hence, it could be better exploited as a technology approach towards the safe application of these materials.

2) It was reported that adverse effects of GO on nematode reproduction were not 100% mitigated by albumin biocorona formation. In future investigations, a great deal of importance should be devoted to toxicity mechanisms, which could be studied with transgenic strains or multi-omics analyses.

3) It was noticed that the translocation pattern of uncoated or coated materials in *C. elegans* body was correlated to the observed effects. This finding suggests that toxicokinetic studies are primordial to safely applying these materials.

4) It was demonstrated that the biocorona changes the biodistribution of NMs in *C. elegans*. However, its degradation inside the nematode intestine and its by-products must be further assessed. It is important to highlight that there are no accurate and reliable analytical methods to recover the corona-coated materials from the organisms without disturbing their original characteristics, or assessing coronas *in situ* in tissues. Fortunately, with the advancement of scientific knowledge, new protocols and guidelines will be elaborated.

5) It is primordial to investigate whether and how biocorona affects the transferring of carbon nanomaterials to other organisms of other trophic levels (i.e., biomagnification effect). However, traditional approaches to estimating the accumulation of organic chemicals are not accurate for carbon nanomaterials; therefore, further research needs to be focused on suppressing these gaps.

Relating to the Chapter 4:

1) This chapter confirms that a biocorona layer can be formed on the graphene oxide surface after its interaction with biomolecules from *E. coli* lysis. Therefore, the protocols and further studies should be planned considering this influence.

2) The complexity of biocorona formed on the GO surface could be investigated in further works, for example, by exploiting proteomic approaches to identify the protein patterns that compose the biocorona. The protein conformation in *E. coli* corona could be evaluated by circular dichroism (CD) spectroscopy or fluorescence correlation spectrometry (FCS). And the binding affinity of proteins by the NMs surface could be examined by isothermal titration calorimetry (ITC) or quartz crystal microbalance (QCM).

3) This chapter reveals that biocorona formed by the interaction of GO with *E. coli* lysate can potentiate silver toxicity to *C. elegans*. If, on the one hand, it could be a drawback, on the other hand, it can open the door to be explored as an advantage to the development of new advanced materials. In this direction, a patent[8] was deposited suggesting that this material would be strategically introduced as a carrier agent of traditional nematicides to maximize their efficacy and control nematode pests. However, this new approach needs to be investigated in terms of safety, scalability and costs.

[8] Patent published: Côa, F. and Martinez, D.S.T. Corona de proteínas carreadora de agentes antinematóides e seu processo de produção. 2022 BR 10 2022 012202 4.

APPENDIX

Appendix A. Supplementary material of Chapter 3…….149

Appendix B. Supplementary material of Chapter 4…….157

Appendix C. Scientific and Academic Contributions……..163

Appendix A. Supplementary Information of Chapter 3

Toxicity mitigation and biodistribution of albumin corona coated graphene oxide and carbon nanotubes on C. elegans

Experimental Workflow

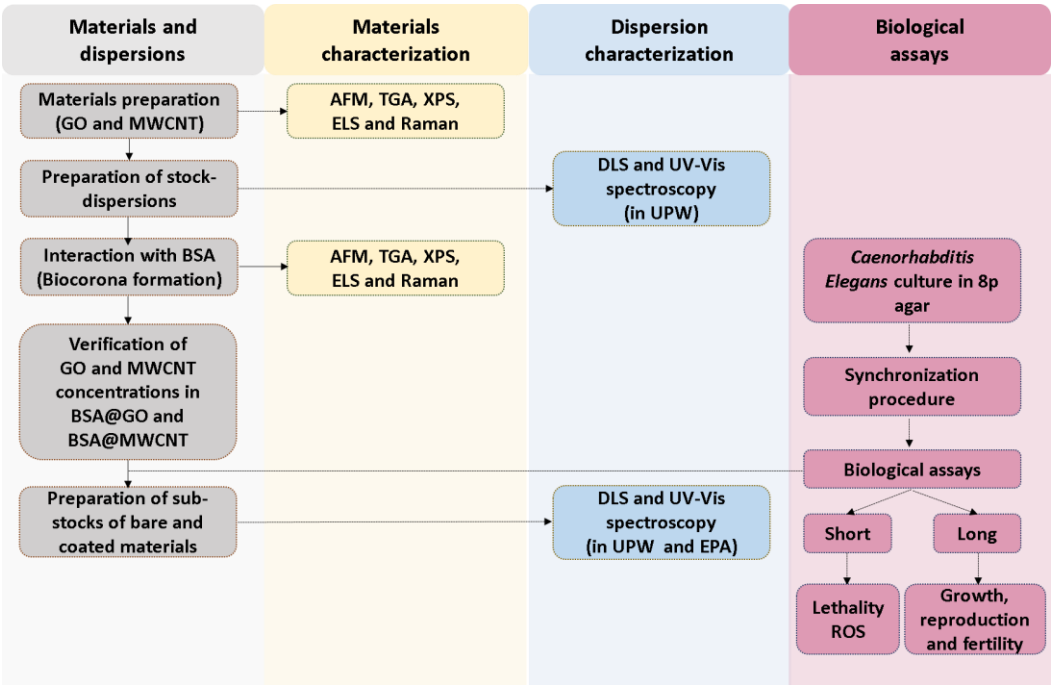

Characterization of GO and MWCNT before and after biocorona formation

Structural information of samples was obtained by Raman spectroscopy. Spectra were acquired with a confocal Raman spectrometer (XploRA PLUS, Horiba) equipped with an optical confocal microscope (100x objective). A laser (638 nm) was used as an excitation source and spectra were with 5 accumulations of 5 s each. Samples were evaluated from stock dispersions that were dropped on a glass side and analysed.

To study the oxygenated functional groups present in bare GO and MWCNT, X-ray photoelectron spectroscopy was performed in a K-Alpha System (Thermofischer Scientific, USA) using Al Kα X-rays and charge compensation during analyses. Pass energies of 50 eV were employed to obtain survey C1s high-resolution spectra. Spectra were collected at four different areas per sample with a spatial resolution of 400 µm. Data were analysed with Thermo Avantage software (version 5.957).

Figure S1 - UV-Vis spectra of GO, BSA@GO and BSA (A), and MWCNT, BSA@MWCNT and BSA (B) from 200 to 800 nm.

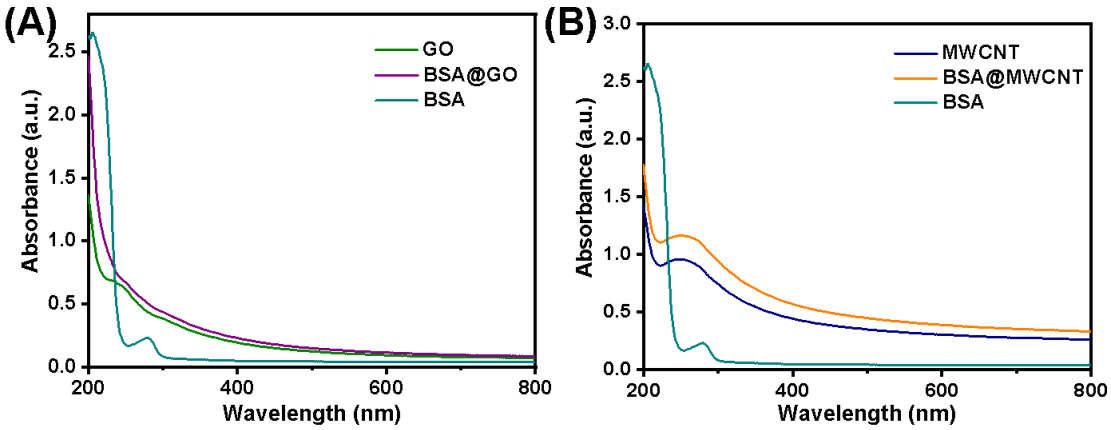

Figure S2 - Calibration curves of GO (A) and MWCNT (B) in ultrapure water obtained from absorbance (at 400 nm wavelength). The straight line is a linear fit of data.

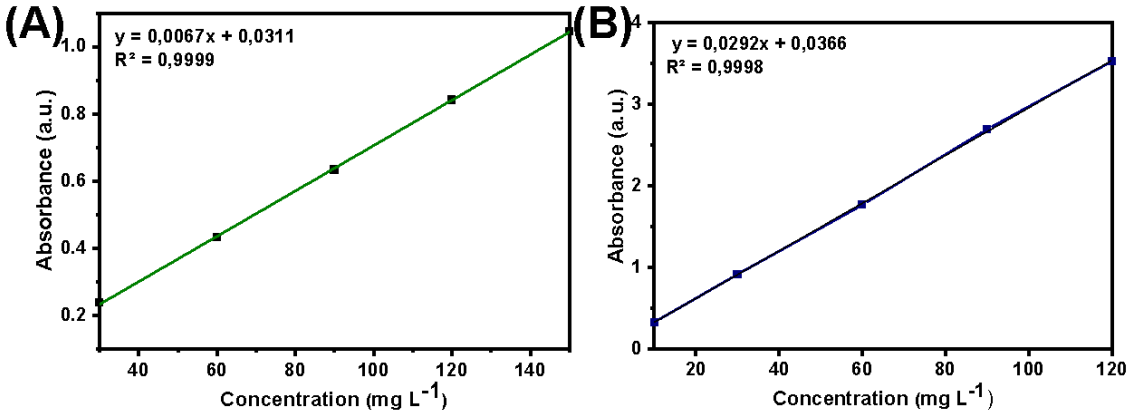

Synchronization procedure details

For performing synchronization procedures, gravid hermaphrodites were collected from 8P agar to a centrifuge tube by washing the plate with EPA medium (50 mL). Washing steps by centrifugation were performed until EPA medium appears clear of bacteria. At each step, centrifugation was carried out at 774 g and 20 °C, the supernatant was discarded and worm pellet was washed with EPA medium (50 mL). After removing bacteria, a lysis solution (1 mL NaOH 10 M, 4 mL NaClO 3%, and 5 mL of ultrapure water) was applied to the worm pellet. The tube was vigorously and manually agitated for 6 minutes to destruct adults and release eggs. The lysis solution containing eggs was transferred to a centrifuge tube of 15 mL and the reaction was disrupted by the addition of EPA medium until filling the tube. Three washing steps by centrifugation were performed at 955 g and 20 °C. At each centrifugation step, the supernatant was discarded, and the worm pellet was washed with EPA medium (15 mL).

The last obtained worm pellet was resuspended in 15 mL of EPA and passed through by a 40 µm cell strainer to remove worm debris. Lastly, depending on the toxicity assay to be realized the eggs were differently treated. For chronic assays, eggs were incubated in 15 mL of EPA medium at 20 °C without food during 20-22 h (L1 stage). For acute assays, eggs were cultured for 48 h at 20 °C on NGM plates seed with *E. coli* OP50, resulting in L3 stage worms (young adults).

Figure S3 - Induction of ROS production in *C. elegans* due to hydrogen peroxide exposure (5 mM).

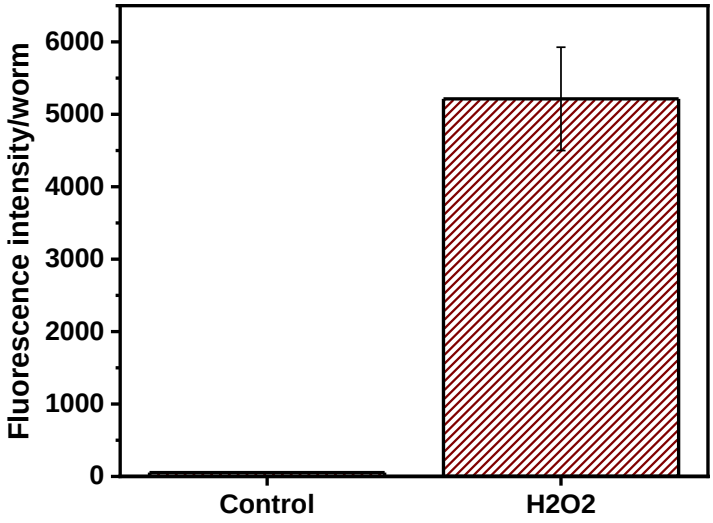

***Escherichia coli* preparation for long-term assays**

The calibration curve for *E. coli* quantification was prepared diluting formazine stock suspension (4000.0 NTU, Merck, Lot 98253) in EPA medium at 250.0; 500.0; 1000.0; 1500.0, and 2000.0 NTU (Figure S4). Absorbance was measured at 600 nm wavelength in a UV–visible spectrophotometer (Multiskan TM GO, Thermo Scientific).

When chronic assays were performed, a suspension of *E. coli* was prepared by inoculating 500 mL of sterilized liquid Luria Broth (LB) medium with 200 µL of *E. coli* OP50 in a shaker incubator at 37 ºC and 100 rpm. After 15 h, the culture was transferred to 50 mL centrifuge tubes and centrifuged at 2,990 g for 5 min. Supernatants containing LB medium were discarded and bacteria pellets were resuspended in 10 mL EPA medium. Then, bacterial densities in *E. coli* suspension were verified and adjusted to 1000 FAU (formazine attenuation units) using the calibration curve. After adjusting bacterial densities, cholesterol solution (5 mg mL^{-1}, dissolved in 100% ethanol) was added to *E. coli* suspension at a concentration of 0.2% v/v cholesterol.

Figure S4 - Calibration curve obtained from absorbance (at 600 nm wavelength) of formazine standards (from 250.0 to 2000.0 NTU) in EPA medium. The straight line is the linear fit of the data.

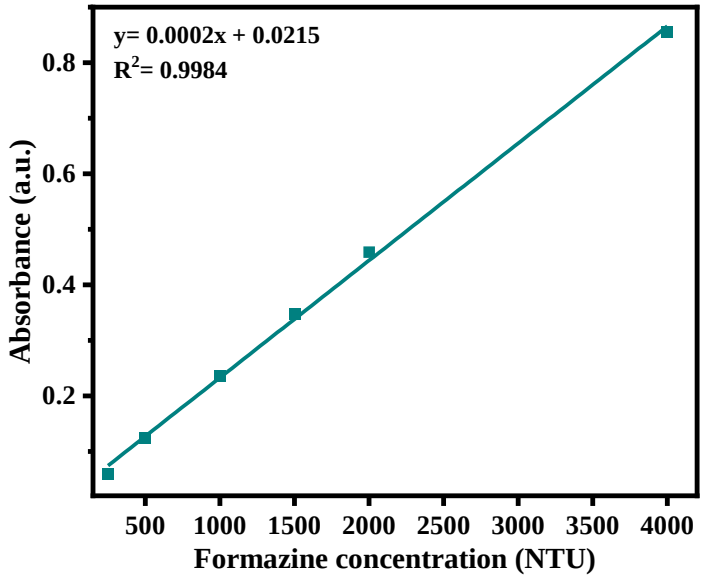

Figure S5 - Inhibition of *C. elegans* growth when it was exposed to 7.61; 10.67; 16.0; 24.0; 36.0; 54.0 and 81.0 mg L^{-1} of BAC-C16.

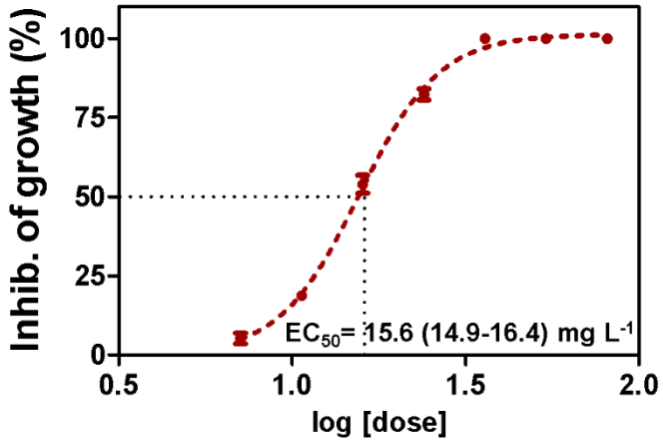

Figure S6 - Raman spectra of GO and BSA@GO (A); MWCNT and BSA@MWCNT (B).

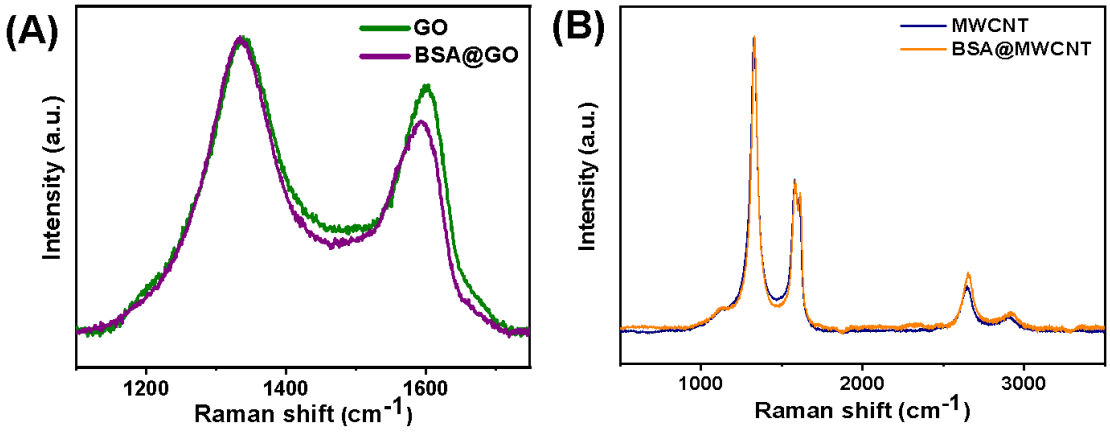

Figure S7 - High-resolution C1s XPS spectra of GO (A) and MWCNT (B).

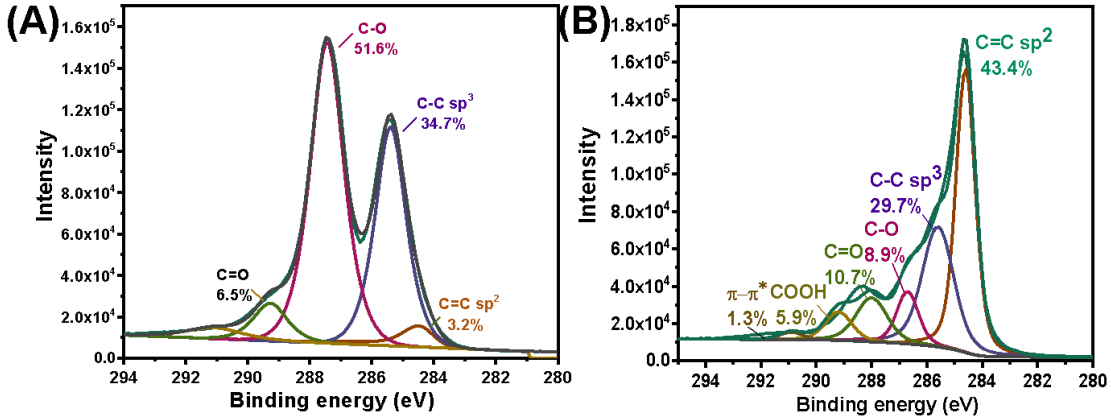

Figure S8 - Hydrodynamic diameters as long as the sonication was performed.

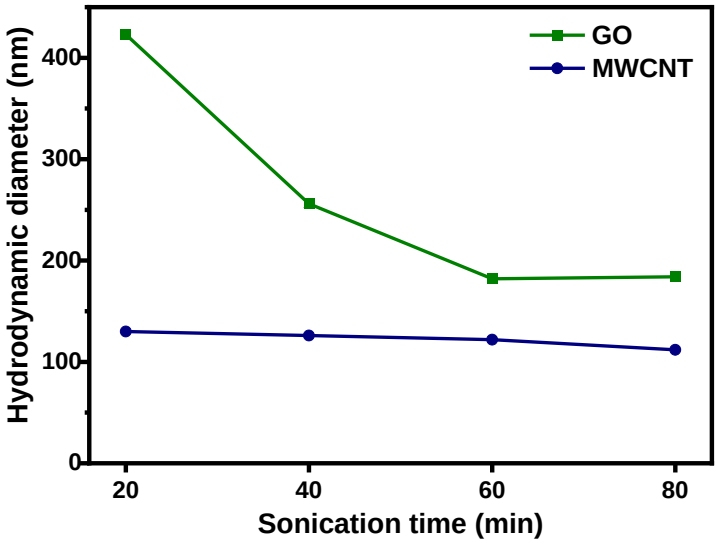

Figure S9 - Stability of GO and MWCNT stock dispersions measured in static (A) and non-static experiments (B) by using UV-Vis spectroscopy to evaluate materials that remained in suspension.

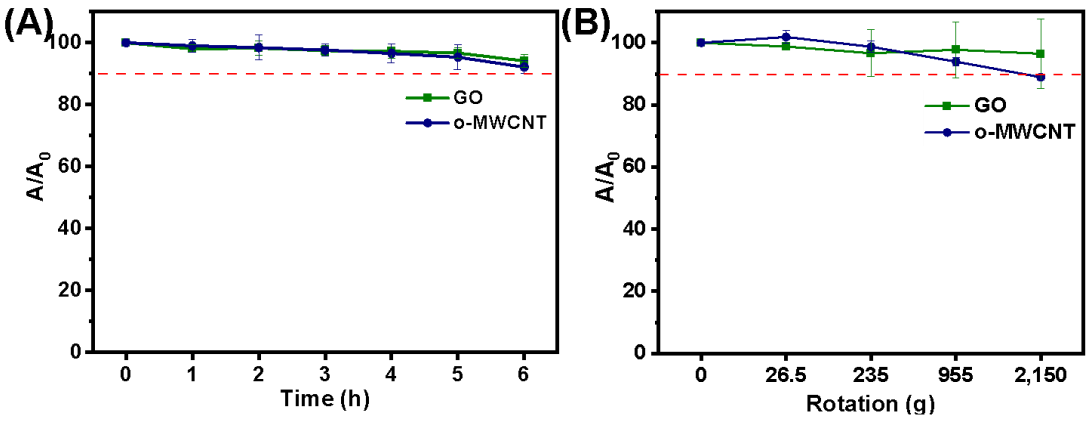

Figure S10 - Correlograms from dynamic light scattering analysis of materials dispersed in EPA medium or ultrapure water, monitored for 96 h.

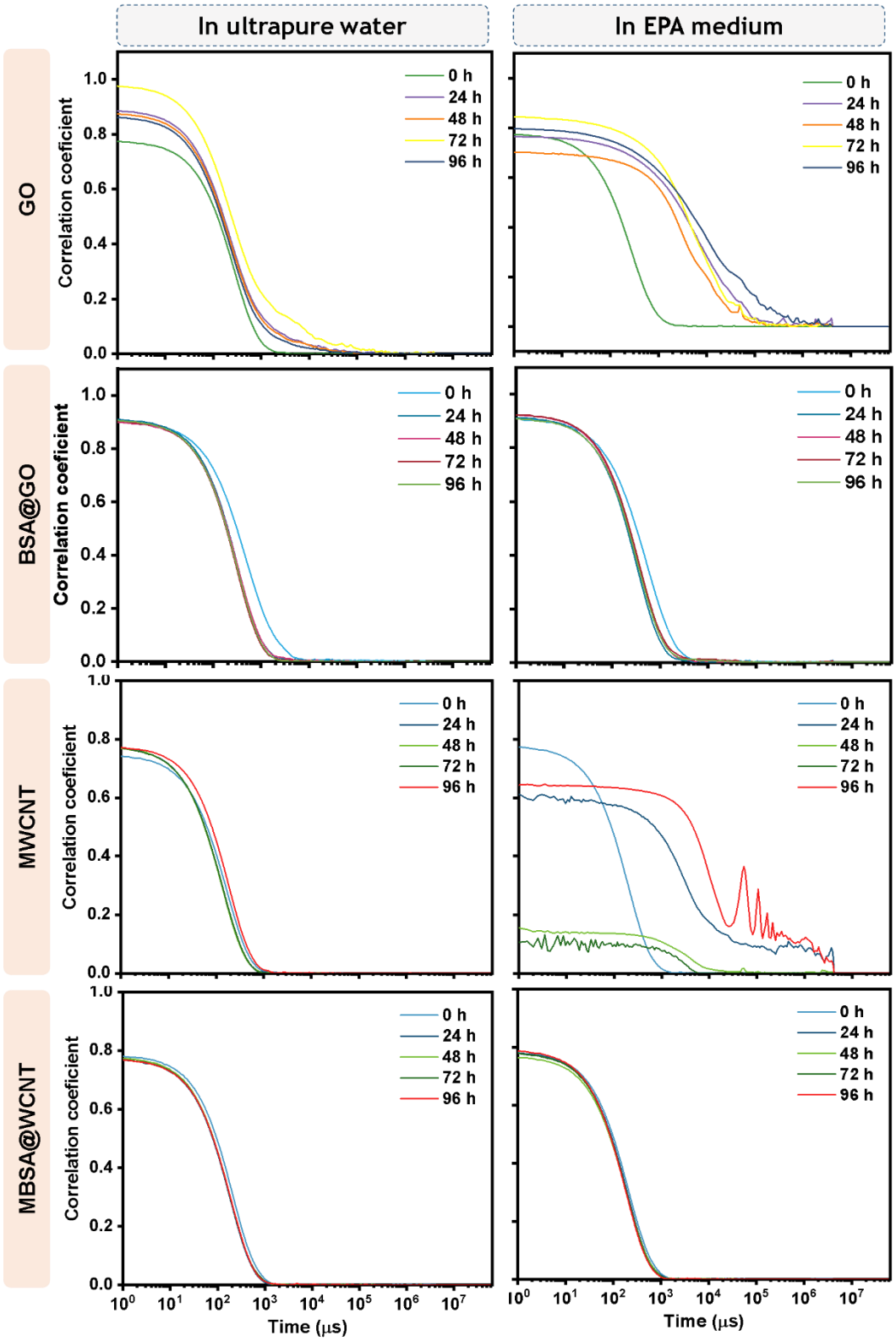

Table S1 - Potential zeta values (mV) of GO, BSA@GO, MWCNT, BSA@MWCNT in ultrapure water and EPA medium obtained by the ELS technique.

	In ultrapure water	In EPA medium
GO	-49.9±0.7	-23.0±0.8
BSA@GO	-32.7±1.3	-25.8±2.1
MWCNT	-50.9±0.4	-25.0±1.3
BSA@MWCNT	-36.7±1.6	-24.2±0.7

Figure S11 - Internalization of GO, BSA@GO, MWCNT, and BSA@MWCNT in nematodes evaluated by Raman confocal spectroscopy.

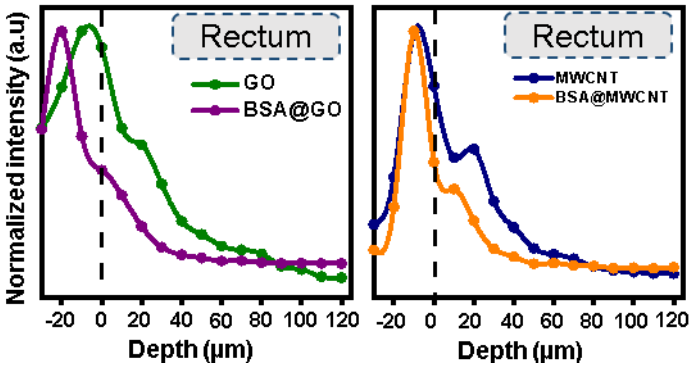

Figure S12 - Excretion experiment. Raman confocal spectroscopy analyses of the intestine of nematodes after being exposed to GO, BSA@GO, MWCNT, and BSA@MWCNT and be transferred to the nematode growth medium (NGM) with or without food for 2 h or 12 h, respectively.

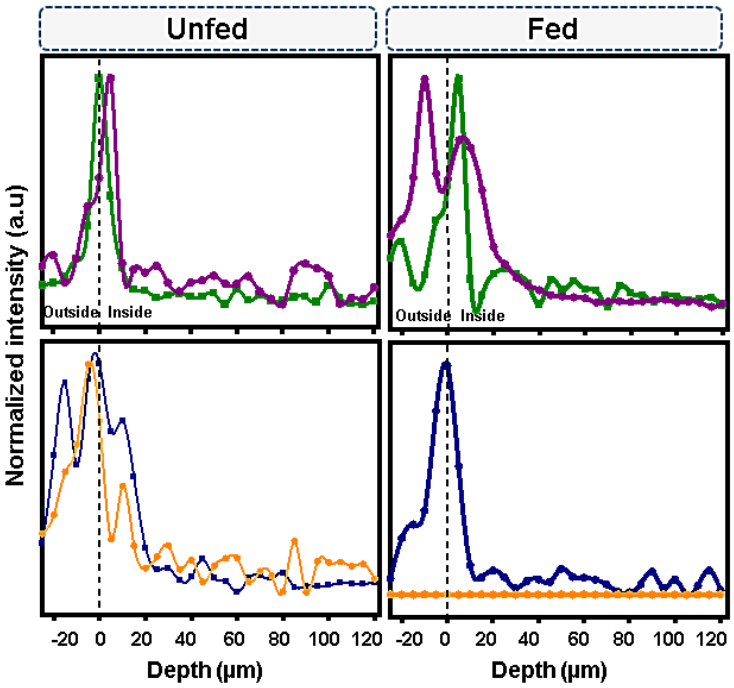

Figure S13 - Optical microscopy images of nematodes exposed to GO, MWCNT, BSA@GO, and BSA@MWCNT at 10 mg L^{-1} for 24 h.

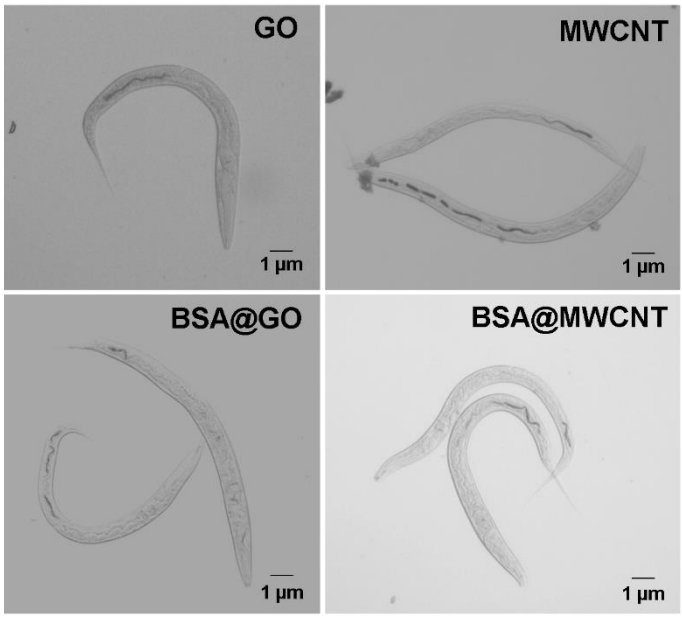

Figure S14 - Inspection visual of aggregated/agglomerated GO, BSA@GO, MWCNT and BSA@MWCNT in long-term assays with *C. elegans*.

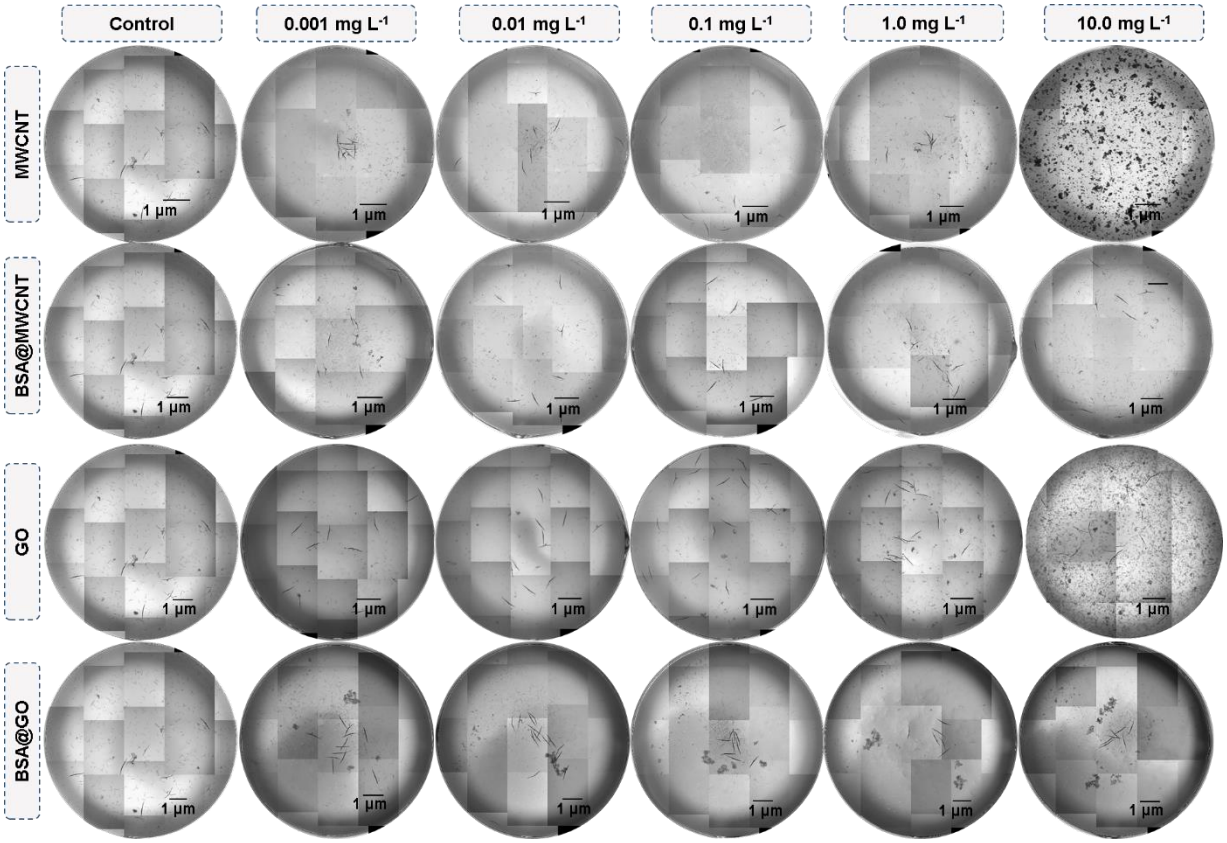

Appendix B. Supplementary Information of Chapter 4

Escherichia coli culture and lysis

OP50 *Escherichia coli* was transferred from Luria-Broth (LB) solid medium with a sterile inoculating loop to sterile LB liquid medium (6 sterile Erlenmeyer flasks of 500 mL) and incubated in an orbital shaker (TE-4200, Tecnal) at 100 rpm and 37 °C. After 14 h, bacteria suspensions were transferred to 50 mL centrifuge tubes and pelleted (Centrifuge 5810R, Eppendorf) at 5,000 rpm, 4 °C for 5 min. Pellets were rinsed with phosphate buffer saline and again centrifuged. Supernatants were discarded and pellets were kept frozen until the extraction. Pellets (~3 g) were resuspended in 100 mL sterile phosphate buffer saline (PBS) solution and this suspension was sonicated in a tip ultrasonic processor (Model Gex 400, Acil Weber) operated at 40 W and controlled temperature (10 °C) for 10 min to promote the extraction of intra-cellular compounds of bacteria. The suspension was centrifuged in 50 mL centrifuge tubes at 10,000 rpm, 4 °C for 10 min. Supernatants were collected and filtered in a 0.22 µm syringe filter to obtain only the soluble compounds from *E. coli* lysed. Proteins were quantified by Bradford assay (Lot #SLBV5669, Sigma-Aldrich) at 595 nm using a microplate reader UV-Vis spectrophotometer (Multiskan TM GO, ThermoScientific) and the protein concentration in suspension was adjusted at 1.0 mg L^{-1} for further use.

Figure S1 - Calibration curve of Bradford assay in PBS from absorbance (at 595 nm). The straight line is a linear fit of data.

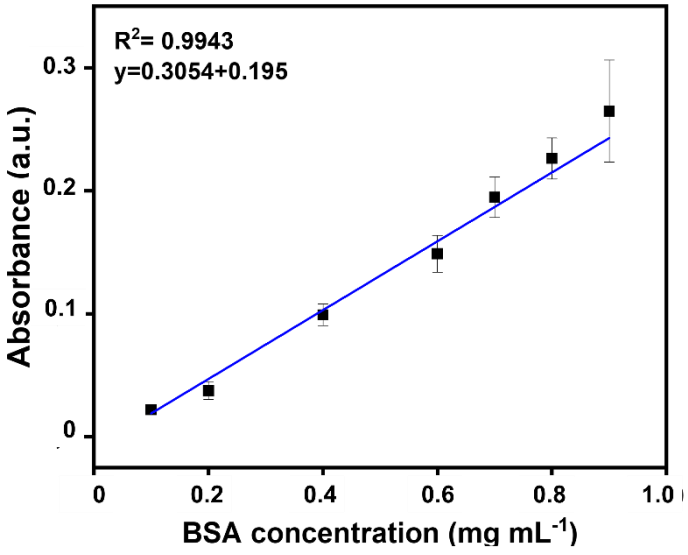

Characterization of graphene oxide with and without corona

The surface roughness and thickness features of GO and EC@GO were evaluated by atomic force microscopy (AFM). Images were obtained in a tapping mode on MultiMode VIII microscope with NanoScope V controller model (Bruker). A silicon tip (NCHR, BudgetSensors) was used with nominal resonance frequency of 300 kHz and nominal force constant of 40 N/m. 5 µL of samples (10 mg L^{-1}) was dropped in a freshly cleaved mica (2 x 2 cm). Images were processed on Gwyddion software (2.5 version). Average height profiles were acquired from 10 different flakes and surface roughness were measured considering an equal area on the flakes (12,808 nm^2).

X-ray photoelectron spectroscopy (XPS) was applied to evaluate the surface elemental composition of GO and EC@GO. A K-Alpha System (Thermofischer Scientific, USA) was employed operated with Al Kα X-rays and charge compensation. Survey spectra were collected with 400 µm spatial resolution at five different areas per sample using a pass energy of 50 eV. Data were processed with Thermo Avantage software (version 5.957).

Functional groups present on GO and EC@GO surfaces were evaluated by ATR-FTIR in IRSpirit-L equipment (Shimadzu). This was performed in the frequency range from 500 to 4000 cm^{-1}, with 2 cm^{-1} resolution and a total of 150 scans.

Sodium dodecyl sulfate-polyacrylamide gel electrophoresis (SDS-PAGE) was performed to separate the proteins adsorbed by GO. Bound proteins were removed from GO by adding 3xSDS-loading buffer (Lot#B77035, New England Biolabs) and 1:10 volume of 1.25M DTT for 3 min at 99 °C. Then, 15 µL of removed proteins were loaded on a SDS-PAGE (4% stacking gel and 15% resolving gel). Positive control was also loaded with all the soluble proteins from *E. coli* lysis. Three independent samples were analyzed and gel run included a color prestained protein standard (Lot 0071601, New England BioLabs). After electrophoresis, separated proteins were stained with silver nitrate.

Figure S2 - Dispersion stability of GO and EC@GO in ultrapure water (UW) and EPA medium evaluated by UV-Vis spectroscopy for 24 h.

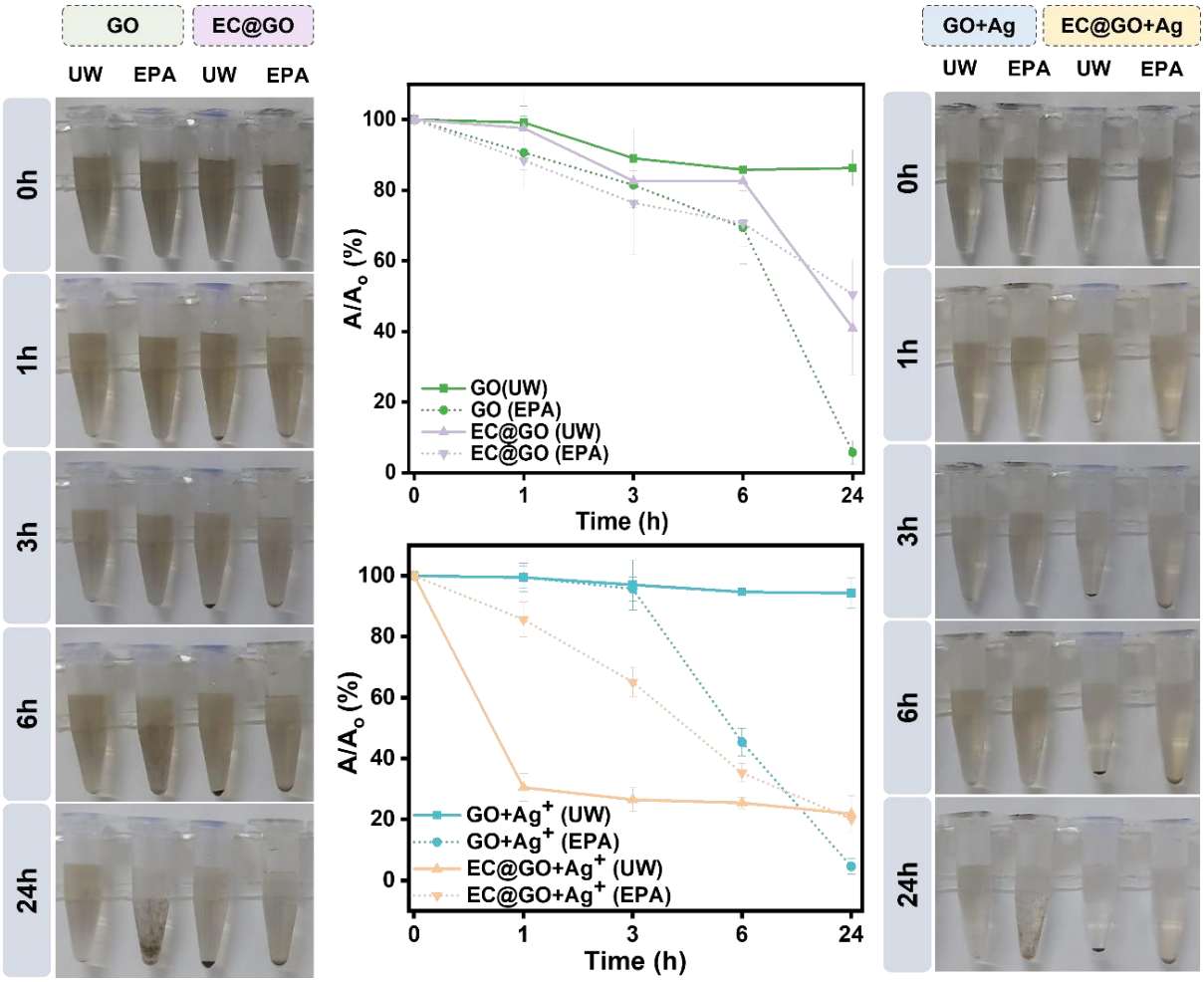

Figure S3 - Internalization of GO+Ag^{+} and EC@GO+Ag^{+} in *C. elegans* evaluated by confocal Raman spectroscopy from -25 to 120 µm depth. Nematode cuticle is represented by point zero and a dotted line. The laser power applied on a sampling point was 1.2 mW.

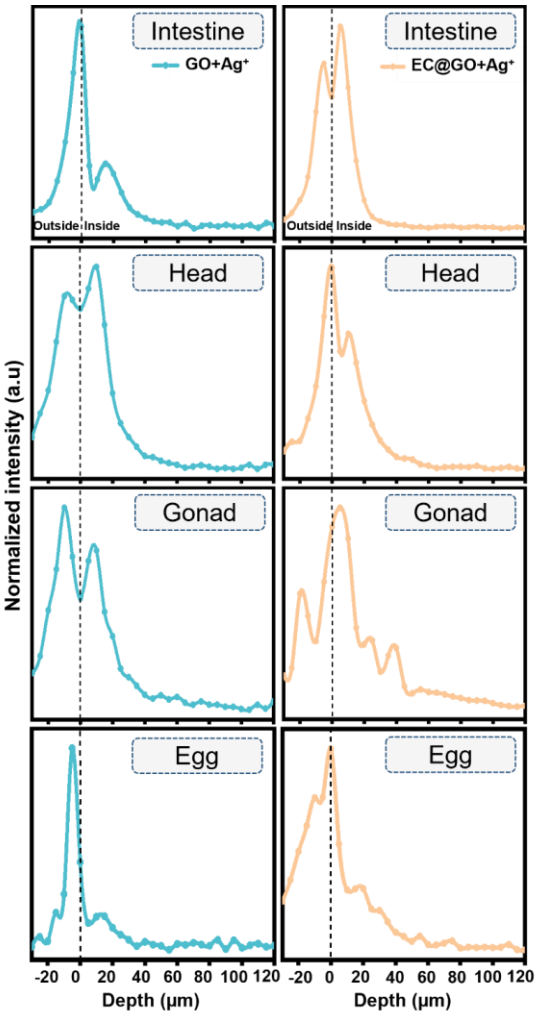

Figure S4 - Amount of silver adsorbed (%) by graphene oxide and graphene oxide coated by *E. coli* corona.

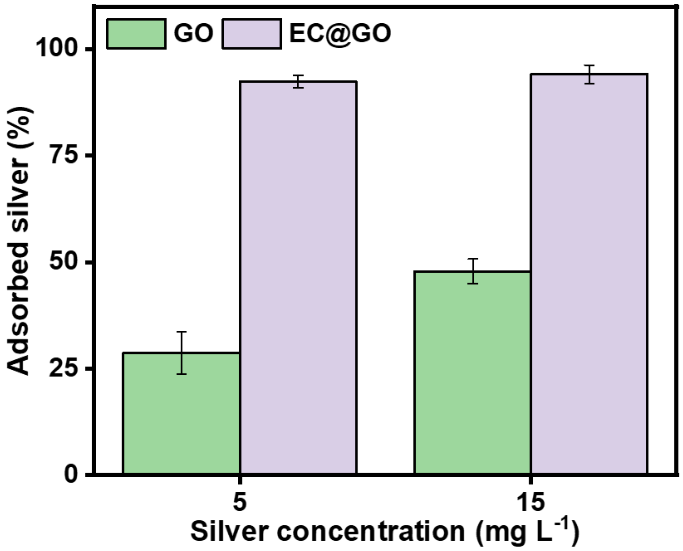

Figure S5 - Calculated distribution of silver species as a function of silver concentration using Spana software.

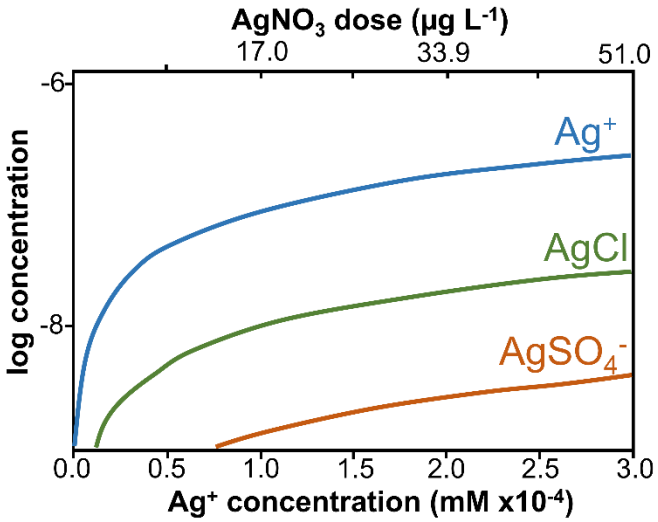

Appendix C. Scientific publications

This list comprises the contributions related to the work developed during this thesis (marked with an asterisk) and indirect contributions in papers, book chapters and patents.

a) Scientific papers

1) ***Côa, F**.; Delite, F.S.; Straus, M.; Martinez, D.S.T. Toxicity mitigation and biodistribution of albumin corona coated graphene oxide and carbon nanotubes in *C. elegans. NanoImpact*, v. 27, 2022.

2) Zanini, C.H.M.; **Côa, F**.; Silva, G.H.; Bettini, J.; Farias, M.A.; Portugal, R.P.; Umbuzeiro, G.A.; Alves, O.L.; Martinez, D. S.T.M. Functionalization of carbon nanotubes with bovine plasma biowaste by forming the protein corona enhances copper removal from water and ecotoxicity mitigation. *Environmental Science-Nano*, v. 1, p. 12, 2022.

3) Martinez, D.S.T.; **Côa, F**.; Knobel, M. Nanossegurança para inovação sustentável. *Ciência & Cultura* (SBPC), v. 74, p. 01-11, 2023.

4) Bortolozzo, L. S.; ***Côa, F.**.; Khan, Latif, U.; Medeiros, Aline M.Z.; Silva, G.H; Delite, F.S.; Straus, M.; Martinez, Diego S.T.M. Mitigation of graphene oxide toxicity in *C. elegans* after chemical degradation with sodium hypochlorite. *Chemosphere*, v. 278, p. 130421, 2021.

5) Melo, C.B.; **Côa, F**.; Alves, O.L.; Martinez, D.S.T.; Barbieri, E. Co-exposure of graphene oxide with trace elements: Effects on acute ecotoxicity and routine metabolism in *Palaemon pandaliformis* (shrimp). *Chemosphere*, v. 223, p. 157-164, 2019.

6) Medeiros, A.Z.; **Côa, F**.; Alves, O.L.; Martinez, D.S.T.; Barbieri, E. Metabolic effects in the freshwater fish *Geophagus iporangensis* in response to single and combined exposure to graphene oxide and trace elements. *Chemosphere*, v. 2, p. 125316, 2019.

7) Silva, G.H.; Clemente, Z.; Khan, Latif U.; **Côa, F**.; Neto, L.L.; Carvalho, Hudson W.P.; Castro, V.L; Martinez, D.S.T.; Monteiro, R.T. Toxicity assessment of TiO_2-MWCNT nanohybrid material with enhanced photocatalytic activity on *Danio rerio* (Zebrafish) embryos. *Ecotoxicology and Environmental Safety*, v. 165, p. 136-143, 2018.

b) Scientific papers (in preparation)

1) ***Côa, F**.; Straus, M.; Delite, F.S.; Ávila, D.; C.A. Pérez, Abreu Junior, C.H.; Lynch, I.; Martinez, D.S.T. Impacts of *E. coli* corona formation on combined toxicity of graphene oxide with silver ions in the *C. elegans* model.

2) ***Côa, F**.; Bortolozzo, L.; Ávila, D.; Martinez, D.S.T. Nanotoxicology of Carbon Nanomaterials in the *C. elegans* model: Current status, Characterization and Perspectives for testing harmonization.

c) Book chapters

1) **Côa, F**.; Gubert, P.; Ávila, D. S. Bianchini, M.C. Modelos de exposição em *C. elegans* e especificidades no uso de nanomateriais. In: Guia para pesquisadores iniciantes em *C. elegans*. 1ed: E-Publicar, 2022.

2) Souza, D.C.; **Côa, F**.; Nunes, F.K.Q.; Silva, I.IM.; Santos Junior, J.A.; Costa, L.P.S.; Bezerra, I.C.; Gubert, P. Pathogenic microorganisms when applied to the animal model *Caenorhabditis elegans* in a One Health Perspective. In: Topics in *C. elegans*. 1ed.: E-Publicar, 2022.

3) **Côa, F**.; Gubert, P.; Identificação colorimétrica/fluorescência de biomomoléculas e estruturas. Guia para pesquisadores iniciantes em *C. elegans*. 1ed.: E-Publicar, 2022.

4) **Côa, F**.; Bortolozzo, L. S.; Petry, R.; Silva, G.H.; Martins, C.H.Z.; Medeiros, A.M.Z.; Sabino, C.M.S.; Costa, R.S.; KHAN, L.U.; Delite, F. S.; Martinez, D.S.T. Environmental Toxicity of Nanopesticides Against Non-Target Organisms: The State of the Art. In: Nanopesticides. 1ed.: Springer International Publishing, 2020, p. 227-279.

5) Gonçalves, S. P. C.; Delite, F.S.; ***Côa, F**.; Neto, L.L.R.; da Silva, G.H.; Bortolozzo, L.S.; Ferreira, A.G.; Medeiros, A.M.Z.; Strauss, M.; Martinez, D.S.T. Biotransformation of Nanomaterials in the Soil Environment: Nanoecotoxicology and Nanosafety Implications. In: Nanomaterials Applications for Environmental Matrices. 1ed.: Elsevier, 2019, p. 265-304.

d) Patents

1) ***Côa, F.**; Martinez, D.S.T. Corona de proteínas carreadora de agentes antinematoides e seu processo de produção. 2022, Brasil. Register number: BR10202201220. Register Institution: INPI - Instituto Nacional da Propriedade Industrial. Deposited: 20/06/2022.